UNIVERSITÀ DEGLI STUDI DI TRIESTE

XXXIV CICLO DEL DOTTORATO DI RICERCA IN

Scienze della Terra e Meccanica dei Fluidi

Restoration of vintage gravity data and comparison with new satellite-derived models in two case studies: the Gulf of Manfredonia and the Friulian Plain / North Adriatic

Settore scientifico-disciplinare: GEO/11 GEOFISICA APPLICATA

DOTTORANDO / Ph.D. STUDENT
Luigi Sante ZAMPA Luigi Sante Zampa

COORDINATORE / COORDINATOR
Prof. Stefano MASET Stefano Maset

SUPERVISORE DI TESI / THESIS SUPERVISOR
Prof. Angelo CAMERLENGHI

CO-SUPERVISORI TESI / THESIS CO-SUPERVISOR
Dr. Martina BUSETTI Martina Busetti
Dr. Emanuele LODOLO E. Lodolo
Dr. Nicola CREATI Nicola Creati
Dr. Carla BARNABA Barnaba Carla

ANNO ACCADEMICO 2020/2021

. . . **To my grandpa,**

who used to say

"*Meglio un asino vivo che un dottore morto*"

"*A living donkey is always better than a dead doctor*"

He encouraged me in my studies till the very end

"The past is not a package one can lay away"

(Emily Dickinson, June 1883 - Letter 830 - to Maria Whitney)

Extended Abstract

The central aspect of this thesis is the recovery, homogenization, and validation of the enormous amount of vintage gravimetric and magnetic data acquired by OGS since the early 1960s, both at sea and onshore in the Italian territory. It is a wealth of geophysical data that today would be unthinkable to acquire because of the unsustainable costs and logistic difficulties. A further important aspect of the work is the comparison with satellite-derived data, analyzed through two specific case studies: the northern Adriatic/Friulian Plain and the Manfredonia Gulf (SW Adriatic). A great effort has been made to evaluate whether gravimetric data acquired in different periods, with different tools and processing techniques, can be used for geological studies after appropriate corrections and homogenization.

Nowadays, with the new interpretation techniques, it is possible to extract further and more accurate information from the same datasets and merge them with the more recent acquisition technique, including satellite-based models. Moreover, data restoration is often a crucial factor in addressing new research projects and scientific explorations.

Starting with this premise, the Ph.D. project have been focused on restoring offshore and onshore gravity data available in the archives of the OGS. New data analysis, conducted in areas where seismic reconnaissance and boreholes partially intercepted known discontinuities in the rock basement, has improved previous geological models giving more spatial continuity to the current interpretation of the targeted structures.

Three different gravity data types were collected and merged to create the most detailed and homogeneous view of gravity anomalies in the study regions: (i) sea-bottom, (ii) sea surface, and (iii) land-based gravity.

Different processing methods have been tested to reduce all possible data errors and signals unrelated to the investigated targets.

Firstly, to remove the gravity effects of elevation above the reference gravity model and the effects of topographic and water masses, we merged high-resolution and low-resolution Digital Topographic Models (DTMs), covering both seafloors and continental areas.

Several merging methods have been considered (Hell & Jakobsson, 2011), finding the best alternative in the solution proposed by Gallant (2019). This approach uses the differences between the high-resolution and the low-resolution models. Then the differences are extrapolated with lowpass filtering techniques over the low-resolution models and smoothing the transitional zones connecting the different models. We adopted this kind of solution because of its significant advantage in preserving all the original accuracy within the high-resolution areas.

The gravity effect of topography was finally computed using both prism and tesseroid elements, respectively near and far from the computational points (Uieda, Barbosa, & Braitenberg, 2016).

Moreover, we processed the sea bottom data using a slightly different computational scheme from the one generally adopted in sea surface and land data processing, which considers the effect of water masses above the measurement point (Hildebrand, et al., 1990). Additionally, sea-bottom data were also upward-continued to the sea surface using the equivalent layer method (Soler & Uieda, 2021). This solution allowed a correct interpolation of sea-bottom with the sea-surface gravity when computing the final anomaly maps.

We reduce crossover errors in sea-surface gravity lines using a remove-restore method which combines the long-wavelength signals of satellite altimeter-derived models with the short-wavelength of shipborne data. Finally, an additional correction was applied to minimize the differences at the line intersections, statistically (Mittal, 1984).

The calculated Free-air anomaly and the Bouguer anomaly were corrected for the geophysical Indirect Effect, using the geoid model EIGEN-6C4, obtaining a final gravity anomaly free from the components related to the geoid and ellipsoid differences(Xiong & Götze, 2001; Hinze et al., 2005; Bruinsma, 2014).

We tested different methods, including spectral analysis, polynomial approximations, and convolution filters, to separate the regional gravity anomalies from the local components associated with shallow density contrasts.

The resulting local anomalies were further emphasized using combinations of different gravity field derivatives, such as the vertical gradient, the Tilt, and the Terracing functions.

Ultimately, we applied all the described methods in two selected study areas.

We chose the first study area in the Gulf of Manfredonia, in the SE sector of the Adriatic Sea, because: (i) two different sea-bottom gravity surveys were conducted over the years, (ii) the bathymetry is mainly flat, and (iii) seismic data revealed a prominent carbonate ridge covered by hundreds of meters of Oligocene-Quaternary sediments.

In the Gulf of Manfredonia, we compared sea-bottom and satellite altimeter-derived data, knowing that the latter is generally biased in coastal regions by signals back-scattered from the nearby land. We used gravity field derivatives to enhance both deep geological contacts and coastal noise. The analyses outlined a ringing noise compromising the altimeter signals up to 17 km from the coast. The differences between the observed data and gravity calculated from the available geological models showed that all the investigated datasets register approximately the same patterns associated with the Gondola Fault Zone. Still, altimeter-derived gravity data is unreliable near where the contribution of sea-bottom gravity is fundamental for a correct geological interpretation.

The second study area includes the northern Adriatic Sea and the Friulian Plain, the foreland of a continental collision. This zone is the transition between eastern Alps and external

Dinarides, and questions on the geometry of the boundaries and reciprocal roles are still open. In this case, we combined sea bottom data collected in the 60s, sea surface data collected in the 70s, 80s, and 2005, and land gravity data (Ciani, Morelli, & Gantar, 1960; Makris, Morelli, & Zanolla, 1998; Cati, Fichera, & Cappelli, 1987). The new processing and gravity field analysis allowed us to track discontinuities generated by lateral density contrast between carbonates, molasse flysch rocks, and sediments within a depth range of ~6 km, which have been integrated into new geological models.

The results of this Ph.D. project showed the potential for improving the accuracy of gravity anomalies merging information from topography and satellite-based gravity models, together with land, sea-surface, and sea-bottom gravity data. In this regard, new processing strategies have been tested to homogenize and combine all datasets and to retrieve the best possible interpretation of subsurface lateral density contrasts in the first kilometers of depth. Specifically, these results helped outline and better image geological structures, with continuity from in-land towards the offshore in local coastal settings, with more accurate results than those previously achieved using sparse geophysical and geological datasets.

This work represents one of the few examples in which vintage geophysical data have been restored and validated. This is an important dataset that can be made available to the scientific community for joint studies and that allows deepening study areas in which the availability of data is scarce. The procedures and methods that have been applied and discussed in this thesis, through examples of case studies and the realization of geological models in-depth, have demonstrated the validity of the approach and provided a key for future studies involving the use of vintage geophysical data.

The first case of study on the Gulf of Manfredonia, has been recently submitted to the Journal “Earth and Space Science," and the manuscript is awaiting the acceptance of final revision of the english language requested by the editor. Furthermore, we are currently working on a second manuscript about the results obtained for the Friuli Venezia Giulia, and the northern Adriatic Sea.

Contents

1 Introduction

The growing development that geophysical acquisition techniques have had in recent decades through the use of satellites or aircraft and drones have made it possible to cover ever-larger areas of territory, drastically reducing the costs of surveys both at sea and on land and overcoming many logistical difficulties. However, although this information is fundamental for analyzing the geological and structural sub-crustal structure of a given area on a large scale, in most cases, it does not provide a sufficiently detailed and precise picture on a local scale and, above all, does not consider the constraints with the information obtained on the land or sea surface. In many cases of geological/geophysical studies, both for scientific and applicative purposes, the punctual data acquired on land or along transects at sea is decisive, to provide a realistic picture of the subsurface and deep structure of a given area, which it can possibly be integrated with other geophysical information, when available.

The OGS Institute acquired since 1950, and for a period of more than forty years, a large amount of gravity and magnetic data both onshore and offshore: in this regard, the OGS was the first Italian institute to systematically collect this kind of experimental data around the national territory.

The objective of this P.h.D project is to recover the huge vintage datasets from the archives of the OGS institute homogenized data into a new digital database and perform a comparison with satellite-derived data in two case studies in the Manfredonia Gulf – SW Adriatic and in northern Adriatic/Friulian Plain.

Until 1970-1975, all the datasets were archived only on paper. Therefore a consistent part of the first-year project was spent implementing a procedure to digitalize and verify the accuracy of the collected data by comparing old with recent acquisitions over the same areas. In this processing, we often found outliers explicitly due to hand-made typing errors that we could correct.

More difficult was to recover information about the geographic datum and the reference gravity networks used to frame the different surveys. These reference systems have been changed multiple times in the past fifty years. Therefore it was necessary for us to know the exact original frames of each survey and to homogenize them all into one unique system. Some of the information about the original frames has been lost over the years; thus, in these cases, we had to guess values using systematic differences with newly available data and/or background information found in other reports.

We focus on sea-bottom gravity data, which are very numerous and mainly concentrated around the Italian coasts, and have not been included in some of the last compilation of the Italian Bouguer gravity maps. Therefore, this data type required a specific processing procedure to be merged with the sea surface data. We implemented this procedure and tested it in the Gulf of Manfredonia case study. Here we compared sea bottom data with satellite altimeter gravity showing that altimeter data are strongly affected by noise in the proximity of the coasts where sea-bottom data can guarantee a more accurate solution instead.

We recovered the Mediterranean digital dataset containing gravity and magnetic lines, acquired by the OGS from 1960 to 1972, in one of the older versions left by Claudio Gantar (Gantar, Morelli, & Pisani, 1968). The gravity and magnetic values at the line crossings have been reevaluated by automatic tools developed in python for this specific task, revealing crossing errors at least two times greater than those supposed by the previous authors. At the same time, we recovered two more recent shipborne gravity surveys in the northern Adriatic Sea that slightly differ from each other and from the OGS Mediterranean dataset.

To homogenize all the different lines, we decided to tie them to a reference model by choosing (i) a satellite altimeter model for gravity and (ii) a global geomagnetic model for magnetic data. Then, we implemented a simple remove-restore procedure to level the lines according to the reference model's mean value calculated in the nearby area of each measured point.

We tested the sensitivity of the re-processed gravity data to recognize density contrast caused by tectonic discontinuities under the sedimentary cover in the immediate subsurface in order to enhance the hidden fault networks. The study was conducted in the Gulf of Manfredonia and the Friulian Plain/northern Adriatic, where we have the constraints of sparse seismic data and eventually exploration boreholes.

We used high-resolution Digital Topographic Models to reduce commission errors in the computation of the Bouguer anomaly, which may occur when investigating relatively shallow sources. Moreover, because the study areas are located in the transitional zone between land and sea, as it is for most Italian territory, we automatically included high-resolution bathymetric models in the computation. Therefore we implement a fast solution to merge Digital Models at different resolutions and automatically combine them with the bathymetric models.

We wrote specific routines in Python to automatically detect the lateral density contrasts in the subsurface and compare them to the available local fault databases to validate the results. We further investigated the physical nature of these density contrasts creating 2D forward models. In this regard, we conducted a specific survey in the area of Fontanafredda - Budoia (PN).

Generally, we were able to detect the presence of subsurface discontinuities but could not always derive a consistent geological model due to the well-known inherent ambiguity of the potential field methods.

1.1 Data used

From the beginning of 1950, the former Osservatorio Geofisico Sperimentale di Trieste now National Institute of Oceanography and Applied Geophysics (OGS), under the direction of Carlo Morelli, started collecting gravity and magnetic data all over the Italian territory, including marine areas. In 1955, Morelli laid the foundation for the first Italian gravity network using two Worden gravimeters, with final closure errors lower than 0.12 mGal (Morelli, 1952). Then, he proposed and guided the foundation of a world standardized gravity network to connect and homogenize all national/local networks. After 20 years, in 1971, the network was finally approved at the General Assembly of Geodesy and Geophysics in Moscow. The approved global reference system (i.e., the International Gravity Standardization Net, IGSN71) remains a monument to international collaboration to date.

The new networks worked as a starting point for many other second-order networks and local surveys, which formed the basis for the first and the second Italian Bouguer gravity maps (Berrino, 2020).

The geophysical explorations were subsequently extended to the Mediterranean Sea within international cooperation projects endorsed by UNESCO. The results led, in 1981, to the drafting of a new bathymetric map of the Mediterranean (10 sheets at a scale of 1: 1.000.000) and, between 1985 and 1999, to the publication of many important scientific papers, which investigate in detail the geodynamics of the sea, using gravity, magnetic, seismic, and other geophysical data.

The complete gravity database, which allowed the create all the available gravity maps of Italy at different scales, i.e., 1: 1.000.000, 1:500.000, 1: 250.000, consists of numerous acquisition campaigns, started in the fifties with Morelli and continued to the beginning of the nineties (Figure 1-1, Figure 1-2). Various partners have participated in the data collection, including exploration companies and academic or public institutions, e.g., ENI, OGS, USDMA

(U.S. Defense Mapping Agency), the Geological Service (Ferri, Ventura, Coren, & Zanolla, 2005; Cassano & Maino, 1989; Carozzo, Luzio, Margiotta, & Quarta, 1992; Berrino, 2020).

The gravity data archive recently recovered at the OGS institute is also part of the Italian gravity database managed by the Geological Service of Italy and contains three main data types: (i) land gravity, (ii) shipborne gravity, and (iii) sea-bottom gravity data.

The latter was not included in the compilation of the latest published Italian gravity map (Ferri, Ventura, Coren, & Zanolla, 2005), probably because of problems related to the computation of sea bottom anomalies, which differs slightly from the conventional processing and makes it difficult the homogenization with other data types (Figure 1-2a). Nevertheless, sea-bottom anomalies can help identify local geological features in coastal areas where no other data is available. Therefore, it is still essential to preserve the sea-bottom data and possibly include them in the newest compilations.

Figure 1-1 Gravity map of Italy 1:1.000.000 (Cassano & Maino, 1989), downloaded from http://sgi.isprambiente.it/milione_grav/milionegrav_1989.html. Map created by the Geological Service of Italy - Agency for Environmental Protection and Technical Services (SGI-APAT), in cooperation with AGIP company. The map is based on 217000 land gravity stations and 4000 sea-bottom stations, homogeneously covering the Italian territory, including the marine coastal areas.

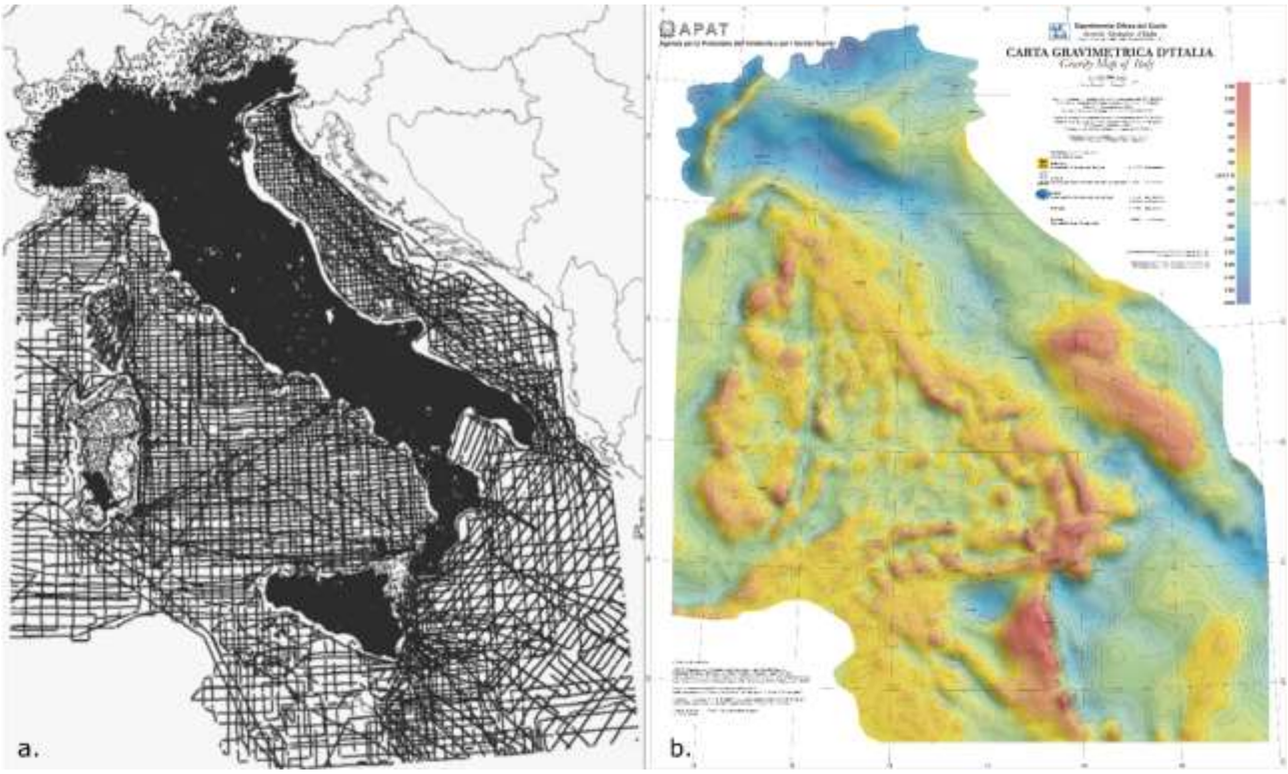

Figure 1-2 - (a) Spatial distribution of the gravity stations used for (b) the Gravity map of Italy 1:250.000 (Ferri, Ventura, Coren, & Zanolla, 2005). Map created by the SGI-APAT, cooperating with the OGS institute the ENI S.p.a Exploration and Production Division. Apparently, no sea bottom gravity data have been used in this newest compilation.

1.2 Land gravity and magnetic datasets

Most of the Italian land gravity data are property of the ENI company and eventually provided by the SGI-APAT, which also manages the archiving. Of these stations, about 27000 refer to relative gravity surveys between 1958 and 1983 (Cassano, 1983; Ferri, Ventura, Coren, & Zanolla, 2005; Berrino, 2020). The remaining part comes from different databases or later acquisitions made by other public/private institutions (Berrino, 2020).

In total, the land coverage consists of about 260.832 relative stations, which distribution can be roughly summarized as follow (Cassano & Maino, 1989):

- 1 station / km in the flat areas;
- 0.7 stations / km in the Apennines;
- 0.1 stations / km in Alpine regions;

For our studies, we re-processed the gravity values of the land stations within the borders of the Friuli Venezia Giulia region with some additional data in the nearby areas.

The observed values come from five different acquisitions, which are briefly described in the following paragraphs.

Moreover, we also digitalized one magnetic dataset acquired by the OGS in the fifties (Veneto Centro Orientale 1953-1954).

1.2.1 Zaule

Zaule is a small village located South East of Trieste, enclosed between the Slovenian border and the Gulf of Trieste. In 1950, Morelli C. recorded 23 gravity stations nearby. He used them to infer the morphology of the rock basement hidden beneath the alluvial sediments (Figure 1-3). The stations were recorded using a western G4A gravimeter (mod. n° 50), with an average accuracy of ±0.03 mGal. The recorded values were tied to the reference station of the Osservatorio Geofisico of Trieste (via R. Gessi), which had a fixed absolute value of 980664.71 mGal (Morelli, 1950).

The geographic coordinates were deduced from topographic maps at a scale of 1:1000 from the Network Update Office of the ACEGAT of Trieste, and other topographic maps at a scale of 1:25.000, with an accuracy of about ±25 m. Instead, station elevations have been measured with a quick assessment survey, reporting a vertical accuracy of 0.01 m.

During that time, the interest in this specific area was mainly related to the port expansion projects. Nevertheless, this data is one of the first examples of an indirect geophysical survey used to study subsurface geology in northeastern Italy.

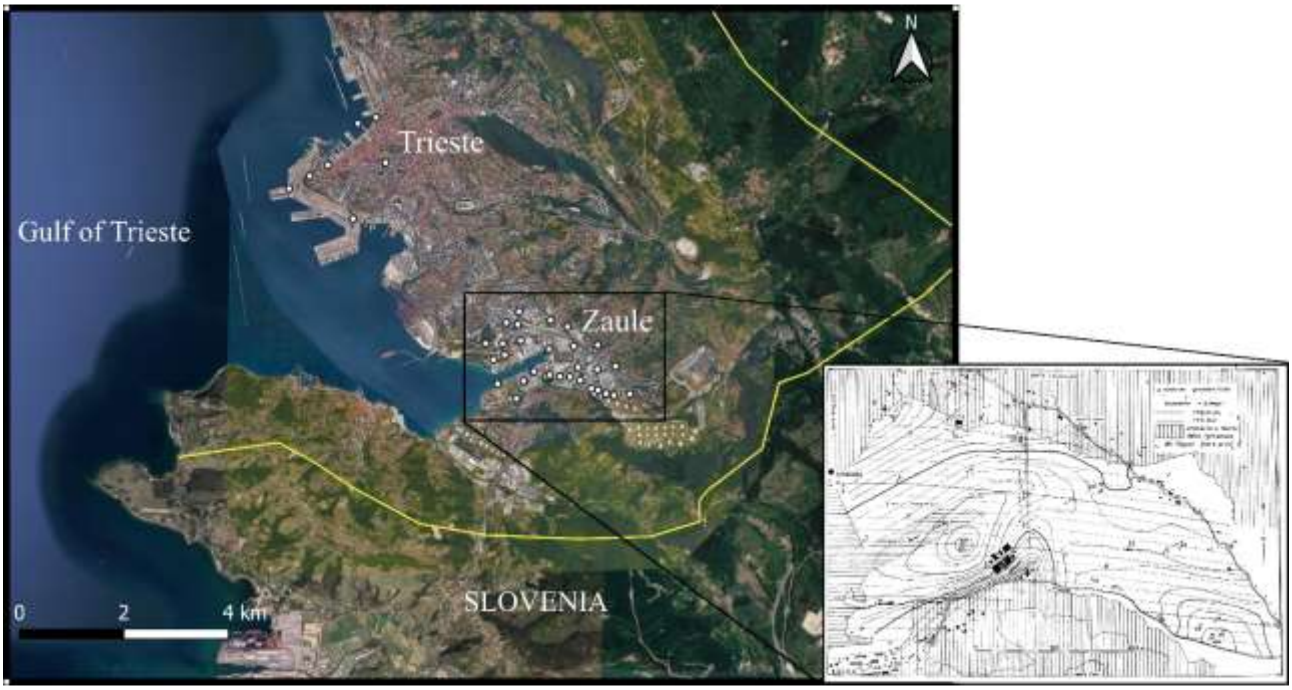

Figure 1-3 - Distribution of the stations in the study area of Zaule and map with the contours of the Bouguer and residual gravity anomalies (Morelli, 1950).

1.2.2 Italia Nord Orientale (ItaNO)

This survey was conducted in 1951 by the OGS between the Friuli and the Veneto regions (Italy). It comprises 180 relative stations measured with a Worden gravimeter (mod. n° 50), with an average accuracy estimated of ±0.5 mGal (Figure 1-4). The starting point of the survey was the reference gravity value measured at the Osservatorio Astronomico of Padova, i.e., 980657.5 mGal. Most of the stations occupy existing trigonometrical points where horizontal and vertical coordinates had been previously measured with metric/sub-metric precision by the Istituto Geografico Militare (IGM). However, the geographic coordinates were then transcripted with the accuracy of 1 arcsec (~25 m) and the elevations with a decimetric precision. Other random errors should be expected since the values were obviously handwritten at the time of the acquisition. Then, by comparing stations' positions with known locations on topographic maps, it is clear that positioning errors have been underestimated, and the expected horizontal accuracy should be around ±100 m.

The initial objective of this survey was the tectonic characterization of the North East of Italy, for which the authors calculated the isostatic anomalies according to both Airy-Heiskanen's and Vening Meisnez's theories. These results offered the first indication that the areas characterized by seismic instability well-correlates with the maximum values of the gravity gradient (Morelli, 1951).

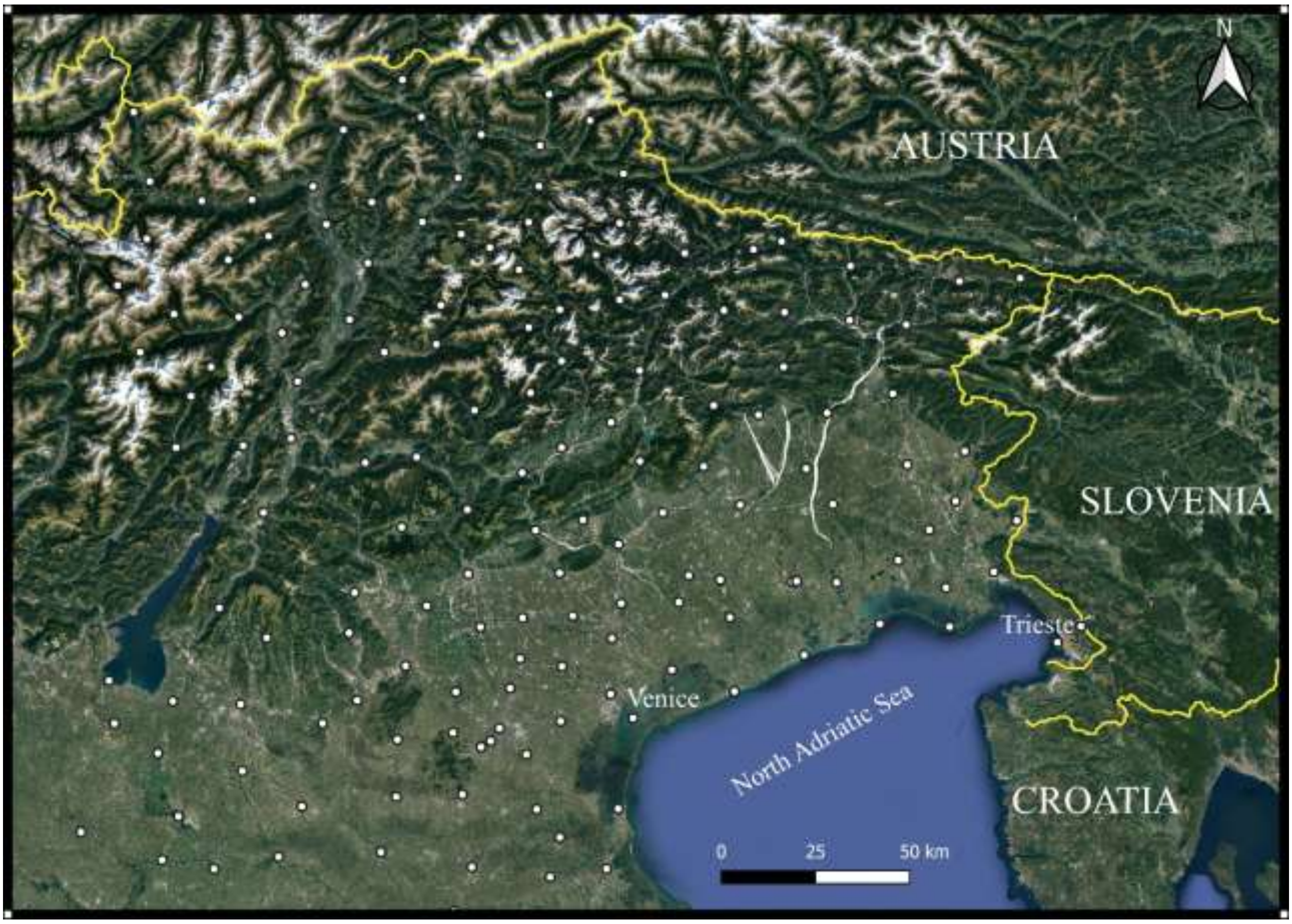

Figure 1-4 - Distribution of the gravity stations ItaNO (Morelli, 1951).

1.2.3 Veneto centro-orientale (GravVenCO)

This survey was a refinement of the one described in the previous paragraph, conducted between 1953 and 1954, with 170 new gravity stations. This refinement aimed to achieve a mean spatial coverage of at least one station every 100 km2 across NE Italy (Figure 1-5). This study used two Worden gravimeters (mod. n°50 and mod. n°52), obtaining an average accuracy of ±0.04 mGal, calculated on repeated stations. In this case, the relative gravity stations were all tied to the Osservatorio Geofisico of Trieste (via R. Gessi), with a reference value of 980657.2 mGal.

The gravity anomalies derived from this data provided the first evidence of Dinaric trending faults buried beneath the Friulian plain. In addition, gravity data analysis also identified some structural boundaries between the Euganian Basin, the Alps, and the Dinarides, finding those in perfect correlation with records of seismic epicenters (Morelli, 1954).

Additional 159 magnetic stations were recorded during the same campaign, using two vertical-field balances, Schmidt type (Askania Werke). The magnetic stations were all placed in the countryside, far from any source of artificial noise (iron artifacts, current lines, etc.). This results in lower positioning accuracy and spatial coverage of magnetic data with respect to gravity. Nevertheless, the magnetic anomalies showed some interesting correlations with the gravity anomalies, suggesting the presence of possible magmatic sources in the crustal sector below the measurement points.

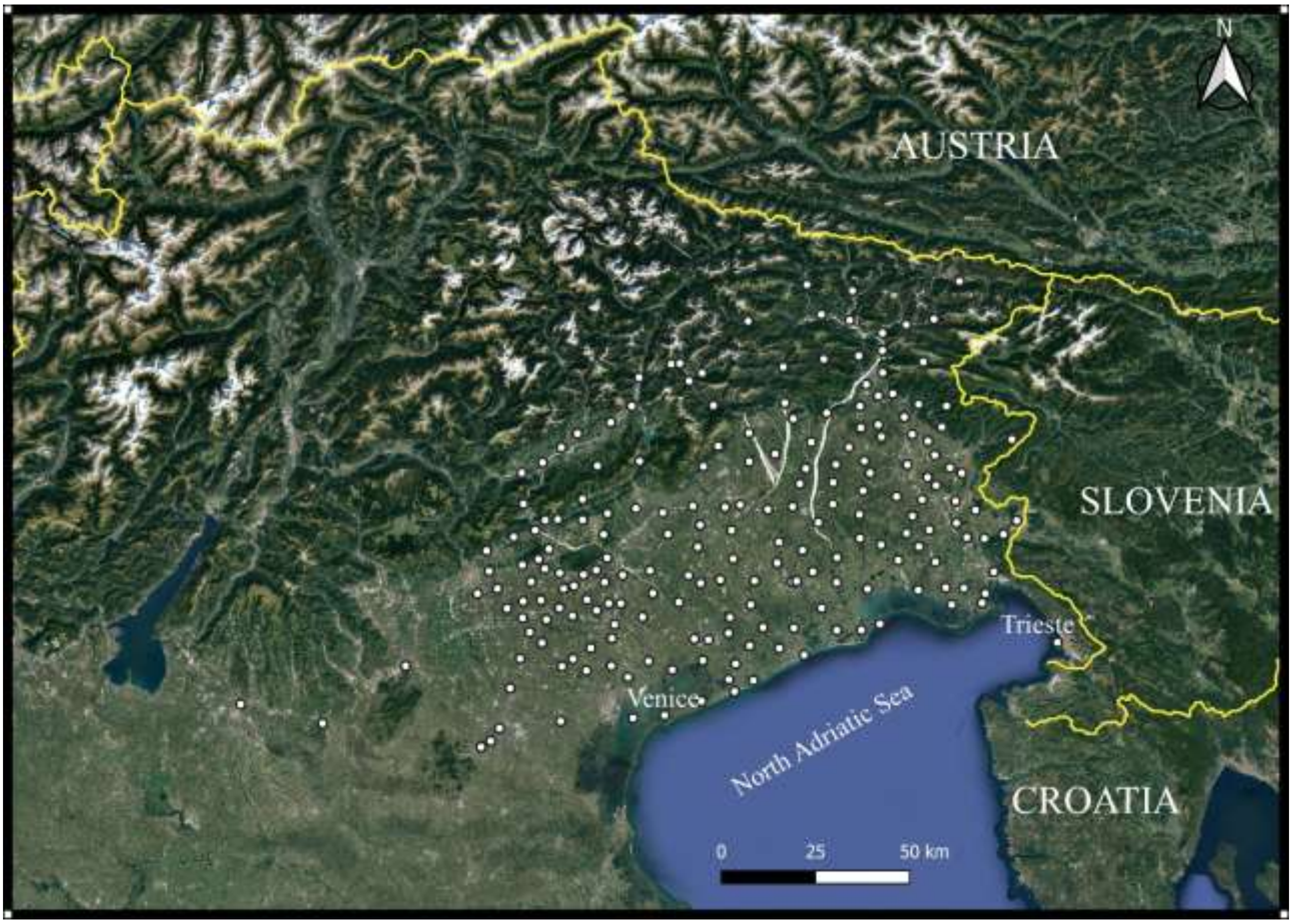

Figure 1-5 - Distribution of the gravity stations GravVenCO (Morelli, 1954).

1.2.4 Trieste - Monfalcone (TriMon)

The dataset comprises multiple surveys conducted mainly for academic research in the Karst region and the city of Monfalcone, close to the Italian-Slovenian border (Prodan, 2002). A total number of 370 stations were recorded using a LaCoste-Romberg gravimeter (mod. D-018), with final closure errors lower than 0.01 mGal (Figure 1-6). The horizontal coordinates and the elevation were derived from regional topographic maps (1:10,000), with ±1 m of accuracy for horizontal coordinates and ±2.5 m for the elevations on average. The gravity data were linked to the TS-SAR first-order network, connected in turn to the reference gravity value of the Osservatorio Geofisico of Trieste (via R. Gessi). The TS-SAR is a microgravity network composed of twelve stations to monitor land subsidence, set up in 2001-2002 (Palmieri & Coren, 2002).

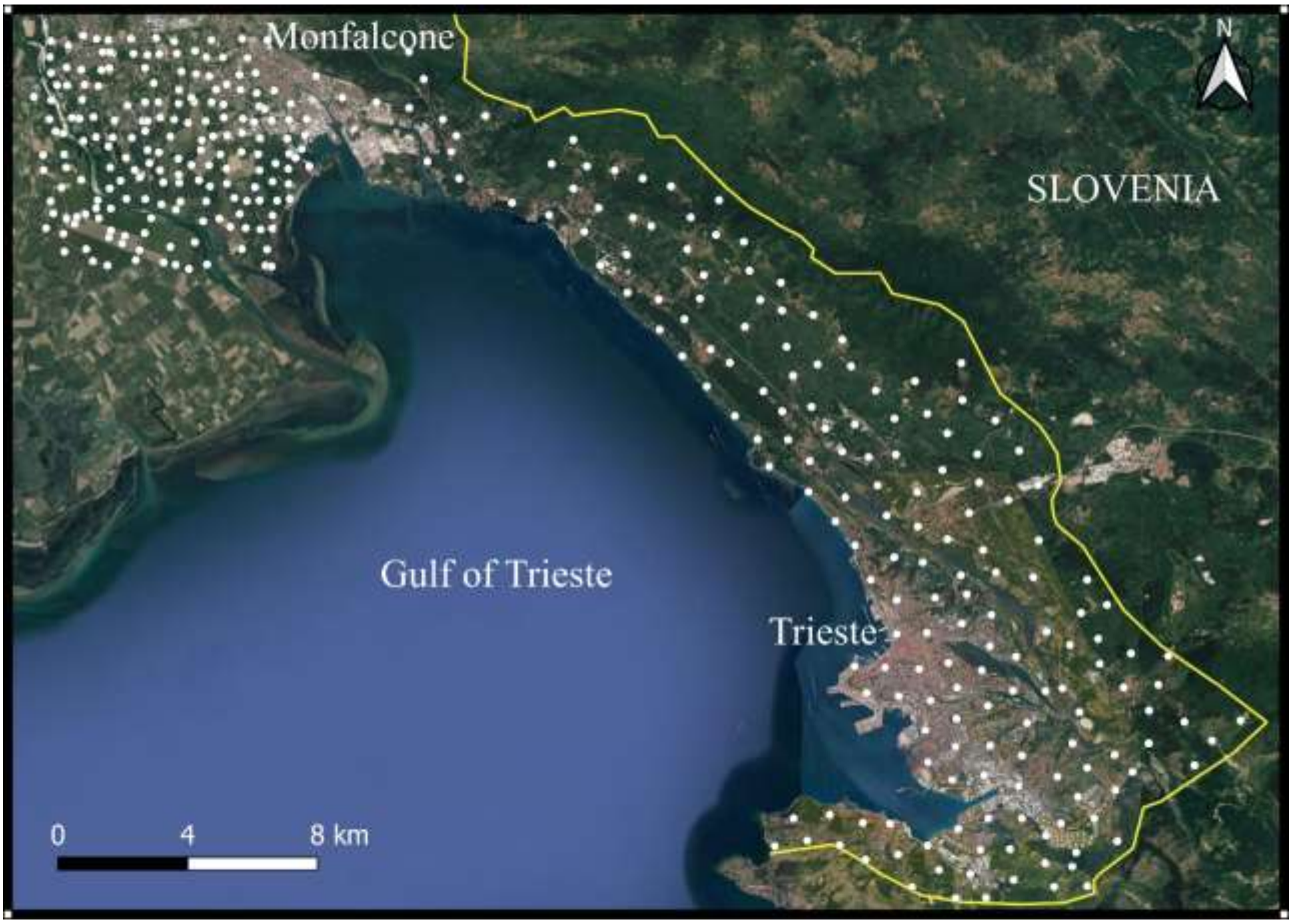

Figure 1-6 - Distribution of the gravity stations TriMon (Prodan, 2002).

1.2.5 TRANSALP - Italian part (TRANSALP_IT)

This dataset comprises around 20000 land gravity stations (in the Italian part), collected in the framework of the international cooperation project TRANSALP, involving Italy, Austria, and Germany (Figure 1-7). The project aimed to increase the data coverage in the south Alpine area and use the newly collected information to model the deep crustal structure of this region (Zanolla, et al., 2006). Most of these gravity stations come from the ENI-E&P Division database and are kindly made available for this project. Most of the stations were recorded before 1980 using western (mod. 4A) and Worden (mod. 654) gravimeters, with nominal accuracies of 0.01 mGal. All the values were tied to the IGSN71 absolute reference system. Instead, coordinates and elevations were deduced from regional topographic maps without specific details on the accuracy. Considering the rough accuracy obtainable from local topographic maps at the scale of 1:10.000, we can assume a maximum error of ±1 m for horizontal coordinates and ±2.5 m for the elevation. However, comparing the stations' coordinates with known locations on topographic maps suggested that previous coordinates transformations may have caused a deterioration in horizontal accuracy of ±25 m.

In addition to the crustal modeling of the TRANSALP project, other interesting findings from the same dataset are described in the previous work of Cati et al. (1987). In this study, the authors used both gravity and aeromagnetic data to define the morphology of the carbonate platform and magnetic basement below the Friulian plain. They identified the margins of the Friulian Platform and the Belluno Basin and some buried segments of the Palmanova line.

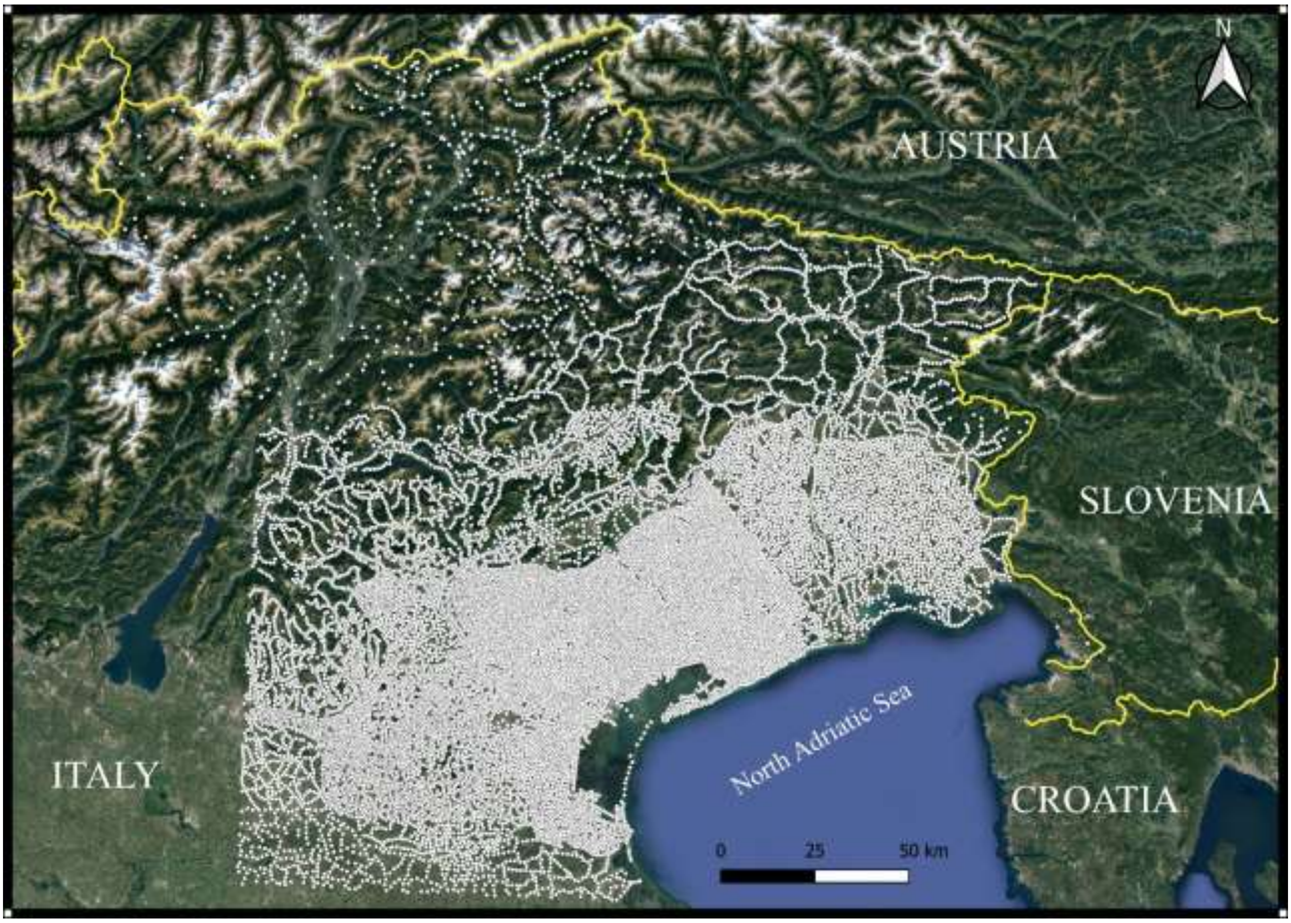

Figure 1-7 - Distribution of the gravity stations TRANSALP_IT (Zanolla, et al., 2006).

1.2.6 Gravity - LTA (Livenza Tagliamento Acque)

In the period 29.09.2020 - 05.11.2020, a detailed gravimetric network was acquired in the area of Fontanafredda - Budoia (PN) to deduce the distribution of densities in the subsoil, i.e., the geometry, thickness, tectonic structure, etc., of the geological elements that characterize it (Busetti, et al., 2021).

The gravimetric survey covers an area of about 90 km^2. The LaCoste & Romberg gravimeter mod. D-018, equipped with a feedback system. A total of 249 stations have been recorded with maximum closure errors on repeated stations of ±0.01 mGal.

The station elevations were derived from the Local topographic maps and high-resolution DTMs with accuracies of ±0.5 m (for more details, see ANNEX 2).

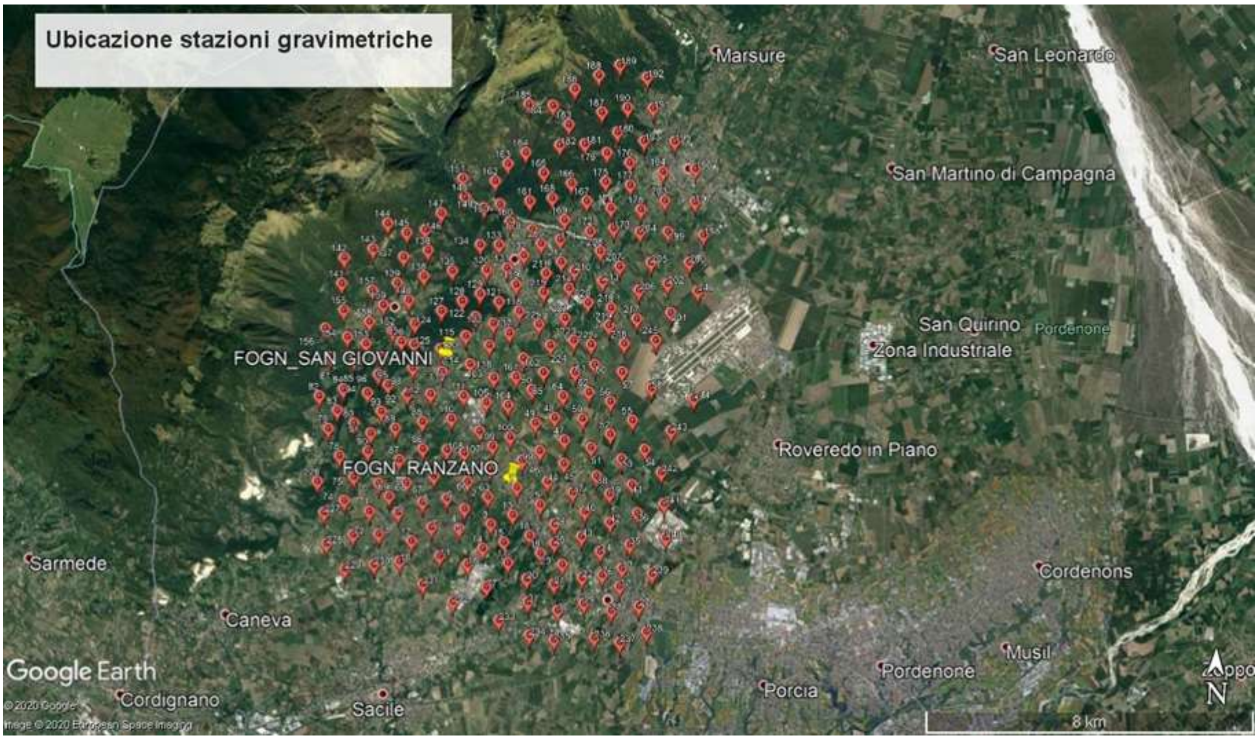

Figure 1-8 - Placement of gravity stations LTA; figure from (Busetti et al., 2021).

1.3 Sea-bottom gravity datasets

Sea-bottom gravity was the first method extensively used by oil companies for marine gravity surveys since 1940 (Nabighian, et al., 2005). Underwater gravimeters are not much different from the inclined zero-length spring meters used on land. The main change is the remote measurement system that allows operating from the vessel while the sensor is lowered down to the seafloor.

In the first models used by OGS, the gravimeter was composed of a metal bell-shaped pressure housing containing a spring-based sensor. Once the instrument was lying at the seafloor, one or more mechanical arms were remotely controlled to level the sensor to the plumb line. Next, the nulling dial was also turned remotely to restore the mass to its null position, and the readings were automatically transmitted back to the vessel via cable (Ciani, Morelli, & Gantar, 1960).

"Underwater gravity measurements have accuracies in the order of 0.01 to 0.3 mGal, depending on sea state, seafloor conditions, and drift rate control" (Nabighian, et al., 2005). In actual practice, the instrument's stability is strongly affected by waves' motion and tidal currents, especially in shallow waters and sandy seabeds. Therefore, most of these gravimeters are further equipped with robust dumping systems, ensuring the readings' stability even in bed conditions while slightly reducing the instrument sensitivity (Carmisciano, et al., 2011).

The instrumental drift usually ranges from 0.15 to 0.2 mGal/day in smooth sea conditions, but it can change from 0.3 to 0.5 mGal/day in rough waters (Ciani, Morelli, & Gantar, 1960).

One of the most significant problems of sea-bottom gravity surveys is the cost-to-time ratio: the average acquisition rate is about 10 to 20 stations per day, depending on the depth and distribution of the stations. Since this rate is highly inferior to the shipborne or airborne gravity systems at the exact cost, sea bottom static measurements nowadays are nearly extinct (Nabighian, et al., 2005).

However, compared to other marine systems, the underwater type has the advantage of being closer to the seafloor, increasing its sensitivity to shallow-depth sources. Moreover, an accurate manual stabilization of the sensor gives higher precision and reliability to the resulting measures, close to the land operating systems. In this perspective, new sea-bottom gravity surveys have been recently deployed to monitor subsidence and fluid movements on offshore reservoirs. This required measuring gravity changes in space and time, using permanent or semi-permanent stations with a µGal precision (Ruiz, et al., 2016).

We present here all the sea bottom data found in the OGS archives during this Ph.D. project (Figure 1-8). Most of these stations were recorded near the Italian coasts, where the position of the vessel was easier to triangulate. Moreover, the proximity of the ports guaranteed fast and frequent connections with land-based stations, thereby avoiding significant instrumental drifts.

The recovered sea bottom dataset contains two primary surveys acquired in different periods, which are briefly described in the following paragraphs.

1.3.1 Sea-bottom OGS60 (1953 - 1960)

This first dataset was acquired during a seven-year research campaign on board different vessels from 1953 to 1960. The acquisition aimed to extend the Italian land-based gravity network offshore and create the first gravity maps of the Italian seas (Ciani, Morelli, & Gantar, 1960). Gravity was measured using western sea-bottom meters. The average accuracy ranges from ±0.05 mGal, near the coast or in short circuits, and up to ±0.3 mGal in rough waters or in very long circuits. Stations depth was measured using echo-sounders (Atlas-Werke) and planar coordinates using optical and/or radar devices pointing to coastal marks or reflective buoys. The coordinates precision decreases with increasing distance from the coast: from a minimum of ±50 m inshore to a maximum of ±200 m at 120 km offshore, or even ±600 m when reflective buoys were not available. Furthermore, the stations are not equally spaced:

the relative distances increase offshore, from a minimum of ~1.6 km to a maximum of ~10 km at 60—70 km from the coast.

1.3.2 Sea-bottom OGS83 (1982-1983)

This second dataset was collected in 1982 as part of a 98-day marine gravity survey to create high-resolution gravity maps of the Adriatic coast from Ancona to Ortona (the "northern Zone") and from Manfredonia to Brindisi (the "sorthern Zone"), and commissioned by the Agip Mineraria company (Gantar, 1983). Gravity values were recorded using the LaCoste and &Romberg sea-bottom meter (mod. 19 G), which, like the western, has a nominal accuracy of 0.05 mGal (Gantar, 1983). Station depths were measured by both echo-sounders (Honeywell ELAC, mod. LA2721A) and pressure meters, giving a final combined accuracy of ±0.5 m. Planar coordinates were calculated through radar trilateration from the coast, using the Motorola System, with a nominal precision of 3m±0.01*distance[km]. The stations are distributed on nearly regular grids up to ~10 km from the coast, with a sampling rate of ~1 km (Figure 1-8).

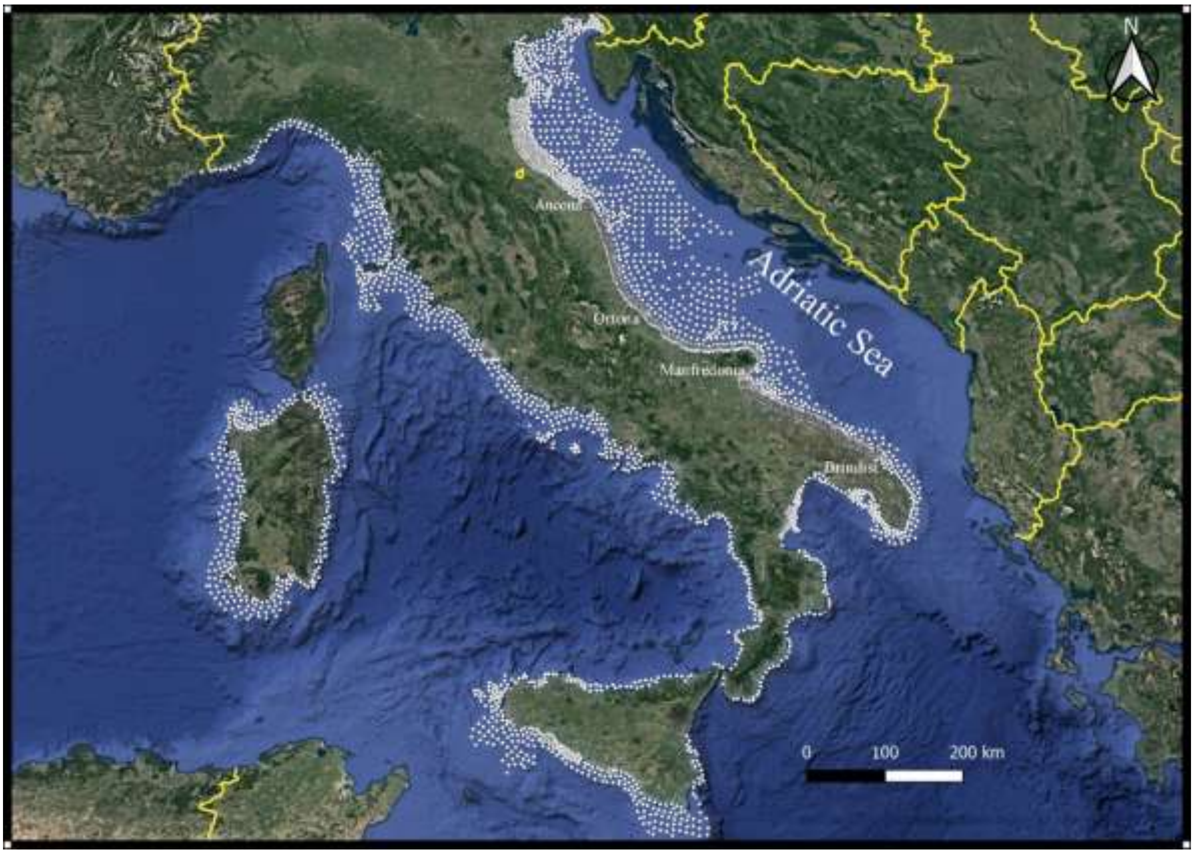

Figure 1-8 Distribution of sea-bottom gravity stations around the Italian coasts (Ciani, Morelli, & Gantar, 1960; Gantar C. , 1983).

1.4 Shipborne gravity and magnetic datasets

Shipborne gravity explorations started approximately in 1950 by oceanographic research institutes and since 1965 by oil companies, after the first successful test of a stabilized-platform L&R instrument (Morelli, 1966; LaFehr & Nettleton, 1967; Nabighian, et al., 2005). These systems have the great advantage of recording many data points along lines together with other measurements (e.g., magnetic or seismic), significantly reducing the time/cost ratio of the field operations compared to the static systems.

However, they also introduced new challenging problems to solve during acquisition and processing. The main difficulty consists of separating the platform acceleration from the static components of the terrestrial gravity field (Morelli, 1966; Fairhead, 2016, p. 63-70). The gyro-stabilized systems minimize the horizontal accelerations, leaving only the problem of the vertical non-gravitational components. These components combine the effects of the vessel and wave motions.

The noise caused by waves can be safely removed using analog or digital filters since it has higher amplitudes and shorter wavelengths than any geological signal.

On the other hand, the vessel motion generates signals easily confused with geological effects. The Eötvös correction can reduce the along-track vessel motion effects when accurately measuring vessel speed (Fairhead, 2016, p. 63-64).

However, other vessel movements may still induce shifts or tiltings of the gravimeter beam to its stable position, despite the gyro-stabilization (e.g., pitch and roll). This additional noise, also known as cross-coupling error, is eventually dimmable using specific algorithms based on the cross-correlation between the gravity signal and the platform motion (Lacoste, 1973).

Nevertheless, non-predicted waves and vessel accelerations may still cause severe signal deterioration, especially in rough waters.

Because of all the above, regardless of the instruments' precision and processing accuracy, discrepancies between survey lines and, more generally, between repeated data points are inevitable. Other additional factors may also contribute to the problem, e.g., non-compensated drifts and local tidal effects. This residual noise is most notable when computing the field derivatives, causing problems for data interpretation.

Leveling algorithms have been developed to limit the problem by averaging the differences at line crossings, and eventually, micro-leveling operations can smoothly remove remaining biases in specific directions. However, this type of processing may also cause the loss of high-frequency signals, reducing data sensitivity.

During our study, together with gravity, we collected and re-processed also shipborne magnetic data.

Even magnetic data suffers from leveling-related problems similar to gravity. However, in this case, the differences between repeated measurements are usually more significant than with gravity. One reason is that the amplitudes of short-wavelength magnetic anomalies have generally broader ranges (±100 nT) compared to gravity (±10 mGal). Moreover, the causes of the errors are different: magnetic data are usually biased by residual diurnal effects or non-compensated artificial noises due to the proximity with unpredicted metallic objects, e.g., other vessels or fishnets.

We used three different shipborne gravity and one magnetic dataset, which are briefly described in the following paragraphs.

1.4.1 The OGS Mediterranean survey (GravOGSMed)

The western and Central Mediterranean, from Gibraltar to approximately the 26°20' E meridian, were surveyed by the OGS institute between 1961 and 1972, with the financial support of the Consiglio Nazionale delle Ricerche (CNR). The cruise took place at two different times (Figure 1-9).

First, from 1961 to 1965, the eastern part of the western Mediterranean was covered by the Saclantcent Research Vessels Aragonese and Maria Paolina.

Second, from 1964 to 1972, the Central and eastern Mediterranean were covered by the CNR Research Vessels Bannock (Morelli, 1966; Morelli, Pisani, & Gantar, 1975).

Gravity was measured using the Graf-Askania (mod. n°13) and Gss-2 (mod. n°11) gravimeters mounted on Auschütz gyro-stabilized platforms. A radar system (Loran C) tracked the vessel's position with an average accuracy ranging from ±200 m to ±600 m. The data were corrected by Eötvös, i.e., subtracting the contribution of the vessel speed. In this first marine acquisition, the time interval required to estimate gravity with an accuracy of at least 0.5 mGal was about 15-25 min (Morelli, 1995; Makris, Morelli, & Zanolla, 1998). This, in addition to the scarce positioning precision, limited the final along-track sampling to an average of 1 point / 1.5 km.

The tidal corrections, which range between ±0.5 mGal, have been neglected since they were considered irrelevant compared to the error estimated for the anomalies at line crossings, i.e., from ±3 to ±7 mGal (Figure 1-10a).

Magnetic data have been recorded on the same tracks as gravity using a towed proton magnetometer, with a sensitivity of ±0.5 nT. However, the subsequent corrections applied to the raw magnetic data may have introduced errors much more significant than those reported by the authors of ±10 nT (Zanolla, Morelli & Marson, 1998). In particular, the diurnal corrections were based all on the Magnetic Observatory at l'Aquila (Italy), which was not necessarily accurate for measurements on the other side of the Mediterranean (Figure 1-10b).

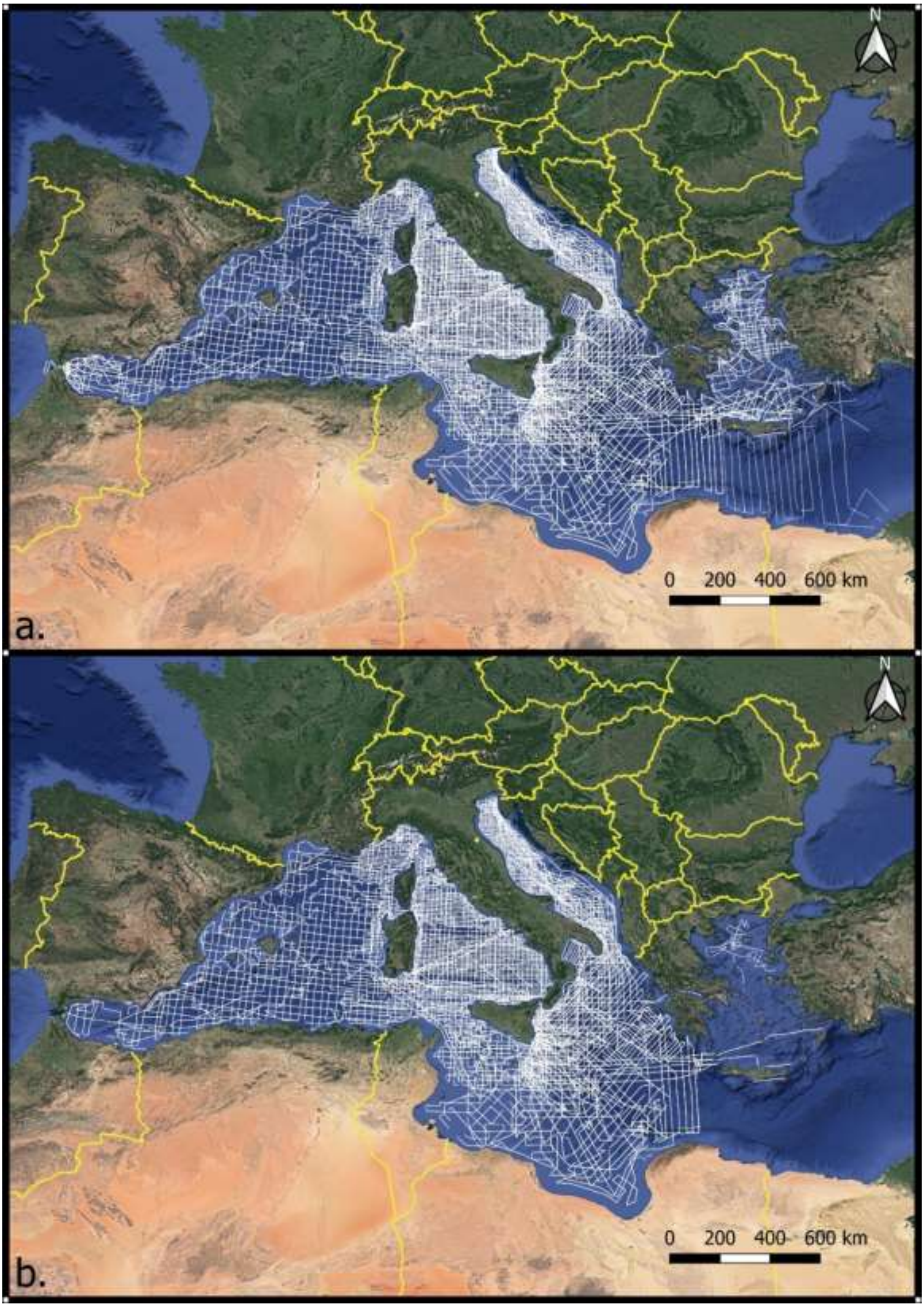

Figure 1-9 - Distribution of shipborne (a) gravity and (b) magnetic stations (GravOGSMed, MagOGSMed), acquired by the OGS between 1961 and 1972 (Makris, Morelli, & Zanolla, 1998; Zanolla, Morelli, & Marson, 1998).

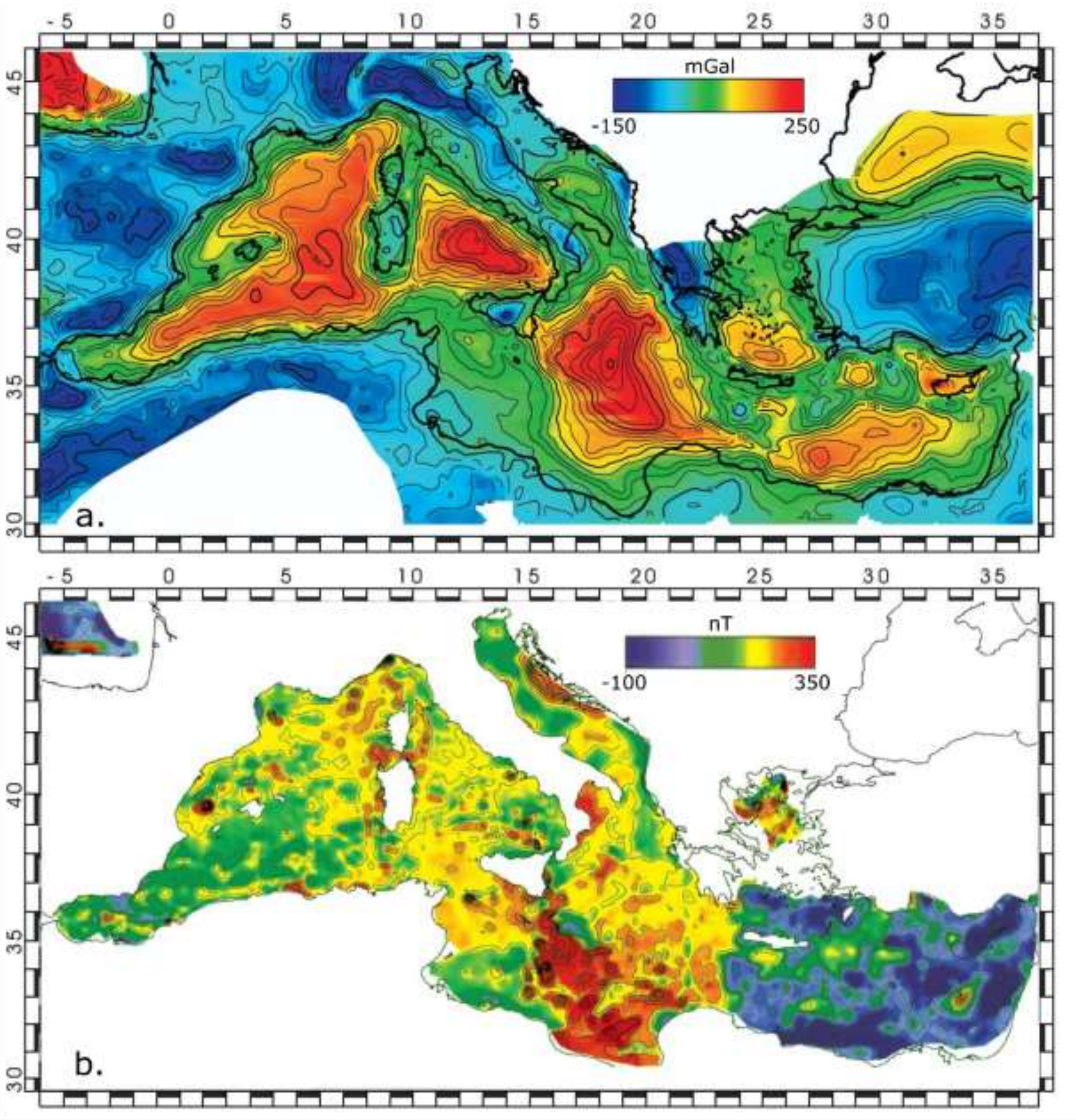

Figure 1-10 Maps of (a) Bouguer gravity and (b) magnetic anomalies in the Mediterranean sea, taken from Makris, Morelli, & Zanolla (1998), and Zanolla, Morelli, & Marson (1998), slightly modified. The anomalies were calculated with the data from GravOGSMed and MagOGSMed (Table 1) and other additional data to cover the eastern Mediterranean.

1.4.2 The RIG northern Adriatic Survey (1982)

This dataset refers to a shipborne survey made by the RIG company of Milano and subsequently integrated within the TRANSALP data (Cati, Fichera, & Cappelli, 1987; Zanolla, et al., 2006). The shipborne data were recorded with along-track sampling rates of ~1 station every 55-70 m, then resampled at every 550-700 m, with a total number of 45 survey lines. The survey was structured in a regular network of lines separated by distances ranging between 3 and 4 km. The dataset covers an area of about 3274 km2 in the western part of the northern Adriatic Sea, ~10 km far from the coast of the Veneto region (Figure 1-11). Unfortunately, not much information was available about the instruments used during the acquisition, coordinates precision, bathymetric depths, or gravity data accuracy. We then considered the same error estimated for land data in the TRANSALP dataset, i.e., ±25 m. Differences in the observed gravity at line crossings range between ±3.5 mGal.

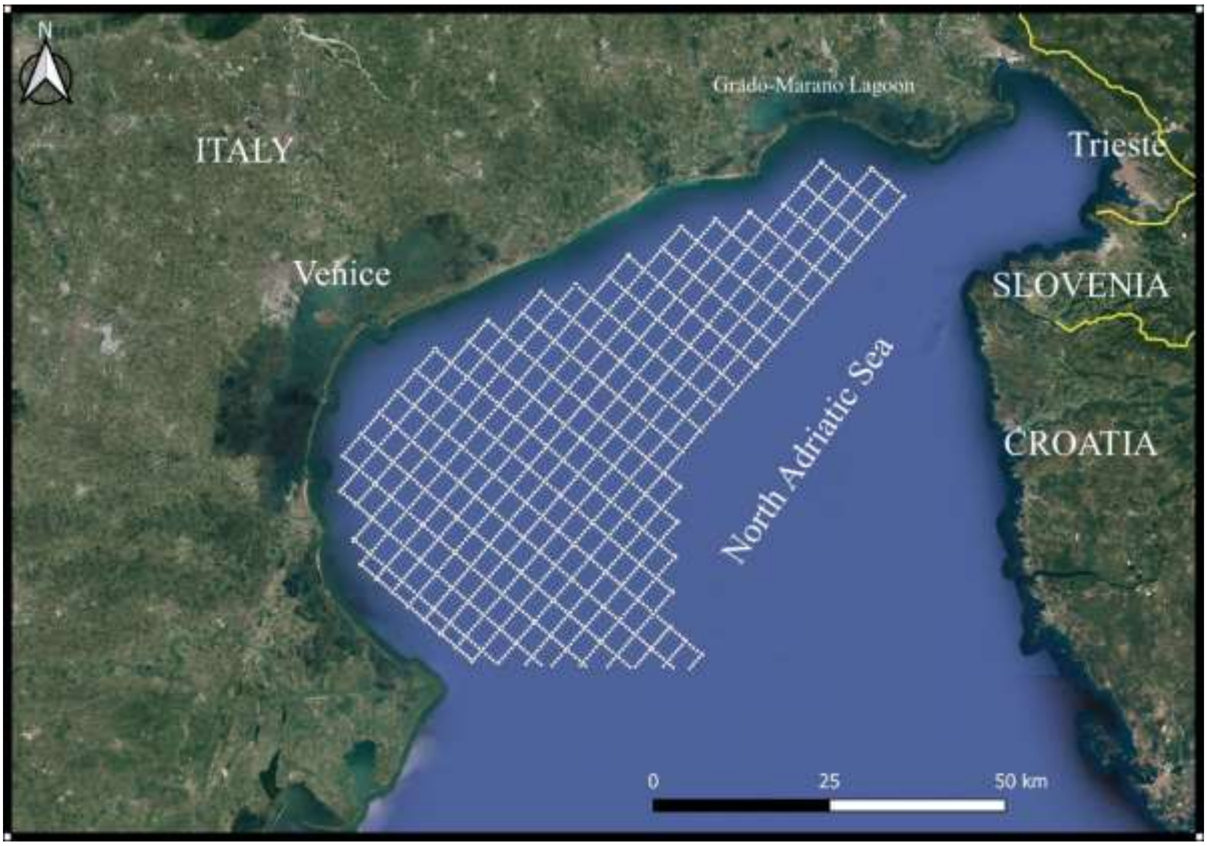

Figure 1-11 - Distribution of sea-bottom gravity stations RIG82 (Cati, Fichera, & Cappelli, 1987; Zanolla, et al., 2006).

1.4.3 The OGS northern Adriatic Survey (OGS_NA05)

The OGS recorded this dataset in 2005. The gravity values were measured with a Bodenseewerk gravimeter (mod. KSS 31) onboard the OGS Research Vessel OGS Explora (Figure 1-12). The survey lines cover the northern Adriatic Sea from the East to the West with a total number of 23 lines (Busetti, et al., 2005). The dataset was re-sampled with an average rate of about 1 point every 200 m. Even in this case, no information was found about the bathymetric depths or data accuracy.

Coordinates were measured with a DGPS receiver with errors up to ±3 m. Differences in the observed gravity at line crossings are about ±0.66 mGal.

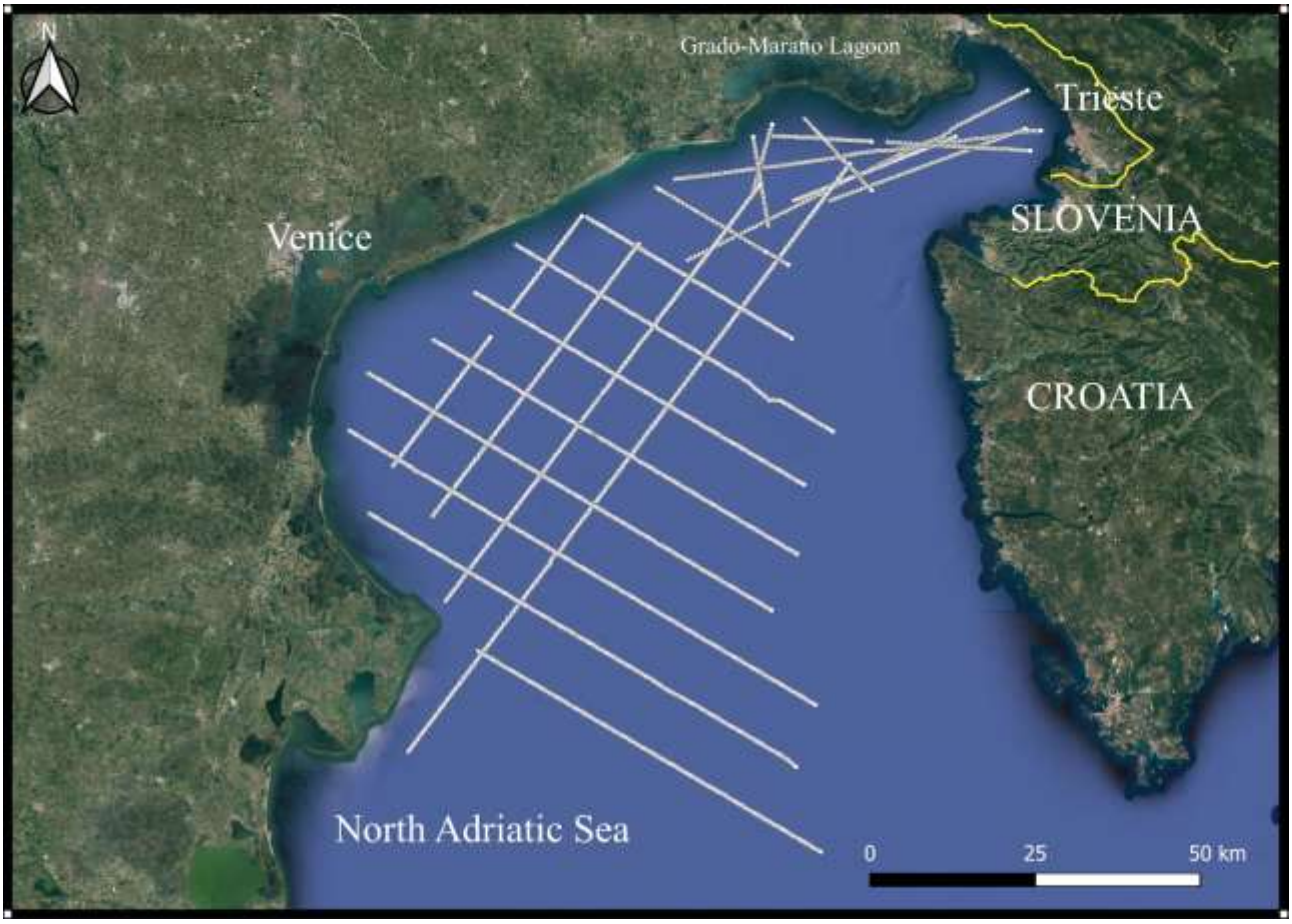

Figure 1-12 Distribution of sea-bottom gravity stations OGS_NA05 (modified after Busetti, et al., 2005).

Table 1 - Re-processed gravity and magnetic datasets with the indication of (i) station type, (ii) identification name, (iii) horizontal accuracy, (iv) vertical accuracy, (v) gravity error, and (vi) references.

Type	ID	n° of stations	ΔXY [m]	ΔZ [m]	Δg [mGal] Δm [nT]	Reference
land (grav)	Zaule	23	25	0.01	0.03	(Morelli , 1950)
land (grav)	ItaNO	180	~100	5	0.5	(Morelli, 1951)
land (grav)	GravVenCO	170	~100	5	0.04	(Morelli, 1954)
land (grav)	TriMon	370	~10	2.5	0.01	(Prodan, 2002)
land (grav)	TRANSALP_IT	20000	25	2.5	0.01	(Zanolla, et al., 2006)
sea-bottom (grav)	OGS60	3135	600 (max)	0.3	0.5	(Ciani, Morelli, & Gantar, 1960)
sea-bottom (grav)	OGS83	2144	3	0.5	0.05	(Gantar C. , 1983)
shipborne (grav)	GravOGSMed	122422	600 (max)	-	7	(Makris, Morelli, & Zanolla, 1998)
shipborne (grav)	RIG82	2632	25	-	3.5	(Cati, Fichera, & Cappelli, 1987; Zanolla, et al., 2006)
shipborne (grav)	OGS_NA05	4240	3	-	0.66	(Busetti, et al., 2005)
land (mag)	MagVenCO	160	25	0.1	3.7	(Morelli C. , 1954)
shipborne (mag)	MagOGSMed	101402	600 (max)	-	10?	(Makris, Morelli, & Zanolla, 1998)

1.5 Absolute gravity reference systems

The analyzed gravity data are all relative measurements: they record differences in the gravitational acceleration from one place to another.

To obtain the absolute gravity, the relative values must be tied to one or more reference stations where the absolute value is known by means of non-relative measurements.

Hence the need for a gravity reference system, i.e., a vast network of stations where the absolute gravity value has been measured with a standard precision over time.

The first global reference system was The Potsdam Gravity System, established by the International Association of Geodesy in 1909. It was structured as a Eurocentric network of relative and absolute stations, tied to the measured value in Potsdam.

Before 1950, absolute gravity was measured by pendulums, which derive gravity from the oscillation periods of a freely swinging mass attached to a fixed support.

Even though the pendulum was enclosed in an evacuated thermostatically controlled chamber, the exact repeatability was not ensured, especially when the instrument was assembled in a different location: it was virtually impossible to determine the exact period of the swings and keep the pendulum length constant over time. Hence, the highest accuracies obtainable with this method in a controlled and stable condition was about ±2 mGal. Furthermore, other unexpected random and systematic errors could easily increase this error by a few mGal (Lowrie, 2007, p. 74-76; Torge & Müller, 2012, p. 176).

In Italy, the first base of the national gravity network was set in 1951 (Figure 1-13), with the reference station in Padua, directly connected to Potsdam (Morelli, 1995; Berrino, 2020). The first Fundamental Gravimetric Network in Italy (RFI 55) was created between 1953 and 1955 with three relative gravimeters (western, North American, Worden). It consists of 119 stations, with the central reference station in Rome (i.e., Roma Ingegneria) tied to the Potsdam System (Cunietti & Inghilleri, 1955; Morelli, 1995).

However, in 1930 a combination of absolute and relative measurements revealed that the Potsdam reference value was wrong by 14.0 mGal, and the same error was repeatedly transferred to the other stations with uncertainties of ± 2.0 mGal (Woollard, 1979).

The Potsdam Gravity System was then changed with the IGSN71, correcting the previous biases with new absolute and relative records. In addition, the network was extended to other locations in America, Europe, and Africa, obtaining a worldwide standardized system with uncertainties of less than ±0.1 mGal (Morelli, Gantar, McConnell, Szabo, & Uotila, 1972).

After 1950, free-fall gravimeters were introduced as a reliable method for absolute gravity measurements, substituting the old bulky pendulums. These instruments record the symmetrical free-fall of a mass within an evacuated chamber using Michelson interferometers. The gravity value, in this case, is derived from the quadratic time-space equation of the free-falling object. These new instruments opened the possibility of improving the IGSN71 accuracy from ±0.1 to ±0.01 mGal.

Given the availability of more accurate absolute and relative gravimeters, a new Italian first-order gravity network, the FOGN77, was created in 1977 (Marson & Morelli, 1978). It covers the whole country, including the RFI55 and IGSN71 stations, with 49 base stations (5 absolute) and 758 connections made with five LaCoste&Romberg meters (four mod. G, and one mod. D). The final standard error after the compensation of the network is confined to the interval [0.006, 0.022] mGal.

Lastly, new atom gravimeters have been developed for absolute measurements. In this case, the instrument records the free-fall acceleration of a cold atom using an atom-interferometer. These new systems can easily reach precisions of a few µGal, and the transportation is relatively more accessible than the previous free-fall meters (dos Santos & Bonvalot, 2016).

Therefore, it has been argued that with the increasing availability of new transportable absolute gravimeters, the gravity standard can be established independently from a global system. Consequently, the IGNS71 should not need further readjustments, but rather a continuous improvement by means of other local networks based on absolute gravimetry (Torge & Müller, 2012, p. 190).

Nevertheless, the maintenance of a global system, supported by regular monitoring, network adjustments, and the supervision of an international committee of geodesists, can guarantee a high level of homogeneity to all the tide gravity surveys, in time and also worldwide (even in the remote areas). Moreover, it may avoid the error propagation caused by unpredicted biases between independent-absolute stations, as were recorded during the compensation of the FOGN77 (Morelli, 1995). Therefore, an update of the present reference Italian gravity network and a plan for its maintenance is fundamental for improving the quality and homogeneity of all the past and present gravity surveys (Berrino, 2020).

In this regard, all the datasets collected for this project were tied to different absolute reference systems, e.g., different upgrades of the RFI before and after the standardization to the IGSN71, or even to different absolute measurements made by independent institutions.

We decided to reduce them all to the standard of the IGSN71, considering the new reference value of the fundamental station of "Roma Ingegneria" as a benchmark (Figure 1-13). However, since not much information was available on the accuracy of the original references, unpredicted systematic errors may still affect some of the data points, even after this correction.

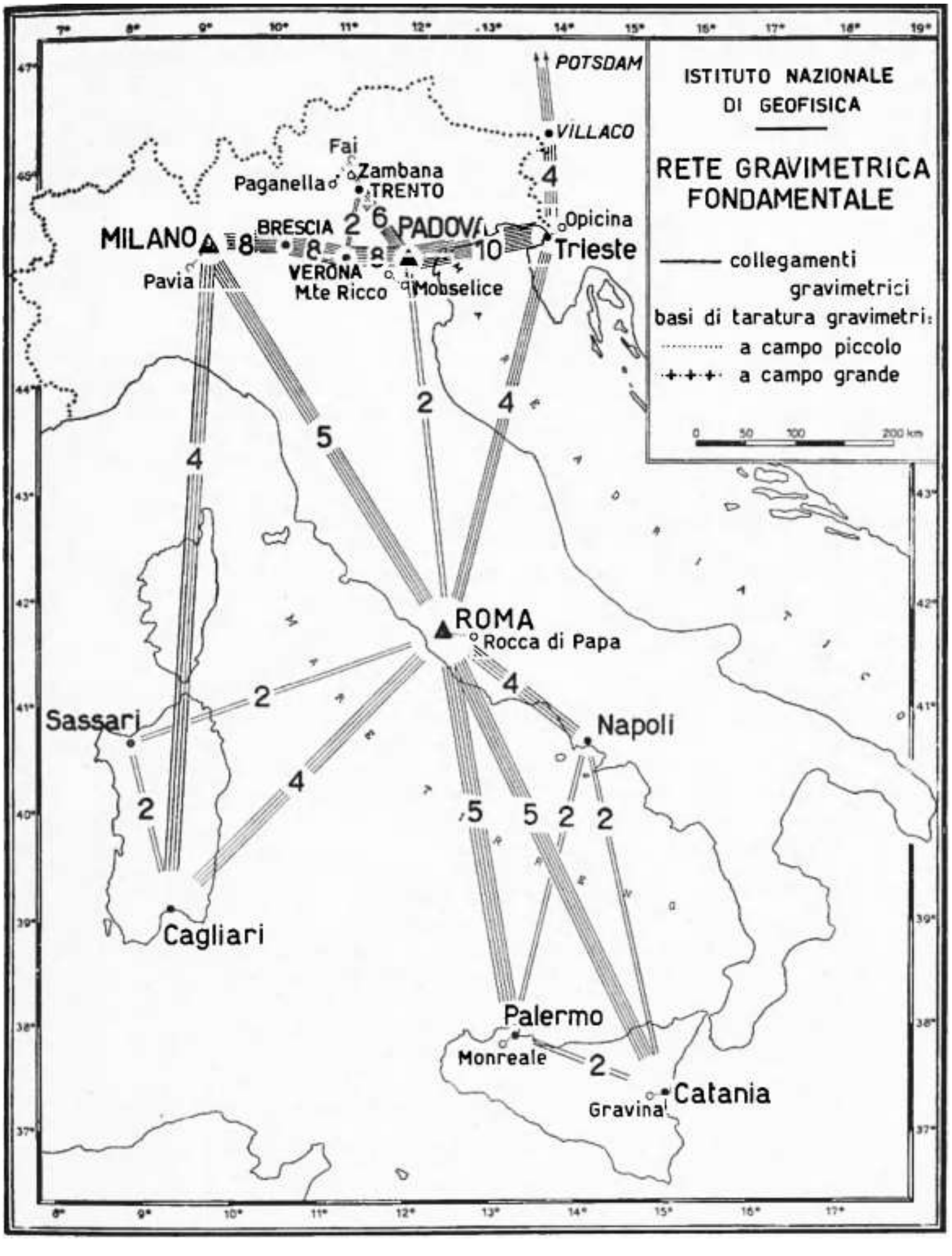

Figure 1-13 Gravity stations and relative connections for a preliminary contribution to the first Italian gravity reference network (Morelli, 1952).

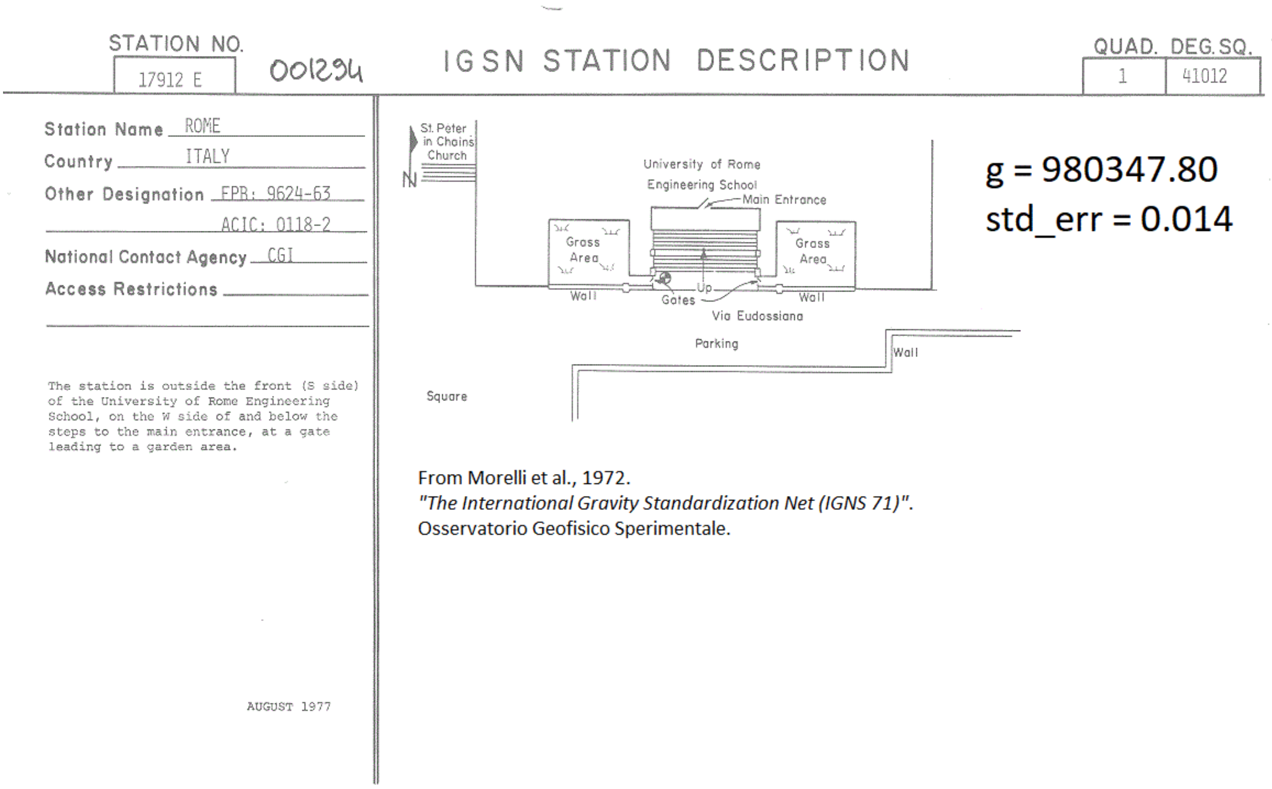

STATION NO. 17912 E 001294

IGSN STATION DESCRIPTION

QUAD. 1 DEG. SQ. 41012

Station Name ROME

Country ITALY

Other Designation FPR: 9624-63

ACIC: 0118-2

National Contact Agency CGI

Access Restrictions

The station is outside the front (S side) of the University of Rome Engineering School, on the W side of and below the steps to the main entrance, at a gate leading to a garden area.

AUGUST 1977

g = 980347.80
std_err = 0.014

From Morelli et al., 1972.
"The International Gravity Standardization Net (IGNS 71)".
Osservatorio Geofisico Sperimentale.

Figure 1-14 Fundamental gravity station of "Roma Ingegneria" framed within the IGSN71 (image downloaded from the International Gravimetric Bureau (BGI) web database, http://bgi.obs-mip.fr/).

1.6 New satellite-based gravity and magnetic models

After 1950, the enormously founded "space race" competition between the United States and the Soviet Union introduced the possibility for measuring gravity from satellites.

It started with the radio tracking of the orbital perturbation of the Sputnik spacecraft, followed by many other missions, which continuously improved the global imaging of the terrestrial gravity field (Rummel, 2020).

As the years passed, also space-based gravity methods changed, becoming more and more sophisticated and accurate. Today, we have two main leading solutions to derive the gravity field from satellites.

The first solution is a dynamic combination of gravity measurements at the satellite height, based on tracking, ranging, and gradiometer systems. The most relevant satellite gravity missions of the last decades, CHAMP, GRACE, and GOCE, are each based on one of the mentioned measurement systems (Pail, 2014). Moreover, the satellite-only models and the derived gravity anomalies are generally computed globally, using spherical harmonic functions (Barthelmes, 2009). The last publicly released geopotential models, based on GOCE data, go to harmonic 330, i.e., full-wavelengths resolution of ~120 km (Gatti, Reguzzoni, Migliaccio, & Sansò, 2016; Ince, et al., 2019).

The second solution is based on the static mapping of the mean sea level using satellite radar altimetry. The derived gravity field can integrate data from many different radar missions succeeded over the years, e.g., SeaSat (1968), GeoSat (1996), CrySat-2 (2011), Jason (2012) HY-2A (2013). This solution allows a complete mapping of the marine gravity field with a full-wavelength resolution of 15 ±3 km and accuracies in the range of ±5 mGal (Andersen, Knudsen, & Am Berry, 2010).

The satellite-only Global Geopotential Models (GGMs) have been integrated with land shipborne, airborne, and altimeter-derived data, generally using least-squares procedures. The combined models increased the resolution of the satellite-only models up to harmonic 2190 or wavelengths of ~18 km (Ince, et al., 2019; Barthelmes, 2009). However, these combined models are degraded by errors propagated during the data processing (commission errors), and they also introduce significant uncertainties in areas not homogeneously covered by non-satellite gravity data (omission errors). These problems inevitably introduce site-dependent errors, which, in some cases, can be higher than ±20 mGal, for wavelengths < 50 km (Torge & Müller, 2012, p. 275-282; Bomfim, Braitenberg, & Molina, 2013).

Since 1965, space missions were also dedicated to recording the Earth's magnetic field: (POGO, Mgsat, Ørsted, CHAMP, SAC-C, and SWARM missions).

Of particular relevance are the CHAMP and SWARM satellite missions. The first, managed by the GeoForschungsZentrum (GFZ), used Fluxgtae and Overhauser magnetometers mounted on the spacecraft, recording the geomagnetic field with accuracies of about 0.1 nT and maximum spatial resolutions of ~300 km (Holme, Olsen, Rother, & Lühr, 2003). The second, managed by the European Space Agency (ESA), is composed of three satellites, orbiting at two different heights (two at 462 km and one at 511 km). Each of the three satellites is equipped with an Absolute Scalar Magnetometer (ASM) and a Vector Field Magnetometer (VFM). This architecture was designed to obtain a high level of accuracy and stability of the magnetic field measurements over time and a better separation between the various field components, i.e., the one generated by sources internal to the Earth (i.e., core, lithosphere, mantle, and oceanic currents), and those generated by external sources in the magnetosphere and ionosphere (Friis-Christensen, Lühr, & Hulot, 2006).

Even in the case of the magnetic field, the derived global models have been integrated with land shipborne, airborne measurements to increase the resolution down to less than 10 km (Fairhead, 2016).

In our work, we used both satellite altimeter-derived gravity and Combined Global geopotential models (CGGMs) for data processing and analysis. The specifics of these datasets are briefly described in the following paragraphs.

1.6.1 Satellite altimeter derived gravity models

Satellite altimeter-derived gravity comes from Sea Surface Heights measurements (SSH). These measurements are based on microwave pulses emitted from satellites orbiting at ~800 km and reflected backward by a portion of the sea surface (footprint).

The product between the travel time and the propagation speed allows the derivation of the distance between SSH, and the reference ellipsoid, with a centimetric precision. Averaging the SSH over long-time intervals (at least one year) removes the time-depending components and gives the resulting Mean Sea Surface (MSS). After correcting the MSS for residual orbital errors and removing the Mean Dynamic Topography MDT (a quasi-stationary component of SSH), the result is a static realization of the marine geoid.

The equation that links the Geoid undulation, $N\ \lambda,\varphi$, to the Free-air gravity anomaly, $Fa\ \lambda,\varphi$. Is known as the *fundamental equation of physical geodesy.* It can be derived from the Bruns formula (eq. 1.1) into the following form (eq. 1.2), by assuming a spherical Earth approximation (Hofmann-Wellenhof & Moritz, 2006, p. 94-97; Andersen, Knudsen, & Am Berry, 2010):

$$T\ \lambda,\varphi \quad = \quad N\ \lambda,\varphi\ \ g_{th} \tag{1.1}$$

$$Fa\ \lambda,\varphi\ = -\frac{\partial T\ \lambda,\varphi}{\partial r} - \frac{2g_{th}}{R} N\ \lambda,\varphi$$

$$= -\ g_{th}\ \frac{\partial N\ \lambda,\varphi}{\partial r} - \frac{2}{R}\ N\ \lambda,\varphi\ \ g_{th} \tag{1.3}$$

where, $T\ \lambda, \varphi, r$ is the disturbing potential, g_{th} is the theoretical (or normal) gravity, R is the mean Earth radius, and λ, φ, r, are the geocentric spherical coordinates of the computational point.

In this equation, the only unknown term is the radial gradient $\frac{\partial N}{\partial r}$, since both N and g_{th} are known from input data and mathematical theory.

Until now, two leading solutions have been used to compute the radial gradient of the geoid from altimetric data: (1) the "geoid-to-gravity method" and (2) the "slope-to-gravity method" (Fairhead, 2016, p. 82-83).

Our study used two altimeter-derived gravity datasets, the S&S and the DTU13, each obtained with one of the mentioned methods.

1.6.2 DTU13

The DTU13 dataset was derived with the "geoid-to-gravity" method, developed by the Technical University of Denmark (Andersen O. B., Knudsen, Kenyon, & Holmes, 2014). In this approach, the vertical derivative is computed starting from 2-D regular grids of the geoid. The geoid grids result from spatial interpolation of radar data, crossover adjusted, and corrected for time-variable and stationary components of the SSH, i.e., all those signals not directly related to the gravity field of the solid-Earth (Andersen, Knudsen, & Am Berry, 2010).

The derivative is calculated using the Fast Fourier Transform (FFT) after removing the effect of the EGM2008 spherical harmonic model to degree 2160 (Pavlis, Holmes, Kenyon, & Factor, 2012), i.e., wavelengths ≤20 km (Barthelmes, 2009). Then, the previously removed harmonic components are added back to the final result (remove-restore method).

The resulting grid of the free-air anomaly is available with a sampling rate of 1 arcmin (Figure 1-15a). However, the maximum resolution is limited by the along-track sampling rate, around 1/7 km^{-1}, and the systematic use of a Wiener lowpass filter with cut-off wavelengths ranging between 5 and 16 km (Andersen & Knudsen, 1998; Andersen, Knudsen, & Am Berry, 2010). As a result, the shortest reliable wavelength hovered around ~13 km (Andersen O. B., Knudsen, Kenyon, Factor, & Holmes, 2013; Fairhead, 2016).

The DTU13 is associated with an interpolation error file, showing uncertainties on the Mean Sea Surface grids (MSSerr), which is defined in units of meters. This error shows the quality of gridded data points, and it roughly indicates the transition between land and marine areas (Andersen O. B., et al., 2008). However, it may underestimate the uncertainties of the MSS grid since it just accounts for interpolation errors, not actual orbit errors, nor other types of errors in various ranges (Andersen & Knudsen, 2009).

The relation between geoid and gravity gives approximately ~1 mGal amplitude for a sea surface slope of 7 mm/7 km (Sandwell, et al., 2013), i.e., 1.4 mGal/cm when considering horizontal distances of 7 km. This simple equivalence can be used as a rule of thumb to convert the MSSerr grid values into mGal. The result is a qualitative indicator of the least expected gravity error in the study area, which, however, does not include the actual error of the EGM2008 model.

1.6.3 S&S

The S&S dataset was derived using the "slope-to-gravity method" based on the same remove-restore principle of the DTU13. However, in this case, the derivatives are directly computed from along-track lines instead of 2-D grids. The resulting slopes are interpolated and convoluted to obtain the 2D grids of W-E, S-N horizontal gravity derivatives. The derivatives are finally combined using the Laplace equation to get the vertical gravity component (Sandwell D. T., 1992; Fairhead, 2016).

The S&S Free-air anomaly dataset is available as a 2D grid with a 1 arcmin sampling rate (Figure 1-15b). An error file is associated with the gravity grid, defining the uncertainties of the model (Figure 1-15d). In this case, the error refers directly to the gravity anomaly, i.e., it is given in mGal units, and it shows the RMS difference between (i) the slope of individual altimeter profiles and (ii) the averaged grid product of W-E and S-N slope (Sandwell & Smith, 2009; Sandwell, Müller, Smith, Garcia, & Francis, 2014).

Thanks to the direct computation of the gradients from the original tracks, the S&S model may preserve high frequencies better than the DTU13 (Figure 1-15c). However, it also amplifies more the residual noises, i.e., non-modeled disturbing components (waves, tides, currents) or blurring scattered spikes, especially in coastal regions.

1.6.4 Costal noise in satellite altimetry data

Errors of satellite altimeter data generally increase close to the coast, where the radar footprint covers part of the land together with the sea (Dawson, Green, & Fletcher, 2015). Reflections from onshore areas generate significant noise obscuring the signal reflected by the sea surface (Figure 1-15d). The exact distance from where these contaminations may occur is not easy to estimate since it depends on a complicated combination of different factors, such as the angle between orbital tracks and shorelines, topographic gradients, local bathymetry, and local tides. In addition to that, a shallow bathymetry may cause reflation from the sea bottom interpreted as from the sea surface. These factors make coastal noise mainly a site-dependent problem. Moreover, the derivation of the gravity field from the geoid undulation required the presence of data all around the computation point, a condition that is, of course, violated near the coast.

Although this noise has been consistently reduced in the last decades, using Interferometric Synthetic Aperture Radar (e.g., CryoSat2 mission), more accurate global gravity models and more sophisticated tracking techniques, signal accuracy up to 7-14 km from the coast may still be compromised (Deng & Featherstone, 2006; Andersen & Knudsen, 2009; Dawson, Green, & Fletcher, 2015).

For these reasons, interpretations of altimeter-derived gravity in coastal regions must be carefully evaluated and preferably integrated with shipborne/airborne gravity measurements or other types of geophysical data.

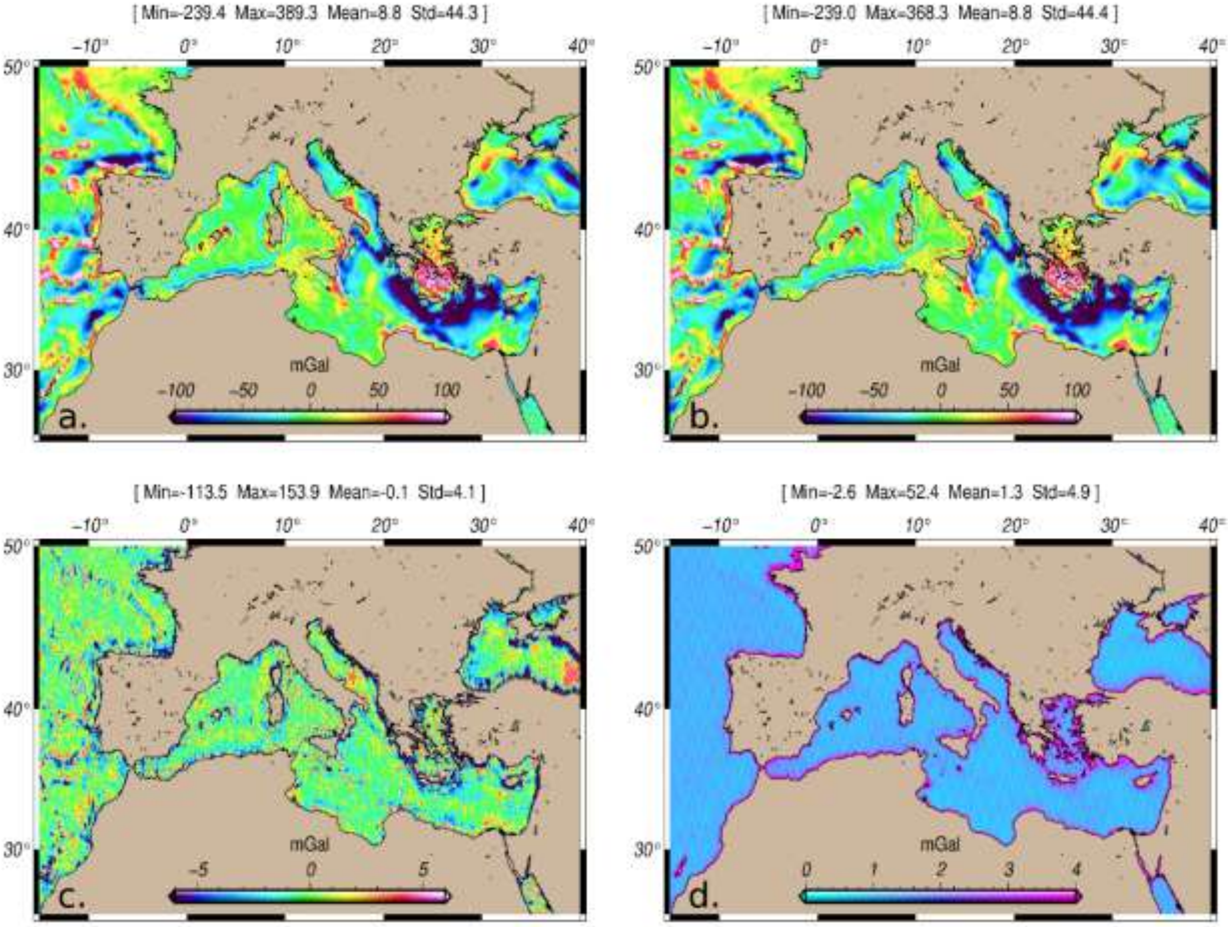

Figure 1-15 Satellite altimeter derived gravity in the Mediterranean sea from (a) DTU13 model, (b) S&S model, and (c) differences between the two. The lower left map (d) shows the error grid associated with the S&S model, in which the highest values occur near the shorelines (coastal noise), in addition to other minor errors in between orbital tracks (e.g., interpolation errors).

1.6.5 EGM08

The EGM08 is a public domain geopotential model, compiled using spherical harmonic functions to degree 2190 and order 2159. The resulting grid has a maximum resolution of 5 arcmins (~10 km) and integrates satellite-only, altimeter-derived, and terrestrial gravity data (Pavlis, Holmes, Kenyon, & Factor, 2012). The satellite component comes from the GRACE mission down to wavelengths of ~270 km, whether the shortest wavelengths on marine areas are essentially based on altimeter-derived gravity, e.g., the DNSC07 (a predecessor of the DTU13). The high-resolution available over continents is derived from the Free-air gravity data provided by multiple institutions to the National Geospatial Agency (NGA). These data have been merged using a Least Square Collocation algorithm (LSC). Therefore, the terrestrial areas with high data coverage (including the northern Adriatic Sea and surrounding regions, Figure 1-16) count on an average resolution down to wavelengths of ~18 km (or to spherical harmonic degree 2159).

This model is the same used in the remove-restore procedure when computing the S&S and DTU13 altimeter-derived gravity anomaly (Andersen O. B., Knudsen, Kenyon, Factor, & Holmes, 2013; Sandwell, Müller, Smith, Garcia, & Francis, 2014).

New and more accurate global gravity models have been developed after the EMG08, e.g., the EIGEN-6C4 (Förste, et al., 2014). However, we decided to use the EGM08 as a reference geoid model for computing the geophysical Indirect Effect, and extending the grid of gravity anomaly over the areas not covered by terrestrial data (paragraphs 2.1.5 - 2.3). This choice allowed us to remain consistent with the mentioned altimeter-derived models, which have been used in our study to evaluate the quality of OGS marine gravity data and in the leveling procedures (paragraph 2.2), since they also uses the EMAG08 in their respective compilations.

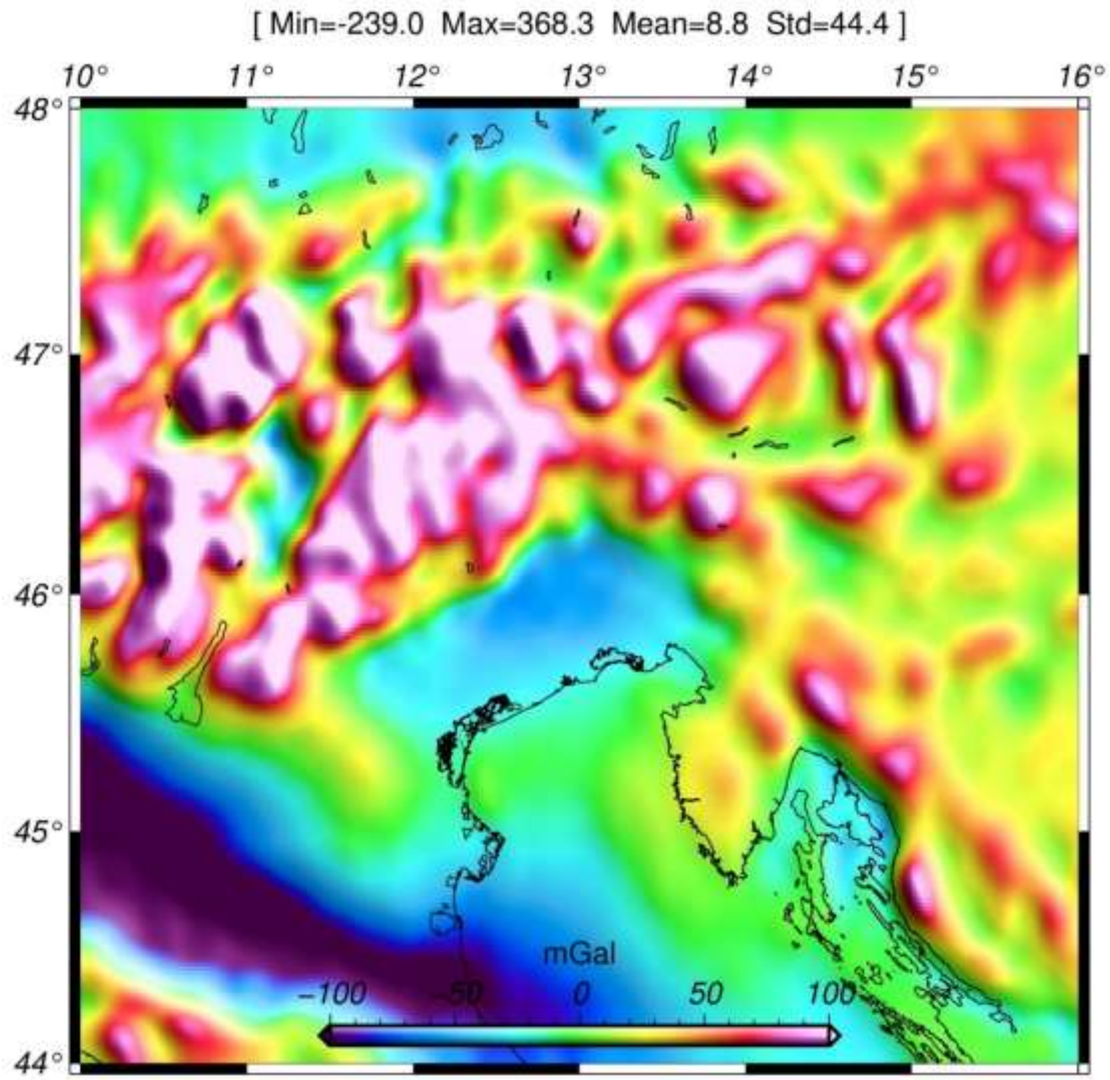

Figure 1-16 - Free Air gravity anomaly derived from the EGM08 (Pavlis, Holmes, Kenyon, & Factor, 2012), centered on the northern Adriatic region, gridded with a sampling-step of 5 km, and low-pass filtered with a sliding average of 20 km size.

1.6.6 EMAG2 version3

The Earth Magnetic Anomaly Grid 02 is a public domain dataset showing the magnetic intensity of the global magnetic crustal field. The 2 arcmin grid integrates data from the CHAMP satellite mission (wavelengths >330 km), shipborne, airborne, and land magnetic data (Meyer, Saltus, & Chulliat, 2017).

As for the gravity-combined models, the errors increase where terrestrial data are scarce and not homogeneously distributed (omission errors), ranging from ±33 nT to ±235 nT (Meyer, Chulliat, & Saltus, 2017). Therefore, the areas with no terrestrial input data within a specific radius have been automatically classified as blank pixels (i.e., to avoid significant uncertainties). One of those areas is the Croatian offshore in the Adriatic sea.

Mean differences between reference shipborne magnetic surveys and the EMAG2v3 have been estimated at a few nanoteslas with standard deviations of about 65 nT for wavelengths > 50 km, but they increase up to 10 nT in standard deviation for shorter wavelengths (Oehler, Rouxel, & Lequentrec-Lalancette, 2018).

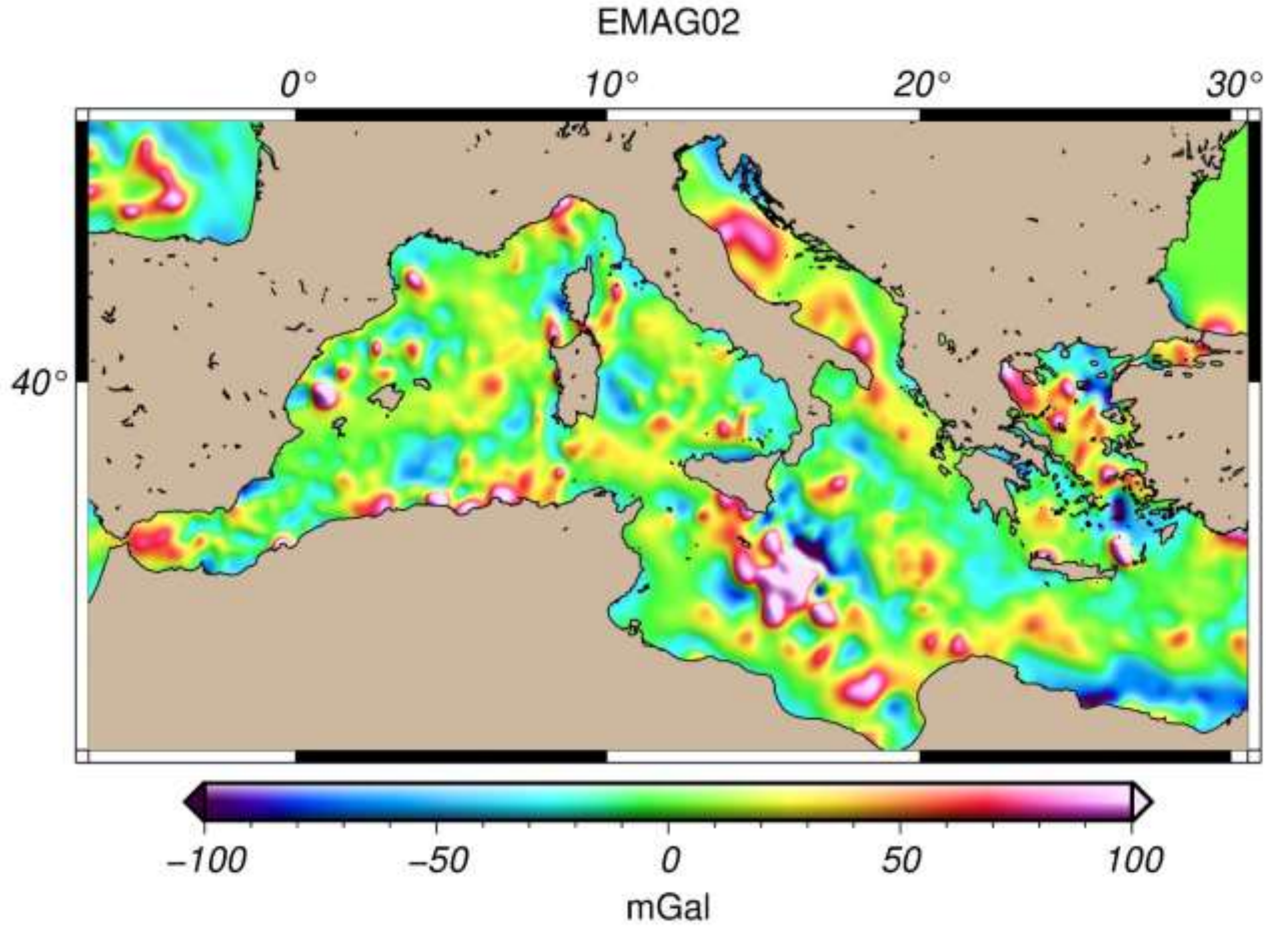

Figure 1-17 - Magnetic anomalies in the Mediterranean sea from the EMAG02 model, filtered using a moving average with a window size of ~55 km.

1.7 Digital Elevation Models (DTMs)

The precision of the station height and elevation models is a key factor for evaluating the accuracy of the resulting gravity anomalies.
The uncertainty resulting from a simple gravity reduction is about ±1 mGal if considering an elevation error of ±5 m and the approximated combined effect of the free-air and the simple Bouguer corrections, i.e., 0.2 mGal/m. This error is generally acceptable for regional studies, but it could exceed the amplitude of investigated signals in microgravity surveys.
The same goes for elevation models in topographic corrections: models with resolutions of about 50 m are generally acceptable in the absence of high topographic gradients (planar regions). However, in the opposite situation (mountain regions), a 25 m or even finer grid is sometimes required. A similar concept can be used for bathymetric models, even though, in this case, the associated water-correction has lower amplitudes than the corresponding crustal-correction in the Bouguer anomalies because of the lower density involved.

In any case, it is always preferable to use accurate elevation models to avoid any additional errors in the resulting anomalies and, when possible, integrate them with bathymetry (Borghi, Carrion, & Sona, 2007). However, high-resolution topographic models are not always available for covering all the study areas, and often they must be integrated with coarser data.

Moreover, the Italian territory, particularly our studied area, is characterized by a varied topography, including high mountains, hills, plains, lagunes, and depressions (land areas below the sea level), all concentrated within a 100 km radius.

To accurately model the gravity effects of all these morphologies, we needed detailed models and an efficient way to separate land from water masses. Therefore, we integrated topographic and bathymetric models with detailed coastlines, keeping land and sea effects separated in the computations. Then, we implemented a processing workflow to merge all the available digital elevation models within a study area in one unique grid, maintaining the accuracy of the original high-resolution data.

To achieve the required accuracy for gravity anomalies, we merged elevation models of different resolutions derived from various sources, including TIN models from quadrangle maps, radar, lidar, multibeam, and seismic data, whose characteristics are briefly described in the following paragraphs.

1.7.1 SRTM model

The Shuttle Radar Topography Mission (SRTM), which last 11-days, was flown aboard the space shuttle Endeavour in 2000, endorsed and supported by the National Aeronautics and Space Administration (NASA) and the National Geospatial-Intelligence Agency (NGA). The mission's primary objective was to acquire a worldwide radar dataset and use it to create the first near-global digital elevation model (Figure 1-18).

The acquisition system was composed of two Synthetic Aperture Radar antennas (SAR), mounted onboard the shuttle and operating with single-pass interferometry. The differences between the signals recorded from both antennas simultaneously enabled the researchers to estimate the surface elevation (Farr, Kobrick, Farr, & Kobrick, 2000).

The absolute vertical and horizontal accuracies of the dataset were found less than ±16 m and ± 20 m, respectively, at 90% confidence (Rodriguez, et al., 2005). However, the expected errors can be more significant in areas of high topographic gradients, e.g., on the Alps (Tarquini, et al., 2012).

Our study used the SRTM Void Filled version, with a resolution of 3 arc-seconds (~90 m), released by the Consortium for Spatial Information (CGIAR-CSI). In this digital version, the dataset voids (areas with insufficient radar contrast) were filled using specific interpolation techniques (Reuter, Nelson, & Jarvis, 2007; Jarvis, Reuter, Nelson, Guevara, et al., 2008).

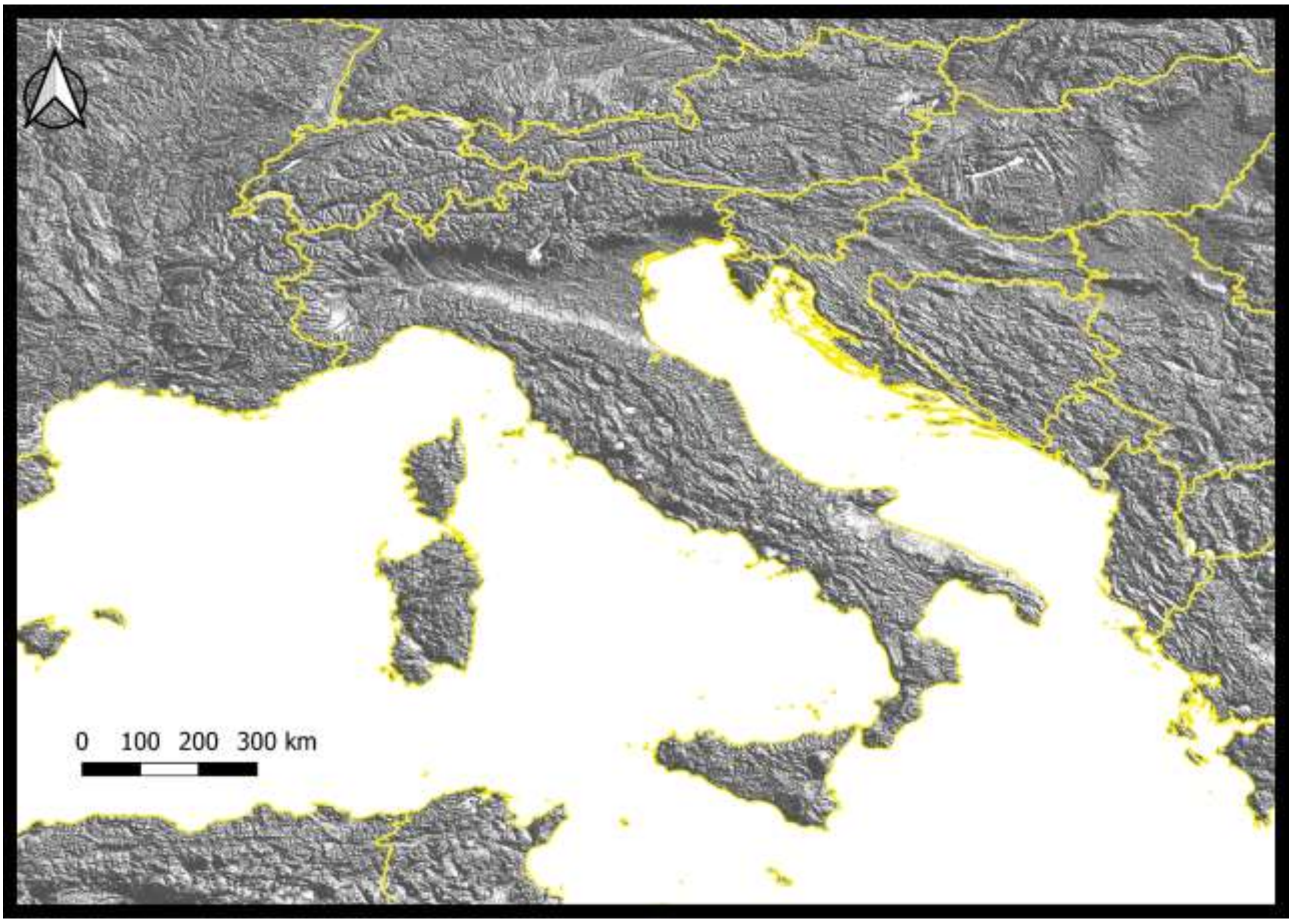

Figure 1-18 SRTM data over Italy and nearest lands (hillshade map)

1.7.2 Lidar models

The Laser Imaging Detection And Ranging (Lidar) is a survey technique based on laser beams measuring the position of targets throughout the travel time or the phase difference of the back-scattered signals.

When mounted on aircraft, these sensors measure the distances to ground points, which are memorized as a cloud of scattered points. After some processing, the point cloud can be converted into highly accurate digital terrain models (DTMs) with sub-metric vertical and horizontal precision.

Our study merges multiple public domain DTMs derived from Lidar surveys, covering the Friuli Venezia Giulia region, Austria, and Slovenia (Figure 1-19). The vertical resolution of these datasets is about 0.1 m, but the accuracy may vary up to ~1 m, depending on the acquisition system, filtering operations, and surface conditions, e.g., the presence of water, forests, or complex infrastructures, generally degrade the signal. Nevertheless, the average accuracy can be considered at ± 0.3 m, as confirmed by independent local studies (Reutebuch, McGaughey, Andersen, & Carson, 2003; Triglav Cekada, et al., 2015; Regione Autonoma Friuli Venezia Giulia, 2020).

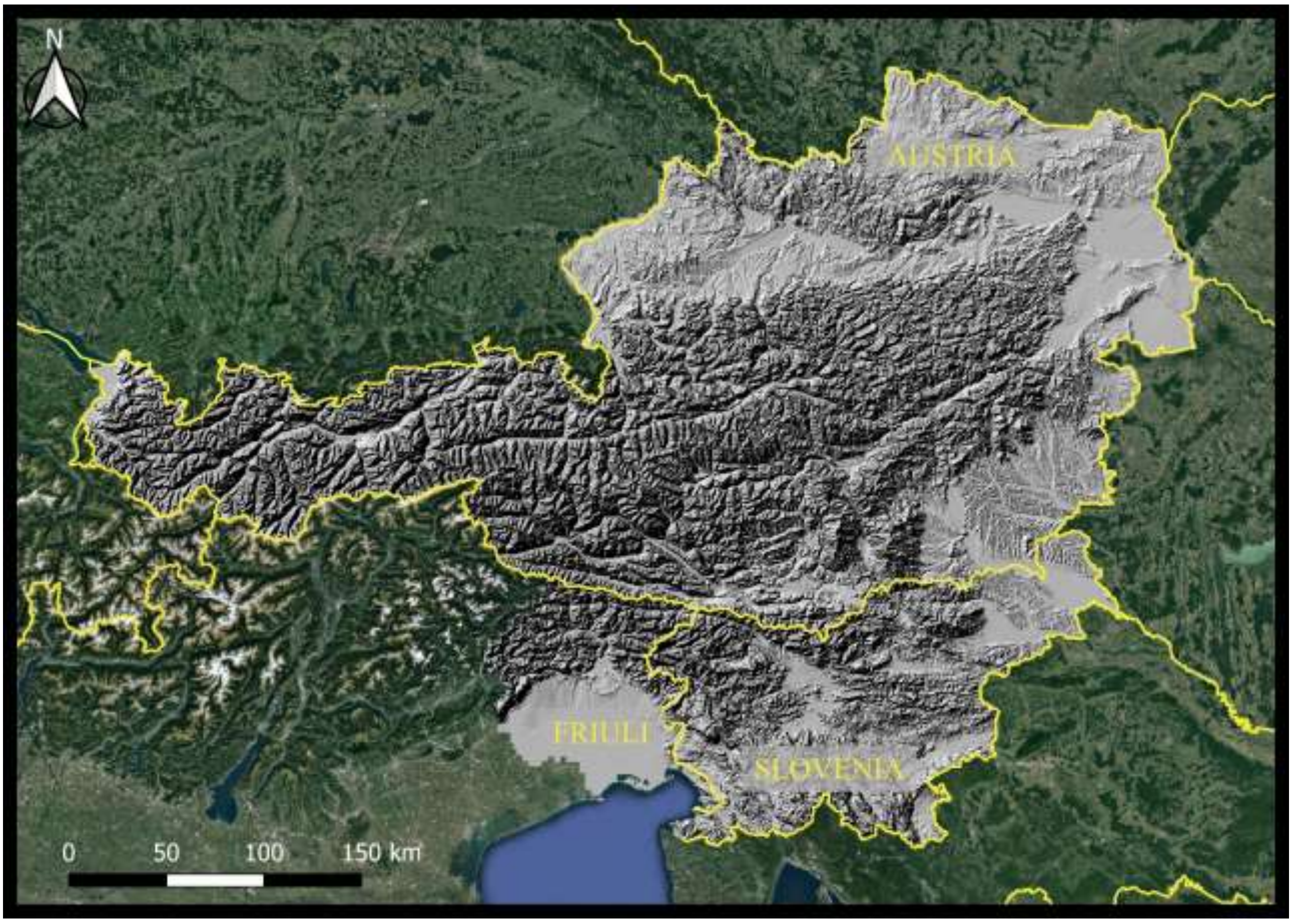

Figure 1-19 Lidar DTM covering Austria, Slovenia, and Friuli Venezia Giulia region, Table 2 (hillshade map).

1.7.3 TIN models (Veneto region)

Detailed elevation models can be created from contours and elevation points digitalized from topographic maps. This is the case of the DTM we used to cover the area of the Veneto region (Figure 1-20). The elevation model, created by the CNR of Pisa, is based on a Triangulated Irregular Network (TIN) of elevation points obtained from the Carta Tecnica Regionale Numerica (CTRN), which have been interpolated using the DEST algorithm developed explicitly for the task (Favalli & Pareschi, 2004). This interpolation method guarantees the best accuracy in modeling slopes, drainage networks, and catchment areas, starting from scattered data (isolated quoted points, contour lines, breaks lines, or photogrammetric information). The final horizontal resolution is 5 m, whether the elevation error is about ± 5 m (Picchio, 2006).

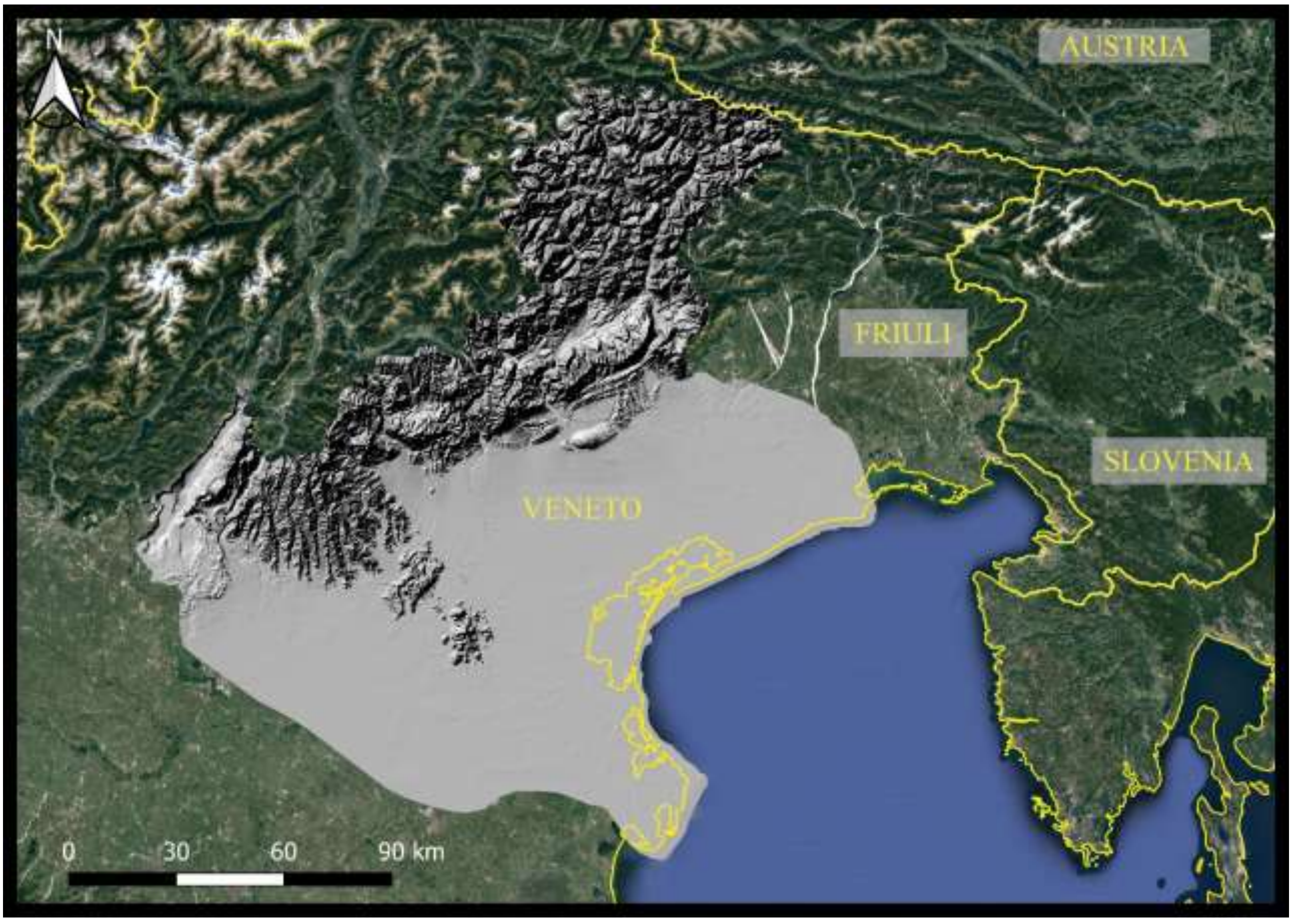

Figure 1-20 Veneto Region DTM, as derived from local topographic maps using TIN-based interpolation algorithms.

1.7.4 Bathymetric models

The bathymetric models used in this study are mainly derived from sonar acquisitions with Multibeam echo-sounders or direct measurements of graduated rods (in shallow waters), and high-resolution seismic profiles (Figure 1-21).
Our study used three different bathymetric datasets (Table 2): the EMODnet bathymetry, the bathymetry of the Gulf of Trieste (GOT), and the bathymetry of Grado and Marano Lagune (GML).

The EMODnet dataset consists of a grid with 1/16 arcminute of resolution (~115 m), covering most international waters. The model integrates a set of heterogeneous data with an uneven spatial distribution. In the case of the Adriatic sea, it comprises Single-Beam echo-sounding profiles, manually contoured on maps and then interpolated using the Kriging algorithm on regular grids with 200 m grid-step. The final dataset was then oversampled to meet the required resolution for the global Emodnet dataset (Trincardi, et al., 2014). According to the EMODnet documentation, the accuracy of the dataset can be empirically estimated using the Zone Of Confidence table (International Hydrographic Organization, 2018). The table indicates horizontal accuracy is ±500 m and maximum vertical accuracy ±7 m, for grid data derived from Single-Beam echo-soundings not homogeneously distributed.

The bathymetry of the Gulf of Trieste (GOT) is a grid database derived from geophysical surveys conducted between 2000 and 2015 by the OGS and Harpha Sea d.o.o. in cooperation with the Department of Geology of the University of Ljubljana. This data includes Multi-Beam and Single-Beam echo-soundings, sub-bottom profiling Chirp, and other sonar acquisitions, in addition to high-resolution boomer seismic profiles and depths from nautical charts. All the collected data were merged using the kriging method, generating two different models: the first with a grid-step of 20 m and the second with a grid-step of 50 m (Trobec, et al., 2018). We used the model at 20 m, resampled with a moving average of 50 m.

The bathymetry of Grado and Marano comprises 700 km of continuous bathymetric profiles, spaced at 150 m, recorded by hydrographic echo-sounders and differential GPS equipment. This survey allowed the generation of a Digital Bathymetric Model of the lagoon plains (DBM), which describes in detail the morphological characteristics of the seabed. This model has been further integrated with high-resolution Multibeam data recorded within the major navigable canals of the Lagoon. The final product is a 1 m resolution bathymetric grid interpolated using a TIN-based algorithm with an estimated sub-metric accuracy (Triches et al., 2011).

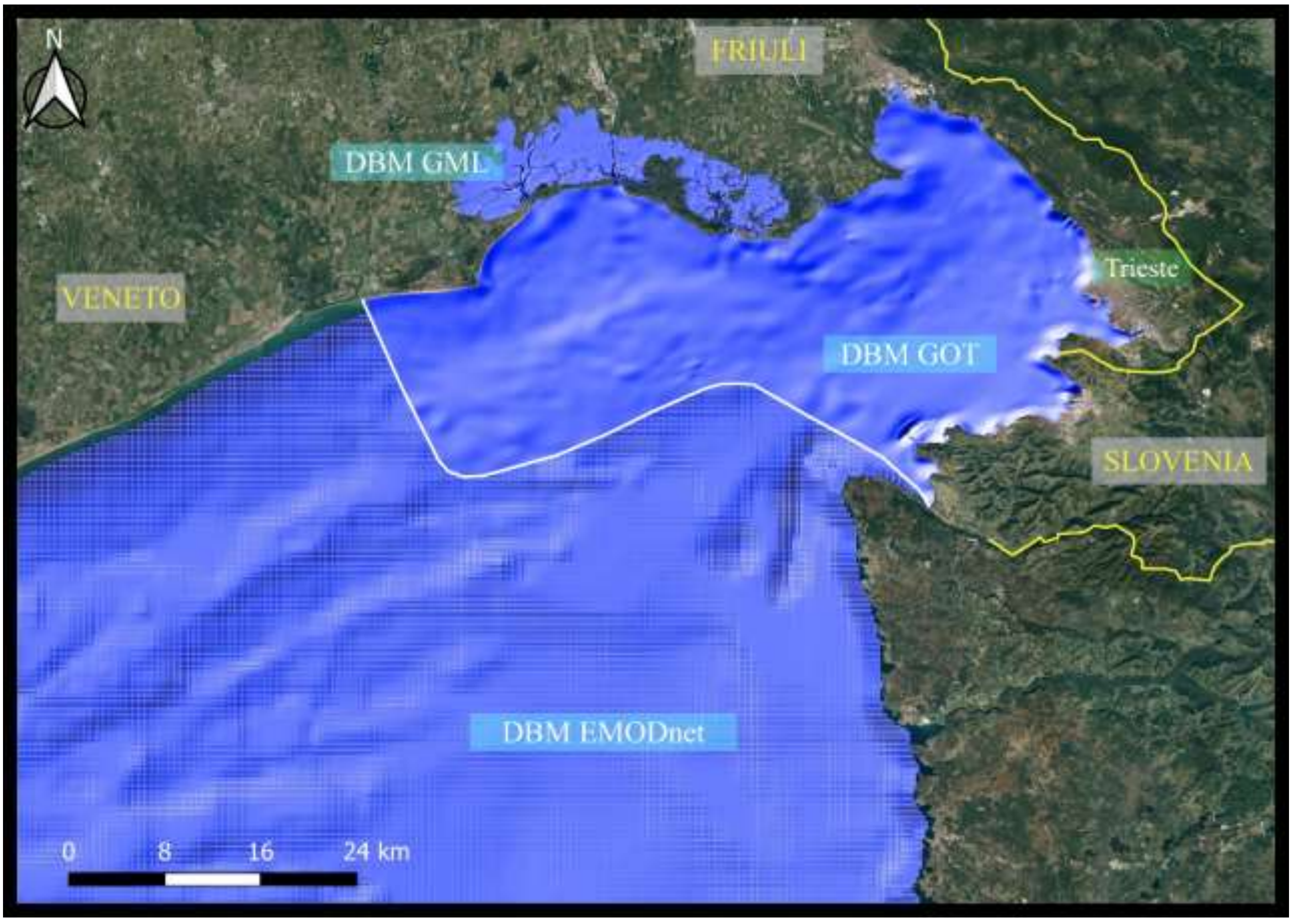

Figure 1-21 - Bathymetric models of the northern Adriatic Sea, derived from EMODnet, the bathymetry of the Gulf of Trieste (Trobec, et al., 2018), and the bathymetry of Grado and Marano Lagoon (Triches, et al., 2011).

1.7.5 The coastline database

In this study, we merged different coastal databases to increase the accuracy of the shorelines in the marine areas where there is a denser coverage of gravity stations.

The main base is the Global, Self-consistent, Hierarchical, High-resolution Geography Database, GSHHG (Wessel & Smith, 2015), which was integrated by more detailed local and regional datasets. Specifically, we use the following additional resources (Figure 1-22):

1. the "GT-Coast-Veneto-WGS84-UTM33.shp" file, with the coastline of the Veneto region digitized from georeferenced rasters taken from different databases (Esri, DigitalGlobe, GeoEye, Earthstar Geographics, CNES/Airbus DS, USDA, USGS, AeroGRID), in 2009, with a resolution of 0.6 m (IDT-RV, 2016).
2. the "GT-Coast-FVG-WGS84-UTM33.shp file, with the coastline of the Friuli Venezia Friuli region, derived from photo-interpretation of aerial and satellite images, topographic maps, and GNSS surveys, with a resolution of 0.5 m (IRDAT-FVG, 2015);
3. the "GT-Coast-Slovenia-WGS84-UTM33.shp" file, derived from the PoligonKopno.shp and PoligonMorje.shp files, with the Slovenian coastline, granted by Ana Trobec from the University of Lubiana (Arso, 2016).

This information is beneficial for accurately separating the gravity effects of topographic and water masses within the Grado and Marano lagoon, where land and sea-bottom stations have been recorded close to each other on island sandbars.

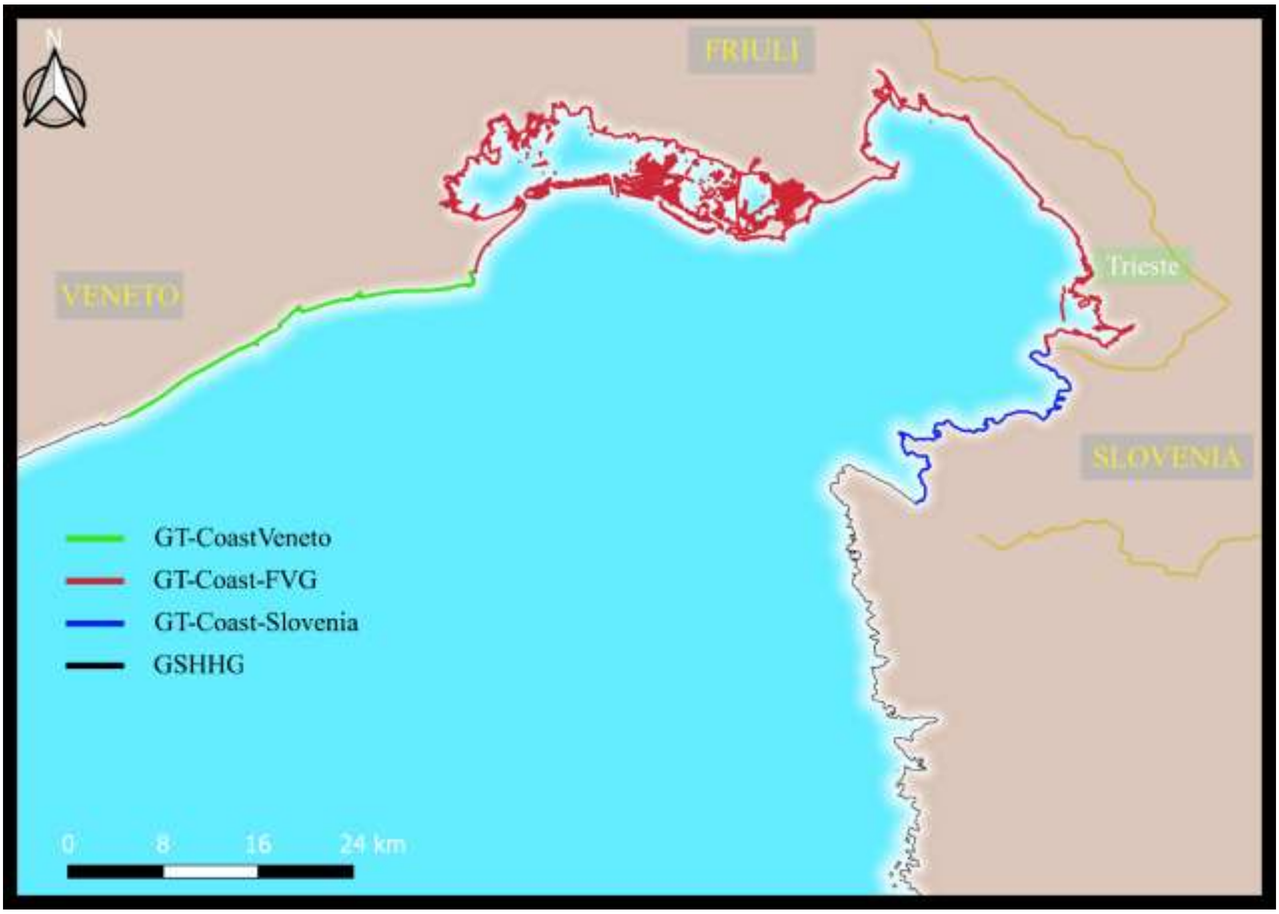

Figure 1-22 Coastline datasets used in the northern Adriatic region

Table 2 Digital Topographic Models used in gravity data processing with (i) reference name, (ii) horizontal resolution, (iii) expected error, and (iv) data source.

Name	**Resolution [m]**	**Error [m]**	**Source**
SRTM	~90	16	http://srtm.csi.cgiar.org
DTM Friuli Venezia Giulia	10	0.5	https://irdat.regione.fvg.it/CTRN/ricerca-cartografia/
DTM Slovenia	20	0.5	http://data.opendataportal.at/dataset/dtm-slovenia
DTM Austria	20	0.5	http://data.opendataportal.at/dataset/dtm-austria
DTM Veneto	5	5	https://idt2.regione.veneto.it/idt/downloader/download
DBM EMODnet (Adriatic sea)	500	7	https://portal.emodnet-bathymetry.eu/
DBM GOT	50	-	https://snap.ogs.trieste.it/cache/doi/6ad9b1e6-c977-cec9-8a2d-db10c7f90adc/58074ea270863f0a32214fab4f43d42c.jsp
DBM GML	1	0.5	On request

2 Methods

2.1 Gravity data reductions

Gravity data reduction methods include various processing steps to adjust an initial Earth-like model to the actual model by adding known measurable effects of the gravity field at the station point. In other words, reductions are meant to approximate a starting theoretical gravity field (or reference field), g_{th}, to the observed gravity field of the solid Earth, g_{obs}. The starting theoretical model commonly used in most applications is the rotating oblate ellipsoid that best approximates the Earth's form (Figure 2-1). The ellipsoid has a constant mass and a precise geometrical definition, which allows deriving its gravitational attraction in a closed mathematical form that only depends on latitude (φ).

The gravity anomalies are the difference between the observed and the reference field, and they show unpredicted later density contrast in the subsurface at different depths.

In geophysical studies, two types of anomalies are of common use: the Free-air and the Bouguer anomaly.

The Free-air anomaly, Fa, is obtained by correcting the reference model for effects of orthometric height, h_{geo} (free-air correction, fac). This correction reduces the theoretical gravity to its approximate value at a vertical distance h_{geo} from the outermost surface of the reference model (i.e., the ellipsoid). However, the fac correction neglects the gravity effect of all masses interposed between the new elevation and the original reference surface. Moreover, the chosen correction distance is taken from the ellipsoid and not from the geoid surface. Therefore the corrected theoretical value does not necessarily correspond to the actual position of the observed gravity station. The inconsistency between the new calculation point and the observed gravity coordinates generates a discrepancy between the actual gravity field and the reference one. This bias is commonly referred to as the Indirect Effect (*IE*), and it is proportional to the geoid undulation N (Li & Götze, 2001). We reduced this error by applying the geophysical Indirect Effect correction discussed in paragraph 2.3.

$$Fa(\lambda,\varphi,h_{geo}) = g_{obs}(\ \lambda,\varphi,h_{geo}\ ) - [\ g_{th}(\varphi) + fac(\varphi,h_{geo})\ ] \tag{2.1}$$

The Bouguer anomaly, Ba, is obtained after the Free-air correction by including the measurable gravity effects of topography and water masses surrounding the station point (topographic effect, te). The topography/water masses considered in this correction are those between the station point and the geoid surface or between the geoid surface and the sea bottom. The residual gravity of the remaining masses interposed between the geoid and the ellipsoid is reduced afterward with the previously mentioned geophysical Indirect Effect correction.

$$\begin{aligned} Ba(\lambda,\varphi,h_{geo}) &= g_{obs}(\lambda,\varphi,h_{geo}) - [\,g_{th}(\varphi) + fac(\varphi,h_{geo}) + te(\lambda,\varphi,h_{geo})\,] \\ &= Fa(\lambda,\varphi,h_{geo}) - te(\lambda,\varphi,h_{geo}) \end{aligned} \tag{2.2}$$

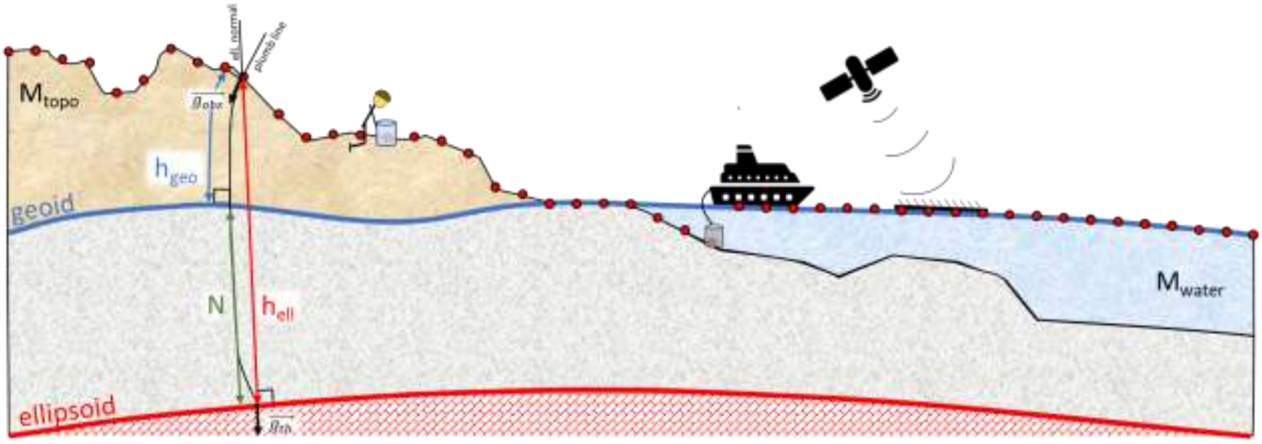

Figure 2-1 - Parameters used to define gravity anomalies (modified after Hackney & Featherstone, 2003). g_{obs} is the measured gravity vector at the Earth's topographic surface, g_{th} *is the theoretical gravity vector at the surface of the ellipsoid.* h_{geo} *is the orthometric height along the curved plumbline,* h_{ell} *is ellipsoidal height along the ellipsoidal surface normal, and N is the geoid–ellipsoid separation.* M_{topo} *and* M_{water} *indicate respectively the topography and the water masses which gravity effect has been removed in the Bouguer anomaly.*

2.1.1 Theoretical gravity

The theoretical or normal gravity, $\mathrm{g_{th}}$, is calculated using the international gravity formula of the Geodetic Reference System 1980 (GRS80).

The GRS80 is an analytically defined rotational geocentric ellipsoid, approximating the shape of the Earth given its total mass and the equatorial and polar radius. Its gravitational field can be written in a closed form, including the centripetal acceleration induced by the Earth's rotation (Table 3).

Table 3 - Parameters of the GRS80 ellipsoid (Moritz, 1980; Torge & Müller, 2012)

Parameter	**Description**	**Formula**	**value/units**
GM	Geocentric gravitational constant	-	3986005×10^{8} $m^{3}s^{-2}$
a	Semimajor axis (equatorial radius)	-	6378137 m
b	Semiminor axis (derived polar radius)	-	6356752.3141 m
f	Flattening	f = (a-b)/a	1 / 298.257222101
e^2	first eccentricity squared	$e^2 = (a^2-b^2)/a^2$	0.00669438002290
w	Rotation rate	-	7.292115×10^{-5} rad s^{-1}
g_e	Normal gravity at the equator	-	978032.67715 mGal
g_p	Normal gravity at the poles	-	983218.63685 mGal

One problem of the GRS80 model is that its total mass, M, also includes the mass atmosphere above the reference surface (Torge & Müller, 2012).

However, we know that the net gravitational force exerted by any homogeneous atmospheric outer shell at any point inside is zero if considering a spherical approximation or close to zero in the case of the ellipsoidal approximation (Newton's shell theorem).

Hence, in geophysical studies, we need to remove the gravity effect of the outer atmospheric shell from the theoretical gravity. This effect decreases with the elevation as the thickness of the atmospheric shell reduces (Hinze, et al., 2005).

We compute the theoretical gravity using the Somigliana equation (Somigliana, 1930).

$$g_{th}(\varphi) = \frac{g_e(1 + k\sin^2\varphi)}{(1 - e^2\sin^2\varphi)^{1/2}} \tag{2.3}$$

where,

$$\mathrm{k} = \frac{bg_p - ag_e}{ag_e} = 0.00669437999013 \tag{2.4}$$

Then, we subtract from $g_{th}(\varphi)$ the atmospheric correction term g_{atm}.

$$g_{atm}(h_{geo}) = 0.874 - 9.9 \times 10^{-5}h_{geo} + 3.56 \times 10^{-9}{h_{geo}}^2 \tag{2.5}$$

2.1.2 Free Air-Water correction

The concept of the Free-air correction (fac), derives from the inverse square law of gravitation, according to which the strength of g_{th} decreases with the distance from the reference surface. In practice, this results in a fall-off of gravity with the elevation (h_{geo}) that can be estimated from eq. 2.3, using a second-order Taylor series approximation (Hinze, et al., 2005).

$$\begin{aligned} fac(\lambda, \varphi, h_{geo}) &= -\frac{\partial g_{th}}{\partial h}\, h_{geo} + \frac{1}{2}\frac{\partial^2 g_{th}}{\partial {h_{geo}}^2}\, {h_{geo}}^2 \\ &\simeq -(0.3087691 - 0.0004398\sin^2\varphi)h_{geo} + 7.2125 \times 10^{-8}{h_{geo}}^2 \end{aligned} \tag{2.6}$$

However, this correction must be slightly modified when dealing with underwater gravity stations (Stacey & Tuck, 1981; Luyendyk, 1984; Dubois & Deplus, 1989; Hildebrand, et al., 1990; Ballu, Dubois, Deplus, Diament, & Bonvalot, 1998). In this case, we used the free-water correction, fwc, in its spherical approximation, g_{th}^{s} (i.e., without the latitude term, φ), which includes the gravity effects of the overlying water masses (eq. 2.7). This correction, in essence, is the same as the Prey reduction as described by Bernhard Hofmann-Wellenhof & Helmut Moritz (2006, pg. 138-140), with the difference that here we used the water density, i.e., ρ_w (1030 kg/m^3), and not the crustal density.

The free-water correction is similar in principle to the atmospheric correction: the water layer overlying the measurement point approximates an outermost homogeneous spherical shell of our reference model, which has a null effect on the inner region.

Then, the total downward gravitational attraction of the theoretical gravity slightly decreases with depth because of the lack of mass contribution from the thickening outer water shell.

This effect contrasts with the more significant increment in gravitational attraction due to the closer proximity with the deep and denser layers of the Earth. The combination of both effects results in a slight decrease of the vertical gravity gradient by a quantity equal to the gravitational attraction of the water shell.

The homogenous-spherical shell approximation holds if (i) the density does not change drastically within the water column and (ii) the Earth curvature effect is negligible. Both assumptions are satisfied for the sea-bottom stations around the Italian coasts where depths do not exceed 250 m and latitudes are limited in a range of ± 8°. Otherwise, the ellipsoidal-shell approximation and water-density profiles must be added in the computation (Stacey & Tuck, 1981).

$$\begin{aligned} fwc(h_{geo}) &\simeq \frac{\partial\; g_{th}^{s} - g_{shell}}{\partial r} h_{geo} \\ &\simeq -\frac{2g_{th}^{s}}{R^{2}} h_{geo} + 4\pi G \rho_w h_{geo} \\ &\simeq -0.222\; h_{geo} \end{aligned} \tag{2.7}$$

2.1.3 Topographic correction

The last correction generally applied to the reference gravity field is the topographic effect, which aims to include the effects of the known topographic and water masses into the model (te, eq. 2.2).

We create a semi-automatic python solution to estimate this effect, adaptable to land, shipborne, and sea-bottom data, and it includes both the gravity effect of the bathymetric and topographic models presented in paragraph 1.7 within a single computation.

Our method is divided into three main steps, each of which uses a specific python library:

1. creating a combined digital topographic and bathymetric model (DTBM) by merging all the available DTMs, DBMs, and coastlines databases, using the GDAL library (GDAL/OGR contributors, 2021).
2. setting a computational mesh suitable for the study area, composed of both prism and tesseroid elements using Pyproj (PROJ contributors, 2021).
3. computing the gravity effect of the mesh, differentiating land and shipborne from sea-bottom stations, using the Harmica library (Uieda, Soler, Pesce, Oliveira Jr, & Shea, 2020).

2.1.3.1 Merging digital topographic and bathymetric models

Topographic effects require accurate topographic data within a radius of at least a few tens of kilometers from the gravity station when searching for relatively shallow sources (e.g., rock basement, caves). Moreover, the modeling domain should be covered by topographic data as homogeneously as possible. Unfortunately, however, the highest resolution topographic models are not available everywhere.

Therefore, joining multiple digital elevation models is often necessary to preserve high resolutions and accuracy where available. But at the same time, abrupt changes in height or slope at the transition zones between areas characterized by different data coverage should be avoided. For example, the proximity of a gravity station with an abrupt discontinuity between different topographic models may introduce artifacts in the derived anomaly, which could be easily confused with geological signals.

We tested different solutions to integrate topographic models at different resolutions, starting with the ones available on the available open-source and commercial software (e.g., Qgis, Arcgis, Global Mapper, GMT) and then turning to other computational methods proposed in research papers (Hell & Jakobsson, 2011; Gallant, 2019).

One of the most promising solutions was a remove-restore procedure that combines the long wavelengths of the low-resolution models, e.g., SRTM, EMODnet, with the short wavelengths of the high-resolutions models, e.g., Lidar or Multibeam (Hell & Jakobsson, 2011). However, with this method, part of the high-resolution signal was inevitably smoothed, especially in areas with high topographic gradients, where differences of more than 15 m occur between the integrated and the original model.

We finally obtained an acceptable result following a simple method recently proposed in a conference paper (Gallant, 2019), which we slightly modified to our purposes.

Our modified solution is a python function that reads multiple input DTMs and outputs a single integrated raster at the chosen final resolution. The function comprises 8 processing steps (Figure 2-2):

1. the input datasets are listed in ascending order, according to the resolution;
2. all the raster are sampled to the final selected resolution, using a moving average, for down-sampling, and bilinear splines, for up-sampling;
3. for each of the sorted rasters, starting from the second, a grid with the differences to the previous raster is computed onto overlapping areas;
4. the grid of differences is extended using a nearest-neighbor interpolation, only over the areas with the lowest resolution;
5. the extended part of the differences is smoothed, firstly using a gaussian filter and then with a moving average, with a 3x3 kernel size;
6. the differences in the extended areas are gradually smoothed to zero with a gaussian filter, to a distance equal to two times the original cell size of the original low-resolution grid, starting from the edges of the high-resolution grid;
7. the voids left by the high-resolution grid are then filled with the sum of the low-resolution grid and the extended differences;
8. the final combined grid is integrated with the next raster in the loop, using the same procedure, etc.

This method does not involve any complex interpolation or minimization algorithm, so it is relatively fast, even with the large matrices from Lidar DTMs (e.g., 20000x20000 px). The input grids are saved and processed using the GeoTIFF file format readable through the optimized algorithms of the GDAL library.

The results from this method have been proven reliable in the most complicated areas (lagoons and mountains), where other tasted methods failed (Figure 2-3, 2-3, 2-4). There are, however, minus points described in the following pros-cons table, which must be considered before blindly using the algorithm.

PROS	CONS
✓ The final DTM does not modify the original data, i.e., it preserves all resolution and accuracy of the input grids (excluding areas near the edges).	✗ Systematic biases are not solved, e.g., discrepancies in the vertical datums and related steps at the edges are only smoothed and not removed.
✓ The algorithm smooths abrupt discontinuities at the grid's edges, consequently avoiding related artifacts in topographic corrections.	✗ The areas near the edges over the low-resolution grids are artificially modified, causing possible artifacts.
✓ The smoothing filter modifies almost exclusively a narrow band over the low-resolution areas without interfering with the high-resolution part.	

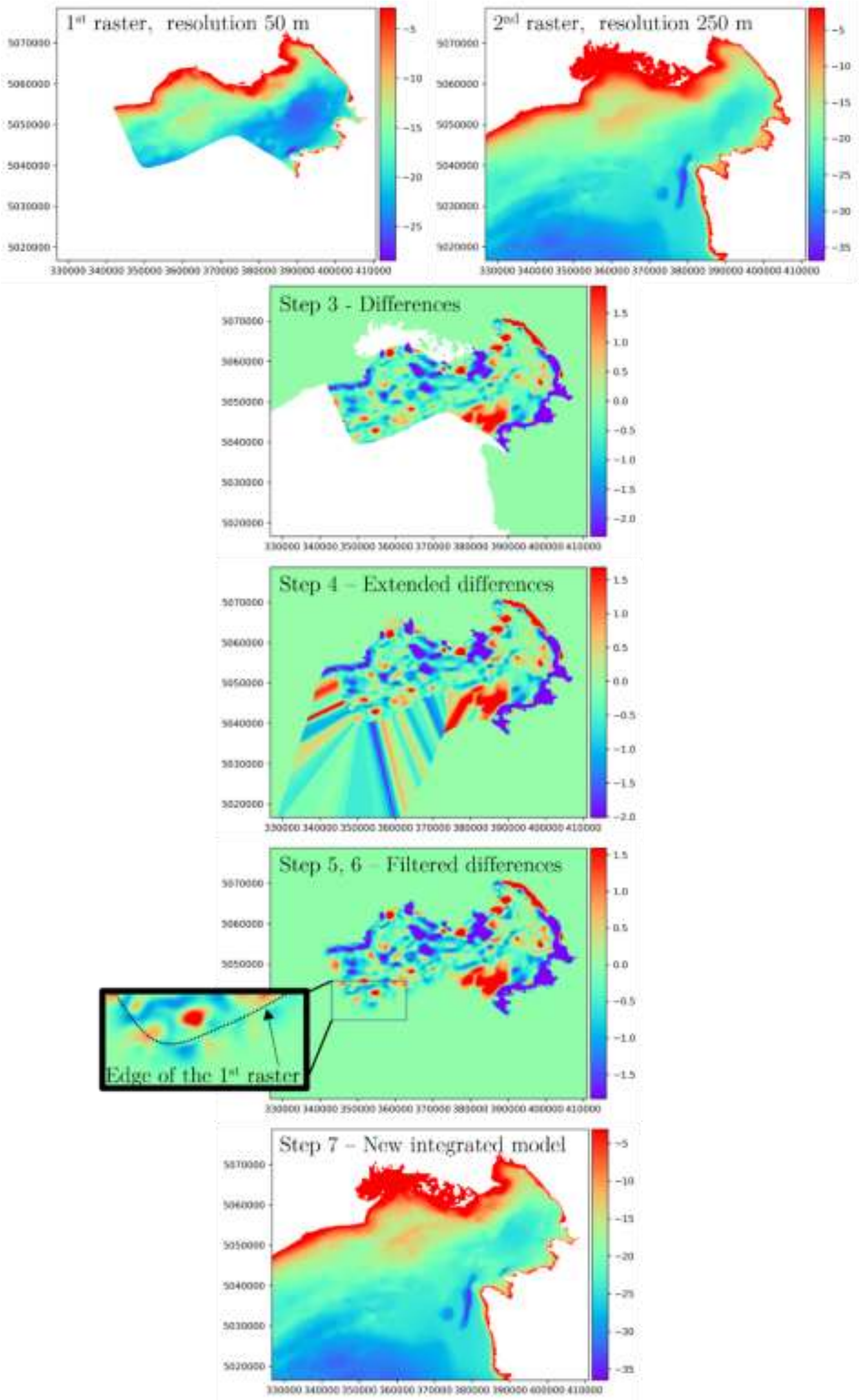

Figure 2-2 Processing steps to merge two digital topographic/bathymetric models at different resolutions. In this example, the two inputs grids are (1) the GOT bathymetry from (Trobec et al., 2018) and (2) the EMODnet bathymetry (Table 2), and each lower panel shows results from one or more of the processing steps described in the text; the last panel (step 7) is the final integrated model with a resolution of 50 m.

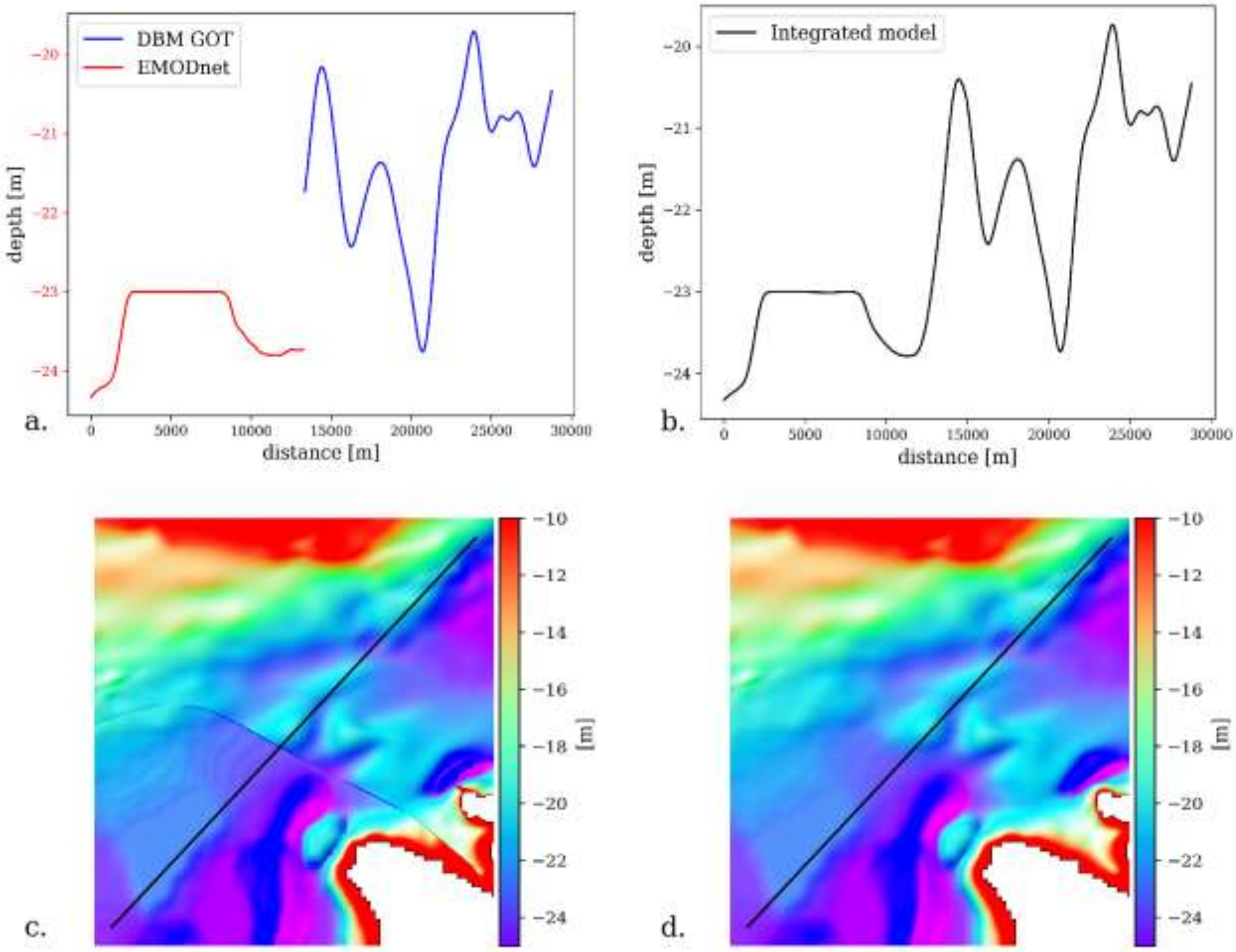

Figure 2-3. Example of integration between the EMODnet bathymetry (250 m) and the GOT bathymetry (50 m) in the northern Adriatic Sea (Trobec et al., 2018), with panels (a) showing the profile from the separated grids (c) before the integration, and (b) the same profile after the integration (grid d).

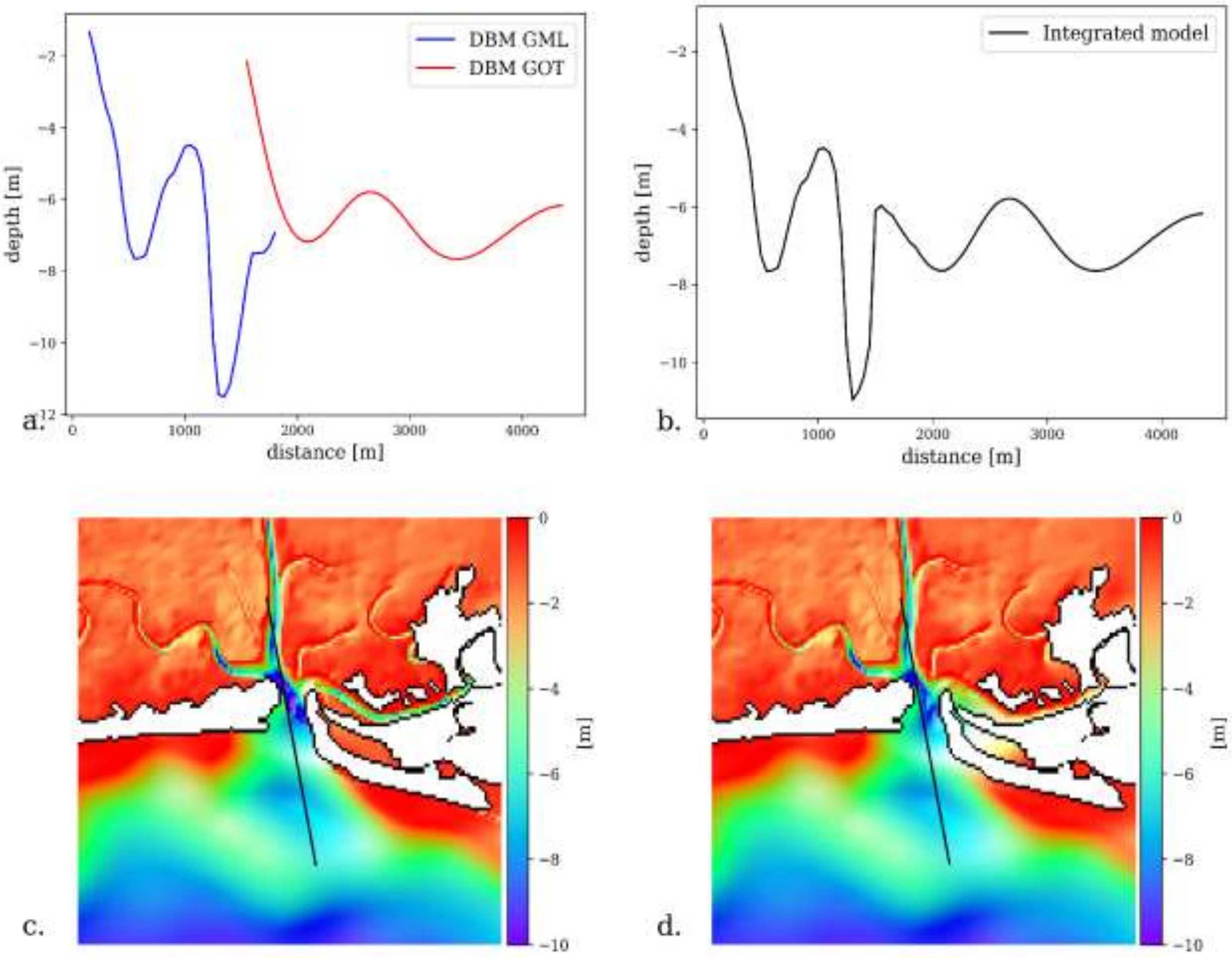

Figure 2-4 Example of integration between the GOT bathymetry (50 m) (Trobec et al., 2018) and the GML bathymetry (1 m), in the northern-East lagoon of the Adriatic Sea (Triches et al., 2011), with padel (a) showing the profile from the separated grids (c) before the integration, and (b) the same profile after the integration (d).

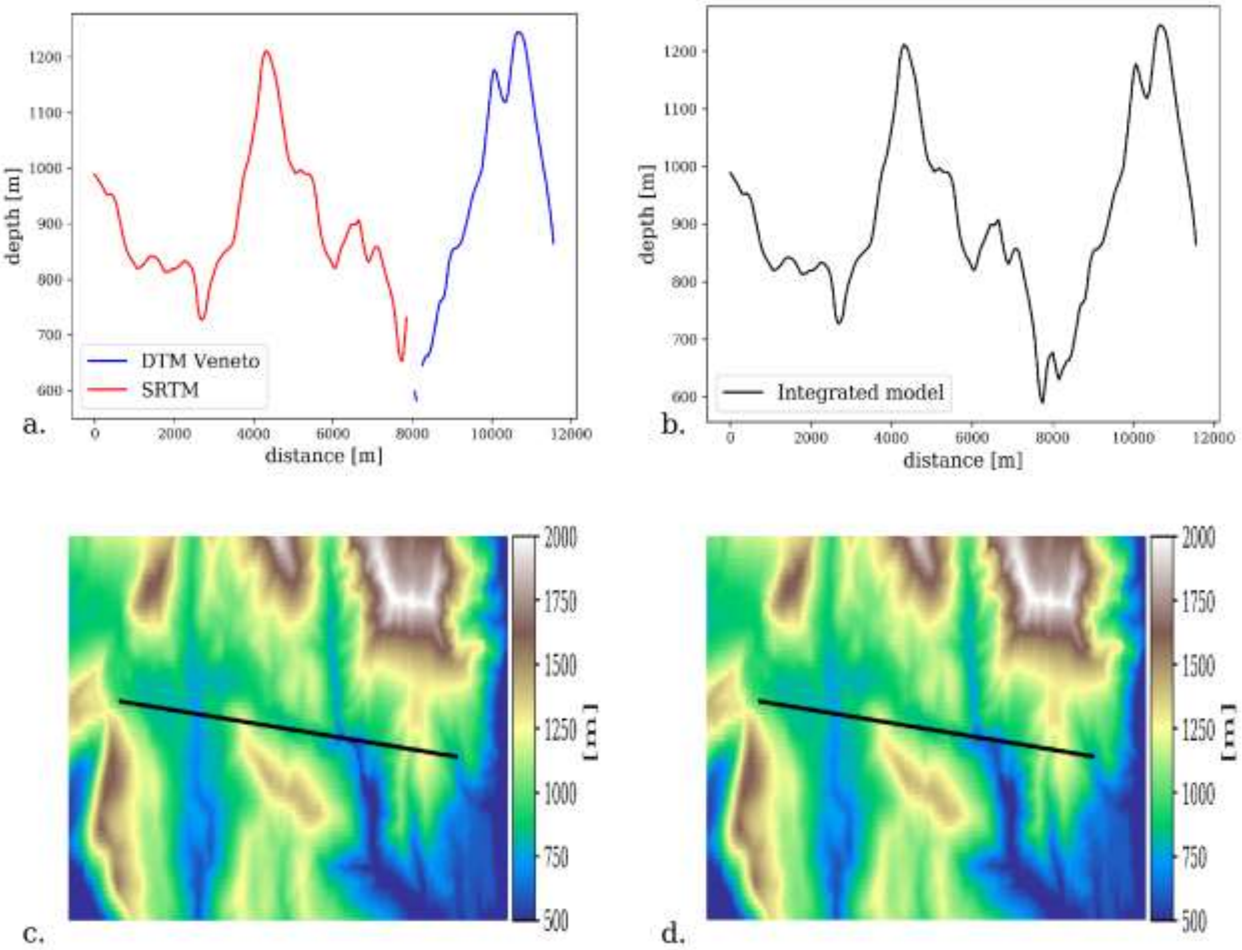

Figure 2-5 - Example of integration between the SRTM topography (90 m) and the Veneto topography (5 m, sampled at 50 m), in the Alps at the border between Veneto and Trentino Alto Adige regions; the panel (a) shows the profile from the separated grids (c) before the integration, and (b) the same profile after the integration (grid d), with the final resolution of 50 m.

Moreover, this merging algorithm automatically keeps separated data points from marine and land areas during the integration procedure when a coastline polygon is provided in the inputs. In this case, a second band is added to the final GeoTIFF file, other than the band with the elevation values. In the second band, all the land areas are classified with 0 values and marine areas with 1 (Figure 2-6). The additional information provided by the integrated coastline allows to automatically and accurately separate water from crustal elements during the computation of the topographic effects.

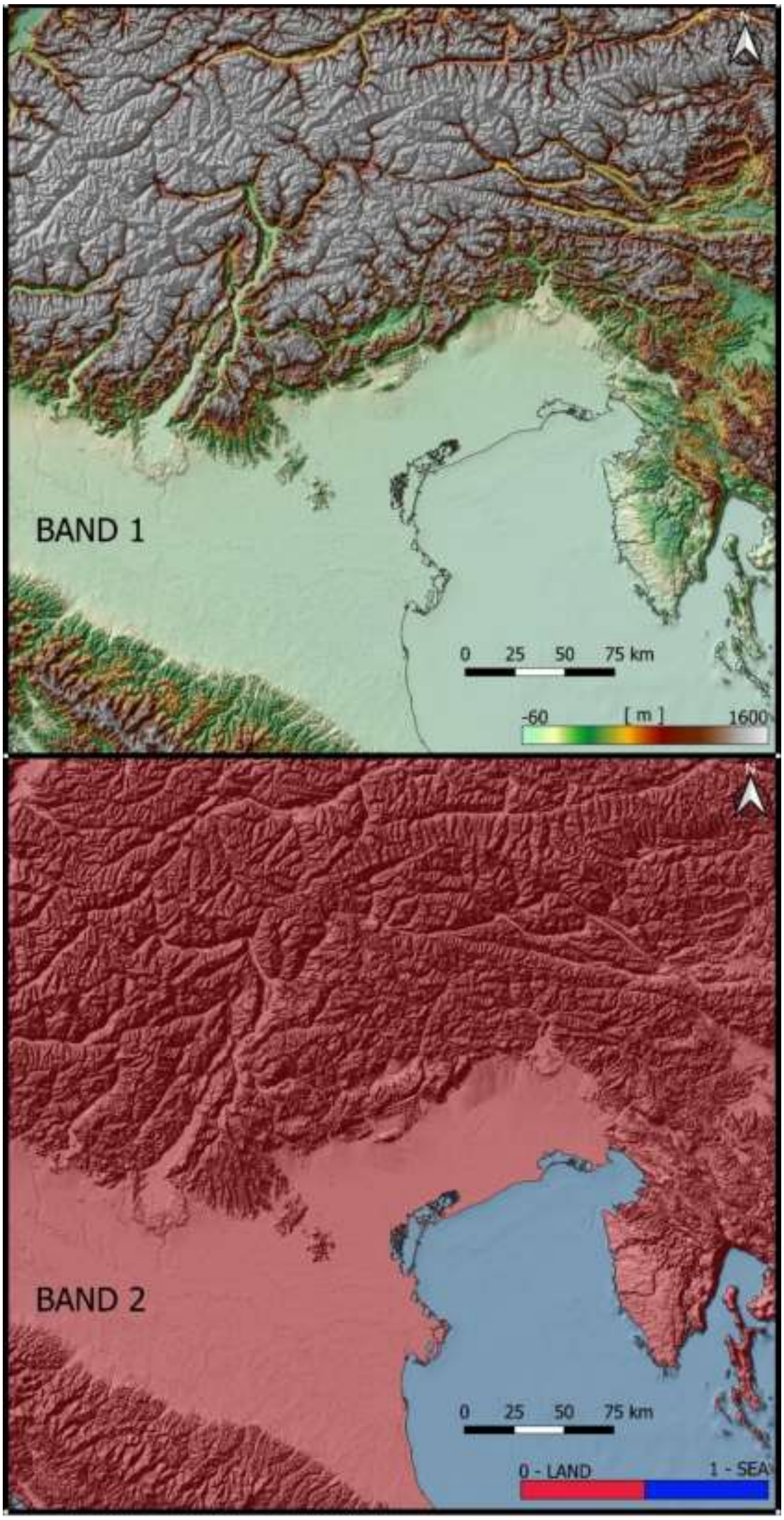

Figure 2-6 - Topographic maps from the Geotiff file used for computing topographic effects in the northern Adriatic Region. The file is composed of two bands with a grid-step of 50 m. The first band contains the elevations; the second band classifies each pixel as marine (1) or land area (2).

2.1.3.2 Topographic correction mesh

Unlike classical approaches used for computing topographic effects, generally based on three different corrections (Nowell, 1999), i.e., the infinite-horizontal slab (BA), the Earth's curvature (BB), and the exceeding topography (BC), we decide to test a solution that condensates those previous steps into two:

1. the effect of a high-resolution inner topographic model, composed of Prism-elements, within a planar reference system;
2. the effect of a low-resolution outer topographic model, composed of Tesseroid-elements, within a spherical reference system;

The idea behind this strategy is relatively simple: in geodesy, a tangent plane can approximate with sufficient accuracy the ellipsoid surface for distances of ~15 km from the tangent point, with horizontal positioning errors of about 0.1 m.

Therefore, the topographic model surrounding the gravity station can be safely approximated using Prism-elements within a few tens of kilometers.

The only required additional correction is the downshift of the prisms (z_{shift}) due to the vertical deviation of the plane from the ellipsoid, which is ~17.5 m at ~15 km from the central point (Forsberg, 1984).

The outer domain, up to 200 km from the central point, is approximated using a local sphere tangent to both the ellipsoid and the plane. The topography on the sphere is discretized by Tessroids-elements (i.e., spherical prisms), and the radius of the local sphere, R_s, is defined as:

$$R_s = \frac{a\sqrt{1-e^2}}{1-e^2\,\text{sen}^2\,\varphi} \tag{2.8}$$

And the mentioned vertical shift of prisms to the sphere is :

$$z_{\text{shift}} = \frac{d^2}{2R_s} \tag{2.9}$$

where, d is the pythagorean distance from the central point of the mesh.

We used the orthographic equatorial projection for the inner domain, which is automatically centered on each computational point using Pyproj library functions.

The orthographic projection has the advantage of preserving both angles and distances approximately equal to those on the sphere for distances < 100 km from the point of tangency, with horizontal positioning errors < 100 m.

The approximative orthogonality and constant relative distances between parallels and meridians on both the tangent plane and the local sphere ensures the mesh not being excessively distorted by the projection, up to the limits imposed to the topographic corrections, which never exceed ~237 km, i.e., $167.375\,\sqrt{2}$ km.

The standard of 166.735 km is the outer radius of the Hayford-Bowie Zone 0, and it marks the distance that minimizes the difference between the spherical cap and the infinite-horizontal slab, for thicknesses < 4 km (LaFehr, 1991).

Moreover, the orthographic projection equations are relatively simple and can be easily handled by either the Gdal or the Pyproj libraries in python (eq. 2.10).

The downside is that this projection depicts only one hemisphere, and it visibly distorts the meridians and reduces the distances between parallels, from approximative 10° to the origin (Figure 2-7).

The transformation equations from spheric to planar coordinates can be derived from simple trigonometry (Snyder, 1987):

$$\begin{cases} x = R_s\, cos\varphi\, sin\lambda \\ y = R_s\, sin\varphi \end{cases} \tag{2.10}$$

where, x and y are the projected coordinates onto the tangent plane at the geographic origin (0,0).

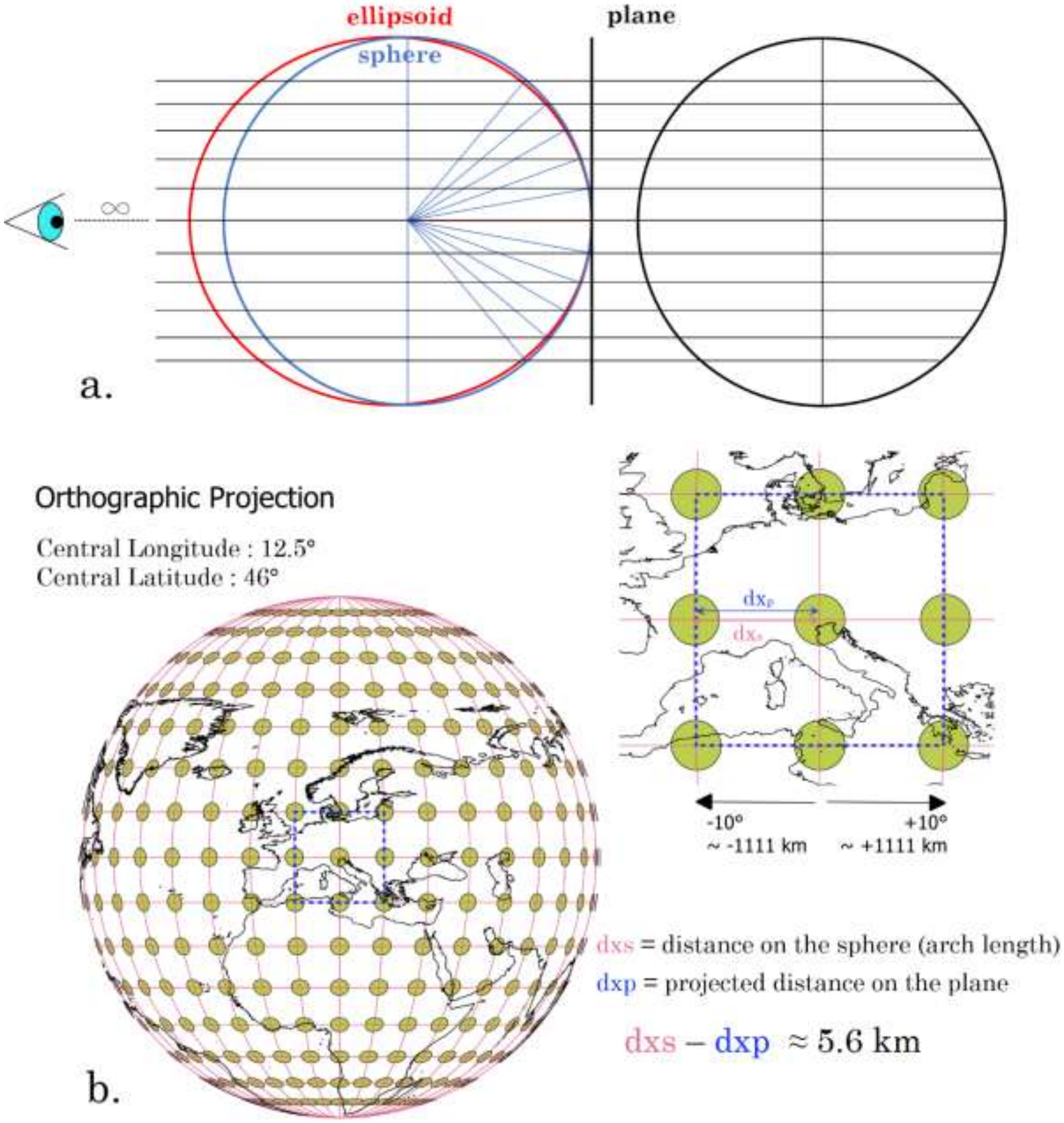

Figure 2-7 Sketch of the orthographic projection at the equator (a), in which both the ellipsoid and the local sphere are tangent to the vertical plane at its central point: all projected parallels are straight lines, whether the meridians are gradually deflected to the hemisphere edges where they form complete circles. The lower image (b) is the half globe orthographic projection tangent to the center of the Friuli Venezia Giulia region (Italy). The green circles are the Tissot indicatrix, which visually proves that distortions between parallels and meridians are not appreciable for a few hundreds of kilometers from the projection center, i.e., the domain of topographic corrections.

Once set in the reference frame, then four parameters control the size and resolution of the final mesh (Figure 2-8a,b): the inner radius (**R1**), the outer radius (**R2**), and the two corresponding grid-steps (**gs1, gs2**).

R1 encloses the area where the positioning errors introduced with the orthographic approximation are lower than the DTBM horizontal accuracy. Generally is R1 < 20 km for horizontal accuracies < 0.5 m. Within this domain, we use the Prism-element discretization.

gs1, is automatically set to the average resolution available on the DTMs covering the local study area. For example, our study cases use 100 m for the Gulf of Manfredonia and 50 m for the northern Adriatic and Friuli Venezia Giulia region.

R2, is the standard radius of 166.735 km, up to which we used the Tesseroid-element discretization, i.e., within the domain [R2, R1].

gs2, is automatically set to the lowest resolution available on the DTMs covering the outer area. In our study cases, we have 250 m for the Gulf of Manfredonia and the northern Adriatic region, which corresponds to the average resolution of the EMODnet bathymetry.

The mesh parameters, once selected, are automatically adjusted to have the inner and outer area perfectly matching onto the projected plane without changing the value of **gs1.**

The use of Prisms over Tesseroids for the inner area (R1) has two main advantages:

1. the possibility to set the computational point directly on the topographic surface, or even below it (e.g., with sea-bottom stations), being the analytical solution of the prism valid on any point, either outside or inside of the element (Nagy, Papp, & Benedek, 2000; Nagy, Papp, & Benedek, 2002; Uieda, Soler, Pesce, Oliveira Jr, & Shea, 2020);
2. faster results in terms of computational time;

However, the straight lines forming the mesh at the inner zone's edges cannot perfectly match the parallels and meridians on the sphere. Therefore, areas of partial superposition between Prisms and Tesseroids occur.

Also, the side of the Tesseroid, which is normal to the sphere's surface, is not congruent to the corresponding Prism lateral side, which is perpendicular to the tangent plane instead.
This inconsistency generates gaps between the two elements, even when the bases are approximately aligned (Figure 2-8c).

Other distortions between the projected mesh and the meridians occur approaching the outer limits of the mesh (167 km). However, the effect is less relevant in this case, being the tesseroids positioned far from the computational point.

We evaluate possible errors in the gravity effect derived from the Prism-Tesseroid mesh by comparing it to a uniform spherical cap computed using a unique Tesseroid-element (Figure 2-9a,b). For the test, we use a mesh extending 167 km (R2), with the inner grid-step of 250 m (gs1), the inner radius of 15 km (R1), and the outer grid-step of 1000 m (gs2). Then, using the harmonica library, we compute the tesseroids gravity effect, imposing a distance-size ratio of 10 (Uieda, Barbosa, & Braitenberg, 2016; Uieda, Soler, Pesce, Oliveira Jr, & Shea, 2020).

The difference between the models increases with the thickness of the cap (Figure 2-9c) and with the elevation of the computational point from the cap up to 5 km (Figure 2-9d). However, it does not exceed 0.02 mGal for cap thickness < 4.5 km, making the Prism-Tesseroid mesh suitable for computing topographic effects in all the alpine regions since the spherical reference cap overestimates any possible real topographic effect.

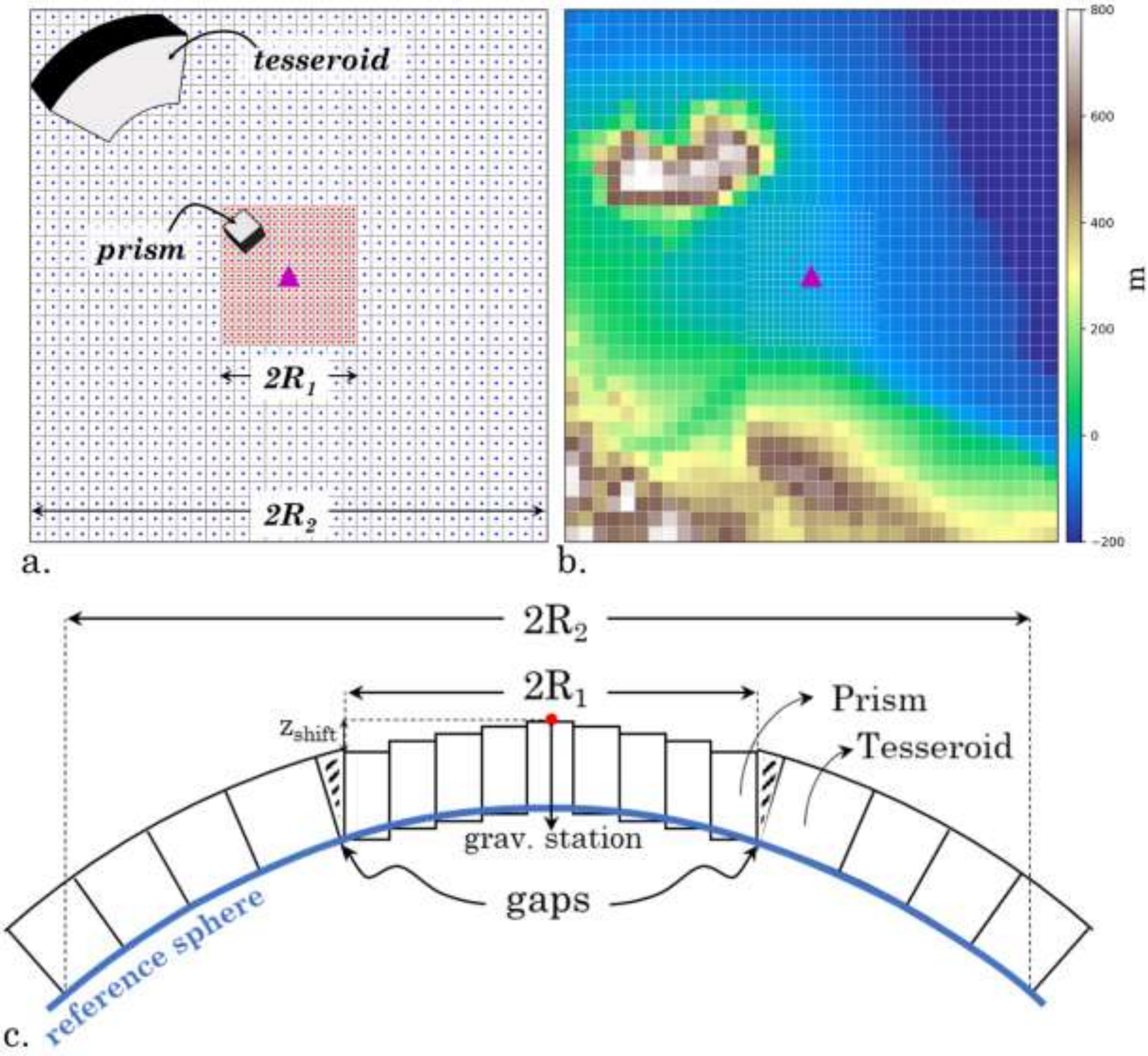

Figure 2-8 - Sketch of the mesh used for topographic corrections (a), defined within the frame of the orthographic projection centered in the Gulf of Manfredonia (b). When re-projected on the sphere in geographic coordinates (sketch, c), the inner Prism-elements and the outer Tesseroid-elements do not match perfectly, and gaps or partial superpositions occur.

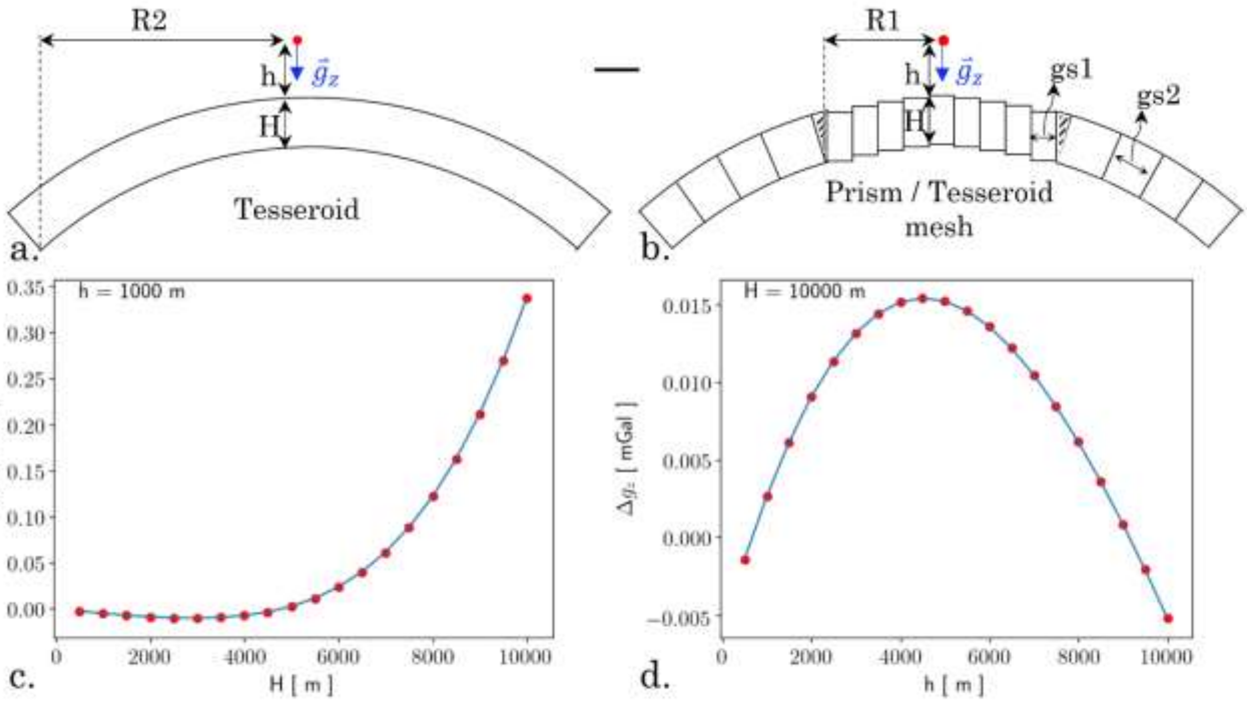

Figure 2-9 - Differences between the gravity effect of (a) a Tesseroid-block (spherical cap), extended for 167 km ***(R2)*** *and (b) the Prism-Tesseroid mesh of the same extent, with the inner radius of 15 km (****R1****), the inner grid-step of 250 m* ***(gs1)*** *and the outer grid-step of 1000 m* ***(gs2).*** *Differences are computed for (c) various cap thicknesses (H) and (d) various elevations of the computational point above the cap (h).*

2.1.3.3 Topographic effects in different conditions

When computing the Bouguer anomaly, we have to consider the position of the gravity station to the surrounding known masses.

If the measurement point lies on the sea surface (as for shipborne or altimeter-derived gravity), the reference model must be corrected for effects of crustal masses above the station and water masses below it (Figure 2-10a,b),

We therefore calculated the topographic effect, Te, by summing (i) the vertical upward attraction of crustal masses above the reference surface (Zone A), and (ii) the drop in the gravitational attraction due to the presence of water in place of the crust in marine areas (Zone B). In this computation we used the constant density of 2.67 g/cm^3 for the crust, ρ_c, and 1.03 g/cm^3 for the water density, ρ_w (Figure 2-9b, eq.2.11).

The same is identical for measurement points above the reference surface (e.g., land-based stations or air-borne measurements). The difference is that the attraction of topographic masses may be either positive or negative, depending on the elevation of the computational point to the surrounding topography.

$$\begin{cases} \text{Zone } (A): \; g_e(h, 0, \rho_c) & \text{if } h > 0 \\ \text{Zone } (B): \; g_e(0, h, \rho_w - \rho_c) & \text{if } h < 0 \end{cases}$$

$$Te_{l,s} = \sum_A g_e(h_t, h_b, \rho) + \sum_B g_e(h_t, h_b, \rho) \qquad (2.11)$$

where g_e is the gravitational attraction of a prism, with h_t and h_b being the top and the bottom height of the element, respectively, and h the height given by the DTBM model.

This approximation may vary locally because of inland depressions (continental areas below the reference surface) or inland water masses (e.g., large lakes or lagoons). Therefore, further corrections should be included in eq. 2.11 to account for these possible local effects, eventually.

The situation is different for sea-bottom stations. In this case, the gravitational effect of the reference model, g_{th}, after the free-water correction, lacks the attraction of masses above the computational point that are not distributed within an homogeneus spherical wa shell, as we assumed in eq. 2.17. Instead, they are spatially divided between crust and water, and their gravitational attraction must be accounted in the final computations (Figure 2-10d).

The gravity effect of all the known masses heterogeneously distributed above the computational point, i.e., within Zone(A) and Zone(B), results in an upward attraction (negative), that must be added to the downward vector of the theoretical gravity (positive).

The remaining effects of masses below the computational point (Zone(C), Figure 4d) should be treated like those of sea-surface stations, i.e., by removing the effect of crust and adding back the effect of water (eq.2.12).

The problem is solved by dividing the DTBM model into three zones (Gantar, 1983; Nowell, 1999).

$$\begin{cases} \text{Zone } (A): \; g_e(h, h_s, \rho_c) & \text{if } h > 0 \\ \text{Zone } (B): \; g_e(0, h, \rho_w) + g_e(h, h_s, \rho_c) & \text{if } h_s < h < 0 \\ \text{Zone } (C): \; g_e(0, h_s, \rho_w) + g_e(h_s, h, \rho_w - \rho_c) & \text{if } h < h_s < 0 \end{cases} \quad (2.12)$$

$$Te_{sb} = \sum_A g_e(h_t, h_b, \rho) + \sum_B g_e(h_t, h_b, \rho)$$

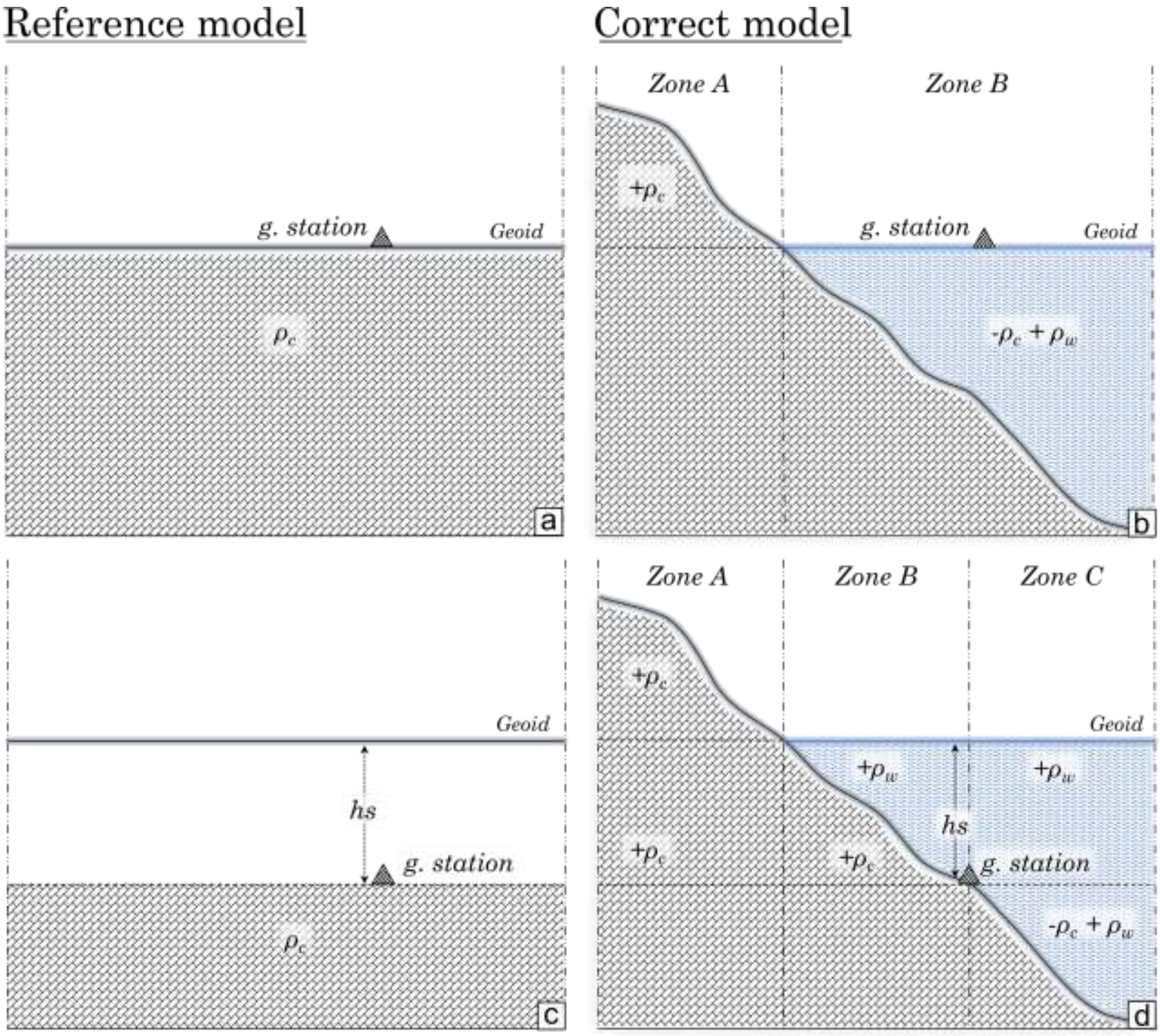

Figure 2-10 Schematic representation of models used to compute the topographic effects of sea-surface gravity (a, b, eq.7) and sea bottom gravity (c, d, eq.8). On the left, the reference model, and on the right, the correct model, including all the density corrections that must be added to the reference model in order to come to a correct estimate of the topographic effect.

The total topographic effect computed using our python workflow (Prism / Tesseroid mesh) was compared to the same calculated with the Tc software (Forsberg, 1984).

Most of the differences are in the range of gravity data error (Table 1), except for higher max values of ±10 mGal, found in mountain regions (Figure 2-11).

The Tc solution is based on prisms only, and it uses spline functions to readjust the topographic grids to the selected limits and resolutions, modifying the initial elevations. The different interpolation strategy is probably the primary cause of differences in areas of rough topography.

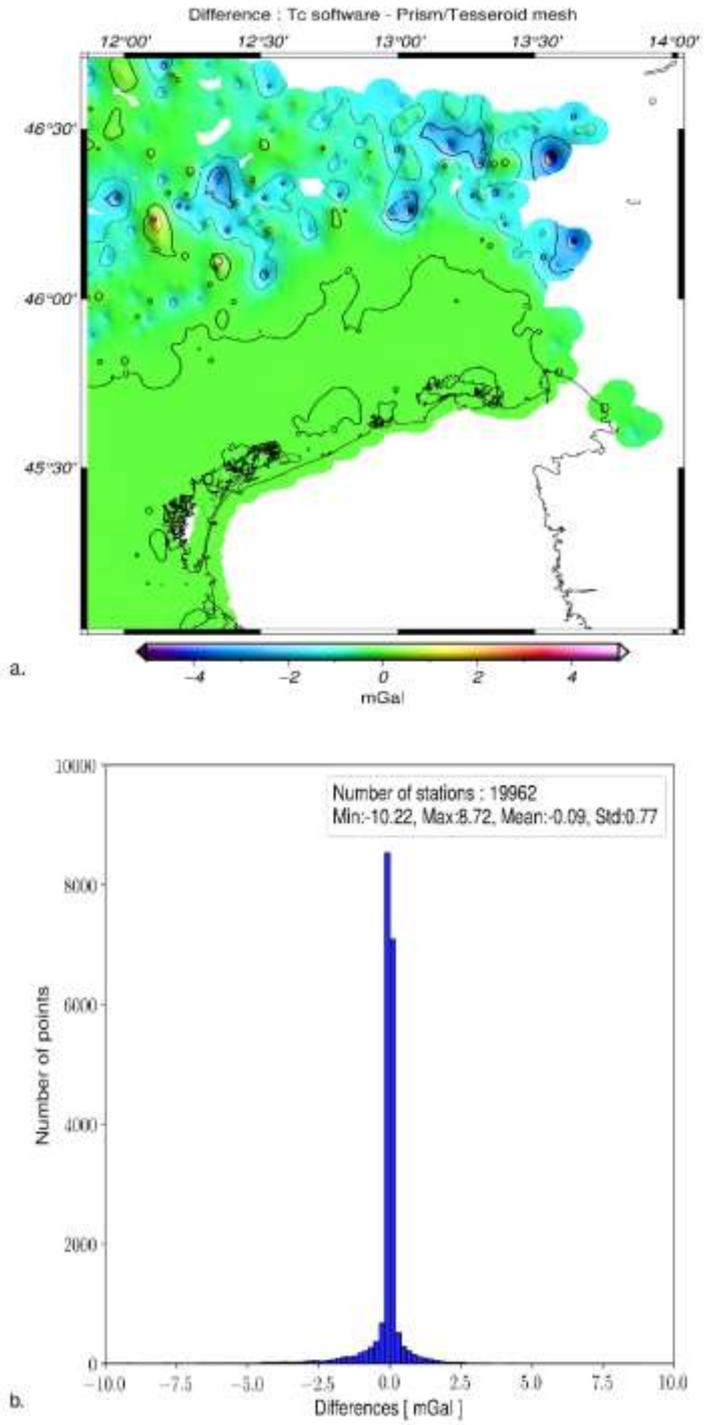

Figure 2-11 - Differences between topographic effects calculated with the Tc software (Forsberg, 1984) and with the Prism/Tesseroid mesh described in the text; the gravity data points used for this comparison-test are taken from the TRANSALP dataset (Figure 1-7), and the input DTMs are created using the merging method described in paragraph 2.1.3.1 (Figure 2-5).

2.1.4 Upward continuation

The Bouguer anomaly of sea-bottom data, as a final step, must be upward continued from the seafloor surface to a constant mean sea level. This processing step is essential to have the sea-bottom values on the same equipotential surface of the altimeter and shipborne gravity data (Ballu, Dubois, Deplus, Diament, & Bonvalot, 1998).
Several methods can be used to compute the upward continuation of potential field data, among which the most popular involve transformations in the wave-number domain and/or the interpolation of the scattered data on regular grids (Pilkington & Boulanger, 2017).

In the case of the sea-bottom stations surrounding the Italian coasts (Figure 1-8), this computation is complicated by the fact that the points are not homogeneously distributed, and the station depths are almost always smaller than the relative distances to the neighboring data points. Therefore, the upward continuation magnitude is often in the same range of the numerical integration or gridding errors occurring with the mentioned solutions.

Thus, we decided to use an upward continuation strategy based on the equivalent layer method, which does not require transformations in the frequency domain or interpolations on regular grids (Dampney, 1969; Soler & Uieda, 2021). The equivalent layer method uses harmonic solutions of the potential field to predict gravity on any point in the source-free space, satisfying the Dirichlet boundary condition. It assumes that the gravity anomaly is generated by an arbitrary set of point-mass sources distributed below the observation point. After setting the relative source's depth, the gravity field of the equivalent-synthetic layer is fitted to the observation points through a minimization process. Thus, the final physical parameters predicted for the fictitious sources can be used to calculate the gravity field at any other point in the space above the sources, i.e., at different elevations.

We used the "*EQLHarmonic*" function from the Harmonica library to obtain the equivalent-layer solution (Uieda, Soler, Pesce, Oliveira Jr, & Shea, 2020). In addition, we included among the inputs the shipborne data collected out of a radius of 2 km from the sea bottom stations, other than the sea-bottom station themselves. This precaution gives a higher constraint to the solution at the sea level.

Finally, after some testing, we set the relative depth of the equivalent sources at 15 km and the dumping regularization parameter equal to 3, which gives an acceptable R^2 score and minimizes the differences between sea-surface and sea-bottom data calculated by linear interpolation to the coordinates of sea-bottom data.

We used the upward continuation only in the northern Adriatic Sea area and not in the Gulf of Manfredonia, where we considered it a negligible effect.

2.1.5 Merging local data with global gravity models

The Bouguer gravity resulting from our processing in the different study areas was interpolated on regular grids using a 1x1 km grid step with the minimum curvature algorithm named "surface" available in the GMT software utilities (Wessel et al., 2019).

However, not all the grid nodes were sufficiently close to the gravity stations. In particular, we have no data points in the areas near the borders of Austria and Slovenia.

The resulting gaps are often a problem for numerical analysis on gravity anomaly grids such as filtering, derivations, or wave-number transformation.

Therefore, instead of using classical interpolation methods to fill the gaps (e.g., minimum curvature or kriging), we used the data from the EGM08 model, gridded at the resolution of ~18 km.

To merge multiple gravity datasets at different resolutions, we adopted the same computational strategy used for topographic models described in paragraph 2.1.3.1

Before this operation, we shifted our grids to the same mean of the EGM08 data avoiding systematic biases between the two datasets.

Despite being relatively trivial to the more sophisticated Least Square Collocation strategies (Torge & Müller, 2012, p. 301-303), our solution has the great advantage of not modifying the original high-resolution grids except for small amounts at the edges. At the same time, it creates a smooth-gentle transition to the surrounding EMG08 values without changing the frequency content of any of the integrated datasets.

2.2 Leveling

When merging shipborne gravity or magnetic data recorded with different instruments and at different times, the most problematic issue is the line-leveling.

Differences between parallel and crossing survey lines can have various origins :

1. poor navigation data (gravity and magnetic);
2. residual velocity effects after non-accurate Eötvös correction (gravity);
3. residual tidal effects (gravity);
4. residual instrumental drift (gravity);
5. non-accurate instrument calibration (gravity – magnetic);
6. non-accurate diurnal corrections (magnetic).

We used the combination of a remove/restore solution and a statistical redistribution of the cross-over errors to reduce any possible bias occurring between the different lines.

The remove-restore method takes the long-wavelength Free-air anomaly of each line and substitutes it with the same derived from satellite altimeter data (Figure 2-12a).
We use the S&S gravity data as a reference for the first step of the computation, which proved to be slightly more accurate than the DTU13. Thus, we selected wavelengths > 16 km from the S&S data and substituted them with those recorded in the shipborne gravity lines. We considered this resolution reliable for altimeter data since the average orbital-track spacing is about 6÷7 km (Fairhead, 2016).

We weighted the remove restore solution using a gaussian function from 0, within the coastline, to 1, at ~16 km offshore (Figure 2-12b). The weighting function avoids the contamination of coastal errors from the altimetry data into the leveled lines. We used the coarser coastline from the GSHHG database to build the grid of the gaussian weights (Wessel & Smith, 2015).

The remove-restore processing can be summarized in four steps and by eq 2.13 :

1. the grid with the gaussian weights is interpolated onto points along the line using a cubic spline;
2. for each point of the line, the mean value of the shipborne gravity is computed by taking into account only the nearest points along that specific line, within a circular window of 8 km radius which filters out the wavelengths < 16 km;
3. the same circular window is used to compute the average of the nearest satellite altimeter gravity data;
4. the shipborne-derived mean is then subtracted from the original gravity value, the altimeter-derived mean is added back, and in both cases, the average values are multiplied by the gaussian weight assigned to that point in the first step.

The process is iterated for each line, independently from the others.

$$Fa_s(\lambda_i, \varphi_i) = Fa_s(\lambda_i, \varphi_i) - W_i \sum_{\Omega\mathrm{i}(\lambda s, \varphi s)}^{Ns} \frac{Fa_s(\lambda_s, \varphi_s)}{N_s} + W_i \sum_{\Omega\mathrm{i}(\lambda a, \varphi a)}^{Na} \frac{Fa_a(\lambda_a, \varphi_a)}{N_a} \qquad (2.13)$$

where, Fa_s are the Free-air shipborne data, λi, and φi the coordinates i-th point along a line, Wi the gaussian weight assigned to the same point, $\Omega\mathrm{i}$ the domain defined by the circular window of 8 km radius, Ns the number of shipborne data within $\Omega\mathrm{i}$, all belonging to the same line, and Na the total number of altimeter-derived values within the same domain, $\Omega\mathrm{i}$.

The following step involves a specific algorithm for distributing random errors in the network adjustment of potential field data (Mittal, 1984).
The algorithm is based on a weighted average, W_i^* that minimizes the differences at the line intersections, obtaining a vector of cross correction values $C_{i,j}$ (eq., 2.14). The correction values are then interpolated through the lines with spline functions, and the resulting line-correction vectors are added to the original lines.

$$C_{i,j} = \frac{Fa_i W_i^* + Fa_j W_j^*}{W_i^* + W_j^*} - g_{obs} \tag{2.14}$$

where, Fa_i is the Free-air value of the i-th line, at the intersection with the j-th line, Fa_j is the Free-air value of the j-th line at the same intersection; W_i^* is the weight calculated for the i-th line, and W_j^* for the j-th line both at the same ij intersection. Finally, g_{obs} is the observed original anomaly at the crossing point under consideration (for more details about the derivation of W_i^*, see the referenced Mittal, 1984).

Although the gaussian weight (W_i) avoids coastal noise to contaminate the leveled data, it also introduces an artificial bias in the coastal segments of the survey lines. By checking for this effect in the leveled lines, with and without the remove restore component, we found a slight systematic tilt < 1 mGal, at distances < 16 km from the coast, plausibly caused by the gaussian weight. However, we considered this bias an acceptable and predictable cost if compared to the errors introduced when omitting W_i, which are in the order of 3 to 20 mGal and unpredictably distributed along the coasts.

We use the same method to level the magnetic data MagOGSMed (Table 1, Figure 1-9). In this case, the reference model is the EMAG02, from which we selected wavelengths > 55 km for the remove-restore procedure, based on its tested accuracy up to the 720 spherical harmonic degree and order (Oehler, Rouxel, & Lequentrec-Lalancette, 2018).

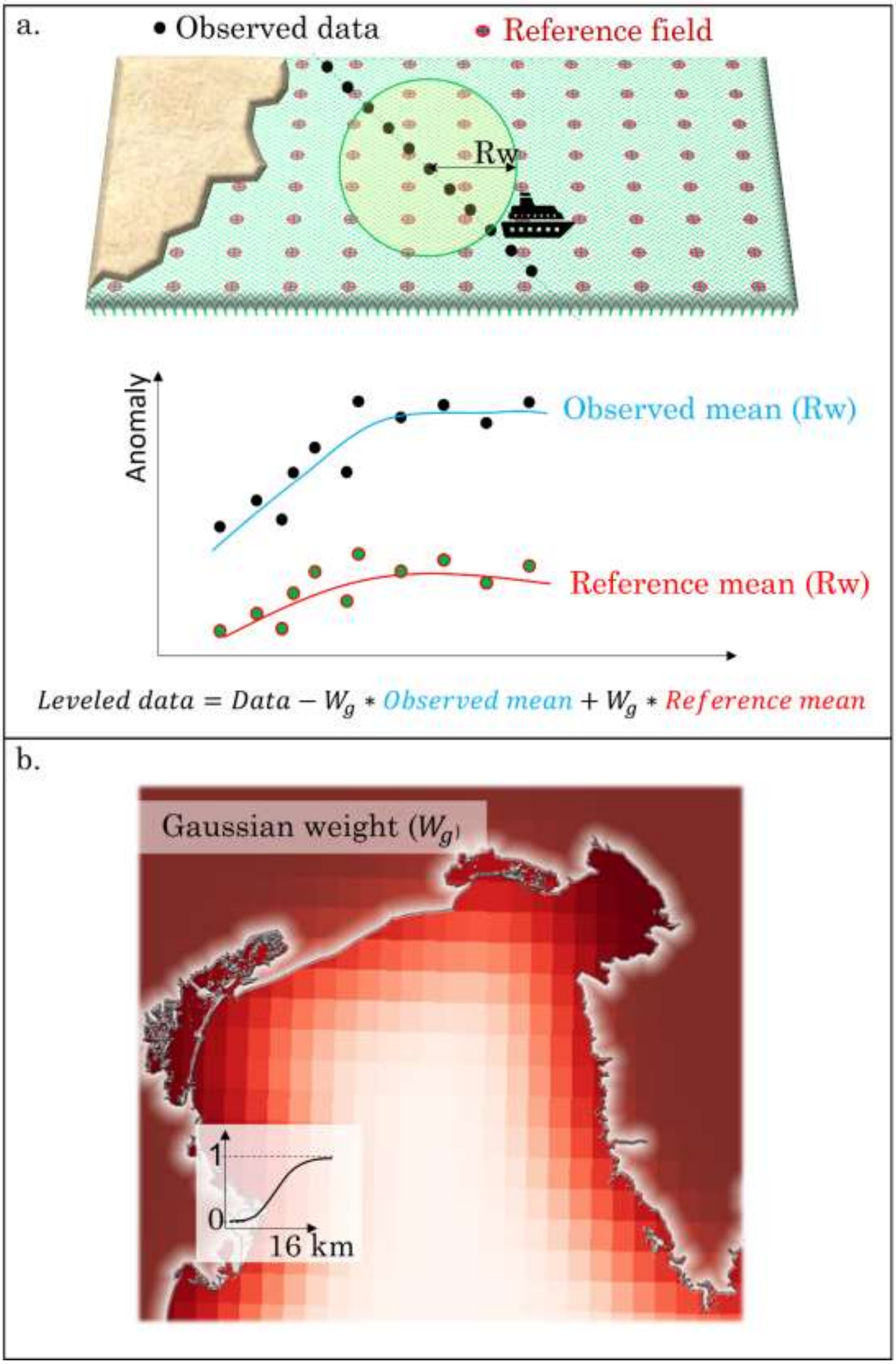

Figure 2-12 - (a) Explanatory sketches of the remove-restore leveling method discussed in the text and (b) grid of gaussian weights used in the computation to avoid coastal-noise from altimeter data to fill in the leveled signals; the grid of weights is the one used for the northern Adriatic Sea.

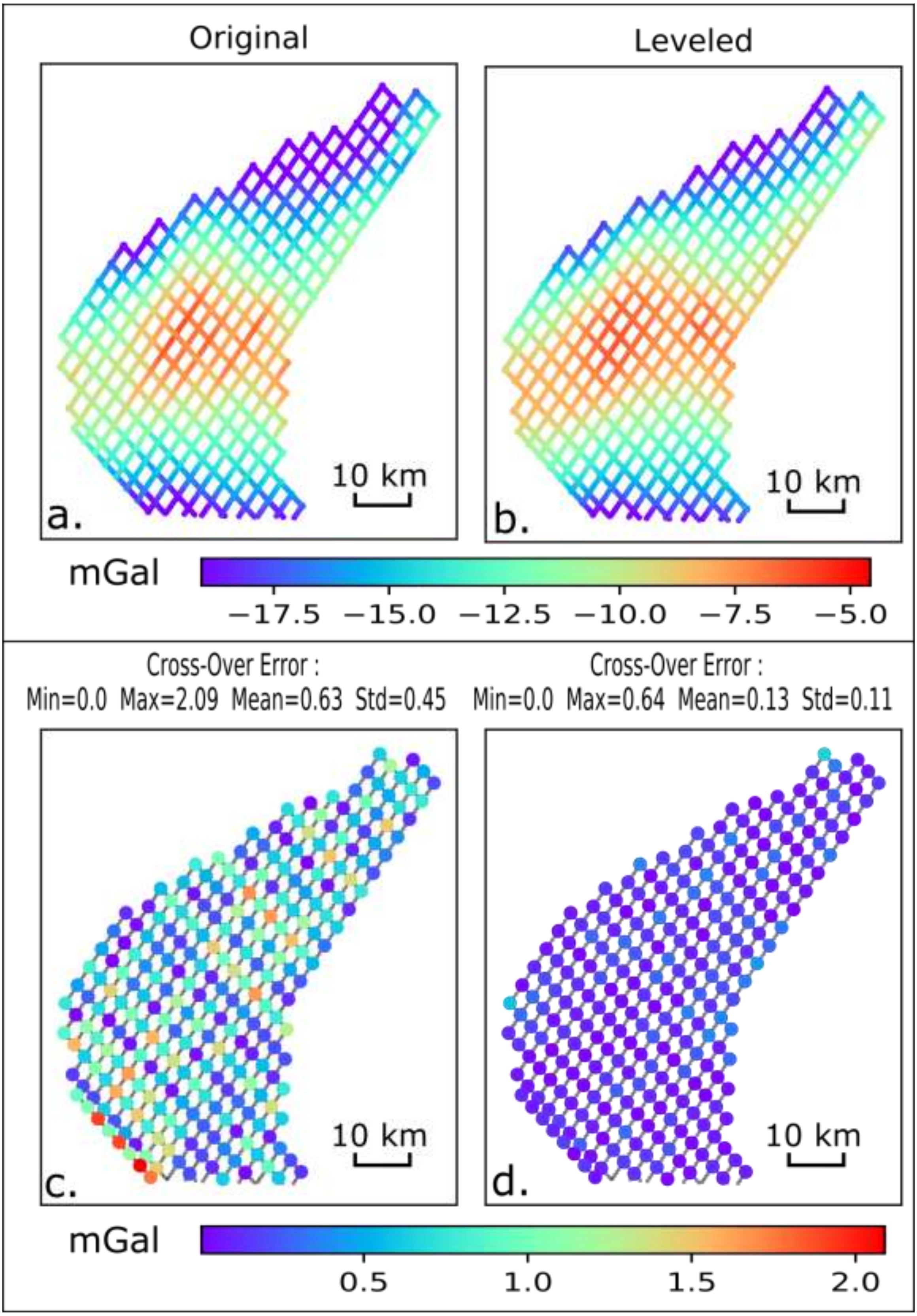

Figure 2-13 - Example from the leveling of the RIG82 shipborne gravity dataset; the diagrams show (a) the original Free-air anomaly, (b) the leveled anomaly, (c) the differences at the intersections before leveling, and (d) after the leveling.

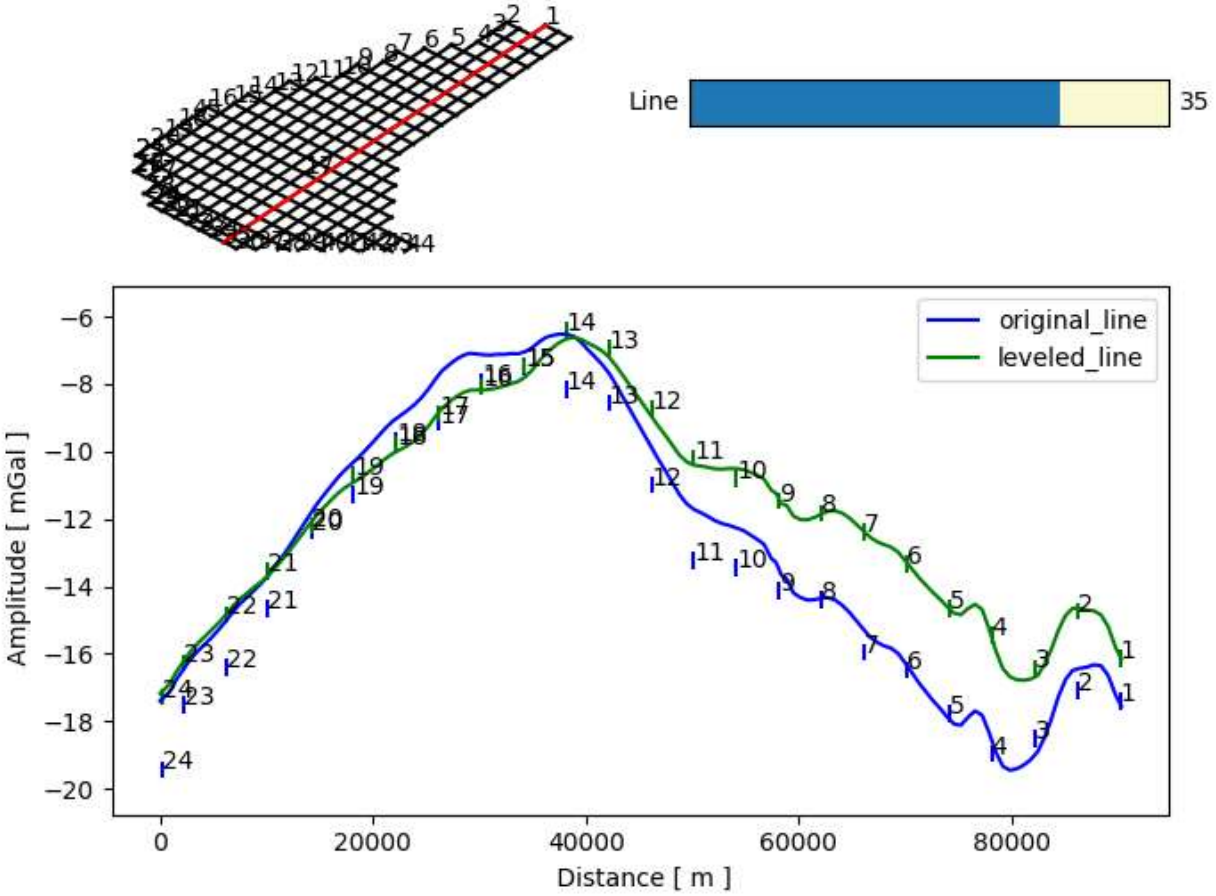

Figure 2-14 - Example of the result from the leveling of a line extracted from the RIG82 shipborne data (Table 1, Figure 2-13). The high-frequencies > 1/16 km are perfectly preserved from the original line, and all the crossings (vertical bars) match the leveled line.

2.3 The geophysical Indirect Effect

The Bouguer anomaly was further adjusted for the additional geophysical Indirect Effect, δg_{IE}. This correction (eq. 2.14) includes two components (Hinze, et al., 2005):

$$\delta g_{IE} = 0.3086\, N - 2\pi G\rho\, N \tag{2.14}$$

The first member on the right side of the equation is the first-order approximation of the quantity introduced in section 2.1, i.e., the Indirect Effect (Li & Götze, 2001). It accounts for differences between the orthometric heights (above the geoid) and the actual elevation of the gravity stations above the reference ellipsoid surface (ellipsoidal heights). The second member accounts for the gravity effect of the masses interposed between the ellipsoid and the geoid, and it is calculated using the simple plate approximation with a reference density ρ, of 2.67 g/cm^3.

For this computation, we used the geoid undulation (N), as derived from the EGM08 spherical harmonic model to degree and order 2190, using the calculation service of the International Centre for Global Earth Models (Ince, et al., 2019).

The amplitudes of the geoid undulation are considerably small for wavelengths <100 km (Hinze, et al., 2005). Therefore, in smaller areas, the correction δg_{IE} it is usually just a constant shift of the anomaly that can be safely neglected since geophysical studies investigate the gravity variation in space and not its absolute value.

However, the Indirect Effect may not be a simple constant shift in regions characterized by known geological complexities at the crustal/mantle level, such as collision zones. In these areas, N could be closer approximated by a first or a higher-order polynomial surface, which can sometimes be confused with real geological signals (e.g., the gravity effect of the foredeep sedimentary basins).

In this regard, a complex geodynamic setting characterizes the Italian peninsula, shaped by two very different orogens, the Alps and the Apennines, a few hundred kilometers apart and verging in almost opposite directions, and by the front of the Dinaric Arc to the East. All these elements, related to crustal dynamics, presumably contribute to the shape of the Italian geoid, which can not be approximated to a simple constant surface in almost none of the Italian regions. Consequently, also the geophysical Indirect Effect can not be considered constant, despite its low amplitudes, i.e., ~2 mGal (Figure 2-15).

The removal of δg_{IE} from the Bouguer anomaly could have been avoided by directly using ellipsoidal height in the previous gravity reductions, which would have meant to compute the gravity disturbance instead of the classical Free-air anomaly.

However, the satellite altimeter gravity used in the leveling procedure is originally a Free-air anomaly, and the sea-water depths of marine data are measured relative to the geoid (i.e., mean sea level). Therefore it was more straightforward to correct gravity data for δg_{IE}, afterword.

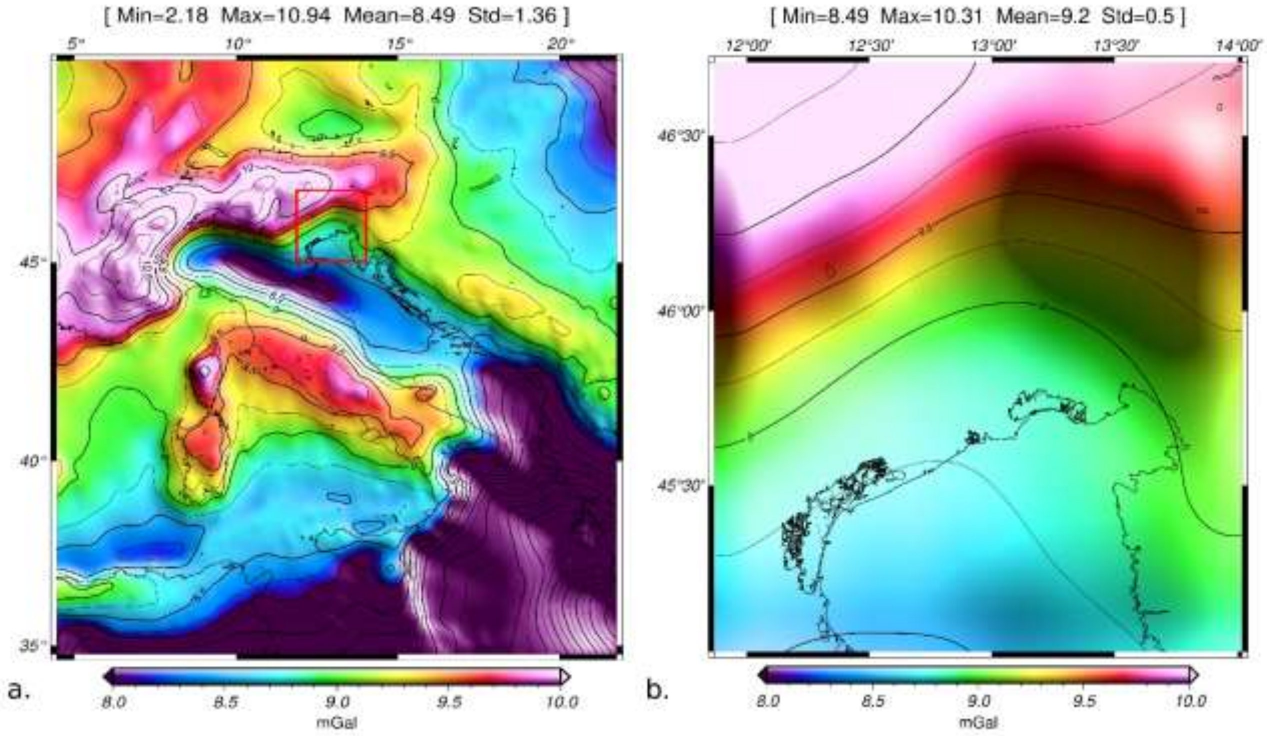

Figure 2-15 - Geophysical indirect effect (eq. 2.14) calculated over Italy (a), with a focus to the north-east of the peninsula, on the Friuli Venezia Giulia Region and northern Adriatic Sea (b).

2.4 Gravity data analysis

2.4.1 Regional-residual separation

When investigating local-shallow density contrasts, it is usual to remove the effects of long-wavelength regional signals from the Bouguer anomaly.

In most cases, long-wavelength signals are generated by deep sources, such as the Moho or the crystalline basement. For example, in Italy, both these interfaces are characterized by wavelengths longer than 100 km, and the remaining short-wavelengths are mainly the result of variations in the bedrock/sediments interface (Corrado & Rapolla, 1981).

We tested different classical regional-residual separation methods, i.e., polynomial regression (Agocs, 1951), wavenumber domain filtering using low-pass Butterwort operators (Keating & Pinet, 2011), and upward continuation filters (Kebede, Alemu, & Fisseha, 2020).
All these methods involved the arbitrary choice of different parameters: the polynomial order, the cut-off wavelength, or the continuation height, which may vary from place to place. Moreover, the Fast Fourier Transform (FFT) involved in wavenumber methods may also introduce nasty artifacts in the presence of high gravity gradients or when the gridded data are not correctly padded (which leads to Gibs effects).
Another possible solution was to remove the gravity data within the investigated area and fill the gaps by interpolating the inner region given the outer values using spline functions (Mickus, Aiken, & Kennedy, 1991; Cella, Nappi, Paoletti, & Florio, 2021). However, this is possible when the anomalies are confined to a specific geological setting (e.g., a closed sedimentary basin) and the boundary with the outer data is somehow "naturally defined".

We then decided to test an alternative method based on a detrend operator, suitable for the study case of the Friuli Venezia Giulia region.

The idea is based on the assumption that the long-wavelength components of the gravity field can be approximated by a first-order polynomial trend within small domains (local areas), framed with a sliding window. We considered this assumption valid on areas < 25 km^2, assuming regional field wavelengths longer than ~100 km. Thus, we define a moving window operator with a size of ~25 km, sliding over the Bouguer anomaly grid, which removes the effect of a first-order linear trend fitting the sparse data found within the window.

This operator is conceptually similar to a high-pass filter in the frequency domain but with the advantage of being unbiased by FFT artifacts and directly tied to the original gravity values.

If the gravity grid is considered reliable enough (i.e., not affected by significant interpolation errors), the detrend function can be computed directly using the grid values instead of the sparse stations' points.

2.4.2 Amplitude derivatives

Gravity field derivatives are commonly used in geophysical studies to enhance lateral density contrasts in-depth (Fedi & Florio, 2001; Aydogan, 2011; de Lerma et al., 2015).

We tested different combinations of field-derivatives to track the fault network system intercepting the bedrock beneath the sedimentary cover of the Friuli Venezia Giulia Region and the Gulf of Manfredonia.

Specifically, we used the ISVD, the Tilt, the Theta, the Terracing functions, which are briefly described in the following paragraphs.

2.4.2.1 ISVD

The integrated second vertical derivative (ISVD) is an alternative method to compute the first vertical derivative of the gravity anomaly (VDR). Unlike the classical one-step derivation in the Fourier domain (Blakely R. J., 1996, p. 326), The ISVD computes the derivative in three different steps (Fedi & Florio, 2001):

1. the vertical integration of the gravity anomaly grid in the frequency domain (eq. 2.15);
2. the computation of the second-order horizontal derivatives using finite-differences, i.e., using the convolution operator, "$*$" (eq. 2.16, eq. 2.17);
3. the computation of the first-order vertical derivative, which combines the results from the previous step through the Laplace equation (eq. 2.17, eq. 2.18).

$$U(x,y) \approx FFT^{-1}\left\{ \frac{1}{|k|}\, FFT\,[\,g(\,x,y\,)\,]\,\right\} \tag{2.15}$$

$$\frac{\partial \mathrm{U}^2(x,y)}{\partial \mathrm{x}^2} \approx \left(U(x,y) * \begin{vmatrix} 0 & 0 & 0 \\ 1 & 0 & -1 \\ 0 & 0 & 0 \end{vmatrix} \right) * \begin{vmatrix} 0 & 0 & 0 \\ 1 & 0 & -1 \\ 0 & 0 & 0 \end{vmatrix} \tag{2.16}$$

$$\frac{\partial \mathrm{U}^2(x,y)}{\partial \mathrm{y}^2} \approx \left(U(x,y) * \begin{vmatrix} 0 & 1 & 0 \\ 0 & 0 & 0 \\ 0 & -1 & 0 \end{vmatrix} \right) * \begin{vmatrix} 0 & 1 & 0 \\ 0 & 0 & 0 \\ 0 & -1 & 0 \end{vmatrix} \tag{2.17}$$

$$\frac{\partial \mathrm{g}(x,y)}{\partial \mathrm{z}} = \frac{\partial \mathrm{U}^2(x,y)}{\partial \mathrm{z}^2} \approx - \frac{\partial \mathrm{U}^2(x,y)}{\partial \mathrm{x}^2} - \frac{\partial \mathrm{U}^2(x,y)}{\partial \mathrm{y}^2} \tag{2.18}$$

The first integration works as a low-pass filter to the gravity field, and together with the space-domain derivations, it generates better quality VDR maps than those created with the corresponding FFT method. Indeed, the FFT direct derivation tends to amplify the residual noise, and it may also generate unwanted artifacts in the presence of high gravity gradients (e.g., Gibbs effects).

The vertical derivative is essentially a high-pass filter that enhances relatively shallow density contrasts of the gravity anomaly (Figure 2-16a). Notably, it has the advantage of approximately marking lateral contacts or faults where its value is equal to 0. However, this property is not reversible: not all the zero values can be interpreted as geological features. Thus, in practice, only specific segments of the zero contours should be considered in the interpretations, and specifically where other evidence suggested the presence of buried geological contacts (Fairhead, 2016, p. 189-192).

2.4.3 Tilt and Theta

The tilt derivative is the angle obtained from the ratio of the VRD (in our study, we used the ISVD) and the first-order horizontal gravity gradient (Miller & Singh, 1994). In this function, the gravity gradient is simply the Pythagorean sum of the horizontal derivatives of the gravity anomaly, each computed using the finite-difference convolution.

$$\mathrm{Tilt} = \mathrm{atan}\left(\frac{\mathrm{ISVD}}{\sqrt{\left(\frac{\partial \mathrm{g}\ \mathrm{x,y}}{\partial \mathrm{x}}\right)^2 + \left(\frac{\partial \mathrm{g}\ \mathrm{x,y}}{\partial \mathrm{y}}\right)^2}}\right) \tag{2.19}$$

The tilt has the advantage of being normalized within ± $\pi/2$; thus, it saturates faster than other functions on the top of the investigated bodies, even in the case of anomalies with low amplitudes. Therefore, the Tilt does not strictly depend on the intensity of the local gravity field but rather on the positivity of the residual anomalies. Moreover, the Tilt inherits the ISDV property of enhancing the fault's edges with zero values (Figure 2-16 b).

The Theta function is simply the cosine of the Tilt. Thus where the Tilt is 0, Theta is equal to 1, which corresponds to the maximum value of its domain [0, 1]. Hence, this function saturates approximately over the top of the edges of the causative sources (Figure 2-16 c).

$$\mathrm{Theta} = \cos\ \mathrm{Tilt} \tag{2.20}$$

2.4.3.1 Terracing

The terracing operator uses the sense of the measured field's local curvature to produce a field comprised of uniform domains separated by abrupt domain boundaries (Cordell & McCafferty, 1989; Nabighian, et al., 2005; Cooper & Cowan, 2009). This operator relies on the curvature of the gravity anomaly: it saturates to the maximum value within the moving window when the local curvature is negative and to its minimum value when the local curvature is positive. We used a Laplacian 2D filter (3x3) rolled over the gravity anomaly grid to estimate the curvature positivity (eq. 2.21, 2.22). The process is iterated multiple times, generally from one to 30, until the investigated targets are well defined in the resulting grid.

$$C(x,y) = \frac{\partial^2 g(x,y)}{\partial x^2} + \frac{\partial^2 g(x,y)}{\partial y^2} = g(x,y) * \begin{vmatrix} 0 & -1 & 0 \\ -1 & 4 & -1 \\ 0 & -1 & 0 \end{vmatrix} \tag{2.21}$$

$$Terr(x,y) = \begin{cases} Max[\, g(x_i, y_i) \,]_{i\pm1, j\pm1}, & if\ C(x_i, y_i) < 0 \\ Min[\, g(x_i, y_i) \,]_{i\pm1, j\pm1}, & if\ C(x_i, y_i) > 0 \\ g(x_i, y_i), & if\ C(x_i, y_i) = 0 \end{cases} \tag{2.22}$$

The terracing operator, at each iteration, verticalizes the gravity gradient over local density contrasts, reducing the gravity anomaly to a composed step-function.

Mapping and profiling with the terracing algorithm make it easier to identify the horizontal shape of the targeted sources and the position of the lateral density contrasts (Figure 2-16 d). Nevertheless, the operator is also quite sensitive to the data noise amplified by the second-order derivation iterated multiple times. Thus, a good practice is to filter the gravity grid before running the algorithm.

One of the most efficient methods to remove the unwanted high-frequency noises is the integration filter used in the ISVD (eq. 2.15), which is also consistent with the physical theory of the potential fields. However, the vertical integration may also remove local signals that could be important in the final interpretation. Thus, we decide to use the Hanning filter instead, which works well by removing local random noise without drastically modifying the original high-frequency content, although it has a more "cosmetic" than any actual physical meaning (Fairhead, 2016, p. 180).

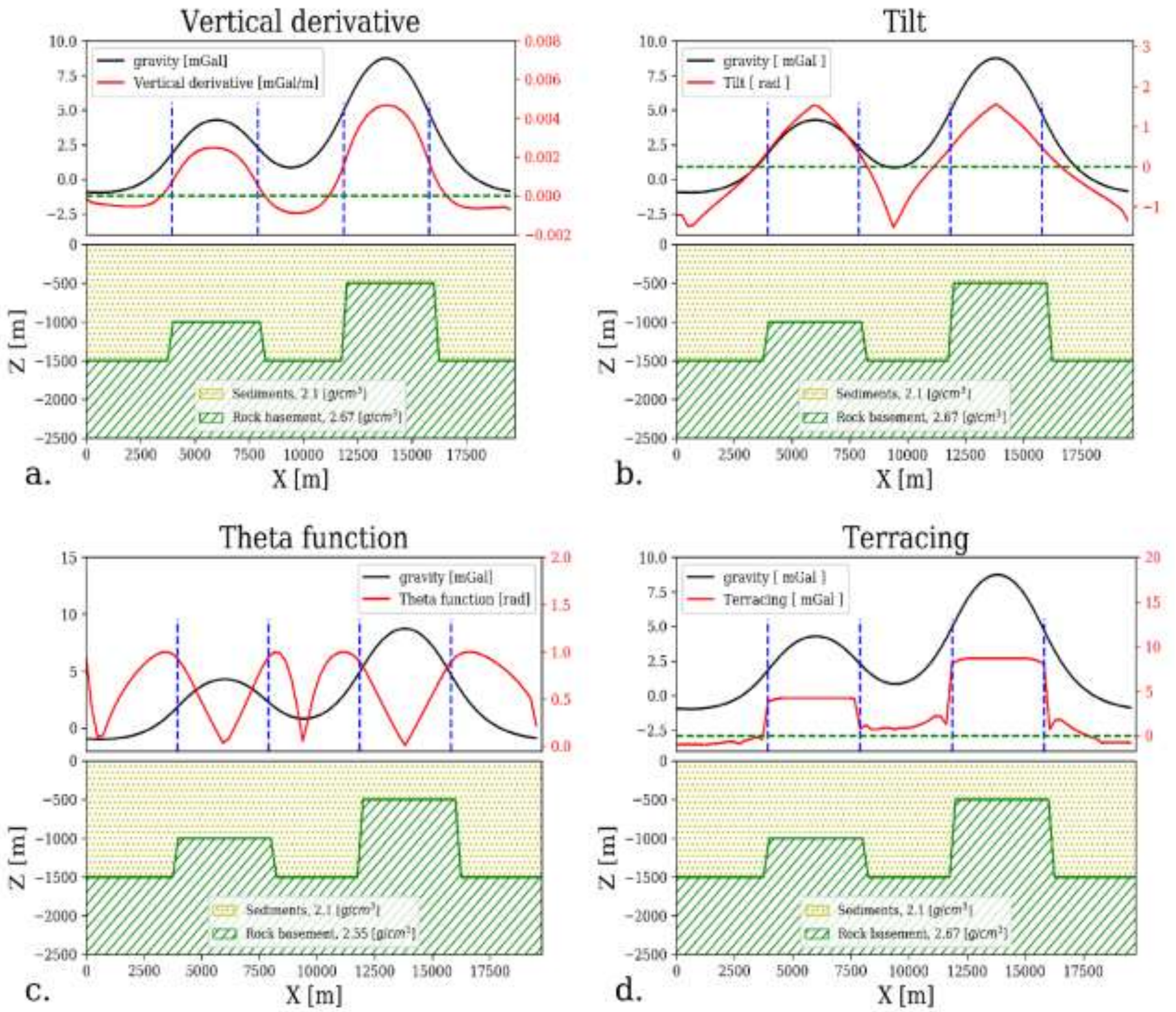

Figure 2-16 - Synthetic tests for different combinations of gravity field derivatives described in the text; the density contrast is that of a simplified case of sediments (2.1 g/cm³) in lateral contact with the lower bedrock (2.55 cm³).

2.4.4 Semi-automatic edge-tracking

We used the Terrace operator combined with the Texture and the Maximum Detection algorithms to obtain a set of lines marking subsurface lateral density contacts from gravity data (Blakely & Simpson, 1986; Hildebrand, et al., 1990).

The Texture operator is a filter transformation that computes the standard deviation $\sigma(x, y)$ of each pixel neighborhood within a window that slides on the Terrace grid (eq. 2.22).
The standard deviation peaks where two or more values exceed the mean within the same window, averaging the variation to the total number of neighboring pixels, Np. This filter property guarantees the spatial continuity and similarity of the edge values from one window to the next.

$$\sigma(x, y) = \sqrt{\frac{1}{Np} \sum_{i=1 \in \Omega}^{N} [\, Terr(x_i, y_i) - \mu \,]^2} \tag{2.23}$$

where, μ is the mean of the squared moving window Ω, composed of N elements.

The Maximum Detection algorithm scans the pixels of the Texture grid (σ) with a 3x3 moving window operator (Ω). This operator verifies whether or not the central value of the window is a relative maximum. It does so by calculating the "inequality indicator", MD, which gives the number of values higher than the central one within the same window.
Best practice indicates that the edges are better outlined when MD is >= 2 or 3 (Fairhead, 2016, p. 212).

$$MD(x, y) = \sum_{\mathrm{i,j} \in \Omega} \left\{ \begin{array}{ll} 1, & if \;\; \sigma_{i-1,j-1} < \sigma_{i,j} > \sigma_{i+1,j+1} \\ 1, & if \;\; \sigma_{i,j-1} < \sigma_{i,j} > \sigma_{i,j+1} \\ 1, & if \;\; \sigma_{i-1,j} < \sigma_{i,j} > \sigma_{i+1,j} \\ 1, & if \;\; \sigma_{i+1,j-1} < \sigma_{i,j} > \sigma_{i-1,j+1} \end{array} \right\} \tag{2.24}$$

We then converted the edges of the MD grid into line vectors using the "r.to.vect" algorithm from the Grass GIS software library (GRASS Development Team, 2017).

We tested this procedure on a simple synthetic model showing the gravity effect of a few simple blocks with different shapes, laying on a tilted plane at an average depth of 2000 m.

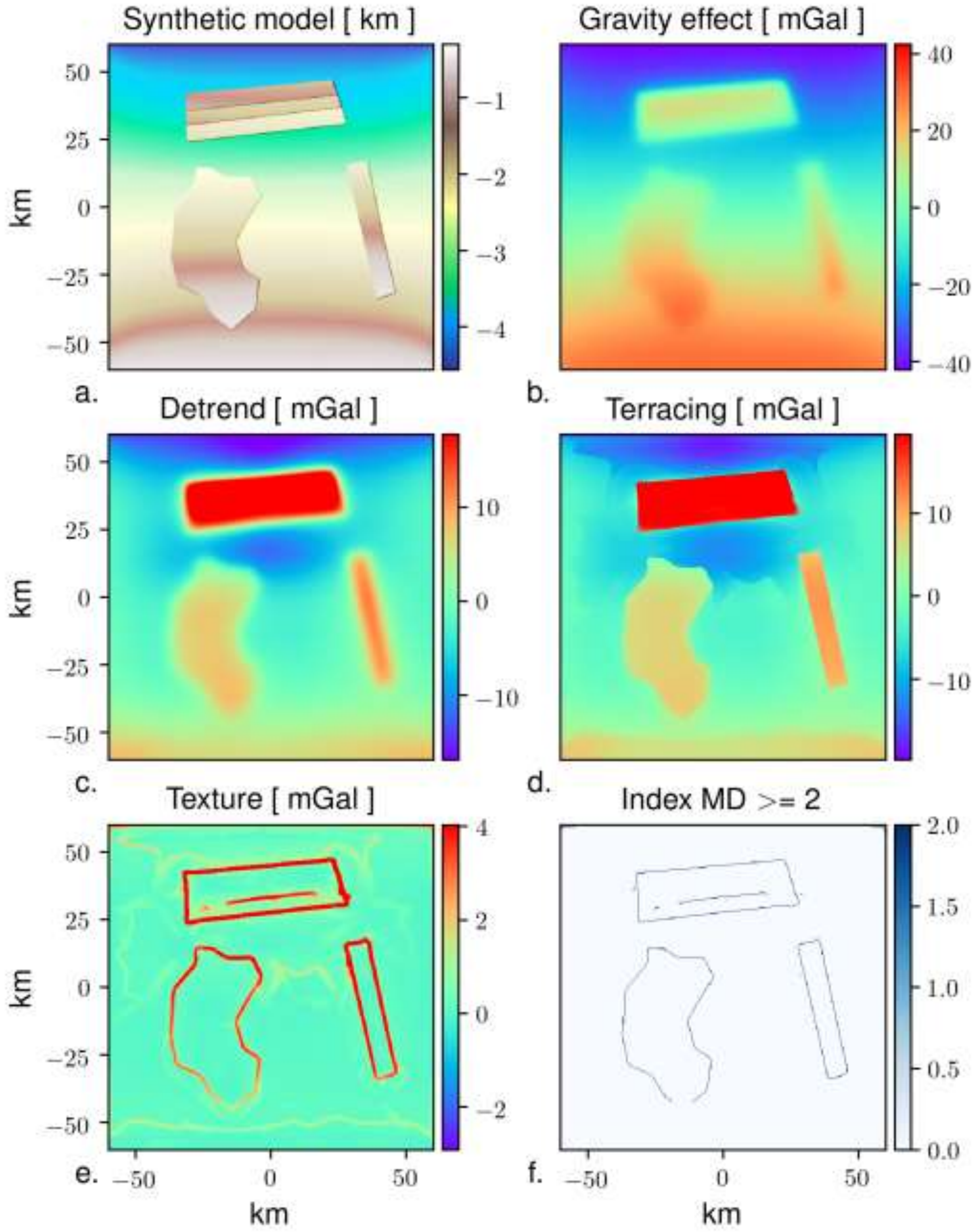

Figure 2-17 - Simple synthetic model used to test the edge-detection workflow; the model (a) combines five blocks with different shapes laying on a tilted plane. First, the gravity effect (b) is computed using Parker (1973), imposing a density contrast of 450 kg/m^3; the following step (c) removes the regional component using the Detrend algorithm described in paragraph 2.4.1, then (d) the terracing algorithm (eq. 2.22) sharpen the gravity gradient over lateral contacts, and (e) the texture operator (eq. 2.23) enhance the edges. Finally, (f) the Maximum Detection algorithm (eq. 2.24) extracts the edge lines.

2.5 Forward modeling

We tested the sensitivity of our gravity data by modeling hidden faults in a few sites where we have the constraints of 2D seismic lines and borehole data.

The objective was to extend the model perpendicularly to the 2D sections obtaining a new 3D model constrained by gravity.

We used three different modeling methods, each of them in different study areas.

2.5.1 Forward modeling using FFT

This type of modeling required a 3D geological interface (e.g., carbonates/sediments) to be created from the interpolation of sparse data, which can be obtained from seismic horizons or well log data. The gravity effect of the interface is then computed by the FFT operator (Parker, 1973):

$$\Delta \mathrm{g}\ x, y\ = FFT^{-1}\left\{-2\pi G\Delta\rho e^{-h_0|\vec{K}|}\sum_{n=1}^{\infty}\frac{|\vec{K}|^{n-1}}{n!}FFT[h(x,y)^n]\right\} \tag{2.25}$$

where $\Delta \mathrm{g}$ is the gravity effect of the 2D interpreted seismic layers, depth-converted, h is the depth of the layer, $\Delta\rho$ is density contrast between the two layers forming the interface, h_0 is the mean depth of the interface, and $\vec{K}$ is the wavenumber.

The advantage of this algorithm is the high-speed computation compared to all the other forward modeling methods and the fact that it can be easily written in Python using the FFT modules of the SciPy library (Virtanen, et al., 2020).

On the downside, only continuous surface grids can be modeled by this method. Thus geological complexities, such as thrusts belts, or vertical intrusions, can not be included.

This method was used in the forward modeling of the gravity field in the Gulf of Manfredonia.

2.5.2 Forward modeling using IGMAS+

IGMAS+ is an interactive graphical software for 3-D numerical modeling, visualization and interdisciplinary interpretation of potential fields and their applications (Götze & Lahmeyer, 1988; Schmdit, Götze, Fichler, & Alver, 2010; Schmidt, et al., 2020).

The computation of the gravity field is based on 3D triangulated polyhedra which are sectioned into 2D polygons, allowing interactive modeling of the gravity anomaly and eventually of the gravity gradients directly onto the 2D sections.

The software gives the possibility to import horizons layers, seismic sections, borehole data and project them directly in the 2D sections, to be used as a constraint for the model.

Thus, this software gives the advantage of starting with 2D models in well-constrained areas and then extending them to the third dimension by adding new parallel sections. The resulting 3D-density model can be voxelized into a regular mesh of points at the desired resolution.

On the downside, the sections can only be set parallel to each other, making it challenging to model structures with perpendicular strikes.

The software has been used for modeling the northern Adriatic Region.

2.5.3 GM-SYS

This software is part of the Geosoft Oasis Montaj - Seequent package (Montaj, 2017).

It allows the 2D interactive modeling of subsurface sections using the polygon approximation. The gravity effect of each polygon is computed with the analytical solution by Talwani (Talwani, Worzel, & Landisman, 1959; Talwani, 1964; Won & Bevis, 1987), which assumed a two-dimensional flat earth model. It means that the modeled section is virtually repeated equally towards infinity in the direction perpendicular to the section itself, and no density variations outside of the 2D plane are contemplated in the model.

Therefore this modeling strategy is suitable for geological models with axial symmetry and elongated in one specific direction (e.g., linear mountain belts or narrow basins).

This software has been used for modeling the area of the LTA dataset (Table 1).

3 Case studies

3.1 Gravity and Magnetic anomalies in the Mediterranean Sea

We reprocessed the shipborne gravity and magnetic data acquired by the OGS between the 60s the 70s in the Central and western Mediterranean (GravOGSMed and MagOGSMed, Table 1), as retrieved from the archives of the institute.

The coordinates of the data points were first converted from the ED50 to the WGS84 datum, introducing transformation errors in the order of ±100 m, verified at known locations at docking ports. This error can be considered acceptable, being less than half of the accuracy of the vessel's positioning system and ~10 times lower than the relative distances between points along the lines (Table 1).

We corrected the gravity data by removing the normal gravity of the GRS80 model (eq. 2.1 - 2.3) and by leveling the lines according to the adjustment method described in chapter 2.2.

Previous authors recognized differences at the track crossings of the same dataset in the order of ±2 mGal, suggesting accuracies for the Bouguer anomalies of ±7 mGal (Makris, Morelli, & Zanolla, 1998). However, this estimate was most likely hand-verified on a few sets of crossing lines and then extrapolated to all the datasets since no maps or tables with cross-over values have ever been reported.

We recalculated all the cross-over values in the dataset using an automatic linear interpolation method created in Python, reporting an STD error at crossings of 4.31 mGal, and max. and min. errors of -42.78 and 27 mGal, which is more than two times the previously expected values (Figure 3-1a).

After the leveling adjustment, based on the S&S model wavelengths > 16 km, these errors have been reduced by more than 50% (Figure 3-1d).

Therefore the new dataset is clean from most line biases, which created notable artifacts when computing field derivatives in geophysical data analysis and modeling (Figure 3-1b).

On the downside, the amplitudes of long-wavelengths, i.e., the same as the S&S altimeter model, are slightly reduced by a few mGal compared to those of the original lines, possibly due to the averaging solution adopted in the remove-restore procedure, which may have introduced some smoothing (Figure 3-1c).

Nevertheless, the algorithm only uses a sliding average tide to the original shipborne data points and the altimeter grid nodes without additional interpolations. And, the average value within the considered intervals should be statistically more accurate than every isolated value by definition.

Therefore the final leveled dataset can be considered accurate to the same level predicted for the altimeter-derived gravity of about ~2 mGal (Sandwell, Müller, Smith, Garcia, & Francis, 2014), at least on wavelengths > 16 km.

Regarding the magnetic anomalies, we found that the previously estimated accuracies, of about ±10 nT (Zanolla, Morelli, & Marson, 1998), have been way too optimistic. Indeed, our calculated cross-over differences range between -657 and +607 nT, with an STD error of ± 44 nT (Figure 3-2a).

These errors could result from a non-accurate diurnal correction, which at that time was only based on the recorded hourly values of the horizontal and vertical components at the magnetic observatory of l'Aquila, then applied to all the Mediterranean datasets.

After the leveling procedure, which in this case was based on the EGM02 model at wavelengths > 55 km, the final differences at line crossings were drastically reduced to STD errors of ±12 nT, with only a few scattered spikes exceeding 100 nT, which can be manually-removed with no effort (Figure 3-2b,c,d).

In the magnetic dataset, we found a significant and almost constant bias of ~100 nT from comparing the data points before and after the leveling. This near-systematic shift is only present in the Central-East Mediterranean between 14° and 25° longitude degrees (Figure 3-2a), i.e., the marine area covered by the CNR Vessel "Bannok" between 1966 and 1972.

This error could have been introduced by a wrong calibration of the towed proton magnetometer during the acquisition since it appears stable for several years of acquisition with the same instrument, and therefore, unlikely caused by unpredicted long-term temporal variation of the magnetic field (Gantar, Morelli, & Pisani, 1968).

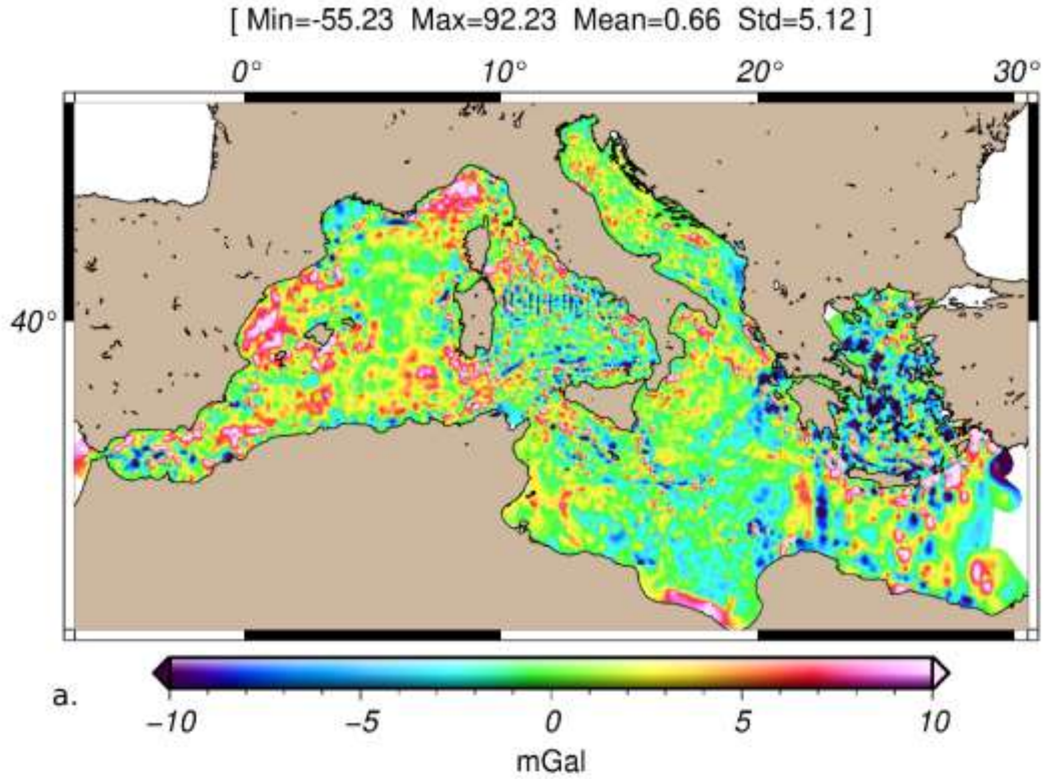
[Min=-55.23 Max=92.23 Mean=0.66 Std=5.12]
0°
10°
20°
30°
40°
−10
−5
0
5
10
mGal

a.

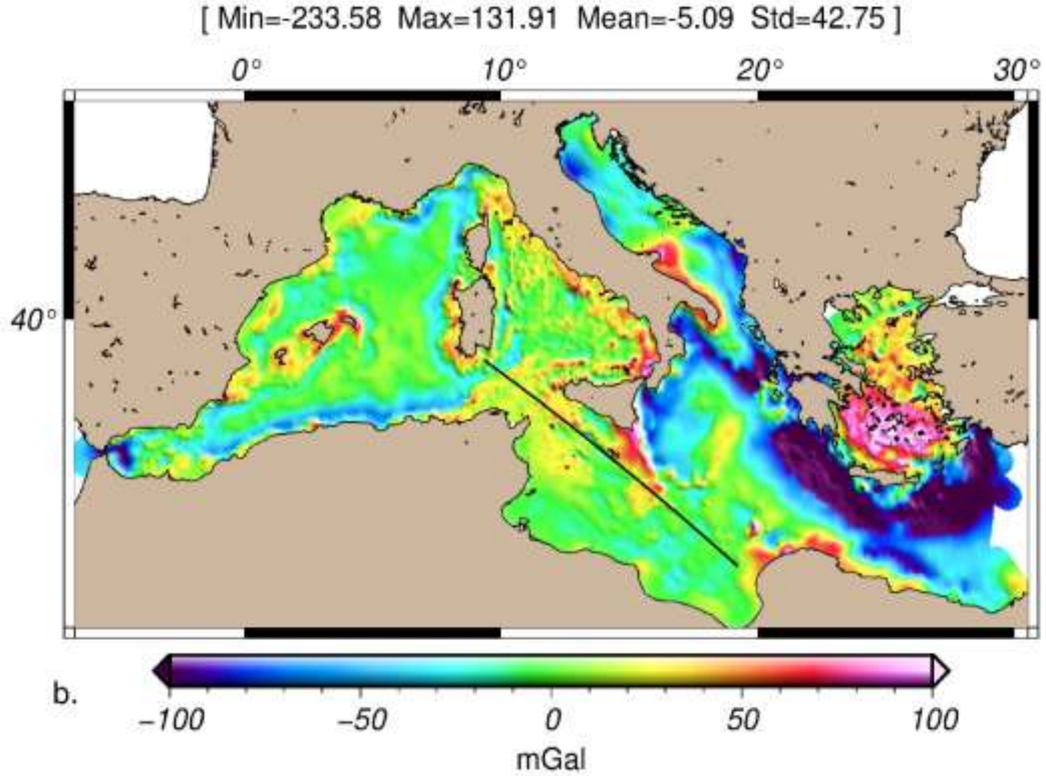
[Min=-233.58 Max=131.91 Mean=-5.09 Std=42.75]
0°
10°
20°
30°
40°
−100
−50
0
50
100
mGal

b.

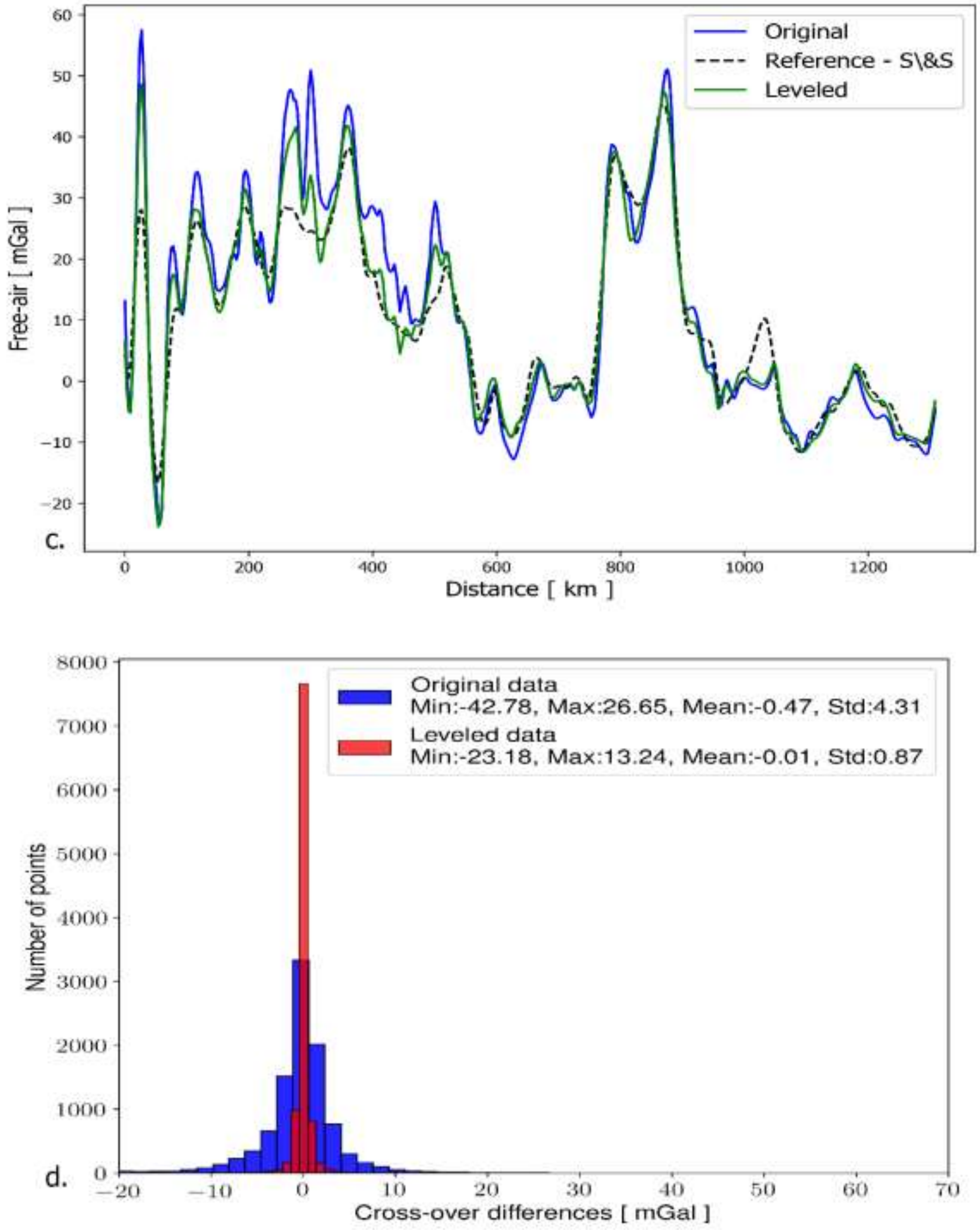

Figure 3-1 - (a) Map of differences between the Free-air anomalies before and after the leveling process (3x3 km grid-step). (b) Free-air anomaly after leveling. (c) Profile crossing the Central South Mediterranean from East to West, plotted in figure (b), in which the original and the leveled anomaly are visible together with the S&S altimeter-derived gravity filtered at ~16 km. (d) Histogram of cross-over differences of the entire GravOGSMed dataset, before and after the leveling.

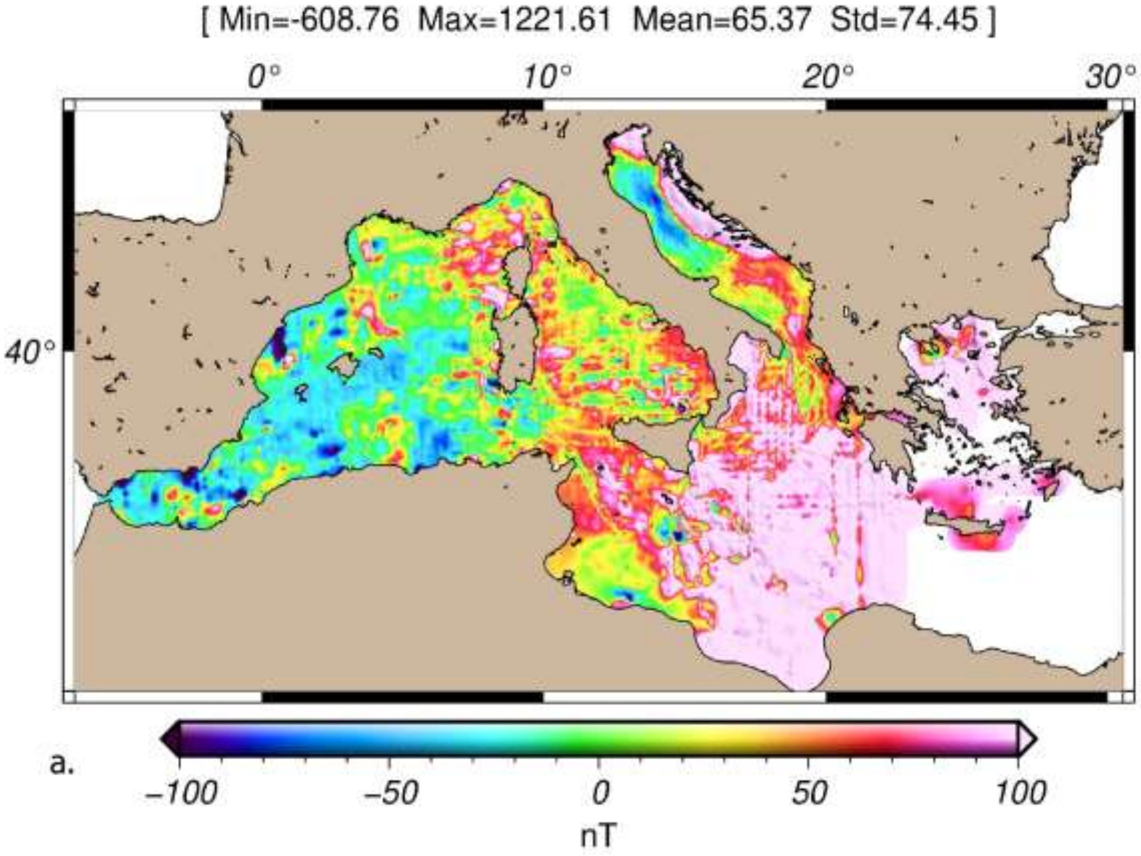
[Min=-608.76 Max=1221.61 Mean=65.37 Std=74.45]
0°
10°
20°
30°
40°
a.
−100
−50
0
50
100
nT

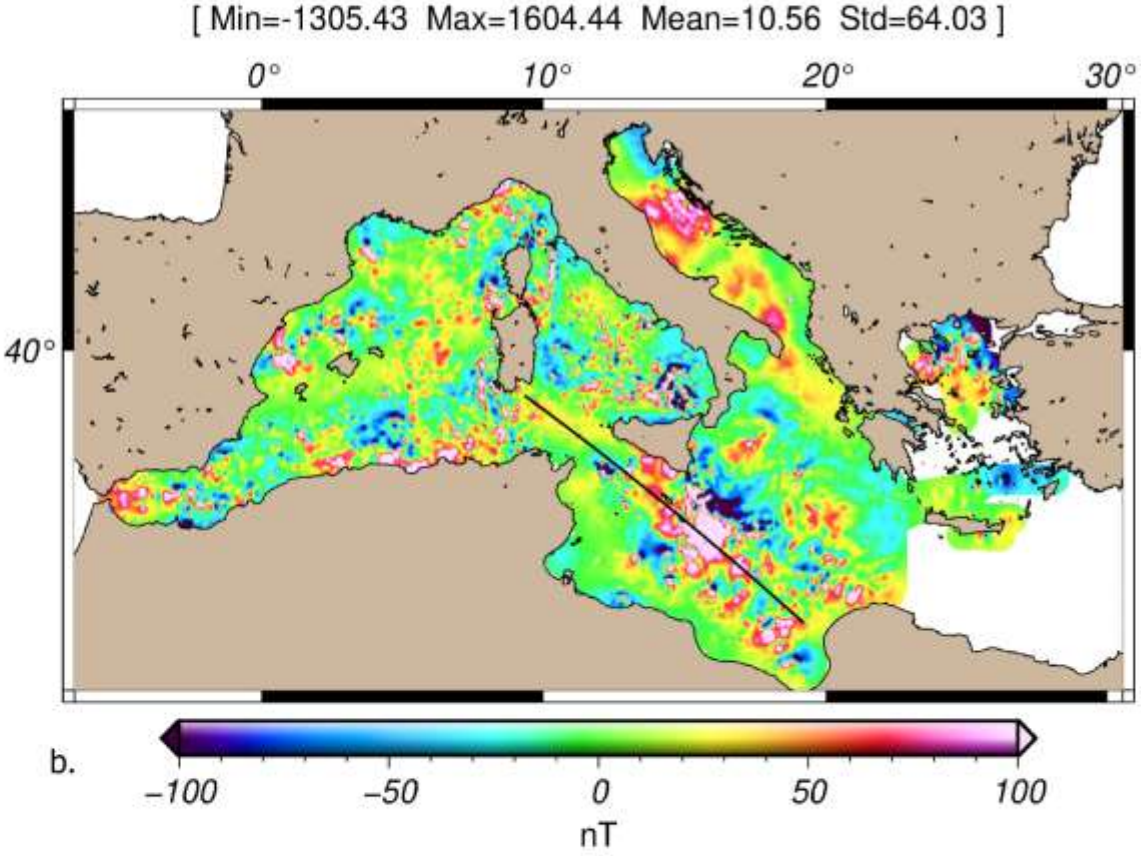
[Min=-1305.43 Max=1604.44 Mean=10.56 Std=64.03]
0°
10°
20°
30°
40°
b.
−100
−50
0
50
100
nT

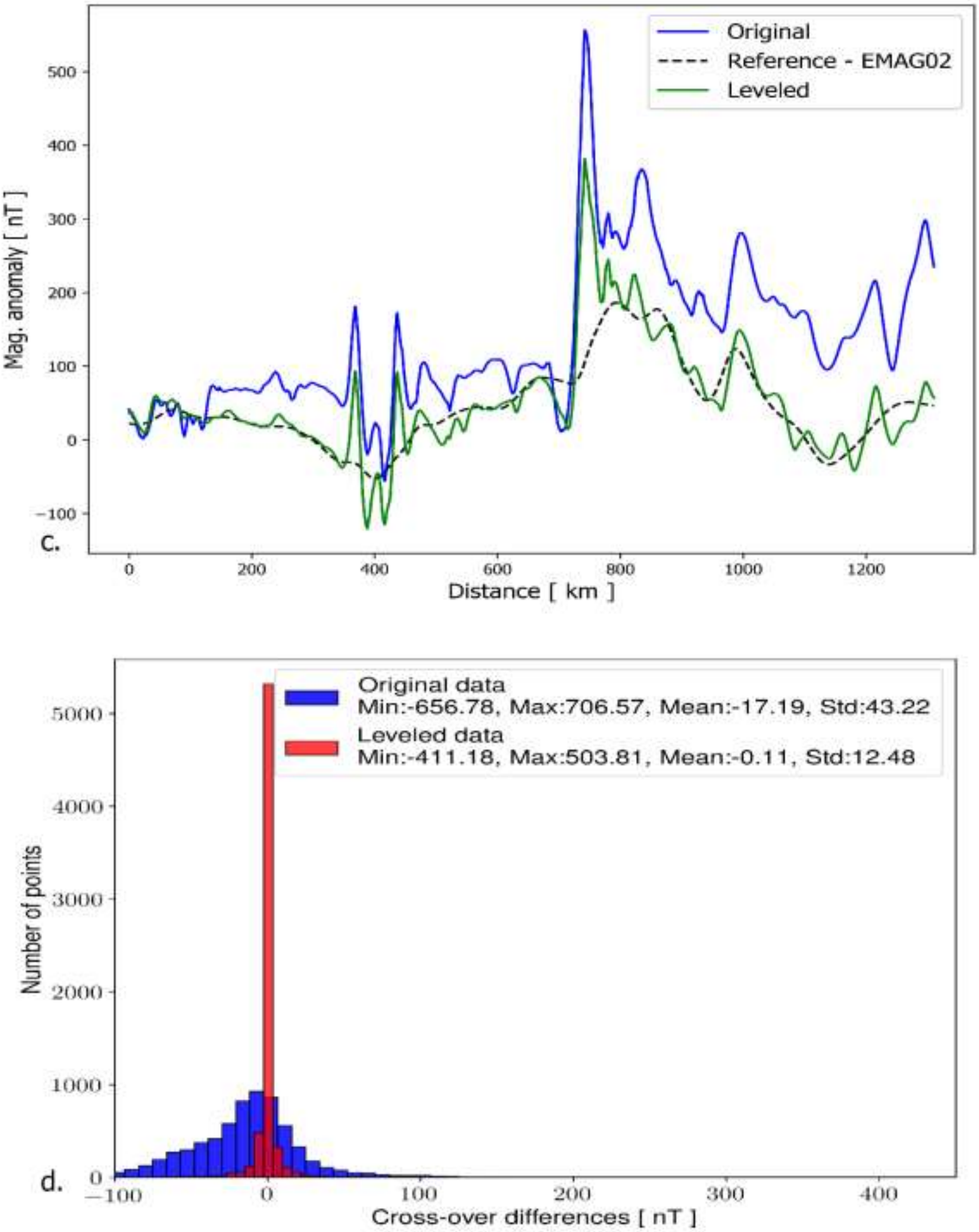

Figure 3-2 - (a) Map of differences between the magnetic anomalies before and after the leveling process (3x3 km grid-step). (b) Magnetic anomaly after leveling. (c) Profile crossing the Central South Mediterranean from East to West, plotted in figure (b), in which the original and the leveled anomaly is visible together with the EMAG02 magnetic model filtered at ~55 km. (d) Histogram of cross-over differences of the entire MagOGSMed dataset, before and after the leveling.

3.2 The Gulf of Manfredonia

The Italian marine-coastal areas host a high-resolution sea-bottom gravity network created between the '50s and the '60s, including 2144 stations, integrated in the '80s with other 3135 stations.

The stations are highly concentrated in the first 10 km from the coast, where the network has a max. resolution of 1 station/km, with an estimated accuracy of 0.5 mGal. These data offer the possibility to study short-wavelength components of the gravity field, often related to later changes in the contact surface between the unconsolidated sediments and the bedrock. The discontinuities of that surface are mostly part of fault networks propagating from the inland, the study of which assumes particular relevance in areas classified with high seismic risk.

Nowadays, new satellite altimeter gravity models allow studying the marine gravity field at approximately the same resolutions of the sea-bottom data, with continuous improvements during the last 20 years. These models offer the possibility to cover most of the global sea surfaces homogeneously, with accuracies of ±2 mGal, which are reliable almost everywhere, except the coastal areas. The altimeter-derived gravity near the coast is generally degraded by signals back-scattered from the nearby land, generating high-frequency noise, which can be easily confused with the geological-related signals. Therefore in Italy, particularly in the Adriatic Sea, the areas hindered by the altimeter coastal noise are the same densely covered by the sea-bottom stations.

We decided to use the case study of the Gulf of Manfredonia to compare satellite altimeter with sea-bottom data to try quantifying the coastal noise and also verifying the quality of geological models inferred from both gravity data types.

The gulf is located in the southeastern sector of the Adriatic Sea, where the bathymetry is a tilted flat surface that does not show any relevant morphological feature. Nevertheless, seismic reflection data intercept a significant structural element beneath the sedimentary cover, i.e., the Gondola Fault Zone, including several E-W and NW-SE trending fault segments that define an elongated, buried structure that extends for ~70 km across the shelf and continuing on-shore, on the Gargano promontory with the Mattinata fault.

We mapped the differences between two satellite altimeter models (DTU13 and S&S) and the sea-bottom dataset, recording max. values of ~20 mGal in the proximity of the Gargano promontory, up to ~17 km from the coasts.

These values validate the hypothesis that satellite altimeter gravity in coastal areas is not usable for geophysical analysis and modeling, and it must be integrated with other data types, e.g., the sea-bottom data.

Moving far away from the coast, where the sea-bottom stations are sparse and separated by relative distances > 6 km, the satellite altimeter data identifies the same structures with more accuracy and continuity than sea-bottom gravity. This was demonstrated by comparing the gravity anomaly, the vertical derivative (ISVD), and the Tilt function of sea-bottom and satellite altimeter data to the same calculated for a forward gravity model derived from seismic chosen.

The comparative analysis has allowed tracking the edges of the Gondola Fault Zone by integrating both satellite altimeter and sea bottom data, revealing shallow near-shore features only visible with the additional information of the sea bottom data.

This result shows the potential for implementing gravity anomalies from satellite altimetry with high-resolution near-shore data, such as the sea-bottom gravity network available around the Italian coasts, and using this information to understand better the geological connection between the offshore and onshore areas.

The complete Section 3.2 The Gulf of Manfredonia is included as ANNEX 1, including the revised manuscript “A comparison between sea-bottom gravity and satellite altimeter-derived gravity in coastal environments: A case study of the Gulf of Manfredonia (SW Adriatic Sea)” by L. S. Zampa, E. Lodolo, N. Creati, M. Busetti, G. Madrussani, E. Forlin, A. Camerlenghi submitted to the Journal “Earth and Space Science" . At the time of submission of this thesis, the manuscript is accepted for publication and is awaiting the acceptance of final revision of the english language requested by the editor.

3.3 The Friulian Plain and the northern Adriatic Sea

The Friulian Plain and the northern Adriatic Sea lie in the north-eastern corner of the Adria Plate and presently constitute part of the Dinaric/South Alpine foreland (Figure 3-3).

The geological assessment of the region results from three main tectonic phases: the Mesozoic extension, the Dinaric compression, and the Alpine compression. In addition, the southwestern part of this area was also affected by the Apennine compression.

Figure 3-3 - Scheme of the regional structural domains and setting of the northern Adriatic Sea and the North-eastern Italy. The area is part of the foreland of the Dinaric and Alpine thrust-belts (modified after Dal Cin, 2018).

During the Early Jurassic extensional phase, the thick and stiff Permo-Triassic carbonate platform was disaggregated by a horst-graben system delimited by N-S trending faults that provide the formation of the Belluno Basin (westward) and Slovenian Basin (eastward), separated by the structural high on which the Friuli Dinaric Carbonate Platform (FDCP) developed during the Cretaceous/Paleogene (Cati, Fichera, & Cappelli, 1987; Zanferrari, et al., 2013).

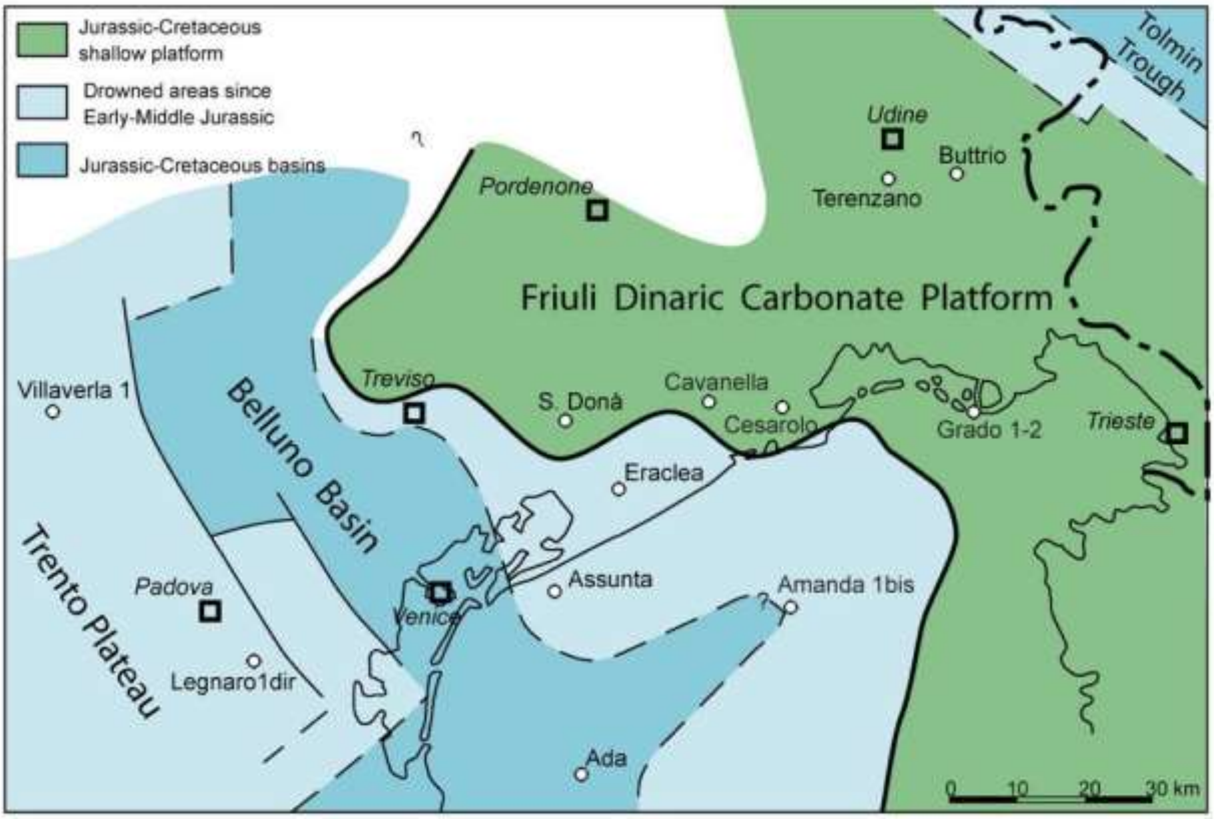

Figure 3-4 - Paleogeographic sketch of the Friuli Dinaric Carbonate Platform during the Late Cretaceous (modified after Cati et al., 1987).

The early stage of the Alpine orogeny, the Mesoalpine phase (Upper Cretaceous-Middle Eocene) is characterized by the NE-SW-oriented compressions, which generated the Dinaric fold-and-thrust belt (Kastelic, Vrabec, Cunningham, & Gosar, 2008).

During this event, the eastern part of the Friuli Dinaric Carbonate Platform was uplifted by the Dinaric thrusts, while the western part was flexured in the foreland domain. The depositional space available in the foredeep brought to the deposition of a conspicuous amount of turbidite sediments derived from the erosion of the chain to the nearest front, overlying the carbonatic platform and incrementing the platform subsidence process. The westernmost Dinaric thrusts beneath the Friulian Plain are constituted by the Palmanova System, which provides a detachment of more than 1500 m at the top of the carbonates (Merlini, Doglioni, & Ponton, 2002; Barison, 2008). sorthern, along the Karst coast, the Dinaric frontal ramp is delineated by the Karst Thrust, with an estimated vertical through of 1800 m of the carbonate units (Busetti et al., 2010a,b; Dal Cin, 2018).

The last alpine orogenic phase (Valsuganese phase, Serravallian-Tortonian) and the present time compressions, characterized by NNW-SSE and N-S axes orientation, respectively (Ponton, 2015), accommodate the counter-clockwise rotation and indentation of the Adria plate (Anderson & Jackson, 1987) towards the European Plate, with presently about 2.0 mm/y of shortening (Bechtold, Battaglia, Tanner, & Zuliani, 2009; D'agostino, et al., 2005). These compressions determined the formation of SW-NE, WE, and NE-SW oriented thrusts, at the most advanced front of the Julian Alps, in the northern sector of the Friulian Plane, e.g., the Budoia-Aviano line. The rapid uplift of the Alps brought the deposition of Molassa terrigenous sediments (clays and sends), during the Miocene, to the front of the mentioned thrusts. Part of the diagonalized Miocene Molasse lays in onlap on the underlying Eocene Flysch. The flexure of the Adria crust under the weight of the uplifting Alps and sediments accumulating at the front generates the Friuli Dinaric Carbonate Platform's tilting towards the approximate North-South direction. Moreover, the new tectonic imprinting generates the reactivation of the previously formed Dinaric structures, which are almost perpendicular to the Alpine lines. The reactivation acts accordingly to a transpressive mechanism pushing in the S, S-E direction. Some anti-Dinaric lineaments have been suggested in the South-East part of the Friulian Plane, in the Karst region, and in the Gulf of Trieste, e.g., the "Sistiana Line" (Barison, 2008).

In the present work, we used the reprocessed gravity data to integrate and validate the information derived from seismic about the subsurface fault network hidden below the sedimentary cover of the Friuli plane and the northern Adriatic Sea.

We first created the Bouguer anomaly map (Figure 3-5) by integrating marine and land gravity data, processed according to the sequence described in chapter 2.1. Then, we integrate the resulting grids at 1 km resolution with the EGM08 grid (Figure 1-16) in the areas exceeding the Italian borders (i.e., Austria, Slovenia, Croatia), using the method described in paragraphs 2.1.3.1 and 2.1.5.

The Bouguer anomaly shows the known negative trend approximately N-S oriented, caused by the flexure of the crust under the weight of the North eastern Alps, as already outlined by previous authors (Morelli, 1951; Cati, Fichera, & Cappelli, 1987; Zanolla, et al., 2006).

At the immediate front of the Alpine range, north of Udine, there is a significant local minimum of -70 mGal, extended for ~65 km W-E, and ~25 km N-S. The minimum to the northeast corresponds to the area occupied by the Morainic Amphitheatre of the Friuli Venezia Giulia. In the central and western parts, the local minimum covers the area partially occupied by the Tagliamento riverbed and by the fans of the Cellina-Meduna system. The minimum corresponds to the deepest part of the Neogene foredeep basin at the Alpine front.

The negative Bouguer anomaly becomes zero around the center of the northern Adriatic Sea, and is slightly positive (~20 mGal) over the Istria region to the south. This is due to the uplift of the Moho, which rises from ~55 km below the Alps to an average of 35 km under the northern Adriatic (Finetti, 2005; Magrin & Rossi, 2020). A slight positive bulge, NW-SE oriented, is also recognizable south of Udine, corresponding to the Dinaric thrust initially named "*Linea di Palmanova*", which is discordant to the N-S Alpine trend.

We used the Detrend algorithm described in paragraph 2.4.1 to remove the regional field from the Bouguer anomaly, with a window size of 25 km, obtaining the map of residual anomalies (Figure 3-7).

The regional field map (Figure 3-6) outlines wavelengths of approximately 100 km, generally caused by the crystalline basement and the Moho variations, at least for what concerns the Italian territory (Rapolla, 1986). The regional variations create perpendicularly-oriented bulges: the SW-NE or WE Alpine bulges or the opposite NW-SE Dinaric bulges. These crossing trends were not evident in the previous work of Cati et al. (1987), where the authors used a spectral low-pass filtering method to separate regional and local signals, and they did not integrate the gravity anomaly with other data outside of the Italian borders.

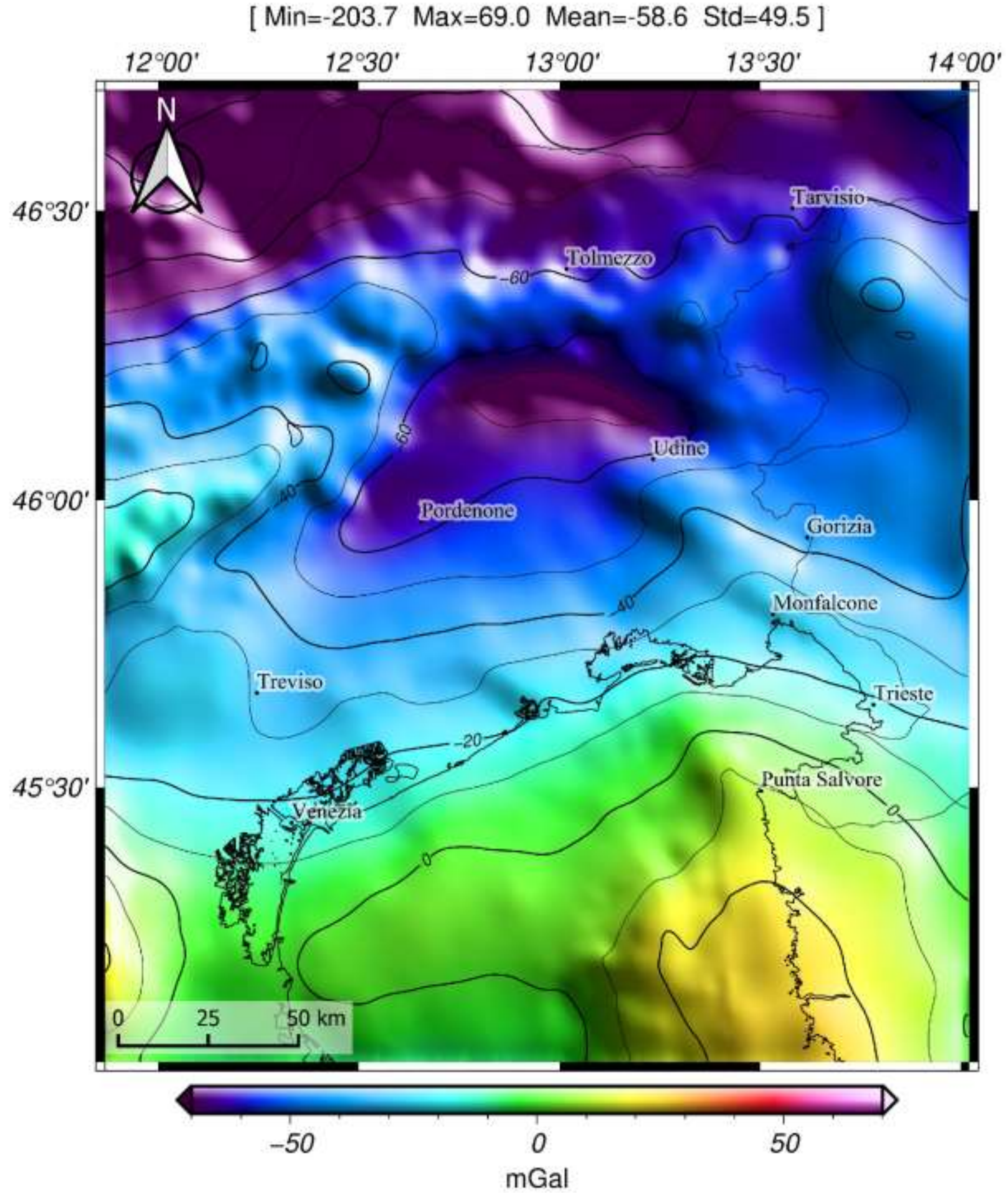

Figure 3-5 - Bouguer map of the Friuli Venezia Giulia Region and the northern Adriatic Sea.

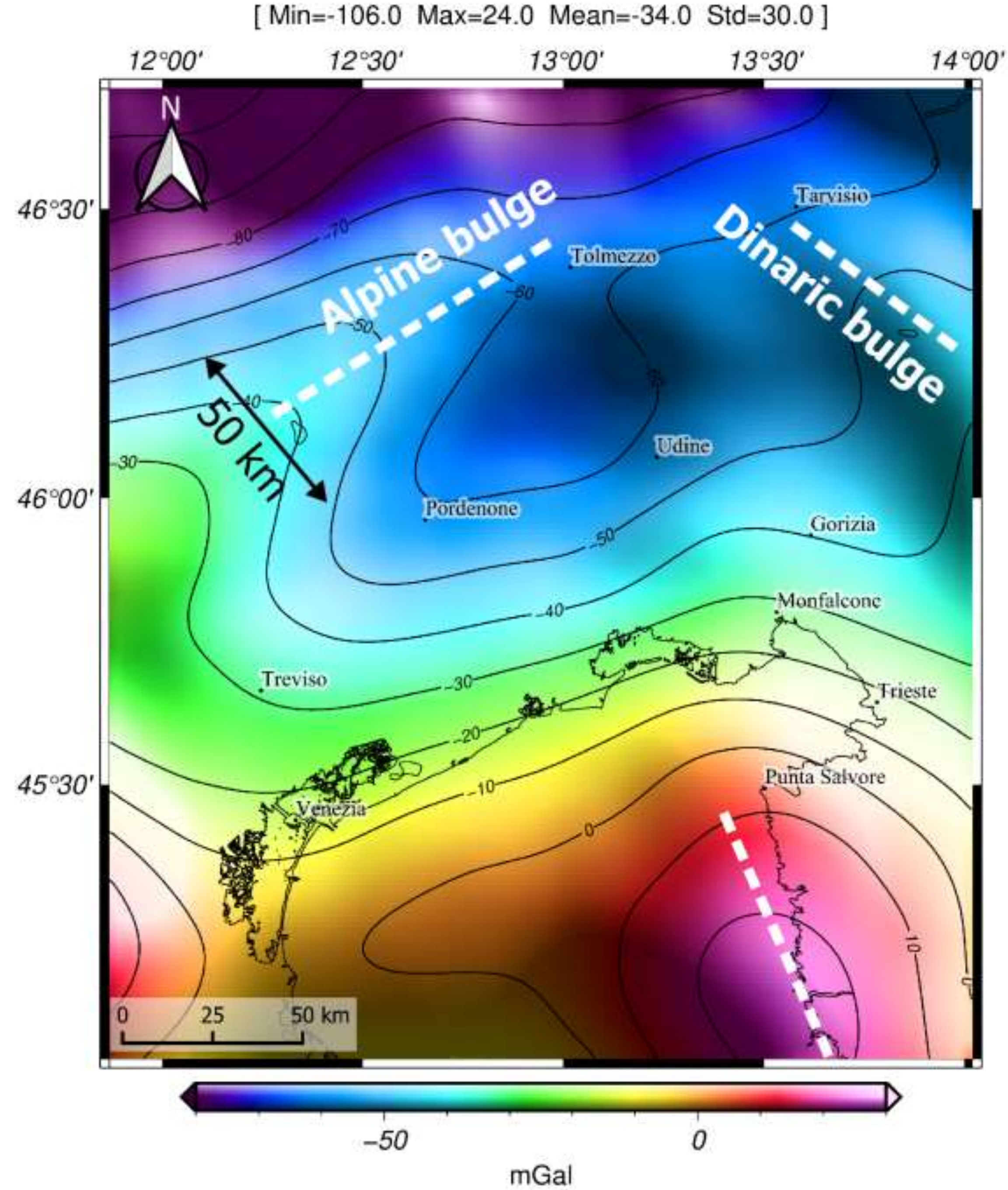

Figure 3-6 - Map o regional anomalies of the Friuli Venezia Giulia Region and the northern Adriatic Sea, obtained using the Detrend algorithm described in paragraph 2.4.1.

The map of residuals showed two main prominent positive anomalies (Figure 3-7). The first emphasizes the Dinaric front, NW-SE oriented, that runs from just to the south of Udine to the Karst region of Trieste.

The second is located in correspondence of the Friuli Dinaric Carbonate Platform, which correspond also to the Dinaric bulge located at the center of the north-eastern Adriatic sea, which runs from Punta Salvore (western corner of Istria) to the Grado and Marano lagoon.

In both cases, bathymetry and topography do not show any relevant morphological expression of these anomalies in an area characterized by the flexure of the Friuli Dinaric Carbonate Platform.

Seismic reflection profile, however, suggest the presence of an almost vertical detachment of the Carbonate platform below the sediments. Here, the limestones are in lateral contact with the overlaying flysch or Molasse and eventually with the Pliocene sediments.

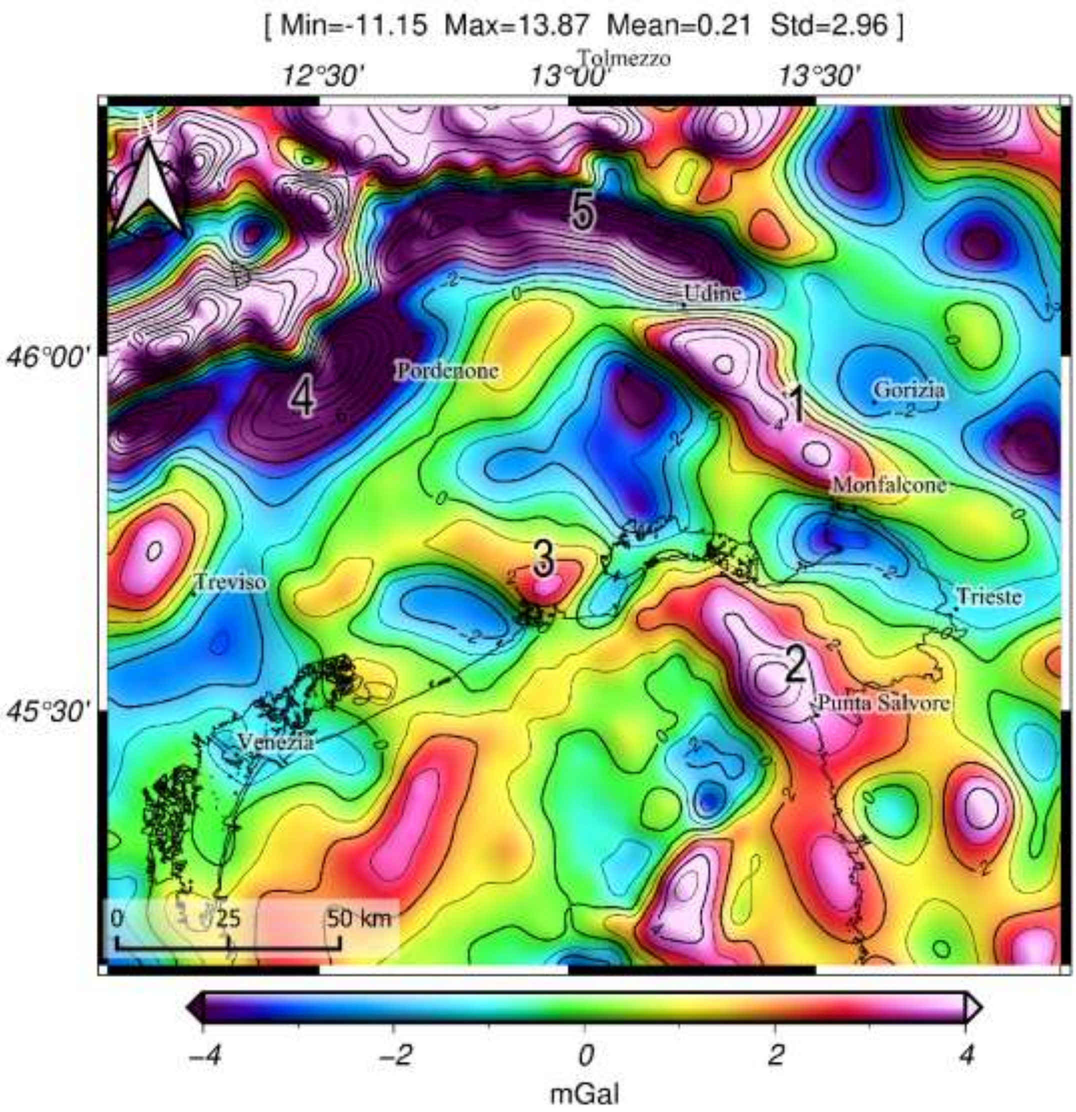

Figure 3-7 Map of residual anomalies in the Friuli Venezia Giulia and northern Adriatic Sea, with labels indicating the anomalies discussed in the text.

We then tested the Terracing function to track the steep edges of the Friuli Dinaric Carbonate Platform automatically.

The terracing map confirmed the presence of at least three main geological features and helped to outline them (Figure 3-8):

1. the Dinaric thrusts uplifting the FDCP to the east;
2. the FDCP shelf margin/ Dinaric peripheral bulge in the northern Adriatic Sea, resulting from the tilting of the Carbonate platform to the east;
3. the FDCP shelf margin buried below the Friulian ;

Moreover, the map emphasizes other lateral density contrast, which has not been clearly explained yet. Among these, the negative anomalies in between the southern front of the Alps and the city of Pordenone to the west and Udine to the east (i.e., numbers 4 and 5 in Figure 3-8).

These two minima correlate with the flexure of the Friuli Dinaric Carbonate Platform due to the Alpine compression, as mapped from seismic lines (Figure 3-9). However, the depth map of the top of the Friuli Dinaric Carbonate Platform shows a gentle deepening instead of the abrupt discontinuity mapped by gravity. There are at least four different hypotheses to explain the discrepancy between gravity and seismic in these areas:

1. a lower density in the Plio-Quaternary cover than in the southern part of the Friulian Plain;
2. a lower density of the basement, caused by a higher degree of fracturing as a consequence of the more intense tectonic deformation acting at the immediate front of the Alps;
3. a deeper source of the anomaly, related to the dolomite or crystalline basement variations below the carbonate platform;
4. errors in the depth-conversion and interpretation of the seismic lines

Moreover, in the central part of the Friulian plain, the terracing shows a slightly negative but relatively extended minimum which does not precisely mimic the depths of the carbonates mapped from seismic. This minimum was already outlined in the previous work of Cati et al., 1987, in which the author suggested the presence of a central Friulian basin dividing the platform. However, the inconsistency with the re-interpreted seismic data may support the hypothesis of a relatively deeper anomaly source.

We then used the edge-tracking procedure described in the methods to extract the faults from the terrace function and compare this result with the Friuli Venezia Giulia Region Active Faults geodatabase (Marchesini et al., 2021).

Four edges correlate with the interpreted fault lines, within the range of the estimated errors:

1. The *Pozzuolo Medea* Thrust,
2. the *Panzano Thrust*,
3. the *Susan-Tricesimo* Thrust;

The reliability of the edges is strictly connected to the distribution of the gravity stations and gravity data error. For example, in the Friulian Plain and the northern Adriatic Sea, we have an average density of 1 station/km^{2,} and the accuracy of the Bouguer anomaly is about ~1 mGal. Therefore, all the edge segments that emerged from the analysis shorter than 2 km have been removed. Moreover, we imposed a threshold on the algorithm to select only the edges with horizontal gravity gradients higher than 1 mGal/m. However, other types of error that we did not consider may contribute to the deterioration of the positioning accuracy of the gravity edges (e.g., interpolation errors). Therefore the results of the edge-detection should be considered more of a guideline for the interpretation of lateral tectonic contacts or density contrast, which, in any case, must be verified by other geophysical/geological methods.

Nevertheless, an interesting result emerged from the gravity edge obtained immediately North of the city of Monfalcone, which is ~7 km East from the near-vertical step in the carbonates as mapped from seismic (Figure 3-5). The problem of this area is that the few available seismic lines used in the interpretation do not continuously cover the edge, and the lines have a very poor resolution. Therefore, it is challenging to locate the faults' position by seismic-only precisely.

On the contrary, the area is well covered by gravity data, which suggests the vertical step being western to the previous seismic interpretation, aligned to the inferred Panzano Thrust, which is more likely the actual position of the carbonate thrust (Figure 3-10).

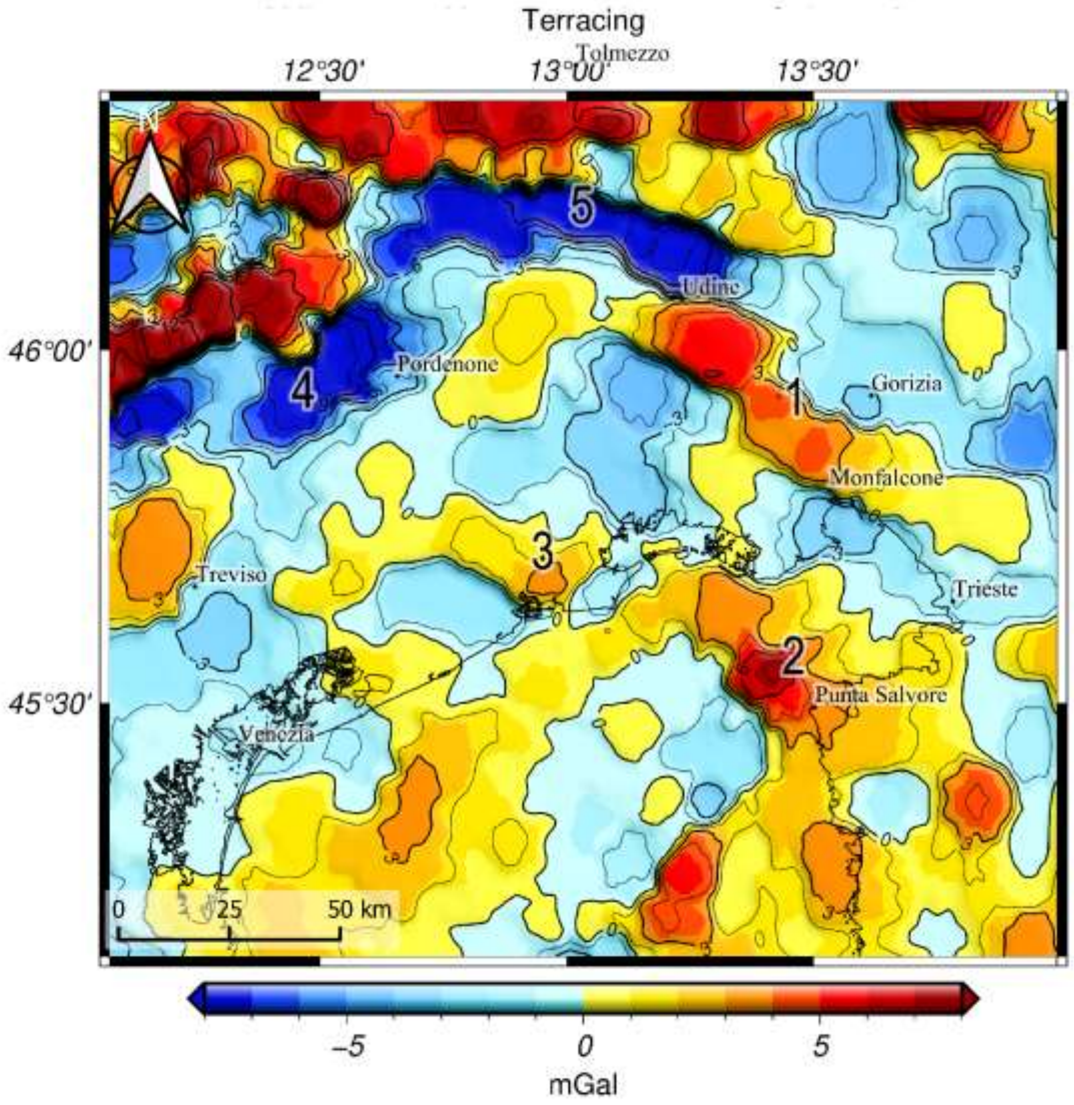

Figure 3-8 - Map of terracing function in the Friuli Venezia Giulia and northern Adriatic Sea, with labels indicating the anomalies discussed in the text, with labels indicating the anomalies discussed in the text.

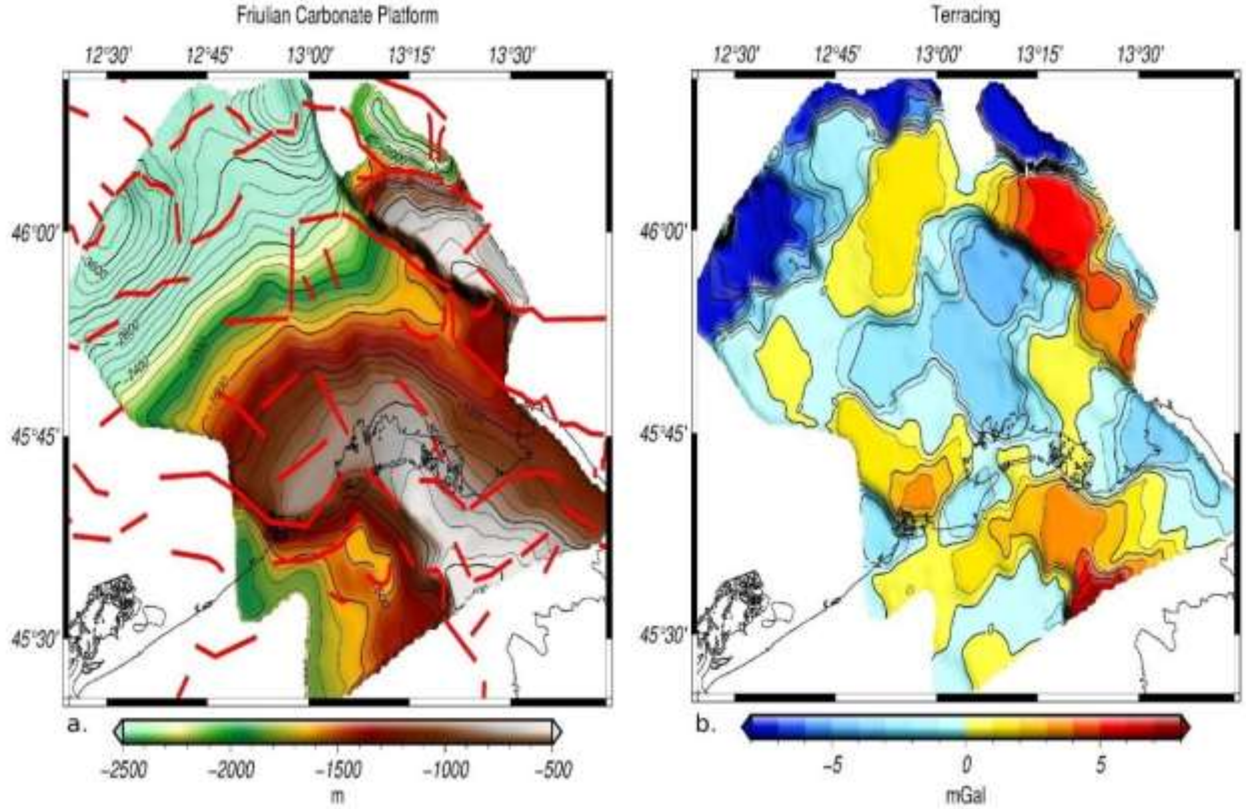

Figure 3-9 - Comparison between two independent results: (a) the map of the top of the Friuli Dinaric Carbonate Platform derived from the interpretation of seismic reflection profiles (Nicolich, Della Vedova, Giustiniani, & Fantoni, 2004; Busetti et al., 2010a), with the edges inferred from gravity and obtained from the edge detection analysis described in section 2.4.4 (red segments). (b) Terracing function derived from gravity data only. The tested hypothesis is whether or not the terracing function can delineate the edges of near-vertical steps at the top of the Carbonates.

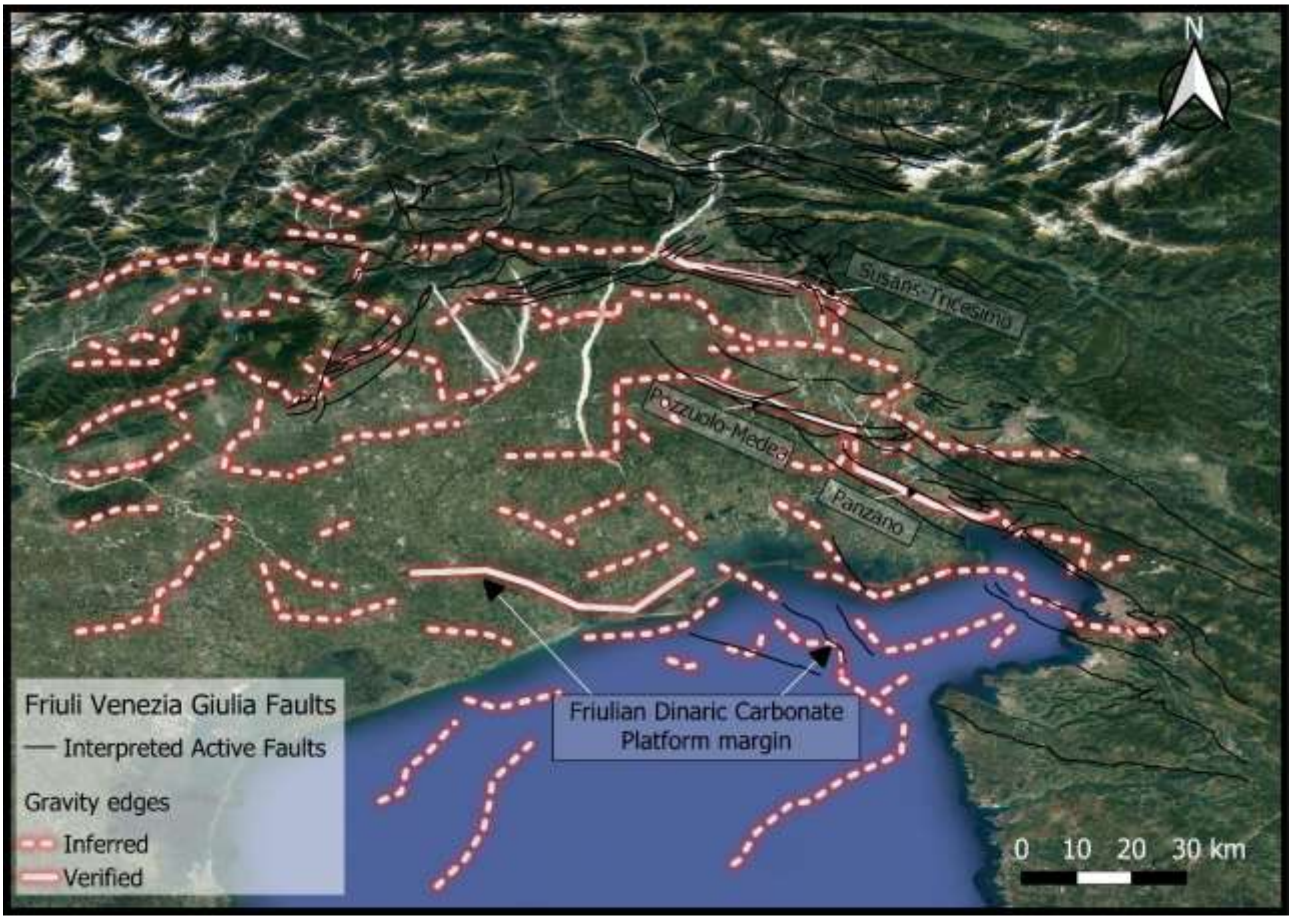

Figure 3-10 - Map with the edges of the terracing function extracted with the semi-automatic method described in paragraph 2.4.4*. We can distinguish between verified edges that correspond to morphological vertical steps and faults that caused the contact between the carbonate and terrigenous units.*

We hypothesize that the edges inferred from gravity are related to depth variations of the Friuli Dinaric carbonate platform (e.g., sub-vertical steps) and its consequent lateral contact with the cenozoic terrigenous units (flysch, molasse, Plio-Quaternary sediments). We should consider that flysch and molasse have approximately similar velocities and densities. Therefore it is difficult to distinguish between the two in the gravity data analysis.

We tested this hypothesis in three different study areas, with 2D forward models constrained by seismic data (Figure 3-11). We used the IGMAS software for modeling profiles 1 and 2 and the GM-SYS software for modeling 4 profiles in the LTA study area (see paragraph 2.5).

We have to underlie that the analysis performed in the LTA area, located at the foot of the Alpine chain, has been commissioned for specific purposes of identifying, mapping, and evaluating subsurface aquifers with the aid of integrated geophysical methodologies. In this case, the field procedure in data acquisition has been oriented accordingly, as for the gravity surveys and modeling. For these reasons, the analysis for the LTA area has been inserted in ANNEX 2 of this Ph.D. thesis.

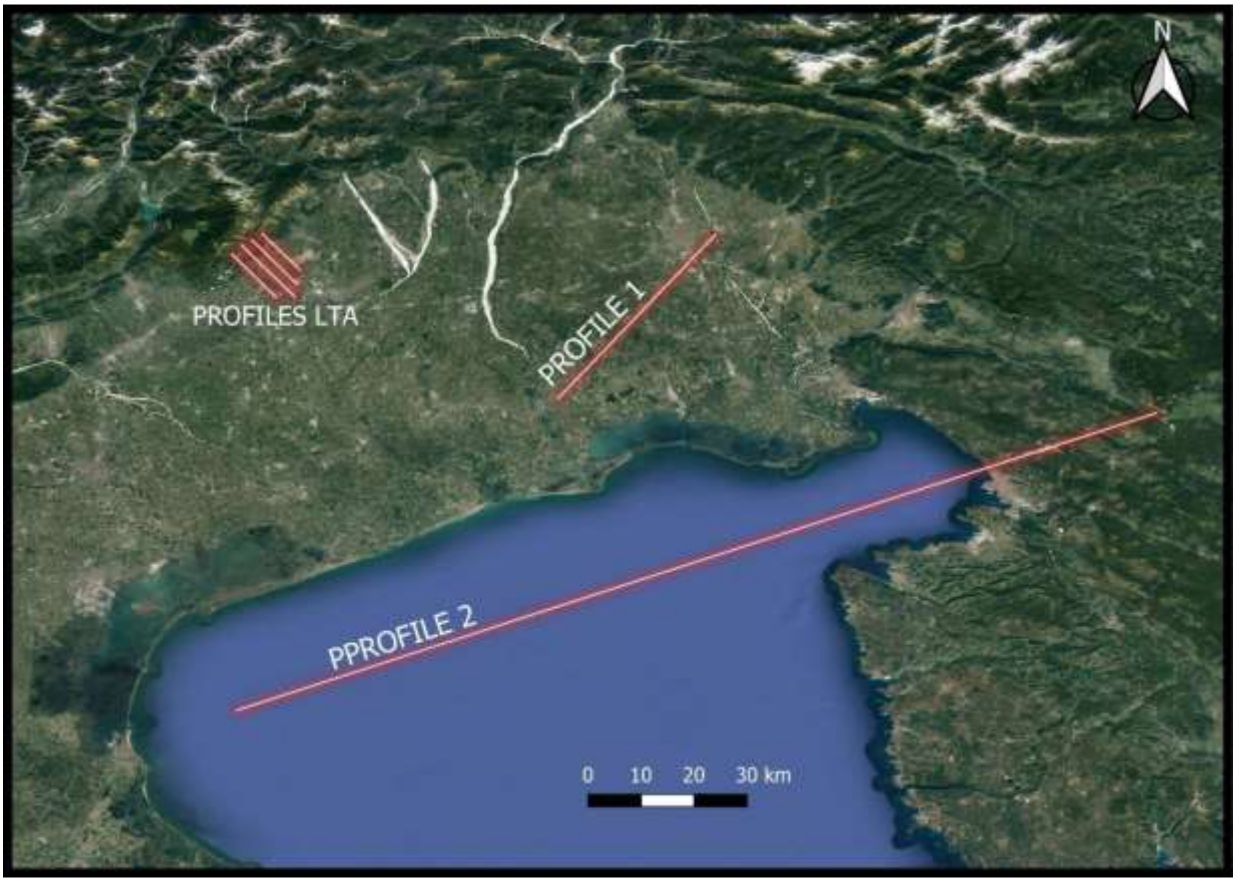

Figure 3-11 - Map showing the location of the 2D-forward gravity models.

PROFILE 1

This model crosses the Dinaric thrust in the eastern part of the Friulian Plain south of Udine (Figure 3-12c). We used the seismic depth-converted horizons of the top of the Friuli Dinaric Carbonate platform and the base of the Quaternary sediments to constrain the 2D-gravity model (Nicolich, Della Vedova, Giustiniani, & Fantoni, 2004). The overlying seismic profile is available as a courtesy of the ENI.

Moreover, we added the direct information from the borehole Cargnacco, which intercepts the profile south of Udine and reaches a depth of ~7250 m (Venturini, 2002).

The densities chosen for the model have been derived from collected seismic velocities using the empirical law after Ludwig, Nafe & Drake (1970). Moreover, we imposed a reference background density of 2.67 g/cm^3.

Thus, we adjusted the depth of the Base of the Quaternary sediment and the top of the Friuli Dinaric Carbonate Platform within a range of ~100 m to fit the residual gravity at best.

The result of the modeling gives us further confirmation that the positive anomaly in the eastern part of the Friulian Plain is due to the lateral density contrast between the flysch and the carbonate rocks. Moreover, the location of the south-west margin of the Friuli Dinaric Carbonate Platform identified by seismic data is also confirmed by the positive gravity anomaly between the cities of Caorle and Lignano Sabbiadoro.

In summary, this model confirmed that the residual gravity could be used to interpret the edges of the carbonate platform, validating the information obtained from seismic lines and boreholes or completing it where it lacks spatial coverage.

PROFILE 2

This model crosses the Karst region and the northern Adriatic Sea from west to east (Figure 3-12d).

To constrain the stratigraphic architecture and geometries of the sedimentary cover and the shallow to intermediate geological structure we used the post stack depth migrated seismic line *CROP-M18* (courtesy of G. Brancatelli) and the well Amanda 1bis for the western and central area, and the seismic interpretation of depth converted seismic profile and a geological section for the eastern part/Karst highland (courtesy of M. Busetti and M. Dal Cin).

We converted the velocities from the well-log Amanda 1bis (Patricelli & Pali, 2020) to densities using the empirical law after Ludwig, Nafe & Drake (1970), and then we modeled the upper/lower crust and the Moho, starting from the initial models EuCRUST-07 (Tesauro, Kaban, & Cloetingh, 2008) and NAC (Magrin & Rossi, 2020).

We try to obtain the best fit with the observed Bouguer anomaly by changing the depth of the lower crust and Moho within a range of ~10 km, starting from the cited crustal models and keeping the densities fixed.

The results obtained with this gravimetric model are different from a seismic-only solution by Finetti & Del Ben (2005). Specifically, in the central part of the profiles, the gravity constrained the presence of the crust that reaches a depth of 37 km, while in the previous model was at 31.5 km.

Moreover, the maximum pick of the anomaly in the central part of the profile appears not strictly related to the lower crust geometry but mainly to the tilting of the carbonate platform in the first 7 km of depth, which culminates with the positive bulge visible in the ISVD map (Figure 3-12b).

Another interesting finding is the positive anomaly in the western part of the northern Adriatic Sea (south of Venice), which has never been studied in detail. We hypothesized that this is due to a slight local uprise of the mantle, which justifies the observed gravity in the 2D model. However, the anomaly is observed only in a small area extending less than 40 km^2, which is less than half of the expected wavelength of the Moho. Thus, a source shallower than the

Moho might justify the anomaly. However, we do not have other evidence from other geophysical or geological data to confirm this hypothesis. Finally, the model does not fit in the Slovenian Karst area, where we do not have geologic or geophysical constraints, and even the gravity data are those integrated from the EGM08 model. Therefore, we decide not to force a solution for this part of the model, leaving it as an open problem.

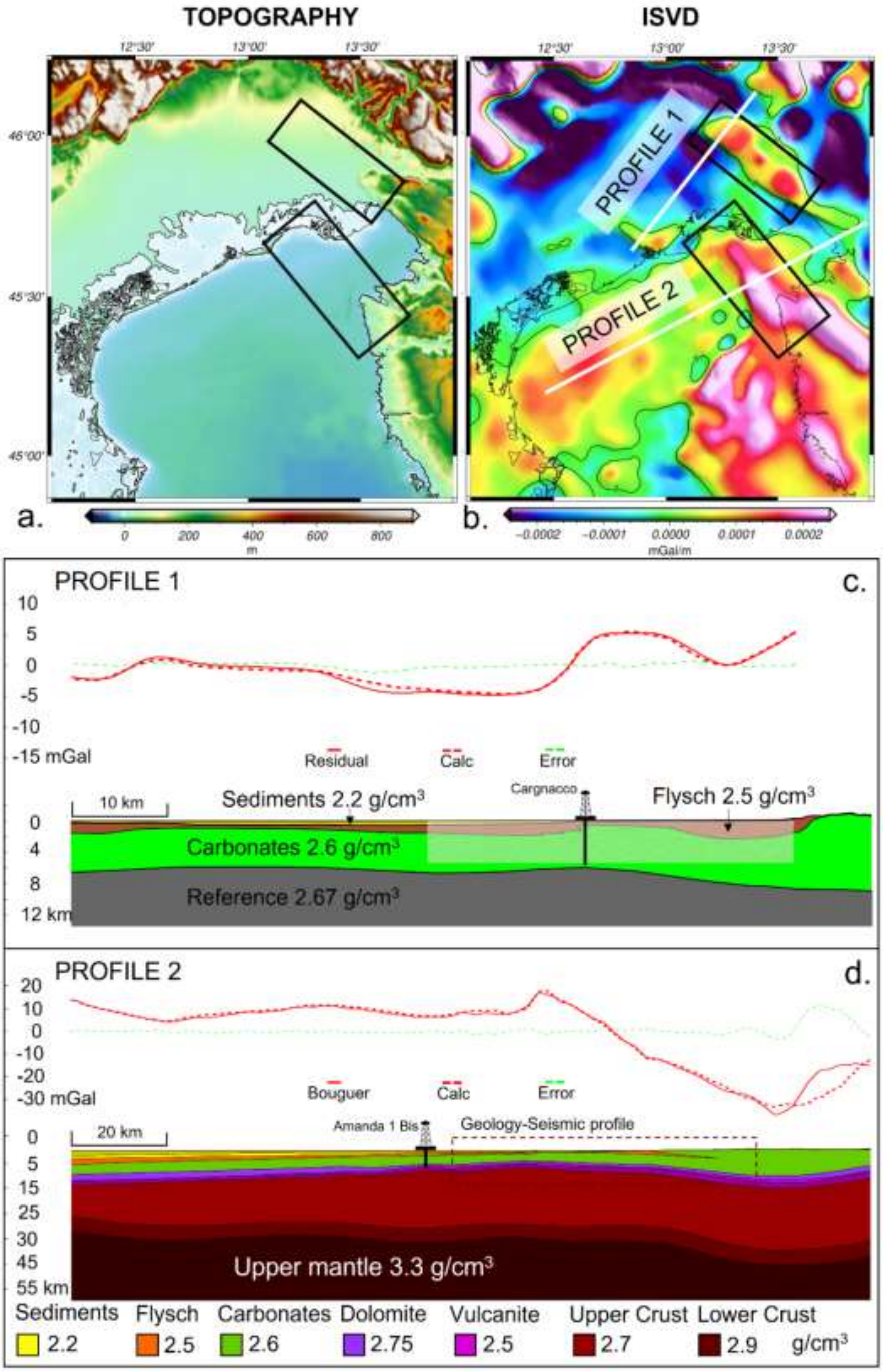

Figure 3-12 - (a) Map of topography/bathymetry of the Friuli Venezia Giulia Region and northern Adriatic Sea and (b) gravity map of the Integrated Second Vertical Derivative (ISVD), where positive anomalies pick in areas with no relevant morphologies. In the lower panels, the 2D-forward gravity models discussed in the text, the first (c) compared to the observed residual values and the second (d) to the Bouguer anomaly.

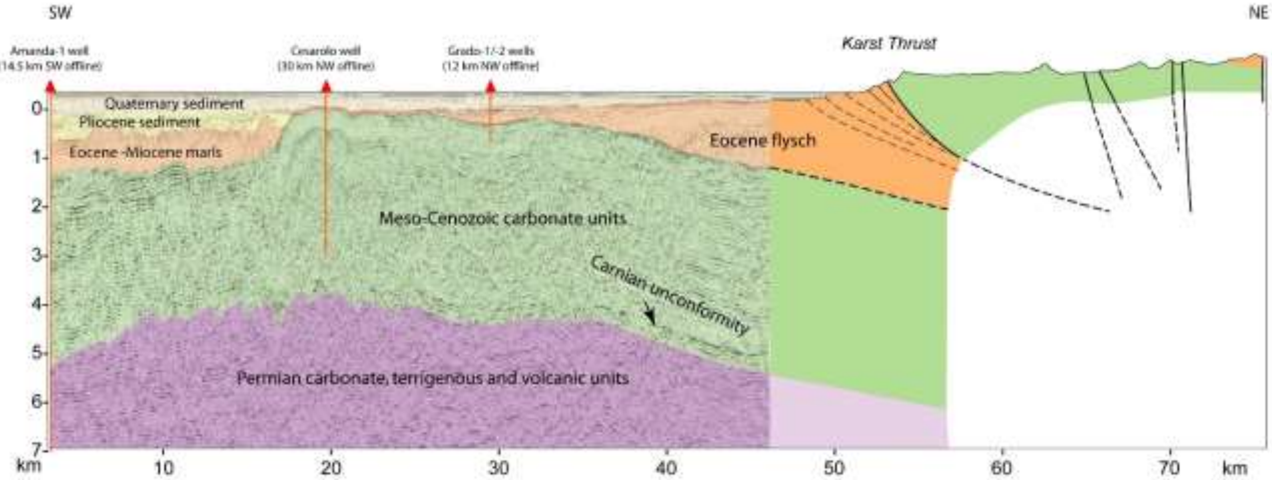

Figure 3-9 - Seismic/geological profile crossing from west to east the Gulf of Trieste, courtesy of M. Busetti and M. Dal Cin (see Figure 3-8d for the location). In the seismic profile is clearly visible the vertical detachment of the carbonates of ~1 km in correspondence with the Cesarolo well and the deepening of the carbonate platform towards the east.

4 Conclusion

In the geophysical field, the potential data represent the primary information to reconstruct the medium and large-scale structural arrangement of a given region, as they are able to determine the distribution of masses in-depth (in the case of gravimetry) and provide important information on the type of subsurface rocks (in the case of magnetometry). This information, combined with other more superficial geophysical data, such as for example the multi-channel seismic profiles, allow to determine with a certain reliability the geological and structural framework of a specific study area. Through the models (i.e., forward or inversion procedures), these geophysical practices represent the basis for any application in the geological, environmental, geotechnical field on a regional and local scale.

The logistical needs and the relative costs of carrying out geophysical surveys that involve a sufficiently large number of stations to allow a robust interpretation is, in any case, high. Today, they are very often unsustainable for research institutes and public bodies in general. The OGS, in the course of various geophysical surveys commissioned both by private companies and in the frame of scientific projects, has collected in a period of time ranging from the end of the 50s to the beginning of the 80s an immense number of gravimetric and magnetic data, both on land and at sea. Only a small percentage of these data have been published and made available to the scientific community. A consistent part is still in non-digital form and has not been made public yet. With a great work of research, recovery, collection, and homogenization, which started a few years ago, we are now trying to recover this immense amount of information, impossible today to replicate with new, financed research campaigns. The fact that these campaigns have been carried out over the years with different methodologies, with different instruments, and different investigation strategies linked to particular purposes, has made this dataset extremely inhomogeneous. The techniques that have been described in this PhD thesis to try to homogenize the data, paying particular attention to the inevitable errors at the crossing points between data acquired in different epochs and with different tools, and comparing the trends of the anomalies with those provided by the data derived from satellite, have been applied in two case studies: Gulf of Manfredonia and northern Adriatic Sea / Friulian Plain.

The choice of these two particular areas was conditioned by the following factors: (1) availability of gravimetric data (of different nature and acquired in different epochs) both at sea and on land, to verify the possibility of linking the datasets also in the areas of transition (coastal strips); (2) availability of geophysical data such as multi-channel seismic lines that offer a structural, albeit shallow, picture of the areas studied; (3) availability of high-resolution morphological data (i.e. DTM's), both from satellite and from airborne surveys, to apply the necessary terrain corrections to the greatest possible detail; (4) surface morphologies that tend to be flat or not very prominent (both on land and at sea), characterized by a sufficient sedimentary cover that masks the presence of important buried structures identified by other geophysical methods; (5) possibility of applying new processing techniques in order to map, perimeter and characterize the buried structural geological elements, so as to compare them with the information present in the literature and evaluate the improvements related to their application.

With regard to the Gulf of Manfredonia area, gravity data at the seabed were available, acquired in different epochs, land-based and satellite gravity data. In addition, multi-channel seismic lines were used. They revealed the presence of a buried structure linked to the tectonic system of Mattinata, which crosses the Gargano and crosses to the east the Gulf of Manfredonia. The seabed in this area, mainly flat, shows no morphological evidence of this structure. Therefore, the challenge was to demonstrate how gravimetric information can be of great help in reconstructing the geometries of these structures, even at great depths, through non-standard data derivation procedures (e.g., tilting), appropriate filtering, and data modeling along specific transects. Another important aspect was to verify if near the coast the satellite and ground datasets were compatible and able to detect similar anomalies. It has been seen that the data derived from satellites present considerable noise problems near the coast, and that, therefore, they are not very useful for land/sea correlations; meanwhile, the information derived from gravity at the sea-bottom made it possible to detect structures also of local importance, otherwise invisible.

In the northern Adriatic/Friulian Plain area, a significant gravimetric dataset was available, derived from a series of geophysical campaigns at sea and from a vast number of land stations. All this is extremely inhomogeneous and not easily correlated, especially regarding the coastal sector where there are large lagoon areas (Marano and Grado). The phase of homogenization of the data and the topographic corrections to be applied to the data, which in this case required the use of datasets with different resolutions, were particularly laborious but allowed to provide a much more detailed picture of the distribution of anomalies and timely with respect to what was previously published. In fact, gravimetric anomalies generated by the presence of Friuli-Dinaric Carbonate Platform displaced by faults, including the main SE-NW oriented ones and linked to the external front of the Dinarides, have been identified and bounded. In addition, the application of techniques such as Terracing has made it possible to discriminate these anomalies more accurately and has made it possible to compare the edges of the short-wavelength anomalies with the features recognized with other geophysical methodologies such as multi-channel seismic profiles. Ultimately, this made it possible to propose more reliable geological interpretations, with a greater number of constraints, so as to produce new gravimetric models.

Finally, the techniques described in this thesis have also been applied to the two large gravimetric and magnetic datasets available for the entire Mediterranean Sea, characterized by the presence of various intersection problems due to the use of data from different surveys. The applied leveling has recognized these errors, has minimized them and through appropriate filtering has homogenized the maps.

The examples reported here have shown how new techniques of analysis and processing of "vintage" data, suitably applied according to the quality of the information available, and compared with more recent data such as satellite-derived data, allow their full use.

A non-negligible economic value is also linked to this, considering the current logistical difficulty in acquiring new data for exploratory and scientific purposes. The examples have shown that the processed potential data and the related models have provided a geological and structural picture of the subsoil in many cases more precise and reliable than that produced in the recent past, perhaps using the same data.

5 Acknowledgments

Technical

***

We thank ENI for kindly providing us the gravity data of the TransAlp project (TRANSALP_IT) and the sea-bottom data in the Gulf of Manfredonia, OGS83 (see Table 1 and chapter 1.1 for details). We also thank them for the availability of the seismic data along which we modeled the gravimetric profiles.

***

Grids and maps were created using Generic Mapping Tools (GMT) version 6.1.1, the Python libraries Scypy and Matplotlib (Virtanen, et al., 2020; Hunter, 2007), and the QGIS software ("*QGIS Development Team, 2021. QGIS Geographic Information System. Open Source Geospatial Foundation. URL http://qgis.org*")

***

We used the python library Harmonica for the topographic corrections, which is part of the project Fatiando a Terra (Uieda et al., 2020), available at https://www.fatiando.org.

Personal

***

I would first like to thank my supervisor, Angelo Camerlenghi, and my co-supervisors, Emanuele Lodolo, Martina Busetti, Nicola Creati e Carla Barnaba, whose expertise was invaluable in formulating the research questions and improving the quality of my work.

***

A particular thanks to Gianni Mandrussani for his help collecting, digitalizing, processing, and archiving gravity and magnetic data from old papers records.

***

I warmly thanks Francesco Palmieri for sharing with me his extremely rare expertise in the field of gravimetry and his support in gravity data processing and modeling, and for the acquisition of gravity data in the frame of the LTA project

***

A kind thanks to prof. Carla Braitenberg and her collaborators, dr. Alberto Pastorutti and dr. Tommaso Pivetta, for their advice and supervision on gravity data processing.

***

In addition, I would like to thank my three sisters, Susanna, Lia, and Antonia, for their wise counsel and support in the time of need and my parents too.

***

Finally, I could not have completed this dissertation without the support of Sabrina, who stood by me with the utmost care and patience, despite my mood swings.

6 References

Agocs, W. B. (1951). Least squares residual anomaly determination. *Geophysics, 16*, 686–696.

Andersen, O. B. (2013). Marine gravity and geoid from satellite altimetry. I *Geoid Determination* (s. 401–451). Springer.

Andersen, O. B., & Knudsen, P. (1998). Global marine gravity field from the ERS-1 and Geosat geodetic mission altimetry. *Journal of Geophysical Research: Oceans, 103*, 8129–8137. doi:10.1029/97JC02198

Andersen, O. B., & Knudsen, P. (2000). The role of satellite altimetry in gravity field modelling in coastal areas. *Physics and Chemistry of the Earth, Part A: Solid Earth and Geodesy, 25*, 17–24. doi:10.1016/S1464-1895(00)00004-1

Andersen, O. B., & Knudsen, P. (2009). The DNSC08 mean sea surface and mean dynamic topography. *Journal of Geophysical Research: Solid Earth*, C11. doi:10.1029/2008JC005179

Andersen, O. B., Knudsen, P., & Am Berry, P. (2010). The DNSC08GRA global marine gravity field from double retracked satellite altimetry. *Journal of Geodesy, 84*, 191–199. doi:10.1007/s00190-009-0355-9

Andersen, O. B., Knudsen, P., & Stenseng, L. (2015). The DTU13 MSS (mean sea surface) and MDT (mean dynamic topography) from 20 years of satellite altimetry. I *IGFS 2014* (s. 111–121). Springer.

Andersen, O. B., Knudsen, P., Berry, P., Freeman, J., Pavlis, N., & Kenyon, S. (2008). The DNSC08 ocean wide altimetry derived gravity field: EGU Meeting Programme. *Abstract EGU2008-A-07163, G1-1MO1O-003*.

Andersen, O. B., Knudsen, P., Kenyon, S., & Holmes, S. (2014). Global and arctic marine gravity field from recent satellite altimetry (DTU13). *76th EAGE Conference and Exhibition 2014*, *2014*, s. 1–5. doi:10.3997/2214-4609.20140897

Andersen, O. B., Knudsen, P., Kenyon, S., Factor, J., & Holmes, S. (2013). The DTU13 Global marine gravity field—first evaluation. *Ocean Surface Topography Science Team Meeting, Boulder, Colorado.*

Anderson, H., & Jackson, J. (December 1987). Active tectonics of the Adriatic Region. *Geophysical Journal International, 91*, 937-983. doi:10.1111/j.1365-246X.1987.tb01675.x

Arso. (2016). Ministry of the environment and spatial planning, Slovenian environment agency. Shapefile of the Slovenia coastline retrieved from: https://gis.arso.gov.si. *Ministry of the environment and spatial planning, Slovenian environment agency. Shapefile of the Slovenia coastline retrieved from: https://gis.arso.gov.si*.

Aydogan, D. (2011). Extraction of lineaments from gravity anomaly maps using the gradient calculation: Application to Central Anatolia. *Earth, Planets and Space, 63*, 903–913. doi:10.5047/eps.2011.04.003

Ballu, V., Dubois, J., Deplus, C., Diament, M., & Bonvalot, S. (1998). Crustal structure of the Mid-Atlantic Ridge south of the Kane Fracture Zone from seafloor and sea surface gravity data. *Journal of Geophysical Research: Solid Earth, 103*, 2615–2631. doi:10.1029/97JB02542

Barison, E. (2008). *Il contributo dei dati sismici per la valutazione delle risorse idriche e geotermiche della pianura friulana.* Ph.D. dissertation, Università degli studi di Trieste.

Barthelmes, F. (2009). Definition of functionals of the geopotential and their calculation from spherical harmonic models: theory and formulas used by the calculation service of the International Centre for Global Earth Models (ICGEM), http://icgem. gfz-potsdam. de. doi:10.2312/GFZ.b103-09026

Bechtold, M., Battaglia, M., Tanner, D. C., & Zuliani, D. (2009). Constraints on the active tectonics of the Friuli/NW Slovenia area from CGPS measurements and three-dimensional kinematic modeling. *Journal of Geophysical Research: Solid Earth, 114*.

Berrino, G. (2020). The state of the art of gravimetry in Italy. *Rendiconti Lincei. Scienze Fisiche e Naturali, 31*, 35–48.

Billi, A., Gambini, R., Nicolai, C., & Storti, F. (2007). Neogene-Quaternary intraforeland transpression along a Mesozoic platform-basin margin: The Gargano fault system, Adria, Italy. *Geosphere, 3*, 1–15. doi:10.1130/GES00057.1

Blakely, R. J. (1996). *Potential theory in gravity and magnetic applications.* Cambridge university press.

Blakely, R. J., & Simpson, R. W. (1986). Approximating edges of source bodies from magnetic or gravity anomalies. *Geophysics 51.7*, 1494–1498. doi:10.1190/1.1442197

Bomfim, E. P., Braitenberg, C., & Molina, E. C. (August 2013). Mutual evaluation of global gravity models (EGM2008 and GOCE) and terrestrial data in Amazon Basin, Brazil. *Geophysical Journal International, 195*, 870-882. doi:10.1093/gji/ggt283

Borghi, A., Carrion, D., & Sona, G. (2007). Validation and fusion of different databases in preparation of high-resolution geoid determination. *Geophysical Journal International, 171*, 539–549.

Bullard, E. C. (1936). Gravity measurements in east Africa. *Philosophical Transactions of the Royal Society of London. Series A, Mathematical and Physical Sciences, 235*, 445–531.

Busetti, M., Cova, A., Marchi, M., Romeo, R., Volpi, V., & Zgur, F. (2005). *Realizzazione della carta geologico-tecnica della risorsa geotermica regionale.* Tech. rep., Istituto Nazionale di Oceanografia e Geofisica Sperimentale.

Busetti, M., Volpi, V., Barison, E., Giustiniani, M., Marchi, M., Ramella, R., . . . Zanolla, C. (2010a). Meso-Cenozoic seismic stratigraphy and the tectonic setting of the Gulf of Trieste (northern Adriatic). *GeoActa, SP, 3*, 1–14.

Busetti, M., Volpi, V., Nicolich, R., Barison, E., Romeo, R., Baradello, L., . . . others. (2010b). Dinaric tectonic features in the Gulf of Trieste (northern Adriatic Sea). *Bollettino di Geofisica Teorica ed Applicata, 51*.

Carmisciano, C., Berrino, G., Cocchi, L., Muccini, F., Gasparoni, F., Furlan, F., & De Paulis, R. (2011). *Aggiornamento tecnologico e test funzionali del gravimetro da fondo LaCoste&Romberg modello U-HG24.* ISSN 2039-7941, NationalInstitute of Geophysics and Volcanology (INGV).

Carozzo, M. T., Luzio, D., Margiotta, C., & Quarta, T. (1992). Gravity map of Italy, scale 1: 500,000. *Quaderni de "La Ricerca Scientifica, 114*.

Cassano, E. (1983). Contributo AGIP alla carta gravimetrica d'Italia. *Atti II Conv. GNGTS*, *1*, s. 183–188.

Cassano, E., & Maino, A. (1989). Carta gravimetrica d'Italia. *Scale, 1*, 000.

Cati, A., Fichera, R., & Cappelli, V. (1987). Northeastern Italy. Integrated processing of geophysical and geological data. *Memorie della Società Geologica Italiana, 40*, 273–288.

Cella, F., Nappi, R., Paoletti, V., & Florio, G. (2021). Basement Mapping of the Fucino Basin in Central Italy by ITRESC Modeling of Gravity Data. *Geosciences, 11*, 398.

Ciani, A., Morelli, C., & Gantar, C. (1960). Rilievo gravimetrico sullo zoccolo epicontinentale dei mari italiani. *Boll. Geofis. Teor. Appl*, 101p.

Colantoni, P., Tramontana, M., & Tedeschi, R. (1990). Contributo alla conoscenza dell'avampaese apulo: struttura del Golfo di Manfredonia (Adriatico meridionale). *Giornale di Geologia*.

Consortium, E. B., & others. (2018). EMODnet Digital Bathymetry (DTM 2018).

Cooper, G. R., & Cowan, D. R. (2009). Terracing potential field data. *Geophysical prospecting, 57*, 1067–1071.

Cordell, L., & McCafferty, A. E. (1989). A terracing operator for physical property mapping with potential field data. *Geophysics, 54*, 621–634.

Corrado, G., & Rapolla, A. (1981). The gravity field of Italy: analysis of its spectral composition and delineation of a tridimensional crustal model for central-southern Italy. *Boll. Geofis. Teor. Appl.*, 17–29.

Cunietti, M., & Inghilleri, G. (1955). *La rete gravimetrica fondametale italiana.* Biblioteca Centrale del Politecnico.

D'agostino, N., Cheloni, D., Mantenuto, S., Selvaggi, G., Michelini, A., & Zuliani, D. (2005). Strain accumulation in the southern Alps (NE Italy) and deformation at the northeastern boundary of Adria observed by CGPS measurements. *Geophysical Research Letters, 32*.

Dal Cin, M. (2018). *3D velocity depth model in the Gulf of Trieste by means of tomographic analysis from multichannel seismic reflection data.* Ph.D. dissertation, University of Trieste.

Dampney, C. N. (1969). THE EQUIVALENT SOURCE TECHNIQUE. *GEOPHYSICS, 34*, 39-53. doi:10.1190/1.1439996

Dawson, G. J., Green, C. M., & Fletcher, K. M. (2015). Using the SAR Mode from CryoSat-2 to Improve Satellite Derived Gravity near the Coast. *77th EAGE Conference and Exhibition 2015*, *2015*, s. cp–451. doi:10.3997/2214-4609.201412985 de Alteriis, G. (1995). Different foreland basins in Italy: examples from the central and southern Adriatic Sea. *Tectonophysics, 252*, 349–373. doi:10.1016/0040-1951(95)00155-7

de Alteriis, G., & Aiello, G. (1993). Stratigraphy and tectonics offshore of Puglia (Italy, southern Adriatic Sea). *Marine Geology, 113*, 233–253. doi:10.1016/0025-3227(93)90020-V

de Lerma, D., Green, C. M., Cheyney, S., & Campbell, S. J. (2015). Improved high order vertical derivatives of potential field data-extending the ISVD Method. *77th EAGE Conference and Exhibition 2015*, *2015*, s. 1–5. doi:10.3997/2214-4609.201412755

Decker, B. L. (1986). World Geodetic System 1984.

Decker, B. L. (1986). World geodetic system 1984: Defense Mapping Agency Aerospace Center St Louis Afs Mo. *World geodetic system 1984: Defense Mapping Agency Aerospace Center St Louis Afs Mo*.

Deng, X., & Featherstone, W. E. (2006). A coastal retracking system for satellite radar altimeter waveforms: Application to ERS-2 around Australia. *Journal of Geophysical Research: Oceans, 111*. doi:10.1029/2005JC003039

dos Santos, F. P., & Bonvalot, S. (2016). Cold-Atom Absolute Gravimetry. *Cold-Atom Absolute Gravimetry*, 1-6. doi:10.1007/978-3-319-02370-0_30-1

Dubois, J., & Deplus, C. (1989). Gravimetry on the Erimo seamount, Japan. *Tectonophysics, 160*, 267–275.

Earth Resources Observation And Science (EROS) Center. (2017). Shuttle Radar Topography Mission (SRTM) Void Filled. *Shuttle Radar Topography Mission (SRTM) Void Filled*. U.S. Geological Survey. doi:10.5066/F7F76B1X

Fairhead, J. D. (2016). *Advances in gravity and magnetic processing and interpretation.* EAGE Publications.

Farr, T. G., Kobrick, M., Farr, T. G., & Kobrick, M. (2000). Shuttle Radar Topography Mission produces a wealth of data. *Eos, Transactions American Geophysical Union, 81*, 583–585.

Favalli, M., & Pareschi, M. T. (2004). Digital elevation model construction from structured topographic data: the DEST algorithm. *Journal of Geophysical Research: Earth Surface, 109*.

Fedi, M. (2002). Multiscale derivative analysis: A new tool to enhance detection of gravity source boundaries at various scales. *Geophysical Research Letters, 29*, 16–1. doi:10.1029/2001GL013866

Fedi, M., & Florio, G. (2001). Detection of potential fields source boundaries by enhanced horizontal derivative method. *Geophysical Prospecting, 49*, 40–58. doi:10.1046/j.1365-2478.2001.00235.x

Fedi, M., Cella, F., Florio, G., & Rapolla, A. (2005). Multiscale derivative analysis of the gravity and magnetic fields of Southern Apennines (Italy). *CROP Project, Deep seismic exploration of the Central Mediterranean and Italy (Atlases in Geoscience, Volume 1)", I. Finetti, ed., Elsevier Science*, 281–318.

Ferri, F., Ventura, R., Coren, F., & Zanolla, C. (2005). Gravity Map of Italy and Surroundings Seas 1: 1250000. *APAT Agenzia per la protezione dell'ambiente e per i servizi tecnici. Dipartimento Difesa del Suolo*.

Finetti, I. (1983). Struttura ed evoluzione della microplacca adriatica. *Boll. Ocean. Teor. Appl. II (2), 115–123*.

Finetti, I. R., & Del Ben, A. (2005). Crustal tectono-stratigraphic setting of the Adriatic Sea from new CROP seismic data. *CROP project: Deep seismic exploration of the Central Mediterranean and Italy, 1*, 519–548.

FitzGerald, D., & Milligan, P. (2013). Defining a deep fault network for Australia, using 3D'worming'. *ASEG Extended Abstracts, 2013*, 1–4. doi:10.1071/ASEG2013ab135

Forsberg, R. (1984). A study of terrain reductions, density anomalies and geophysical inversion methods in gravity field modelling. *A study of terrain reductions, density anomalies and geophysical inversion methods in gravity field modelling*.

Förste, C., Bruinsma, S. L., Abrikosov, O., Lemoine, J.-M., Schaller, T., Götze, H. J., . . . others. (2014). EIGEN-6C4 The latest combined global gravity field model including GOCE data up to degree and order 2190 of GFZ Potsdam and GRGS Toulouse. *GFZ Data Services, 10*. doi:https://doi.org/10.5880/icgem.2015.1

Friis-Christensen, E., Lühr, H., & Hulot, G. (2006). Swarm: A constellation to study the Earth's magnetic field. *Earth, planets and space, 58*, 351–358.

Fu, L.-L., & Cazenave, A. (2000). *Satellite altimetry and earth sciences: a handbook of techniques and applications.* Elsevier.

Fullea, J., Fernandez, M., & Zeyen, H. (2008). FA2BOUG—A FORTRAN 90 code to compute Bouguer gravity anomalies from gridded free-air anomalies: Application to the Atlantic-Mediterranean transition zone. *Computers & Geosciences, 34*, 1665–1681. doi:10.1016/j.cageo.2008.02.018

Gallant, J. (December 2019). Merging lidar with coarser DEMs for hydrodynamic modelling over large areas. Modelling and Simulation Society of Australia and New Zealand. doi:10.36334/modsim.2019.k24.gallant

Gantar, C. (1983). Rilievo gravimetrico offshore mgb002: Sullo zoccolo continentale nel mare Adriatico, per l'Agip Mineraria. *Rilievo gravimetrico offshore mgb002: Sullo zoccolo continentale nel mare Adriatico, per l'Agip Mineraria.* Osservatorio Geofisico Sperimentale (OGS), Rel. 5/83 - MNS/1, Rapporto finale N. 82595.

Gantar, C., Morelli, C., & Pisani, M. (1968). Information report on surface gravity and magnetic measurements withthe ship Bannock in the Mediterranean sea. *Boll. Geof. Teor. Appl.*, 134-157.

Gatti, A., Reguzzoni, M., Migliaccio, F., & Sansò, F. (September 2016). Computation and assessment of the fifth release of the GOCE-only space-wise solution. *Computation and assessment of the fifth release of the GOCE-only space-wise solution*. doi:10.13140/RG.2.2.28625.94569

GDAL/OGR contributors. (2021). *GDAL/OGR Geospatial Data Abstraction software Library.* Hentet fra https://gdal.org

Götze, H.-J., & Lahmeyer, B. (1988). Application of three-dimensional interactive modeling in gravity and magnetics. *Geophysics, 53*, 1096–1108.

GRASS Development Team. (2017). *Geographic Resources Analysis Support System (GRASS GIS) Software, Version 7.2.* Hentet fra http://grass.osgeo.org

Green, C. M., Fletcher, K. M., Cheyney, S., Dawson, G. J., & Campbell, S. J. (2019). Satellite gravity – enhancements from new satellites and new altimeter technology. *Geophysical Prospecting, 67*, 1611-1619.

Hackney, R. I., & Featherstone, W. E. (2003). Geodetic versus geophysical perspectives of the 'gravity anomaly'. *Geophysical Journal International, 154*, 35–43.

Hell, B., & Jakobsson, M. (2011). Gridding heterogeneous bathymetric data sets with stacked continuous curvature splines in tension. *Marine Geophysical Research, 32*, 493–501.

Hidayat, R., & Green, R. (2009). Real-time texture boundary detection from ridges in the standard deviation space. *Proceedings of the British Machine Vision Conference* (s. 5.1-5.10). BMVA Press.

Hildebrand, J. A., Stevenson, J. M., Hammer, P. T., Zumberge, M. A., Parker, R. L., Fox, C. G., & Meis, P. J. (1990). A seafloor and sea surface gravity survey of Axial Volcano. *Journal of Geophysical Research: Solid Earth, 95*, 12751–12763. doi:10.1029/JB095iB08p12751

Hinze, W. J., Aiken, C., Brozena, J., Coakley, B., Dater, D., Flanagan, G., . . . others. (2005). New standards for reducing gravity data: The North American gravity database. *Geophysics, 70*, J25–J32. doi:10.1190/1.1988183

Hofmann-Wellenhof, B., & Moritz, H. (2006). *Physical geodesy.* Springer Science & Business Media.

Holme, R., Olsen, N., Rother, M., & Lühr, H. (2003). CO2 — A Champ Magnetic Field Model. I C. Reigber, H. Lühr, & P. Schwintzer (Red.), *First CHAMP Mission Results for Gravity, Magnetic and Atmospheric Studies* (s. 220–225). Berlin, Heidelberg: Springer Berlin Heidelberg. doi:10.1007/978-3-540-38366-6_32

Hunter, J. D. (2007). Matplotlib: A 2D graphics environment. *Computing in Science & Engineering, 9*, 90–95. doi:10.1109/MCSE.2007.55

IDT-RV. (2016). Infrastruttura Dati Territoriali della Regione del Veneto. Shapefile of the Veneto coastline and Lagoon of Venice at scale of 1:5000 retrieved from: https://idt2.regione.veneto.it. *Infrastruttura Dati Territoriali della Regione del Veneto. Shapefile of the Veneto coastline and Lagoon of Venice at scale of 1:5000 retrieved from: https://idt2.regione.veneto.it*.

Ince, E. S., Barthelmes, F., Reißland, S., Elger, K., Förste, C., Flechtner, F., & Schuh, H. (2019). ICGEM – 15 years of successful collection and distribution of global gravitational models, associated services, and future plans. *11*, 647-674. doi:10.5194/essd-11-647-2019

International Hydrographic Organization. (2018). Regulations of the IHO for International (INT) Charts and Chart Specifications of the IHO. *Regulations of the IHO for*

International (INT) Charts and Chart Specifications of the IHO. International Hydrographic Organization Principauté de Monaco, Monaco.

IRDAT-FVG. (2015). Infrastruttura Regionale di Dati Ambientali e Territoriali per il Friuli Venezia Giulia. Shapefile of the Friuli Venezia Giulia coastline at scale of 1:5000 retrieved from: https://irdat.regione.fvg.it/WebGIS/. *Infrastruttura Regionale di Dati Ambientali e Territoriali per il Friuli Venezia Giulia. Shapefile of the Friuli Venezia Giulia coastline at scale of 1:5000 retrieved from: https://irdat.regione.fvg.it/WebGIS/*.

Jarvis, A., Reuter, H. I., Nelson, A., Guevara, E., & others. (2008). Hole-filled SRTM for the globe Version 4. *available from the CGIAR-CSI SRTM 90m Database (http://srtm. csi. cgiar. org), 15*, 25–54.

Kastelic, V., Vrabec, M., Cunningham, D., & Gosar, A. (2008). Neo-Alpine structural evolution and present-day tectonic activity of the eastern Southern Alps: The case of the Ravne Fault, NW Slovenia. *Journal of structural geology, 30*, 963–975.

Keating, P., & Pinet, N. (2011). Use of non-linear filtering for the regional–residual separation of potential field data. *Journal of Applied Geophysics, 73*, 315-322. doi:https://doi.org/10.1016/j.jappgeo.2011.02.002

Kebede, H., Alemu, A., & Fisseha, S. (2020). Upward continuation and polynomial trend analysis as a gravity data decomposition, case study at Ziway-Shala basin, central Main Ethiopian rift. *Heliyon, 6*, e03292.

Lacoste, L. J. (1973). CROSSCORRELATION METHOD FOR EVALUATING AND CORRECTING SHIPBOARD GRAVITY DATA. *38*, 701-709. doi:10.1190/1.1440369

LaFehr, T. R. (1991). An exact solution for the gravity curvature (Bullard B) correction. *Geophysics, 56*, 1179–1184.

LaFehr, T. R., & Nettleton, L. L. (1967). Quantitative evaluation of a stabilized platform shipboard gravity meter. *Geophysics, 32*, 110–118.

Li, X., & Götze, H.-J. (2001). Ellipsoid, geoid, gravity, geodesy, and geophysics. *Geophysics, 66*, 1660–1668.

Lowrie, W. (2007). Fundamentals of Geophysics. *Fundamentals of Geophysics*. doi:10.1017/cbo9780511807107

Ludwig, N. J., & Drake, C. L. (1970). Seismic refraction. *in The Sea,ed. A. E. Maxwell*.

Luyendyk, B. P. (1984). On-bottom gravity profile across the East Pacific Rise crest at 21 north. *Geophysics, 49*, 2166–2177. doi:10.1190/1.1441632

Magrin, A., & Rossi, G. (2020). Deriving a new crustal model of Northern Adria: the Northern Adria Crust (NAC) model. *Frontiers in Earth Science, 8*, 89.

Makris, J., Morelli, C., & Zanolla, C. (1998). The Bouguer gravity map of the Mediterranean Sea (IBCM-G). *Boll. Geofis. Teor. Appl, 39*, 79–98.

Marson, I., & Morelli, C. (1978). First order gravity net in Italy. *Boll. Geodesia e Scienze Affini I.G.M.*, 659-698.

Mastronuzzi, G., Palmentola, G., & Sansò, P. (2002). Lineamenti e dinamica della costa pugliese. *Studi costieri, 5*, 9–22.

Merlini, S., Doglioni, C., & Ponton, M. (2002). Analisi strutturale lungo un profilo geologico tra la linea Fella-Sava e l'avampaese adriatico (Friouli Venezia Giulia-Italia). *Memorie Società Geologica Italiana, 57, 293-300.*

Meyer, B., Chulliat, A., & Saltus, R. (2017). Derivation and Error Analysis of the Earth Magnetic Anomaly Grid at 2 arc min Resolution Version 3 (EMAG2v3). *Geochemistry, Geophysics, Geosystems, 18*, 4522-4537. doi:https://doi.org/10.1002/2017GC007280

Meyer, B., Saltus, R., & Chulliat, A. (2017). EMAG2v3: Earth Magnetic Anomaly Grid (2-arc-minute resolution): National Centers for Environmental Information, National Oceanic and Atmospheric Administration.

Mickus, K. L., Aiken, C. L., & Kennedy, W. D. (1991). Regional-residual gravity anomaly separation using the minimum-curvature technique. *Geophysics, 56*, 279–283.

Migliaccio, F., Reguzzoni, M., Gatti, A., Sansò, F., & Herceg, M. (April 2011). A GOCE-Only Global Gravity Field Model by the Space-Wise Approach., (s. 39-).

Miller, H. G., & Singh, V. (1994). Potential field tilt—a new concept for location of potential field sources. *Journal of Applied Geophysics, 32*, 213–217. doi:10.1016/0926-9851(94)90022-1

Mittal, P. K. (1984). Algorithm for error adjustment of potential field data along a survey network. *Geophysics, 49*, 467–469.

Montaj, G. O. (2017). GM-SYS Gravity and Magnetic Modelling Software. *User's Guide Version, 9*, 8.

Morell, C., Pisani, M., & Gantar, C. (1975). Geophysical anomalies and tectonics in the Wstern Mediterranean. *Bollettino di Geofisica Teorica e Applicata, 18*, 211-249.

Morelli, C. (1948). Discussione e considerazioni sulla compensazione d'insieme della rete internazionale delle stazioni di riferimento per le misure di gravità relativa. *Annals of Geophysics, 1*, 425–454.

Morelli, C. (1950). Rilievo Gravimetrico Sperimentale nella zona di Zaule (Trieste). *Bollettino di Geofisica Teorica ed Applicata, I*.

Morelli, C. (1951). Rilievo Gravimetrico e Riduzione Isostatica nell'Italia Nord-Orientale. *Bollettino di Geofisica Teorica ed Applicata, I*.

Morelli, C. (June 1952). Primo contributo per una rete gravimetrica fondameritale in Italia. *Annals of Geophysics, 5*. doi:10.4401/ag-5837

Morelli, C. (1954). Rilievo Gravimetrico e Magnetico del Veneto centro-orientale. *Bollettino di Geofisica Teorica ed Applicata, II*.

Morelli, C. (1966). The Geophysical Situation in Italian Waters. *The International Hydrographic Review*.

Morelli, C. (1995). Gino Cassinis e la gravimetria in Italia. *Rendiconti Lincei, 6*, 5–17. doi:10.1007/BF03001631

Morelli, C., Gantar, C., McConnell, R. K., Szabo, B., & Uotila, U. (1972). The international gravity standardization net 1971 (IGSN 71). *The international gravity standardization net 1971 (IGSN 71)*.

Moritz, H. (1980). Geodetic reference system 1980. *Bulletin géodésique, 54*, 395–405.

Nabighian, M. N., Ander, M. E., Grauch, V. J., Hansen, R. O., LaFehr, T. R., Li, Y., . . . Ruder, M. E. (2005). Historical development of the gravity method in exploration. *Geophysics, 70*, 63ND–89ND.

Nagy, D., Papp, G., & Benedek, J. (2000). The gravitational potential and its derivatives for the prism. *Journal of Geodesy, 74*, 552–560. doi:10.1007/s001900000116

Nagy, D., Papp, G., & Benedek, J. (2002). Corrections to" The gravitational potential and its derivatives for the prism". *Journal of Geodesy, 76*, 475–475.

Nicolich, R., Della Vedova, B., Giustiniani, M., & Fantoni, R. (2004). Carta del sottosuolo della Pianura Friulana (Map of subsurface of the Friuli Plain). *Regione Autonoma Friuli Venezia Giulia, Direzione Centrale Ambiente e Lavori Pubblici. Servizio Geologico 32.*

Nowell, D. A. (1999). Gravity terrain corrections—an overview. *Journal of Applied Geophysics, 42*, 117–134. doi:10.1016/S0926-9851(99)00028-2

Oehler, J.-F., Rouxel, D., & Lequentrec-Lalancette, M.-F. (2018). Comparison of global geomagnetic field models and evaluation using marine datasets in the north-eastern Atlantic Ocean and western Mediterranean Sea. *Earth, Planets and Space, 70*, 99. doi:10.1186/s40623-018-0872-y

Oliphant, T. E. (2006). *A guide to NumPy* (Årg. 1). Trelgol Publishing USA.

Pail, R. (2014). CHAMP-, GRACE-, GOCE-Satellite Projects. *CHAMP-, GRACE-, GOCE-Satellite Projects*, 1-11. doi:10.1007/978-3-319-02370-0_29-1

Palmieri, F., & Coren, F. (2002). *Progetto TS-SAR. Rete microgravimetrica di controllo: periodo 2001-2002.* Tech. rep., Istituto Nazionale di Oceanografia e di Geofisica Sperimentale.

Parker, R. L. (1973). The rapid calculation of potential anomalies. *Geophysical Journal International, 31*, 447–455. doi:10.1111/j.1365-246X.1973.tb06513.x

Pavlis, N. K., Holmes, S. A., Kenyon, S. C., & Factor, J. K. (2012). The development and evaluation of the Earth Gravitational Model 2008 (EGM2008). *Journal of Geophysical Research: Solid Earth, 117*. doi:10.1029/2011JB008916

Picchio, S. (2006). Analisi delle variazioni altimetriche in un'area studio del delta del Po. *Analisi delle variazioni altimetriche in un'area studio del delta del Po*. ASITA.

Pilkington, M., & Boulanger, O. (May 2017). Potential field continuation between arbitrary surfaces — Comparing methods. *GEOPHYSICS, 82*, J9-J25. doi:10.1190/geo2016-0210.1

Ponton, M. (2015). Depth structural analysis of the external Dinaric chain in Julian Alps and Prealps (Italy and Slovenia). *Gortania Atti Museo Friulano di St Nat Udine 36:23–34*.

Prodan, M. (2002). *Rilievo gravimetrico e interpretazione strutturale nella provincia di Trieste.* Ph.D. dissertation, Università degli Studi di Trieste.

PROJ contributors. (2021). *PROJ coordinate transformation software library.* Hentet fra https://proj.org/; pyproj4.github.io/pyproj

Rapolla, A. (1986). Crustal structure of Central and Southern Italy from gravity and magnetic data. *Giornale di Geologia, 48*, 129–143.

Regione Autonoma Friuli Venezia Giulia. (2020). La costruzione delle banche dati territoriali nel contesto dell'infrastruttura regionale di dati ambientali e territoriali (irdat fvg). *La costruzione delle banche dati territoriali nel contesto dell'infrastruttura regionale di dati ambientali e territoriali (irdat fvg)*. Hentet fra https://www.regione.fvg.it/rafvg/export/sites/default/RAFVG/ambiente-territorio/conoscere-ambiente-territorio/allegati/La_costruzione_delle_banche_dati_territoriali_in_IRDAT_fvg_v3-20.pdf

Reutebuch, S. E., McGaughey, R. J., Andersen, H.-E., & Carson, W. W. (2003). Accuracy of a high-resolution lidar terrain model under a conifer forest canopy. *Canadian journal of remote sensing, 29*, 527–535.

Reuter, H. I., Nelson, A., & Jarvis, A. (2007). An evaluation of void-filling interpolation methods for SRTM data. *International Journal of Geographical Information Science, 21*, 983-1008. doi:10.1080/13658810601169899

Rodriguez, E., Morris, C. S., Belz, J. E., Chapin, E., Martin, J., Daffer, W., & Hensley, S. (January 2005). An assessment of the SRTM topographic products. *An Assessment of the SRTM Topographic Products*.

Ruiz, H., Agersborg, R., Hille, L., Lindgård, J. E., Lien, M., & Vatshelle, M. (2016). Monitoring offshore reservoirs using 4D gravity and subsidence with improved tide corrections. *2016 SEG International Exposition and Annual Meeting.*

Rummel, R. (2020). Earth's gravity from space. *31*, 3-13. doi:10.1007/s12210-020-00889-8

Sandwell, D. T. (1992). Antarctic marine gravity field from high-density satellite altimetry. *Geophysical Journal International, 109*, 437–448. doi:10.1111/j.1365-246X.1992.tb00106.x

Sandwell, D. T. (2002). Reference earth model-WGS84. *Scripps Institution of Oceanography*.

Sandwell, D. T., & Smith, W. H. (2009). Global marine gravity form retracked Geosat and ERS-1 altimetry: Ridge segmentation versus spreading rate. *Journal of Geophysical Reseach, 10*. doi:10.1029/2008JB006008

Sandwell, D. T., Müller, R. D., Smith, W. H., Garcia, E., & Francis, R. (2014). New global marine gravity model from CryoSat-2 and Jason-1 reveals buried tectonic structure. *Science (New York, N.Y.), 346*, 65–67. doi:10.1126/science.1258213

Sandwell, Garcia, E., Soofi, K., Wessel, P., Chandler, M., & Smith, W. H. (2013). Toward 1-mGal accuracy in global marine gravity from CryoSat-2, Envisat, and Jason-1. *The Leading Edge, 32*, 892–899. doi:10.1190/tle32080892.1

Schmdit, S., Götze, H.-J., Fichler, C., & Alver, M. (2010). IGMAS+ a new 3D Gravity, FTG and Magnetic Modeling Software. *Geoinformatik*, (s. 57–63).

Schmidt, S., Anikiev, D., Götze, H.-J., Garcia, À. G., Dacal, M. L., Meeßen, C., . . . Scheck-Wenderoth, M. (2020). *IGMAS+–a tool for interdisciplinary 3D potential field modelling of complex geological structures.* Tech. rep., Copernicus Meetings.

Snyder, J. P. (1987). *Map projections–A working manual* (Årg. 1395). US Government Printing Office.

Soler, S. R., & Uieda, L. (2021). Gradient-boosted equivalent sources. *Geophysical Journal International, 227*, 1768–1783.

Somigliana, C. (1930). Geofisica—Sul campo gravitazionale esterno del geoide ellissoidico. *Atti della Reale Academia Nazionale dei Lincei Rendiconti, 6*, 237-234.

Stacey, F. D., & Tuck, G. J. (1981). Geophysical evidence for non-Newtonian gravity. *Nature, 292*, 230–232. doi:10.1038/292230a0

Talwani, M. (1964). Computation of magnetic anomalies caused by two-dimensional bodies of arbitrary shape. *Computers in the mineral industries, 1*, 464–480.

Talwani, M., Worzel, J. L., & Landisman, M. (1959). Rapid gravity computations for two-dimensional bodies with application to the Mendocino submarine fracture zone. *Journal of Geophysical Research (1896-1977), 64*, 49-59. doi:https://doi.org/10.1029/JZ064i001p00049

Tarquini, S., Vinci, S., Favalli, M., Doumaz, F., Fornaciai, A., & Nannipieri, L. (2012). Release of a 10-m-resolution DEM for the Italian territory: Comparison with global-coverage DEMs and anaglyph-mode exploration via the web. *Computers & Geosciences, 38*, 168-170. doi:https://doi.org/10.1016/j.cageo.2011.04.018

Tesauro, M., Kaban, M. K., & Cloetingh, S. A. (2008). EuCRUST-07: A new reference model for the European crust. *Geophysical Research Letters, 35*.

Torge, W., & Müller, J. (2012). Geodesy. *Geodesy*. doi:10.1515/9783110250008

Triches, A., Pillon, S., Bezzi, A., Lipizer, M., Gordini, E., Villalta, R., . . . Ramella, R. (2011). *Carta batimetrica della Laguna di Marano e Grado.* Tech. rep., Regione Autonoma Friuli Venezia Giulia.

Triglav Cekada, M., Bric, V., Primož, K., Mongus, D., Lukac, N., & Zalik, B. (November 2015). Nationwide aerial laser scanning for 3D-acquisition of water surfaces in Slovenia.

Trincardi, F., Campiani, E., Correggiari, A., Foglini, F., Maselli, V., & Remia, A. (2014). Bathymetry of the Adriatic Sea: The legacy of the last eustatic cycle and the impact of modern sediment dispersal. *Journal of Maps, 10*, 151–158.

Trobec, A., Busetti, M., Zgur, F., Baradello, L., Babich, A., Cova, A., . . . others. (2018). Thickness of marine Holocene sediment in the Gulf of Trieste (northern Adriatic Sea). *Earth System Science Data, 10*, 1077–1092.

Uieda, L., Barbosa, V. C., & Braitenberg, C. (2016). Tesseroids: Forward-modeling gravitational fields in spherical coordinates. *Geophysics, 81*, F41–F48. doi:10.1190/geo2015-0204.1

Uieda, L., Soler, S. R., Pesce, A., Oliveira Jr, V. C., & Shea, N. (2020). Harmonica: Forward modeling, inversion, and processing gravity and magnetic data (Version v0.1.0). doi:10.5281/zenodo.3628742

Venturini, S. (2002). Il pozzo Cargnacco 1: un punto di taratura stratigrafica nella pianura friulana. *Mem. Soc. Geol. It, 57*, 11–18.

Virtanen, P., Gommers, R., Oliphant, T. E., Haberland, M., Reddy, T., Cournapeau, D., . . . Contributors, S. 1. (2020). SciPy 1.0: Fundamental Algorithms for Scientific Computing in Python. *Nature Methods, 17*, 261–272. doi:10.1038/s41592-019-0686-2

Virtanen, P., Gommers, R., Oliphant, T. E., Haberland, M., Reddy, T., Cournapeau, D., . . . Contributors, S. 1. (2020). SciPy 1.0: Fundamental Algorithms for Scientific Computing in Python. *Nature Methods, 17*, 261–272. doi:10.1038/s41592-019-0686-2

Wessel, P., & Smith, W. H. (2015). A Global, Self-Consistent, Hierarchical High–Resolution Geography Database, V2. 3.4. *Digital Media, http://www. soest. hawaii. edu/pwessel/gshhg. rSIR-SMAP Projections and Grids*.

Wessel, P., Luis, J. F., Uieda, L., Scharroo, R., Wobbe, F., Smith, W. H., & Tian, D. (2019). The generic mapping tools version 6. *Geochemistry, Geophysics, Geosystems, 20*, 5556–5564. doi:10.1029/2019GC008515

Won, I. J., & Bevis, M. (1987). Computing the gravitational and magnetic anomalies due to a polygon: Algorithms and Fortran subroutines. *Geophysics, 52*, 232–238.

Woollard, G. P. (1979). The new gravity system: Changes in international gravity base values and anomaly values. *Geophysics 44.8*, 1352–1366. doi:10.1190/1.1441012

Zanferrari, A., Masetti, D., Monegato, G., Poli, M. E., Avigliano, R., Carraro, F., . . . others. (2013). Carta geologica d'Italia alla scala 1: 50.000-Foglio 049 Gemona del Friuli-Note Illustrative. *Regione Friuli Venezia Giulia-Servizio Geologico; ISPRA-Servizio Geologico d'Italia, 262*.

Zanolla, C., Braitenberg, C., Ebbing, J., Bernabini, M., Bram, K., Gabriel, G., . . . others. (2006). New gravity maps of the Eastern Alps and significance for the crustal structures. *Tectonophysics, 414*, 127–143.

Zanolla, C., Morelli, C., & Marson, I. (1998). The magnetic anomalies of the Mediterranean Sea (IBCM-M). *Bollettino di Geofisica Teorica ed Applicata, 39*, 1–36.

ANNEX 1

Manuscript submitted to *Earth and Space Science*

A comparison between sea-bottom gravity and satellite altimeter-derived gravity in coastal environments: A case study of the Gulf of Manfredonia (SW Adriatic Sea)

L. S. Zampa[1,2], E. Lodolo[1], N. Creati[1], M. Busetti[1], G. Madrussani[1], E. Forlin[1], A. Camerlenghi[1]

[1]National Institute of Oceanography and Applied Geophysics - OGS - Italy
[2]Department of Mathematics and Geosciences - University of Trieste - Italy

Key Points:

- Comparison between sea-bottom and satellite altimeter-derived gravity allowed us to estimate noise effects in near-shore altimeter data.
- The high-resolution sea-bottom gravity data along the Italian coasts shows the effects of sources not detected by satellite altimeters.
- Combined analysis of satellite altimetry and sea-bottom gravity data gives a complete view on the offshore continuation of near-shore structures.

Corresponding author: Luigi Sante Zampa, lzampa@inogs.it

Abstract

The marine gravity field derived from satellite altimetry is generally biased, in coastal areas, by signals back-scattered from the nearby land. As a result, the derived gravity anomalies are mostly unreliable for geophysical and geological interpretations of nearshore environments.

We compared two different altimetry models with sea-bottom gravity measurements acquired along the Italian coast to quantify the errors generated by reflections from onshore areas and verify the quality of the geologic models inferred from gravity. We focused on the Gulf of Manfredonia, in the SE sector of the Adriatic Sea, where (i) two different sea-bottom gravity surveys have been conducted over the years, (ii) the bathymetry is mainly flat, and (iii) seismic data has revealed a prominent carbonate ridge covered by hundreds of meters of Oligocene-Quaternary sediments. Gravity field derivatives have been used to enhance deep geological contacts and coastal noise. The analyses point to a ringing noise compromising the altimeter signals up to 17 km from the coast. Differences between observations and gravity calculated from a geological model constrained by seismic data show that all the investigated datasets register approximately the same patterns associated with the Gondola Fault Zone.

This study shows the potential for implementing gravity anomalies from satellite altimetry with high-resolution near-shore data, such as that provided by sea-bottom gravity network available around the Italian coasts. Future applications will use this technique to improve the analysis of the connections between marine and inland geology in transitional areas.

Plain Language Summary

We present a comparative analysis between two types of gravity data used in geophysical studies: satellite altimeter-derived gravity and sea-bottom gravity. It is generally accepted that the quality of satellite altimetry data in the vicinity of the coast is hindered by signals reflected from nearby land. We show how this may affect the interpretation of gravity anomalies and how it could be solved by integrating altimetry-derived gravity with high-resolution marine gravity networks in the proximity of coasts. We chose the Gulf of Manfredonia as a test area on the South Adriatic coast of Italy, which hosts a major tectonic feature, namely, the Gondola Fault Zone. The fault zone is not clearly expressed at the sea floor, which is generally flat, but it dislocates carbonate rocks located hundreds of meters below the sediments. In so doing, it creates lateral density contrasts prone to be detected by gravity data.

Keywords

Sea-bottom gravity, Satellite altimeter-derived gravity, Coastal noise, ISVD, Tilt

1. Introduction

The quality of sea-surface height measurements from satellite radar altimetry in coastal regions is impaired by the noisier radar returns from the generally rougher coastal sea and simultaneous returns from reflective land and inland water (Andersen & Knudsen, 2000). Satellite altimeter-derived gravity data in the vicinity of land is therefore inevitably contaminated by non-gravity signals.

The altimeter-derived results can be improved using the waveform tracking technique, which reprocesses the waveform data through a “coastal retracking system", as performed along the Australian coastal regions (Deng & Featherstone, 2006). The resolution of these methods has continuously improved in the last decades, also thanks to newly available and more accurate radar data. Moreover, radar altimetry has the advantage of near-global coverage and almost homogeneous error characteristics in noncoastal regions (Fu & Cazenave, 2000; Green et al., 2019). When comparative data acquired independently and with different techniques are available, such as marine geophysical measurements, it is possible to provide a more exhaustive and quantitative assessment of the satellite altimetry errors. From the early 1950s to the late 1980s, the Osservatorio Geofisico Sperimentale (OGS) of Trieste (Italy) performed several gravimetric surveys along the Italian coast using sea-bottom gravimeters (Ciani et al., 1960; C. Morelli, 1966; Gantar, 1983), during which thousands of data points were recorded (Figure 1).

In this study, we investigate the compatibility of sea-bottom gravity with satellite altimeter-derived gravity, using both the DTU13 (Andersen et al., 2014) and the S&S (Sandwell et al., 2014) datasets, and provide a quantitative evaluation of the differences between the two types of gravity data. To delineate the effectiveness of this comparison (satellite-derived gravity vs. sea-bottom gravity), this study focuses on a relatively small coastal area in the SW Adriatic Sea, The Gulf of Manfredonia, where two different sets of sea-bottom gravity data have been acquired over the years.

The choice of study area is essentially motivated by the following: (i) it is a very flat sector of the coastal region where a thick, ellipsoidal-shaped sedimentary basin has been identified with seismic reflection profiles; (ii) a dense grid of gravity measurements acquired at the sea-bottom is available; (iii) seismic profiles show the presence of significant geological discontinuities propagating from inland (Gargano Peninsula) towards the offshore (Gulf of Manfredonia), and thus tend to be detectable within the gravity data; (iv) it represents an ideal case in which the flat seafloor does not mimic the trend of the rock-basement below the seafloor sediments, which instead can be easily imaged using gravity anomalies.

The sea-bottom gravity stations in the study area were connected to the national absolute gravity network, which has been upgraded over the years leading to a systematic bias between data points taken in different periods. All measurements were concentrated near the coast due to the vessel position being easier to triangulate from the land. In addition, the proximity of docking harbors guaranteed a fast and frequent connection with land-based gravity stations, thereby reducing large residual drift errors in the final absolute gravity values.

These data had never been coupled with sea-surface gravity, acquisition of which started in the 1960s (C. Morelli, 1966). The great advantage in terms of acquisition time and cost of sea-surface gravity over sea-bottom gravity has made this new data type preferable and more widely used. However, sea-bottom measurements are still more sensitive to sub-bottom density variations and not affected by leveling errors in the same way as sea-surface gravity, which makes them more suitable when it comes to studying the accuracy of gravity fields near the coast (Talwani et al., 1966; Ballu et al., 1998; Fairhead, 2016).

All the gravity datasets analyzed in the current work have undergone preliminary correction using the same reference model: the Bouguer anomaly of sea-bottom data that takes into account the free-water gradient and gravity effects of topography and water masses above and below the sea-bottom station. Meanwhile, the same anomaly computed for the altimeter-derived data considers only the effects of topography and water masses above and below the sea surface, respectively.

We used the Integrated Second Vertical Derivative (ISVD) and the Tilt derivative to enhance both the noise effects and the gravity signals from the edges of causative sources. The results of these analyses were compared with those calculated from a forward gravity model derived from seismic-reflection data. This allowed us to investigate the relative sensitivity of each dataset to the gravity effect of known sources, and provided a better understanding of which dataset would be easier to repair for the interpretation of gravity anomalies.

The results of this current work can be used in the study of continuity and configuration of geological contacts marked by density contrasts from inland to offshore coastal areas. The method described here could potentially be implemented to significantly reduce errors caused by coastal noise in satellite altimeter-derived gravity data in similar coastal regions where sea-bottom gravity measurements are available.

2.1. Geological setting

The Gulf of Manfredonia is located in the SW sector of the Adriatic Sea. It is bounded to the north by the Gargano Peninsula and to the west by the northern part of the Puglia region (i.e., the northern sector of the Salento). Within the gulf, the bathymetry shows maximum water depths of ~90 m, with a smooth seafloor surface, without any relevant morphological features.

The lithostratigraphy of the area to a depth of ~2.5 km has been divided into four main units (D. Morelli, 2002; Volpi et al., 2015): (i) Plio-Quaternary sandy and clayey sediments, (ii) Upper Oligocene–Miocene argillaceous and marly turbidites, (iii) middle Liassic-Paleogene pelagic limestones and marls, and (iv) upper Triassic-lower Liassic evaporitic, dolomitic and shallow-water limestone. The two lowest units (iii and iv), generally called the "Jurassic-Paleogene carbonate succession", form the solid bedrock. Unconsolidated or partially consolidated siliciclastic sediments cover the bedrock up to depths of ~1500 meters in the deepest basin (Figure 2b).

Seismic studies conducted since the 1970s have revealed the presence of an important structural element beneath the sedimentary cover, striking broadly W-E, known as the Gondola Fault Zone. The Gondola Fault Zone includes several E–W and NW-SE trending fault segments that define an elongated, buried structural high called the "Gondola ridge" (Colantoni et al., 1990; de Alteriis & Aiello, 1993; de Alteriis, 1995), which extends ~70 km across the shelf without producing significant morphologies at the seafloor along most of its extension (Ridente & Trincardi, 2006). Conversely, a tectonic-related relief visibly affects the seafloor morphology downslope along the ~50 km-long NW-SE branches of the Gondola Fault Zone (Tramontana et al., 1995; de Alteriis, 1995). The Gondola Fault zone has been related to a Cenozoic reactivation of pre-existing faults (Finetti, 1983;

Tramontana et al., 1995). The deformation of Middle Pleistocene sediment evidence quaternary activity. The overall geometry of the Gondola Fault Zone suggests a significant right-lateral component of motion (Ridente et al., 2008).

The Gondola fault system continues onshore with the Mattinata Fault that cuts through the Gargano Promontory (Figure 2a), which is an E–W elongated relief (maximum elevation ~1000 m) along with the flexural bulge of the Adriatic foreland (Ridente et al., 2008). The Gondola and Mattinata fault zones can be traced for a total length of at least 180 km (Di Bucci et al., 2006), and belong to the ~15 km wide corridor of the fault system that extends from the Adriatic Sea to the core of the Apennines (Ridente et al., 2008). The Mattinata Fault is considered to be a poly-phased belt, subjected to an intense deformation since Mesozoic times and formed by several fault splays (see Billi et al. (2007), and references therein). However, seismic data have shown that the Mattinata Fault is neither in direct continuity nor perfectly aligned with the Gondola Fault Zone, showing an under-lap of ~20 km and right-stepping of ~5 km (Ridente et al., 2008).

2. Data

In this study, we calculate and compare gravity anomalies covering the Gulf of Manfredonia using four different datasets: two satellite altimeter-derived gravity datasets, i.e., the DTU13 (Andersen et al., 2013, 2014, 2015) and the S&S (Sandwell et al., 2014), and two sea-bottom gravity datasets, i.e., OGS60 (Ciani et al., 1960) and OGS83 (Gantar, 1983). To constrain the forward gravity model, we used the geological model produced by Volpi et al. (2015). The model is based on the interpretation of multichannel seismic profiles made available through the Visibility of Petroleum Exploration Data in Italy project (ViDEPI, www.videpi.com, managed by the Italian Ministry of Economic Development) and released in SEG-Y format by the web portal Seismic data Network Access Point (SNAP), managed by the Istituto Nazionale di Oceanografia e di Geofisica Sperimentale (Diviacco, 2018).

2.1. Satellite altimeter derived gravity

Satellite altimeter-derived gravity comes from the Sea Surface Heights (SSH) measurements, obtained by radar satellites orbiting at 800 km and 1,300 km above the Earth's surface. A microwave pulse emitted by the satellite antenna is reflected by a portion of the sea surface (the footprint), whose position is mapped relative to the reference ellipsoid. This allows for a complete reconstruction of the SSH over almost the entire globe. After correcting the SSH for time-dependent components, residual orbital errors, and the Mean Dynamic Topography (a quasi-stationary component of SSH), the result is a static realization of the marine geoid (Andersen et al., 2010). The mathematical relation between geoid undulations (N) and the Free-air anomaly (Fa) is given by the Bruns formula:

$$Fa = -g^{s}_{th}\frac{\partial N}{\partial r} - \frac{2}{R}N g^{s}_{th} \tag{5}$$

where, g^{s}_{th} is the theoretical gravity (spherical approximation), r is the radius vector connecting the computational point to the center of the Earth, N is the geoid undulation, and R is the mean Earth radius.

There are two methods available to compute the vertical geoid gradient $\frac{\partial N}{\partial r}$, using altimetry data: (i) the "geoid-to-gravity" and (ii) the "slope-to-gravity" method (Fairhead, 2016).

2.1.1. DTU13

The DTU13 dataset was obtained using the geoid-to-gravity method, developed by the Technical University of Denmark (Andersen et al., 2014). In this approach, the vertical derivative is computed starting from 2-D regular grids of the geoid. The geoid grids result from spatial interpolation of radar data, crossover adjusted and corrected for time-variable and stationary components of the SSH, i.e., all those components not directly related to the gravity field of the solid Earth (Andersen et al., 2010).

The derivation is performed using the Fast Fourier Transform (FFT), after having removed the effect of the EGM2008 spherical harmonic model up to degree and order 2160 (Pavlis et al., 2012), i.e., wavelengths of ≤20 km (Barthelmes, 2009). The removed harmonic components are the added back into the final result (remove-restore technique). The resulting free-air anomaly is available in a grid format, with a sampling step of 1 arc-min. However, the real maximum resolution is limited by the along-track spacing of observations, which is around 7 km, and by the systematic use of a Wiener lowpass filter with cut-off wavelengths ranging between 5 and 16 km (Andersen & Knudsen, 1998; Andersen et al., 2010). As a result, the shortest reliable wavelength is around full waveforms of ~13 km (Andersen, 2013; Fairhead, 2016).

The DTU13 is associated with an interpolation error file (Figure 3b), showing uncertainties on the Mean Sea Surface grids (MSS_{err}), which is defined in units of meters (Andersen & Knudsen, 2009). This error file shows the quality of gridded data points, and it can be used to roughly identify the transition between land and ocean (Andersen et al., 2008). However, it may underestimate the real uncertainties of the MSS, since it only accounts for interpolation errors and not for actual orbit errors, or other errors in various range corrections (Andersen & Knudsen, 2009).

The relation between geoid and gravity (eq. 1), gives a ~1 mGal amplitude for a sea surface slope of 7 mm/7 km (Sandwell et al., 2013), i.e., 1.4 mGal/cm when considering horizontal distances of 7 km (i.e., full-waveforms of 14 km). This simple equivalence has been used as a rule of thumb to convert the MSS_{err} grid values into mGals (Figure 3b). The result is a qualitative indicator of the least expected gravity error in the study area, which, however, does not include the actual error of the EGM2008 model.

2.1.2. S&S

The S&S dataset uses the slope-to-gravity method, which is based on the same remove/restore principle of DTU13. However, in this case the derivatives are directly computed from along-track signals, instead of the 2-D grids. The resulting slopes are interpolated and convoluted to obtain grids of W-E, S-N horizontal gravity gradients, and finally combined through the Laplace equation to obtain the vertical gravity component (Sandwell, 1992; Fairhead, 2016).

The S&S Free-air anomaly is available in a grid format with a sampling-step of 1 arc-min (Figure 3c), and it is also associated with an error grid that defines its uncertainty (Figure 3d). In this case, the error refers directly to the gravity anomaly, i.e., it is expressed in mGal units, and it shows the RMS difference between (i) the slope of individual altimeter profiles and (ii) the averaged grid product of W-E and S-N slope (Sandwell & Smith, 2009; Sandwell et al., 2014).

Thanks to the direct computation of gradients from along-track signals, the S&S model may preserve high frequencies better than the DTU13, although it may also amplify residual noises, i.e. non-modeled disturbing components (waves, tides, currents) or blurring scattered spikes, especially in coastal regions.

2.1.3. Coastal noise

Errors of satellite altimeter data generally increase close to the coast, where the radar footprint covers part of the inland together with the sea surface (Dawson et al., 2015). Reflections from onshore areas generate large amplitude noise covering signals reflected by the sea surface (Figure 3b,d). The exact distance from where this contamination may occur is not easy to estimate, since it depends on a complicated combination of different factors, such as the angle between orbital tracks and shoreline, topographic and bathymetric gradients, local bathymetry, and local tides. This makes coastal noise mostly a site-dependent problem.

Although this noise has been consistently reduced in the last decades, using Interferometric Synthetic Aperture Radar (e.g. CryoSat2 mission), more accurate global gravity models (e.g. EGM2008), and more sophisticated tracking techniques, signal accuracy up to 7-14 km from the coast may still be compromised (Deng & Featherstone, 2006; Andersen & Knudsen, 2009; Sandwell & Smith, 2009; Dawson et al., 2015).

For these reasons, interpretations of altimeter-derived gravity in coastal regions must be carefully evaluated and preferably integrated with ship-borne/air-borne gravity measurements or other types of geophysical data.

2.2. Sea-bottom gravity data

2.2.1. OGS60

OGS60 is part of a dataset recorded during a seven-year mission (1953 - 1960) to extend offshore the Italian land-based gravity network (RFI) and to create the first gravity maps of the Italian seas (Ciani et al., 1960). Gravity data were measured using a western sea-bottom relative meter, with a nominal accuracy of 0.05 mGal. Station depths were measured by echo-sounders (Atlas-Werke) and coordinates calculated using optical and/or radar instruments pointing to coastal marks or reflective buoys. Planar coordinate precision decreases with increasing distance from the coast: from a minimum of ±50 m inshore to a maximum of ±200 m at ~120 km from the coast, or even up to ±600 m when reflective buoys were not available. OGS60 stations are not regularly distributed; station spacing increases offshore, from a minimum of ~1.6 km to a maximum of ~10 km at 60–70 km from the coast (Figure 3e).

2.2.2. OGS83

OGS83 data were collected in 1982, as part of a 98-day marine gravity survey to create high-resolution gravity maps of the Adriatic coast, from Ancona to Ortona (the "northern zone") and from Manfredonia to Brindisi (the "southern zone"), commissioned by the Agip Mineraria company. Gravity differences were measured with a LaCoste and Romberg sea-bottom relative meter (mod. 19 G), which has a nominal accuracy of 0.05 mGal (Gantar, 1983). Station depth was measured by both echo-sounders (Honeywell ELAC, mod. LA2721A) and pressure meters, giving a final combined accuracy of ±0.5 m. Horizontal coordinates were calculated through radar trilateration from the coast

(Motorola System), with a nominal precision of ±3 m ±0.01*distance[km]. The OGS83 stations are distributed on a nearly regular grid, up to ~10 km from the coast, at a distance of ~1±0.2 km from each other (Figure 3e).

3. Methods

The computation of gravity anomalies from sea-bottom data (OGS60 and OGS83) differs slightly from the procedure generally used with sea-surface data (e.g., DTU13 and S&S). A correct comparison can only be achieved when both data types are adjusted for the same disturbing effects, i.e., all the gravity signals not related to the sub-bottom target sources (Ballu et al., 1998). To achieve this condition, we first calculate the Free-water anomaly, Fw, for the sea bottom gravity data:

$$Fw = g_{obs} - (g_{th} + fwc) \qquad (2)$$

where, g_{obs} is the observed gravity and fwc is the Free-water correction. Then, we calculated the Bouguer anomaly of both altimeter-derived gravity and sea bottom gravity (Ba_{sat} and Ba_{sb}), by using two different solutions based on a common computational scheme to derive the total topographic effect (Te_{sat} and Te_{sb}):

$$Ba_{sat} = Fa - Te_{sat} \qquad (3)$$

$$Ba_{sb} = Fw - Te_{sb} \qquad (4)$$

where, Fa is the free-air of satellite-altimetry datasets (eq. 1).

After computing the Bouguer anomaly, the OGS83 and OGS60 stations were merged into a unique dataset, the OGS. The validity of this merging operation is supported by a statistical analysis of the differences between the two datasets within the overlapping near-shore area. Most of the differences are around ±1.2 mGal, with an average bias that is negligible compared to satellite altimeter errors (Table 1). This finding ensures a precision higher than 1 mGal for sea-bottom gravity, since the repetition of measurements in two different periods over the same area gives an average discrepancy of just ~0.58 mGal (RMS).

As a final step, the Bouguer anomaly of sea-bottom data should have been upward continued from the drape seafloor surface to a constant mean sea level to have all datasets at the same distance from the causative sources (Ballu et al., 1998). However, since the average seafloor is at a ~50 m depth (mean vertical step) and gravity stations were separated by less than 1 km (smallest horizontal step), the upward-continuation amplitude would have been lower than 1 mGal and likely affected by numerical noise. Therefore, we decide to skip this last processing step.

3.1. Theoretical gravity (g_{th})

The theoretical gravity, g_{th}, was calculated using the WGS84 ellipsoid as a reference model (Decker, 1986), i.e., the same used for satellite altimetry. The WGS84 model includes the mass of the atmosphere above the reference surface and the total mass of the solid Earth. The effect of the atmospheric layer must then be removed from the theoretical gravity since the net gravitational force exerted by outer spherical shells on any point inside is zero (Hinze et al., 2005):

$$g_{th}\left(\lambda\right)=\frac{978032.67714\left(1+0.001931851386sin^{2}\lambda\right)}{\left(1-0.00669437999013sin^{2}\lambda\right)^{1/2}}-g_{atm} \qquad (5)$$

where, λ is the geographic latitude and g_{atm} is the value for atmospheric correction at the sea level, i.e., 0.87 mGal.

3.2. Free-water anomaly (Fw)

The theoretical gravity of stations located below the water masses was corrected for the relative depth of each measurement point, using the free-water correction *fwc* (Stacey &

Tuck, 1981; Luyendyk, 1984; Dubois & Deplus, 1989; Hildebrand et al., 1990; Ballu et al., 1998):

$$\begin{aligned} fwc(h) &\simeq \frac{\partial(g^s_{th} - g_{shell})}{\partial r} h \\ &\simeq -\frac{2\, g^s_{th}}{R^2}\, h \,+\, 4\pi G \rho_w h \\ &\simeq -0.222\, h \end{aligned} \qquad (6)$$

where h is the station depth ($h \leq 0$), ρ_w is the water density (1030 kgm^{-3}), g_{shell} is the downward attraction of an homogeneous spherical shell and G is gravitational constant ($6.67 * 10^{-11}$ $m^3 s^{-2}/kg$).

The free-water correction is similar in principle to the atmospheric correction: the water layer overlying the measurement point approximates the outermost homogeneous spherical shell of the reference model, which has a null gravity effect on the inner region. The total downward gravitational attraction of the theoretical model slightly decreases with depth because of the lack of mass contribution from the thickening outer shell. This effect is in contrast with the larger increment in the gravitational attraction due to the closer proximity with the Earth-mass center. The combination of both effects is a slight decrease of the vertical gravity gradient by a quantity ~ equal to the gravitational attraction of the water shell (eq. 8).

The homogenous-spherical shell approximation holds, if (i) the density does not change drastically within the water column and (ii) the effect of Earth curvature is negligible (Bullard, 1936). The study area fills both conditions since it is smaller than 200 km and the water layer is on average ~50 m. Otherwise, the ellipsoidal-shell approximation and water-density profiles should have been included in the computation (Stacey & Tuck, 1981).

3.3. Topographic effect (*Te*)

The gravity effect of topographic and water masses in the Bouguer anomaly (eq. 3, eq. 4), were computed differently in the case of sea-bottom (OGS60, OGS83) and sea-surface gravity (DTU13, S&S) since sea-bottom stations are located at different distances from the surrounding masses than sea-surface measurements.

In both cases, the adopted computational scheme separately considers the effect of (i) a high-resolution Digital Topographic-Bathymetric Model (DTBM) with a grid-step of 100 m, extended for 9 km from the computational point, and (ii) the effect of a low-resolution DTBM, with 3 km grid-step which extends for 159 km from the limits of the high-resolution area.

The DTBM model was created from a combination of SRTM and EMODnet data (Farr & Kobrick, 2000; Consortium et al., 2018), composed of 3-D prisms. The gravity effect of each prism is calculated through the Python library Harmonica (Uieda et al., 2020), which makes use of the analytical solution proposed by Nagy et al. (2000). It has the advantage of being valid on any point, either outside or inside the element (Nagy et al., 2002; Fukushima, 2019).

3.3.1. Topographic effect at the sea-surface (Te_{sat})

When the measurement point lies on the sea surface (as for altimeter-derived gravity), the reference model must be corrected for effects of crustal masses above the point and water masses below it, in order to obtain the complete Bouguer anomaly (Figure 4a,b).

We therefore calculated the topographic effect, Tesat, by summing (i) the vertical upward attraction of crustal masses above the reference surface (Zone A), and (ii) the drop in the gravitational attraction due to the presence of water in place of the crust in marine areas (Zone B). In this computation we used the constant density of 2.67 g/cm^3 for the crust, ρ_c, and 1.03 g/cm^3 for the water density, ρ_w (Figure 4, eq.7).

This approximation may vary locally because of inland depressions (continental areas below the reference surface) or inland water masses (e.g., large lakes or lagoons).

The solution is identical for measurement points above the reference surface (e.g. land-based stations or air-borne measurements). The difference is that the attraction of topographic masses may be either positive or negative, depending on the height of the computational point relative to the surrounding topography.

$$\frac{\begin{cases} Zone(A):\ g_e(h,0,\rho_c) & if\ h>0 \\ Zone(B):\ g_e(0,h,\rho_w-\rho_c) & if\ h<0 \end{cases}}{Te_{sat} \ = \sum_{A} g_e(h_t,h_b,\rho) + \sum_{B} g_e(h_t,h_b,\rho)} \tag{7}$$

where g_e is the gravitational attraction of a prism, with h_t and h_b being the top and the bottom height of the element, respectively, and h the height given by the DTBM model.

3.3.2. Topographic effect at the sea-bottom (Te_{sb})

We assumed, in eq. 5, that the starting reference model is a spherical layered earth (Figure 4c). In this approximation, the outermost layer above sea bottom stations is made of water with a constant density; hence, it has a total null gravity effect on any point inside. However, both water and crustal masses are non-homogeneously distributed above the stations in the real model (Figure 4d).

Therefore, the gravity effect of all the heterogeneously distributed masses above the computational point must be added as an upward attraction to the theoretical gravity (ie., negative effect). The remaining effects of the water masses below the computational point (Zone C, Figure 4d) should be treated like those of sea-surface stations, i.e., by removing the crustal effects and adding back the effect of the water (eq.8).

The problem is solved by dividing the DTBM model into three zones (Gantar, 1983; Nowell, 1999):

$$\begin{array}{l} \begin{cases} Zone(A): \; g_e(h, h_s, \rho_c) & if\; h > 0 \\ Zone(B): \; g_e(0, h, \rho_w) + g_e(h, h_s, \rho_c) & if\; h_s < h < 0 \\ Zone(C): \; g_e(0, h_s, \rho_w) + g_e(h_s, h, \rho_w - \rho_c) & if\; h < h_s < 0 \end{cases} \\ \hline Te_{sb} \;=\; \sum_{A} g_e(h_t, h_b, \rho) + \sum_{B} g_e(h_t, h_b, \rho) + \sum_{C} g_e(h_t, h_b, \rho) \end{array} \tag{8}$$

where *hs* is the depth of the computational point (i.e., negative height).

3.4. Field derivatives

Gravity field derivatives are commonly used in geophysical studies to enhance lateral density contrasts at depth in-depth (Fedi & Florio, 2001; Aydogan, 2011; de Lerma et al., 2015). The multiscale derivative has already proven helpful in identifying the offshore continuation of the Mattinata Fault system (the ”Gondola ridge”) on in larger scale regional analyses (Fedi et al., 2005). In this study, we use the Integrated Second Vertical Derivative (ISVD) and the Tilt derivative (Miller & Singh, 1994; Fedi & Florio, 2001; Fedi, 2002), for a qualitative evaluation of the sensitivity to lateral density contrast of each different gravity dataset (DTU, S&S, OGS). The ISVD was calculated in three steps (Fedi & Florio, 2001): (i) integrating the gravity anomaly grid in within the frequency domain, (ii) computing the second-order horizontal derivatives in the space domain using a 2D convolution, and (iii) calculating the first-order vertical derivative combining the results from the previous step through the Laplace equation.

The Tilt derivative is the angle given by the ratio between the ISVD and the first-order horizontal gravity gradient, which is also computed through a spatial-domain convolution:

$$\mathrm{Tilt} = \mathrm{atan}\left(\frac{ISVD}{\sqrt{\left(\frac{\partial g}{\partial x}\right)^2 + \left(\frac{\partial g}{\partial y}\right)^2}}\right) \tag{9}$$

where g is the gravity anomaly and $\sqrt{\left(\frac{\partial g}{\partial x}\right)^2 + \left(\frac{\partial g}{\partial y}\right)^2}$ is the horizontal gravity gradient.

The calculated functions have been qualitatively evaluated by direct comparison with a forward gravity model. This model includes the interface between the OligoceneQuaternary sediments and the underlying carbonate platform, as per Volpi et al. (2015), in which depths were derived from a 2D inversion of multichannel seismic profiles constrained by well-logs data. The gravity effect of the seismic interface is computed using the Parker method in the FFT domain (Parker, 1973):

$$\Delta \mathrm{g}(x,y) = FFT^{-1}\left\{-2\pi G\Delta\rho e^{-h_0|\vec{K}|}\sum_{n=1}^{\infty}\frac{|\vec{K}|^{n-1}}{n!}FFT[h(x,y)^n]\right\} \qquad (2.15)$$

where Δg is the gravity effect of the 2D interpreted seismic layers, depth-converted, h is the depth of the layer, $\Delta\rho$ is density contrast between the two layers forming the interface, h_0 is the mean depth of the interface, and $\vec{K}$ is the wavenumber.

A first-order polynomial surface was removed from the Bouguer anomaly before computing the derivatives in order to take out the regional component of the gravity field.

We considered the linear trend surface to be an acceptable approximation for the regional gravity effects, under the assumption that over the Italian territory both the Moho and the crystalline basement have wavelengths longer than 100 km (Corrado et al., 1981), and our study area is less than 90 km in extent.

The Tilt function allowed us to map the edges of the gravity sources using the residual gravity field. Lines approximating these edges were outlined through a maximum detection algorithm built using a 3 x 3 km moving window operator (Blakely & Simpson, 1986). The operator slides on the cosine of the Tilt, also known as the Theta derivative. The

Theta derivative is always positive and has its maximum values, i.e., the zero Tilt values, in correspondence with sub-surface lateral discontinuities (Wijns et al., 2005; Fairhead, 2016). The ridge axis of the Gondola system was calculated in the same way but using the Tilt function instead of the Theta function because it shows maximum values immediately above the top-center of the causative sources. The detected edges were divided into two sets: the first containing lines correlating with fault interpretation based on seismic profiles or with visible changes in the trend of a carbonate platform (verified edges); and a second containing lines only registered by gravity (inferred edges). The "gravity edges" combine the results from the OGS data within a coastal strip of ~17 km and the S&S data in the remaining areas.

4. Results and Discussion

The Bouguer anomaly values follow an approximately bimodal distribution (Figure 5a). The first mode, centered at ~60 mGal, represents the near-shore area southwest of the Gondola fault system. The second mode, at ~75 mGal, accounts for values covering the north-eastern sector, with relatively higher positivity than those in the area to the southwest. The differences between the two sectors are mainly related to the abrupt discontinuity of the Gondola Fault Zone. The fault corresponds with a break in the main regional gravity trend associated with wavelengths of ≤200 km. The same discontinuity extends to the north over the Gargano Peninsula, along with the Mattinata Fault, and is also visible in the magnetic data (Fedi et al., 2005). Since regional gravity signals are likely to be related to crustal discontinuities, e.g., the crystalline basement and/or the Moho (Corrado et al., 1981), the presence of a nearly vertical step of ~30 mGal breaking the continuity of the main Bouguer trend may suggest that the base of the fault system is much deeper than the Jurassic layer, which is around a depths of 2-3 km (Volpi et al., 2015).

The relative minimum of about -30 mGal near the western coast extends for ~30 km in the SW-NE direction, ~50 km in the NW-SE direction, and it has a similar amplitude and shape in all the datasets that have been studied (DTU, S&S, and OGS). Based on the information gathered from seismic reflection data, we assert that part of this residual anomaly is related to a local sedimentary basin reaching depths of ~1500 m.

The Bouguer anomaly values from the DTU model (?) show approximately the same statistical information and similar spatial distribution as the S&S (Table 2 and Figure 5b,c). However, the S&S model has higher amplitudes and shorter wavelengths than the DTU, as shown in the data distribution and by the map of data differences (Figure 5a,e). The S&S data register short wavelength anomalies near the SE coast, ~6 km wide, which occur as a “ringing effect” and can reasonably be expected to be caused by the radar signals reflected from adjacent land areas, i.e., coastal noise (Figure 5c). The noise degrades the S&S gravity anomaly up to ~17 km from the coast. This is approximately the size of the most prominent positive anomaly in the SE coastal sector of the study area, calculated as the distance from coast to the first zero value in the ISVD map (Figure 6h).

Differences between OGS and satellite altimeter datasets (DTU and S&S) show values greater than 15 mGal in the vicinity of the NW coast (i.e. the Gargano Promontory). Here, high positive differences correlate with high topographic gradients (Figure 5e,f,g). However, this coastal area is also poorly covered by sea-bottom stations (more than 6 km apart from each other), which means differences may also be caused by interpolation artifacts, rather than by coastal noise. The RMS difference of DTU and S&S compared to OGS data (Table 2), is approximately within the estimated errors of satellite altimeter datasets (Andersen et al., 2014; Sandwell et al., 2014). Nevertheless, the maximum and minimum differences are greater than 20 mGal, meaning that there are local errors a few tens of mGals higher than the predicted uncertainties if considering sea-bottom gravity as a correct reference.

After removing a first-order linear trend, the residual anomaly (Figure 6a, d, g) should correlate with the carbonate basement, i.e. it should respond mainly to the density contrast between carbonate rocks and the overlying terrigenous sequence (Corrado et al., 1981; Rapolla, 1986; Fedi & Rapolla, 1993). This hypothesis is partially confirmed by the forward gravity model based on seismic reflection data, which shows patterns similar to the observed residual gravity. However, amplitudes of residual gravity on the Gondola ridge are almost ~10 mGal higher than the calculated gravity (Figure 7a), which may reinforce the hypothesis of a deeper origin than the Jurassic sequence for the base of this Gondola System.

The residual gravity, the ISVD, and the Tilt maps (Figure 6) provide further evidence that S&S contains higher frequencies than the DTU model: it has both the highest ringing noise near the coast and the sharpest gravity gradient corresponding to the Gondola ridge, as highlighted by the forward gravity model. Furthermore, the ISVD of S&S data correlates positively with the ridge axes. In addition, the dataset resolution allows us to map the slight change in the main ridge axis orientation from NW-SE to E-W, which is less evident in both the DTU and OGS data. This confirms that, of the datasets investigated, the S&S is the most accurate away from the coast and, at the same time, the noisiest in near-shore areas. On the other hand, the OGS data are the most reliable near coasts where there is a near regular distribution of sea-bottom stations that are separated by distances of ~1 km, and do not register any evident systematic bias between data acquired in subsequent surveys (Figure 3e and Table 1).

The ISVD map of OGS data shows local relative minima close to the coast, with sizes ranging from 5 to 6 km (figure 6b). Each of these minima is covered by more than three gravity stations, and they are not related to any local structural discontinuity as shown by seismic reflection profiles on the top of the carbonate layer, which appears to be relatively flat in this sector. Excluding the presence of localized deeper sources and/or measurement biases, these small gradient changes may be related to localized variations within the Pliocene and Pleistocene sediments (D. Morelli, 2002; Volpi et al., 2015). As described in the geological setting above, at least two different sedimentary units have been recognized from the interpretation of seismic profiles (Figure 2b): the upper unit is composed of Plio-Quaternary siliciclastic sediments, which we assumed are less dense and less compacted than the lower Oligocene-Miocene unit composed of silico-clastic and calcareoclastic turbidites (Volpi et al., 2015). The normal superposition of these units has been hypothesized to have been locally modified by tectono-eustatic processes (D. Morelli, 2002) and probably by different sedimentary river inputs and erosion mechanisms, leading to lateral depositional transitions (heterotopic facies). The ISDV map (Figure 6b) shows that one of the relative minima is located directly in front of the mouth of the Ofanto (Figure 7e), the largest river in the Puglia region, which transports and deposits a considerable amount of sediments into the sea (Mastronuzzi et al., 2002). If confirmed, this hypothesis could be an important proof of the capabilities of the Italian sea-bottom gravity network to distinguish even small density variations within sedimentary bodies, which may be extremely useful in the absence of seismic profiles acquired near the coast. The ISVD and the Tilt derivatives enhance lateral density transitions. In both functions, the zero value marks the approximate edges of causative sources, i.e., lateral discontinuities of subsurface interfaces. The Tilt, unlike ISVD, is normalized between ±π/2, and it tends to saturate faster over bodies with relatively higher densities with respect to the surroundings. This property makes the Tilt derivative particularly useful when outlining the planar shape of the carbonate platform, as imaged by gravity maps (Figure 7).

All the datasets investigated show similar results for the positioning of the SW edge of the Gondola ridge. However, they do not have sufficient resolution and perhaps lack the necessary accuracy to outline the ridge's NE side correctly. On the NE side, the shape of the gravity anomaly over the graben is smoother than on the SW side, and the residual anomaly is ~5 km larger than the anomaly calculated from the geological model. In this area, the OGS sea-bottom stations are separated by distances ranging from 6 to 10 km (Figure 3e). As a result, the observed gravity cannot fit with the forward model, which assumes a regular distribution of the stations (i.e., 1 st/km2). The NE side of the ridge is instead better approximated by the Tilt function derived from the S&S model (figure 7c).

South of the Gondola ridge, the gravity edges approximately correspond to the Jurassic faults as interpreted from seismic data (D. Morelli, 2002). In addition, the central axis of the ridge derived from gravity well data correlates with the pre-existing seismic interpretation (D. Morelli, 2002; Volpi et al., 2015). This confirms that part of the information contained in both the sea-bottom and satellite-altimetry gravity represents a 3D sub-surface fault network (Fedi & Florio, 2001; FitzGerald & Milligan, 2013; Fairhead, 2016). The remaining signals are associated with lateral density contrasts, which are not necessarily related to the sub-vertical steps in the rock basement (Figure 7e). Some of the "inferred edges" extracted from S&S data emerge on the NE and NW sides of the map, where the rock/sediment transition is smoother, and the gravity edges outline the center of the tilted sides of the interface, rather than on its upper edge. Other inferred edges, derived from OGS data, instead contour local minima near the coast. Some of these correlate with SW-NE-oriented Paleogene faults cutting the southern shoreline sector (Figure 7e). These lineaments are Dinaric transfer faults, which reactivate an older NE-SW Jurassic horst-graben system (D. Morelli, 2002). The reactivation dislocates the Oligocene-Miocene deposits, forming a lateral transition between them and the upper and less-dense sedimentary unit.

5. Conclusions

In this study sea-bottom gravity measurements (OGS) have been compared with sea-surface satellite altimeter-derived gravity (DTU and S&S) in the Gulf of Manfredonia.

All the gravity data types investigated, once corrected for effects of the free-water gradient and topographic/water masses, show statistical comparability and spatial correlation in the imaging created from this gravity anomaly data. All datasets show the same negative anomaly associated with a ~1500 m deep basin located immediately to the south of the Gondola Fault Zone. The residual gravity, ISVD, and Tilt functions register the effects of the central carbonate ridge as outlined by the seismic reflection profiles.

A comparison with the forward gravity model obtained from seismic interpretation shows that the S&S dataset allows more accurate identification of the lateral sediment/rock transition when compared to the other gravity datasets (i.e., DTU and OGS). However, S&S is severely compromised by coastal noise up to 17 km from the shoreline, where the interpretation of residual gravity is highly inconsistent. The DTU dataset shows a lower high-frequency content than S&S data, despite being less noisy near the shore.

The combined interpretation of the OGS sea-bottom and altimeter-derived gravity data allowed the edges of the carbonate platform to be mapped with a high degree of confidence, both near and away from the coast. Part of the gravity-derived edges correlate with faults within the Gondola Fault Zone that have been detected by seismic profiles. Other edges mark the smooth transition between rock and sediments rather than abrupt discontinuities generated by faults. Some edges, detected only by sea-bottom gravity data near the eastern coast, outline shallow anomalies with low amplitudes, which could be related to relatively small density contrasts in the river deposits and/or differential sediment compaction. In a few cases, these near-shore edges also seem to be partially related to SW-NE-oriented lateral discontinuities, as identified by seismic data. This finding shows how the high-resolution sea-bottom gravity network around the Italian coast contains information about sub-surface geological structures not fully detectable by satellite altimetry or the available seismic data.

The comparative analysis described here shows the effectiveness of coupling information from sea-bottom and satellite altimeter-derived gravity to reduce uncertainties of altimeter signals in localized coastal areas. In particular, the results help to outline and better image geological structures propagating from inland towards the offshore areas of the Salento region with greater accuracy than possible when using only a single gravity or seismic dataset.

Acknowledgments

All grid files and maps were created using Generic Mapping Tools (GMT) version 6.1.1.

The multichannel seismic-reflection data comes from the project ViDEPI (Visibility of Petroleum Exploration Data in Italy), managed by the Italian Ministry of Economic Development, and made available in SEG-Y format on the SNAP (Seismic Data Network Access Point) platform managed by the Istituto Nazionale di Oceanografia e Geofisica Sperimentale (Diviacco, 2018).

We thank ENI for kindly providing the sea-bottom gravity dataset OGS83 (Gantar, 1983).

The S&S dataset is available through Sandwell et al. (2014), at https://www.earthbyte.org/newglobal-marine-gravity-model-sandwell-et-al-2014.

The DTU13 dataset is available through Andersen et al. (2013), at https://ftp.space.dtu.dk.

The OGS sea-bottom gravity dataset is part of the OGS gravity database (Ciani et al., 1960; C. Morelli, 1966).

The DTBM is a combination of SRTM and EMODnet data. The SRTM product is released by the National Aeronautics and Space Administration (NASA) and downloaded from the USGS EROS Data Center, courtesy of the U.S. Geological Survey. The EMODnet product is provided by the EMODnet Bathymetry Consortium (2018): EMODnet Digital Bathymetry (DTM).

For the topographic corrections, we used the python library Harmonica, which is part of the project Fatiando a Terra (Uieda et al., 2020), available at https://www.fatiando.org.

References

Andersen, O. B. (2013). Marine gravity and geoid from satellite altimetry. In *Geoid determination* (pp. 401–451). Springer.

Andersen, O. B., & Knudsen, P. (1998). Global marine gravity field from the ERS1 and Geosat geodetic mission altimetry. *Journal of Geophysical Research: Oceans*, *103*(C4), 8129–8137. doi: 10.1029/97JC02198

Andersen, O. B., & Knudsen, P. (2000). The role of satellite altimetry in gravity field modelling in coastal areas. *Physics and Chemistry of the Earth, Part A: Solid Earth and Geodesy*, *25*(1), 17–24. doi: 10.1016/S1464-1895(00)00004-1

Andersen, O. B., & Knudsen, P. (2009). The DNSC08 mean sea surface and mean dynamic topography. *Journal of Geophysical Research: Solid Earth*(114), C11. doi: 10.1029/2008JC005179

Andersen, O. B., Knudsen, P., & Am Berry, P. (2010). The DNSC08GRA global marine gravity field from double retracked satellite altimetry. *Journal of Geodesy*, *84*(3), 191–199. doi: 10.1007/s00190-009-0355-9

Andersen, O. B., Knudsen, P., Berry, P., Freeman, J., Pavlis, N., & Kenyon, S. (2008). The DNSC08 ocean wide altimetry derived gravity field: EGU Meeting Programme. *Abstract EGU2008-A-07163, G1-1MO1O-003*.

Andersen, O. B., Knudsen, P., Kenyon, S., Factor, J., & Holmes, S. (2013). The dtu13 global marine gravity field—first evaluation. In *Ocean surface topography science team meeting, boulder, colorado.*

Andersen, O. B., Knudsen, P., Kenyon, S., & Holmes, S. (2014). Global and arctic marine gravity field from recent satellite altimetry (DTU13). In *76th eage conference and exhibition 2014* (Vol. 2014, pp. 1–5). doi: 10.3997/2214-4609 .20140897

Andersen, O. B., Knudsen, P., & Stenseng, L. (2015). The dtu13 mss (mean sea surface) and mdt (mean dynamic topography) from 20 years of satellite altimetry. In *Igfs 2014* (pp. 111–121). Springer.

Aydogan, D. (2011). Extraction of lineaments from gravity anomaly maps using the gradient calculation: Application to Central Anatolia. *Earth, Planets and Space*, *63*(8), 903–913. doi: 10.5047/eps.2011.04.003

Ballu, V., Dubois, J., Deplus, C., Diament, M., & Bonvalot, S. (1998).Crustal structure of the Mid-Atlantic Ridge south of the Kane Fracture Zone from seafloor and sea surface gravity data. *Journal of Geophysical Research: Solid Earth*, *103*(B2), 2615–2631. doi: 10.1029/97JB02542

Barthelmes, F. (2009). Definition of functionals of the geopotential and their calculation from spherical harmonic models: theory and formulas used by the calculation service of the International Centre for Global Earth Models (ICGEM), http://icgem. gfz-potsdam. de. doi: 10.2312/GFZ.b103-09026

Billi, A., Gambini, R., Nicolai, C., & Storti, F. (2007).Neogene-Quaternary intraforeland transpression along a Mesozoic platform-basin margin: The Gargano fault system, Adria, Italy. *Geosphere*, *3*(1), 1–15. doi: 10.1130/ GES00057.1

Blakely, R. J., & Simpson, R. W. (1986). Approximating edges of source bodies from magnetic or gravity anomalies. *Geophysics 51.7*, 1494–1498. doi: 10.1190/1 .1442197

Bullard, E. C. (1936). Gravity measurements in east Africa. *Philosophical Transactions of the Royal Society of London. Series A, Mathematical and Physical Sciences*, *235*(757), 445–531.

Ciani, A., Morelli, C., & Gantar, C. (1960). Rilievo gravimetrico sullo zoccolo epicontinentale dei mari italiani. *Boll. Geofis. Teor. Appl*(6), 101p.

Colantoni, P., Tramontana, M., & Tedeschi, R. (1990). Contributo alla conoscenza dell'avampaese apulo: struttura del Golfo di Manfredonia (Adriatico meridionale). *Giornale di Geologia*.

Consortium, E. B., et al. (2018). Emodnet digital bathymetry (dtm 2018).

Corrado, G., et al. (1981). The gravity field of Italy: analysis of its spectral composition and delineation of a tridimensional crustal model for central-southern Italy. *Boll. Geofis. Teor. Appl.*(23), 17–29.

Dawson, G. J., Green, C. M., & Fletcher, K. M. (2015). Using the SAR Mode from CryoSat-2 to Improve Satellite Derived Gravity near the Coast. In *77th eage conference and exhibition 2015* (Vol. 2015, pp. cp–451). doi: 10.3997/2214-4609.201412985

de Alteriis, G.(1995).Different foreland basins in Italy: examples from the central and southern Adriatic Sea. *Tectonophysics*, *252*(1-4), 349–373. doi: 10.1016/0040-1951(95)00155-7

de Alteriis, G., & Aiello, G. (1993). Stratigraphy and tectonics offshore of Puglia (Italy, southern Adriatic Sea). *Marine Geology*, *113*(3-4), 233–253. doi: 10.1016/0025-3227(93)90020-V

Decker, B. L. (1986).*World geodetic system 1984: Defense Mapping Agency Aerospace Center St Louis Afs Mo.*

de Lerma, D., Green, C. M., Cheyney, S., & Campbell, S. J. (2015).Improved high order vertical derivatives of potential field data-extending the ISVD Method. In *77th eage conference and exhibition 2015* (Vol. 2015, pp. 1–5). doi: 10.3997/2214-4609.201412755

Deng, X., & Featherstone, W. E. (2006). A coastal retracking system for satellite radar altimeter waveforms: Application to ERS-2 around Australia. *Journal of Geophysical Research: Oceans*, *111*(C6). doi: 10.1029/2005JC003039

Di Bucci, D., Ravaglia, A., Seno, S., Toscani, G., Fracassi, U., & Valensise, G. (2006). Seismotectonics of the southern Apennines and Adriatic foreland: Insights on active regional E-W shear zones from analogue modeling. *Tectonics*, *25*(4). doi: 10.1029/2005TC001898

Diviacco, P. (2018). *Sismica riconoscitiva legge 613/1967 - zona d.* OGS (Istituto Nazionale di Oceanografia e di Geofisica Sperimentale), Geophysical Section. Retrieved from https://snap.ogs.trieste.it/cache/service/doi/10.6092/SNAP.580bf950a46873e44295a7e29d66f077 doi: 10.6092/SNAP.580BF950A46873E44295A7E29D66F077

Dubois, J., & Deplus, C.(1989).Gravimetry on the Erimo seamount, Japan. *Tectonophysics*, *160*(1-4), 267–275.

Fairhead, J. D. (2016). *Advances in gravity and magnetic processing and interpretation*. EAGE Publications.

Farr, T. G., & Kobrick, M. (2000). Shuttle Radar Topography Mission produces a wealth of data. *Eos, Transactions American Geophysical Union*, *81*(48), 583-585.

Fedi, M. (2002). Multiscale derivative analysis: A new tool to enhance detection of gravity source boundaries at various scales. *Geophysical Research Letters*, *29*(2), 16–1. doi: 10.1029/2001GL013866

Fedi, M., Cella, F., Florio, G., & Rapolla, A. (2005). Multiscale derivative analysis of the gravity and magnetic fields of sorthern Apennines (Italy). *CROP Project, Deep seismic exploration of the Central Mediterranean and Italy (Atlases in Geoscience, Volume 1)", I. Finetti, ed., Elsevier Science*, 281–318.

Fedi, M., & Florio, G. (2001). Detection of potential fields source boundaries by enhanced horizontal derivative method. *Geophysical Prospecting*, *49*(1), 40–58. doi: 10.1046/j.1365-2478.2001.00235.x

Fedi, M., & Rapolla, A.(1993). *I metodi gravimetrico e magnetico nella geofisica della Terra solida*.

Finetti, I. (1983). Struttura ed evoluzione della microplacca adriatica. *Boll. Ocean. Teor. Appl. II (2), 115–123*.

FitzGerald, D., & Milligan, P. (2013). Defining a deep fault network for Australia, using 3D'worming'. *ASEG Extended Abstracts*, *2013*(1), 1–4. doi: 10.1071/ASEG2013ab135

Fu, L.-L., & Cazenave, A. (2000). *Satellite altimetry and earth sciences: a handbook of techniques and applications*. Elsevier.

Fukushima, T. (2019). *Fast computation of prismatic gravitational field*.

Gantar, C. (1983). *Rilievo gravimetrico offshore mgb002: Sullo zoccolo continentale nel mare Adriatico, per l'Agip Mineraria.* Osservatorio Geofisico Sperimentale (OGS), Rel. 5/83 - MNS/1, Rapporto finale N. 82595.

Green, C., Fletcher, K., Cheyney, S., Dawson, G., & Campbell, S. (2019).Satellite gravity – enhancements from new satellites and new altimeter technology. *Geophysical Prospecting*, *67*(6), 1611-1619.

Hildebrand, J. A., Stevenson, J. M., Hammer, P. T. C., Zumberge, M. A., Parker, R. L., Fox, C. G., & Meis, P. J. (1990). A seafloor and sea surface gravity survey of Axial Volcano. *Journal of Geophysical Research: Solid Earth*, *95*(B8), 12751–12763. doi: 10.1029/JB095iB08p12751

Hinze, W. J., Aiken, C., Brozena, J., Coakley, B., Dater, D., Flanagan, G., ... others (2005). New standards for reducing gravity data: The North American gravity database. *Geophysics*, *70*(4), J25–J32. doi: 10.1190/1.1988183

Luyendyk, B. P. (1984). On-bottom gravity profile across the East Pacific Rise crest at 21 north. *Geophysics*, *49*(12), 2166–2177. doi: 10.1190/1.1441632

Mastronuzzi, G., Palmentola, G., & Sans`o, P. (2002).Lineamenti e dinamica della costa pugliese. *Studi costieri*, *5*, 9–22.

Miller, H. G., & Singh, V. (1994). Potential field tilt—a new concept for location of potential field sources. *Journal of Applied Geophysics*, *32*(2-3), 213–217. doi: 10.1016/0926-9851(94)90022-1

Morelli, C. (1966). The geophysical situation in Italian waters. *The International Hydrographic Review*.

Morelli, D. (2002). Evoluzione tettonico-stratigrafica del Margine Adriatico compreso tra il Promontorio garganico e Brindisi. *Mem. Soc. Geol. It*, *57*, 343–353.

Nagy, D., Papp, G., & Benedek, J. (2000). The gravitational potential and its derivatives for the prism. *Journal of Geodesy*, *74*(7-8), 552–560. doi: 10.1007/s001900000116

Nagy, D., Papp, G., & Benedek, J. (2002). Corrections to" The gravitational potential and its derivatives for the prism". *Journal of Geodesy*, *76*(8), 475–475.

Nowell, D. A. (1999). Gravity terrain corrections—an overview. *Journal of Applied Geophysics*, *42*(2), 117–134. doi: 10.1016/S0926-9851(99)00028-2

Parker, R. L. (1973). The rapid calculation of potential anomalies. *Geophysical Journal International*, *31*(4), 447–455. doi: 10.1111/j.1365-246X.1973.tb06513.x

Pavlis, N. K., Holmes, S. A., Kenyon, S. C., & Factor, J. K.(2012). The development and evaluation of the Earth Gravitational Model 2008 (EGM2008). *Journal of Geophysical Research: Solid Earth*, *117*(B4). doi: 10.1029/2011JB008916

Rapolla, A. (1986).Crustal structure of Central and sorthern Italy from gravity and magnetic data. *Giornale di Geologia*, *48*(1-2), 129–143.

Ridente, D., Fracassi, U., Di Bucci, D., Trincardi, F., & Valensise, G. (2008). Middle Pleistocene to Holocene activity of the Gondola Fault Zone (sorthern Adriatic Foreland): Deformation of a regional shear zone and seismotectonic implications. *Tectonophysics*, *453*(1-4), 110–121. doi: 10.1016/j.tecto.2007.05.009

Ridente, D., & Trincardi, F.(2006). Active foreland deformation evidenced by shallow folds and faults affecting late Quaternary shelf–slope deposits (Adriatic Sea, Italy). *Basin Research*, *18*(2), 171–188. doi: 10.1111/j.1365-2117.2006.00289.x

Sandwell, D. T. (1992). Antarctic marine gravity field from high-density satellite altimetry. *Geophysical Journal International*, *109*(2), 437–448. doi: 10.1111/j.1365-246X.1992.tb00106.x

Sandwell, D. T., Garcia, E., Soofi, K., Wessel, P., Chandler, M., & Smith, W. H. F.(2013).Toward 1-mGal accuracy in global marine gravity from CryoSat-2, Envisat, and Jason-1. *The Leading Edge*, *32*(8), 892–899. doi: 10.1190/tle32080892.1

Sandwell, D. T., Mu¨ller, R. D., Smith, W. H. F., Garcia, E., & Francis, R. (2014). New global marine gravity model from CryoSat-2 and Jason-1 reveals buried tectonic structure. *Science (New York, N.Y.)*, *346*(6205), 65–67. doi: 10.1126/science.1258213

Sandwell, D. T., & Smith, W. H. (2009). Global marine gravity form retracked Geosat and ERS-1 altimetry: Ridge segmentation versus spreading rate. *Journal of Geophysical Reseach*, *10*. doi: 10.1029/2008JB006008

Stacey, F. D., & Tuck, G. J. (1981). Geophysical evidence for non-Newtonian gravity. *Nature*, *292*(5820), 230–232. doi: 10.1038/292230a0

Talwani, M., Early, W. P., & Hayes, D. E. (1966). Continuous analog computation and recording of cross-coupling and off-leveling errors. *Journal of Geophysical Research*, *71*(8), 2079–2090. doi: 10.1029/JZ071i008p02079

Tramontana, M., Morelli, D., & Colandoni, P. (1995). Tettonica plio-quaternaria del sistema sud-garganico (settore orientale) nel quadro evolutivo dell'Adriatico centro-meridionale. *Studi geologici camerti, n. speciale, 1995, pp. 467-473*.

Uieda, L., Soler, S. R., Pesce, A., Oliveira Jr, V. C., & Shea, N. (2020). Harmonica: Forward modeling, inversion, and processing gravity and magnetic data (Version v0.1.0). doi: 10.5281/zenodo.3628742

Volpi, V., Forlin, E., Baroni, A., Estublier, A., Donda, F., Civile, D., ... Delprat-Jannaud, F. (2015). Evaluation and Characterization of a Potential CO2 Storage Site in the South Adriatic Offshore. *Oil & Gas Science and Technology– Revue d'IFP Energies nouvelles*, *70*(4), 695–712. doi: 10.2516/ogst/2015011

Wessel, P., Luis, J. F., Uieda, L., Scharroo, R., Wobbe, F., Smith, W. H., & Tian, D. (2019).The generic mapping tools version 6.*Geochemistry, Geophysics, Geosystems*, *20*(11), 5556–5564. doi: 10.1029/2019GC008515

Wijns, C., Perez, C., & Kowalczyk, P. (2005). Theta map: Edge detection in magnetic data. *Geophysics*, *70*(4), L39–L43. doi: 10.1190/1.1988184

Table 1. There are statistics of differences between sea-bottom gravity datasets OGS60 and OGS83 (Figure 3e). The differences are calculated on the OGS60 stations, in the overlapping area between the two datasets, by linearly interpolating the OGS83 values at the exact coordinates.

	Min	Max	Mean	Std	RMS	N°of points
OGS83-OGS60	-0.79	1.7	0.1	0.57	0.58	59

Unit of measurement in mGal

Table 2. Statistic of the Bouguer gravity anomaly calculated for each dataset (DTU, OGS, and S&S) and relative differences within a 17 km wide coastal strip (DTU-S&S, DTU-OGS, DTU-OGS). The differences are calculated on regular grids with 2.5 km grid-step.

	Min	Max	Mean	Std	RMS	N°of points
DTU	41.04	124.49	64.18	11.73	-	1739
S&S	41.78	123.87	66.46	12.01	-	1739
OGS	41.43	102.77	60.58	6.58	-	671
DTU-S&S	-27.33	7.11	-2.89	6.21	6.86	333
DTU-OGS	-20.47	19.18	1.17	4.07	4.23	333
S&S-OGS	-6.99	38.57	4.07	6.66	7.8	333

Unit of measurement in mGal

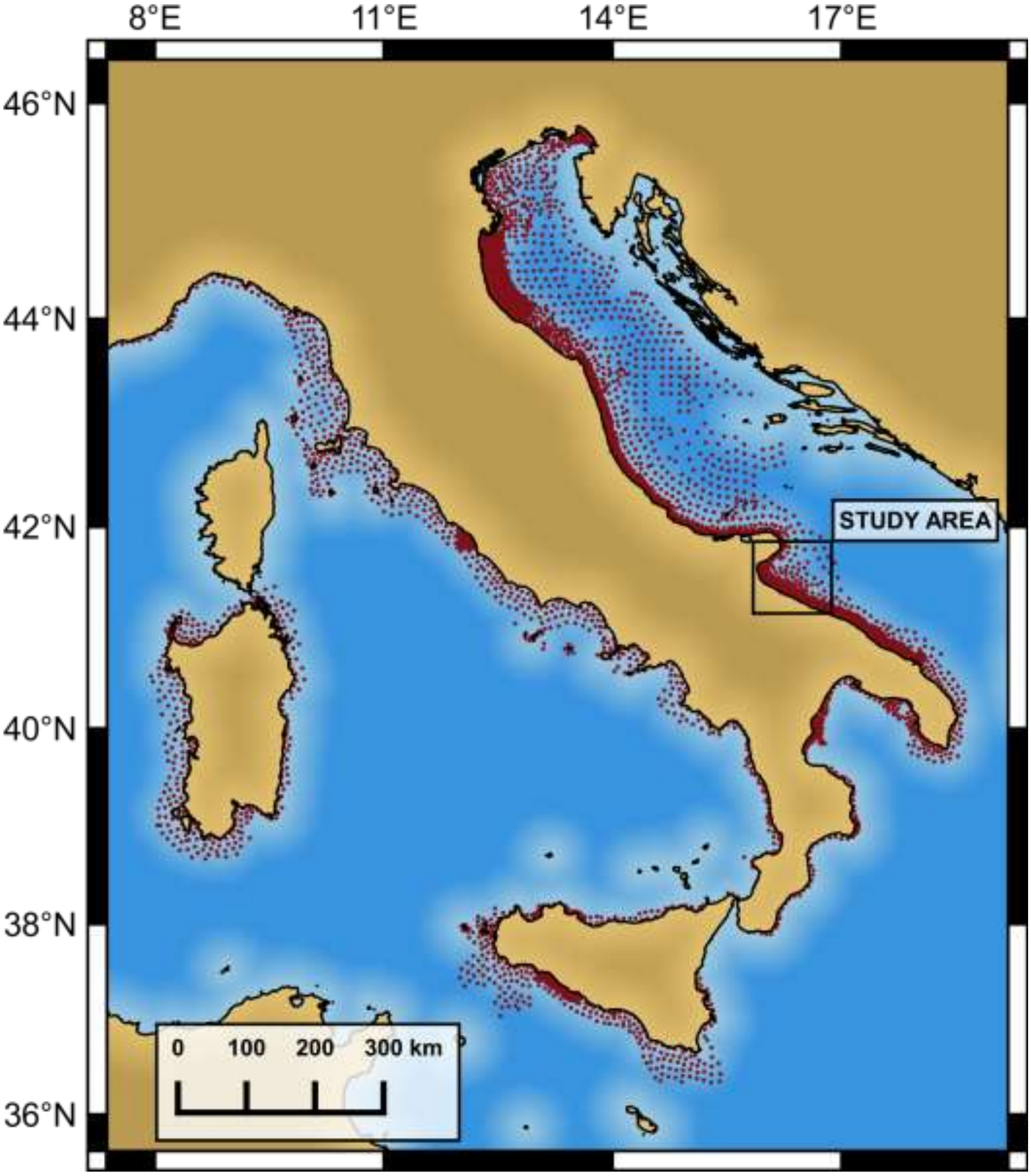

Figure 1. Position of sea-bottom gravity stations (small red dots) from the OGS database, including C. Morelli (1966) and Gantar (1983). Most of the stations recorded from the early 1950s to the late 1980s, a few tens of kilometers from the Italian coasts, with an average spacing of about 1 km. Map frame in WGS 84/World Mercator + EGM2008 height coordinate system (EPSG: 6893).

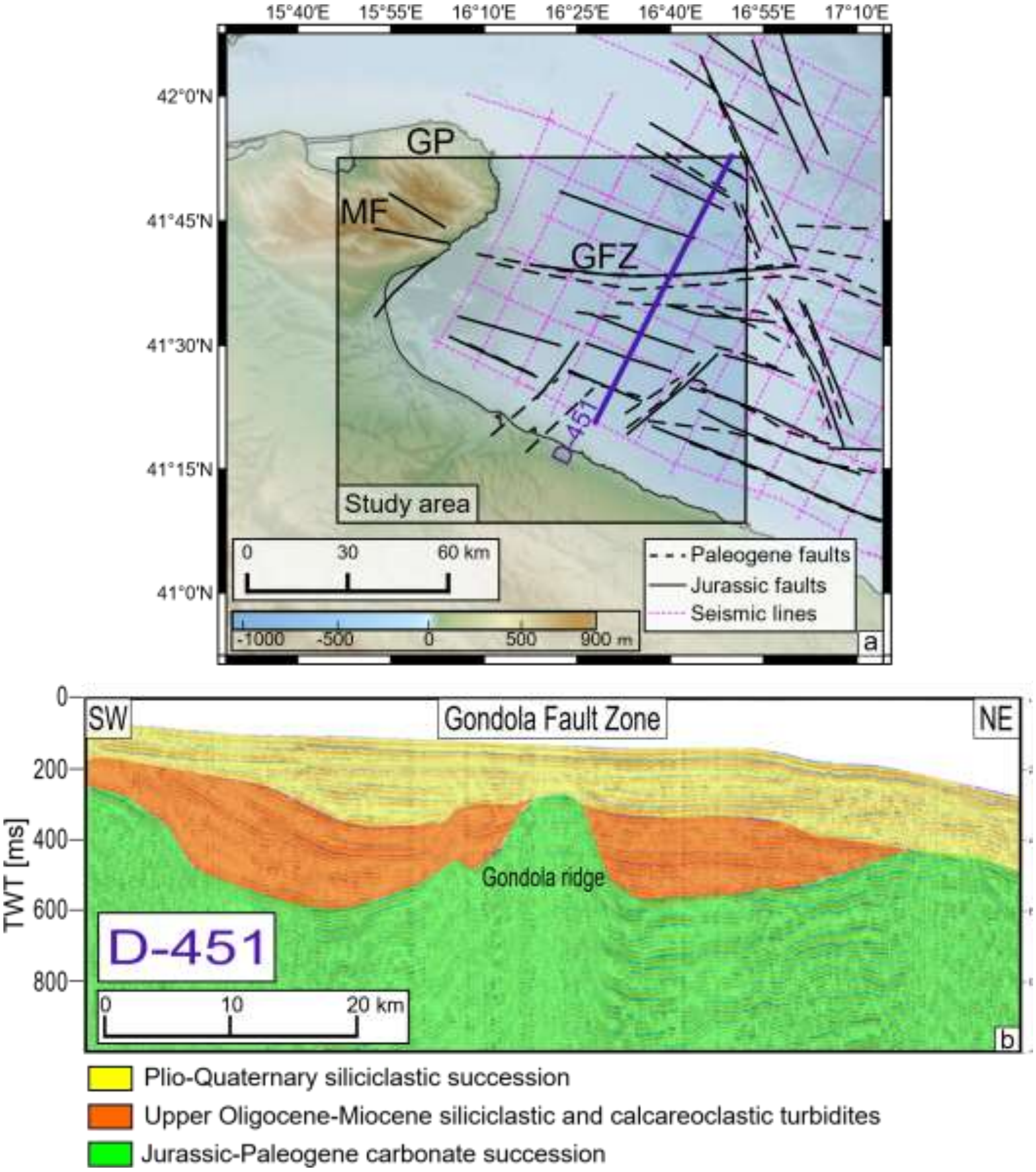

Figure 2. (a) Structural map of the Gulf of Manfredonia, showing the Gondola Fault Zone (GFZ) and its inland continuation with the Mattinata Fault (MF) cutting through the Gargano Promontory (GP). Fault interpretation in the marine sector has been derived from seismic data (D. Morelli, 2002), and position of the multichannel seismic profiles from ViDEPI (violet lines). (b) Seismic profile D-451 (position in Figure 2a), where the Gondola ridge is clearly imaged (interpretation of seismic layers has been taken from Volpi et al. (2015)). Seismic data comes from the project ViDEPI "Visibility of Petroleum Exploration Data in Italy" (URL: www.videpi.com), managed by the Ministry of Economic Development. Data have been made available in the SEGY format on the SNAP "Seismic data Network Access Point" platform, managed by the Istituto Nazionale di Oceanografia e di Geofisica Sperimentale, OGS (Diviacco, 2018).

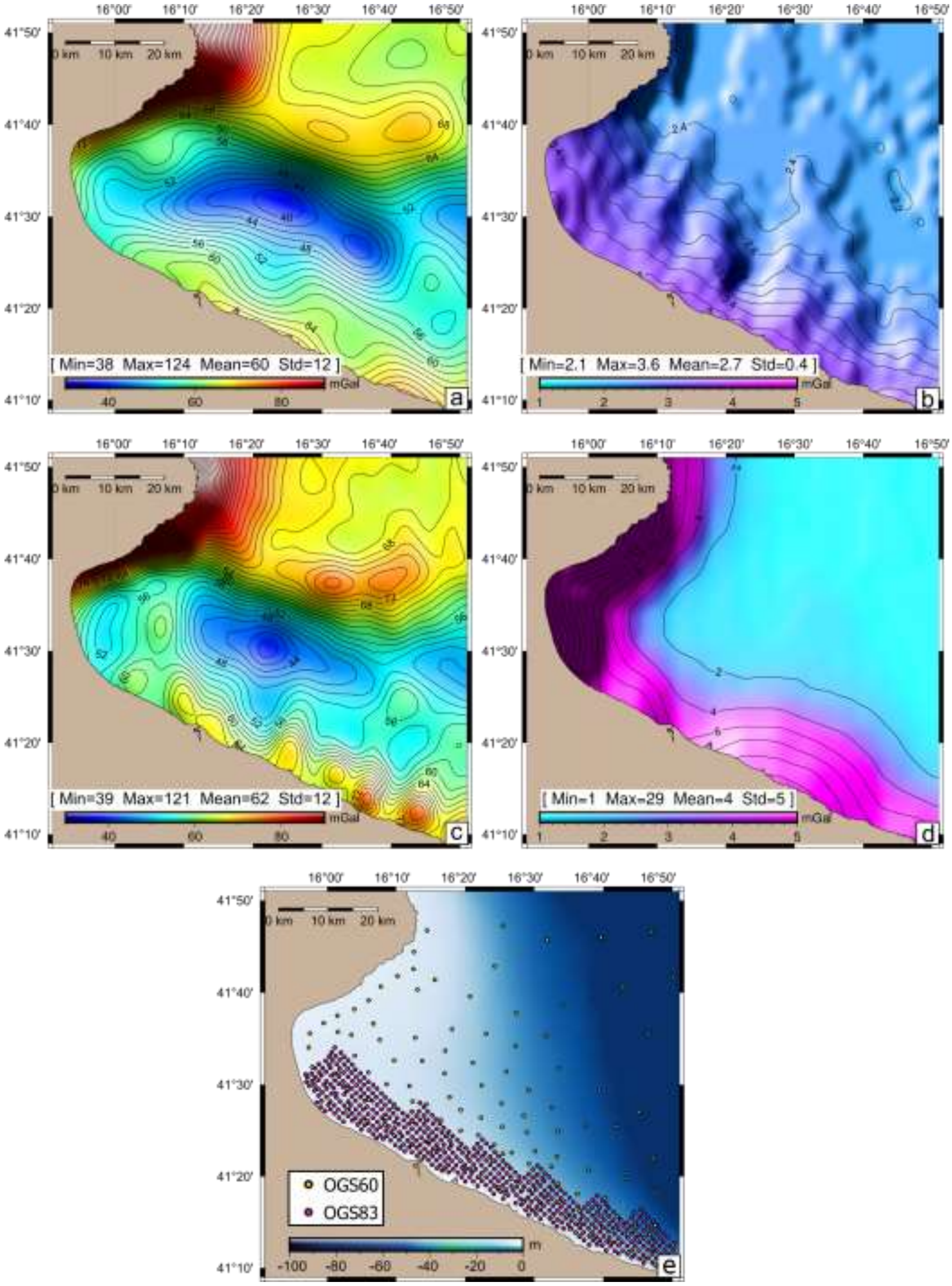

Figure 3. Free air anomaly of DTU dataset with associated MSS interpolation error (a,b) and Free-air anomaly of S&S dataset with associated RMS error (c,d). The error maps show how the quality of the Free-air anomaly deteriorates near the coast, up to a maximum of 29 mGal in S&S data. The lowest map (e) shows the position of sea-bottom gravity stations, plotted onto the Gulf of Manfredonia bathymetry: OGS 1960 (yellow dots) and OGS 1983 (red dots).

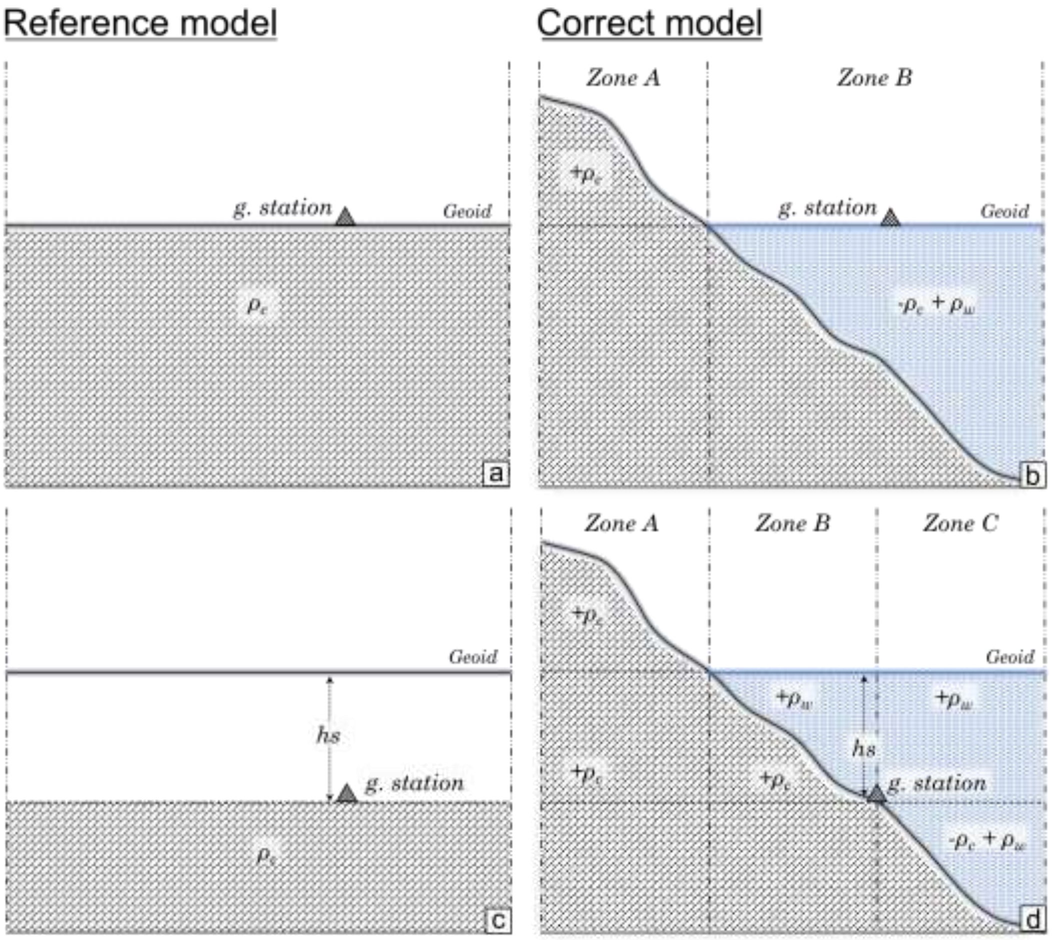

Figure 4. Schematic representation of models used to compute the topographic effects of sea-surface gravity (a, b, eq.7) and sea bottom gravity (c, d, eq.8). On the left, the reference model, and on the right, the correct model including all the density corrections that must be added to the reference model in order to come to a correct estimate of the topographic effect.

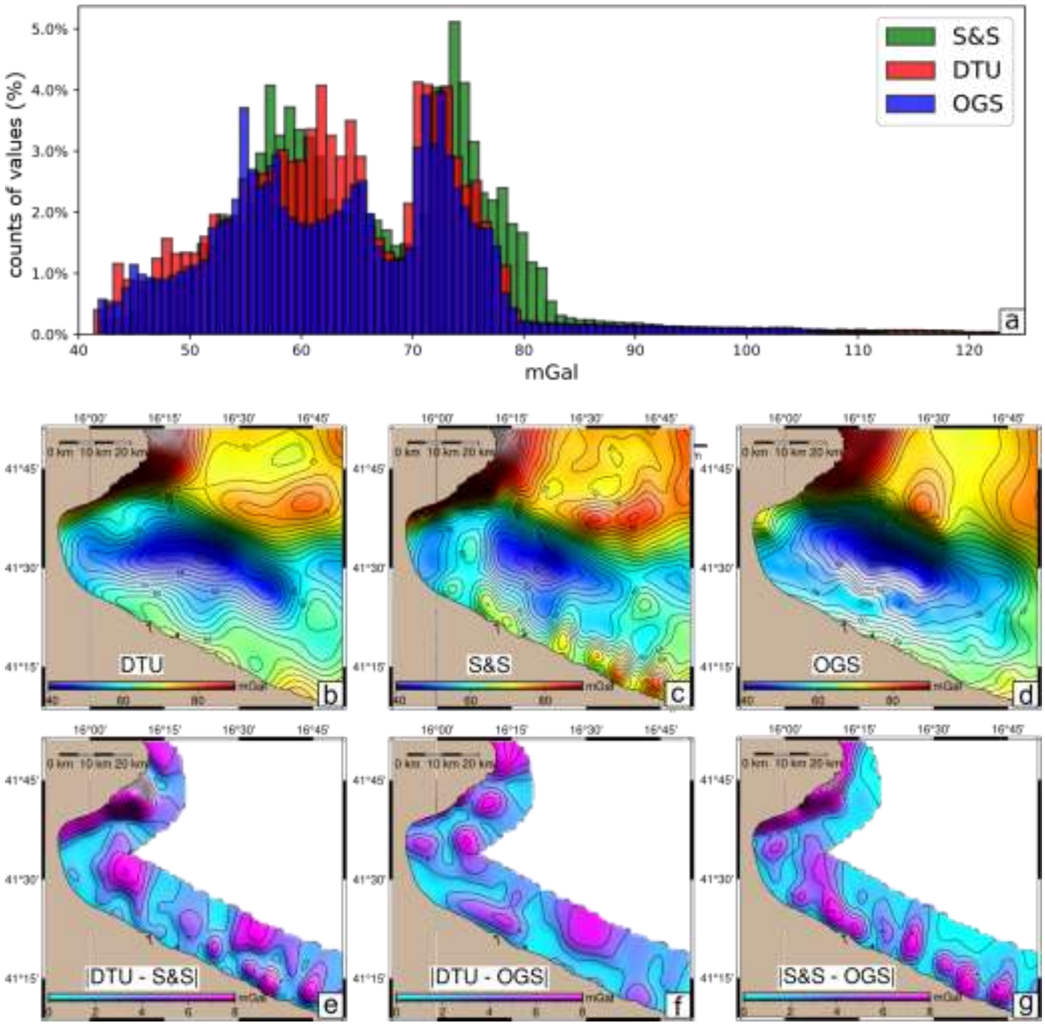

Figure 5. Distribution of Bouguer anomaly values (a), Bouguer anomaly maps (b, c, d), and relative absolute differences of DTU, S&S, OGS datasets (e, f, g). A block-mean average, with ~2 km window size, and a low-pass Gaussian filter, with a 6 km window size, has been used to avoid aliasing errors (Wessel et al., 2019) and bring all datasets to the exact empirical lowest resolution. The differences are mapped within a 15 km wide coastal strip, which is the area most affected by coastal noise in satellite data and, at the same time, densely covered by the OGS sea-bottom stations. The absolute value stresses the total magnitude of differences without the bias of the sign. The coastal noise is easy to identify in the S&S dataset and in the S&S-OGS differences, where it forms a sort of "ringing effect" up to ~17 km seaward.

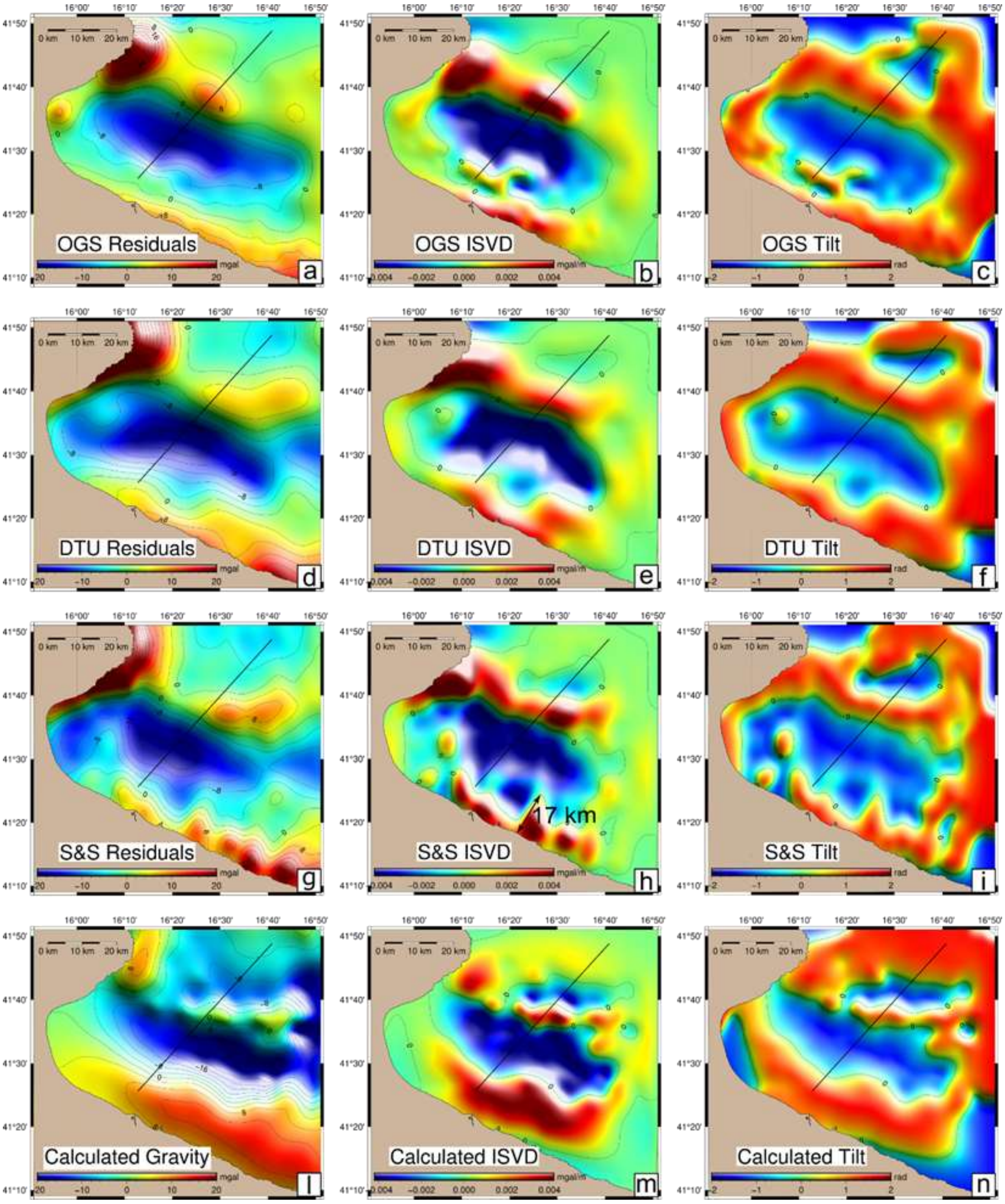

Figure 6. The subplots show, from left to right, (i) the observed gravity residuals, (ii) the Integrated Second Vertical Derivative (ISVD), and (iii) the Tilt function of OGS (a, b, c), DTU (d ,e ,f) and S&S (g, h, i) datasets. The bottom plots (l, m, n) show the calculated gravity effect of the 2D depth interface, obtained from depth-converted seismic reflection data, which separates sedimentary deposits from carbonate rocks. The black line indicates the profile analyzed in Figure 7.

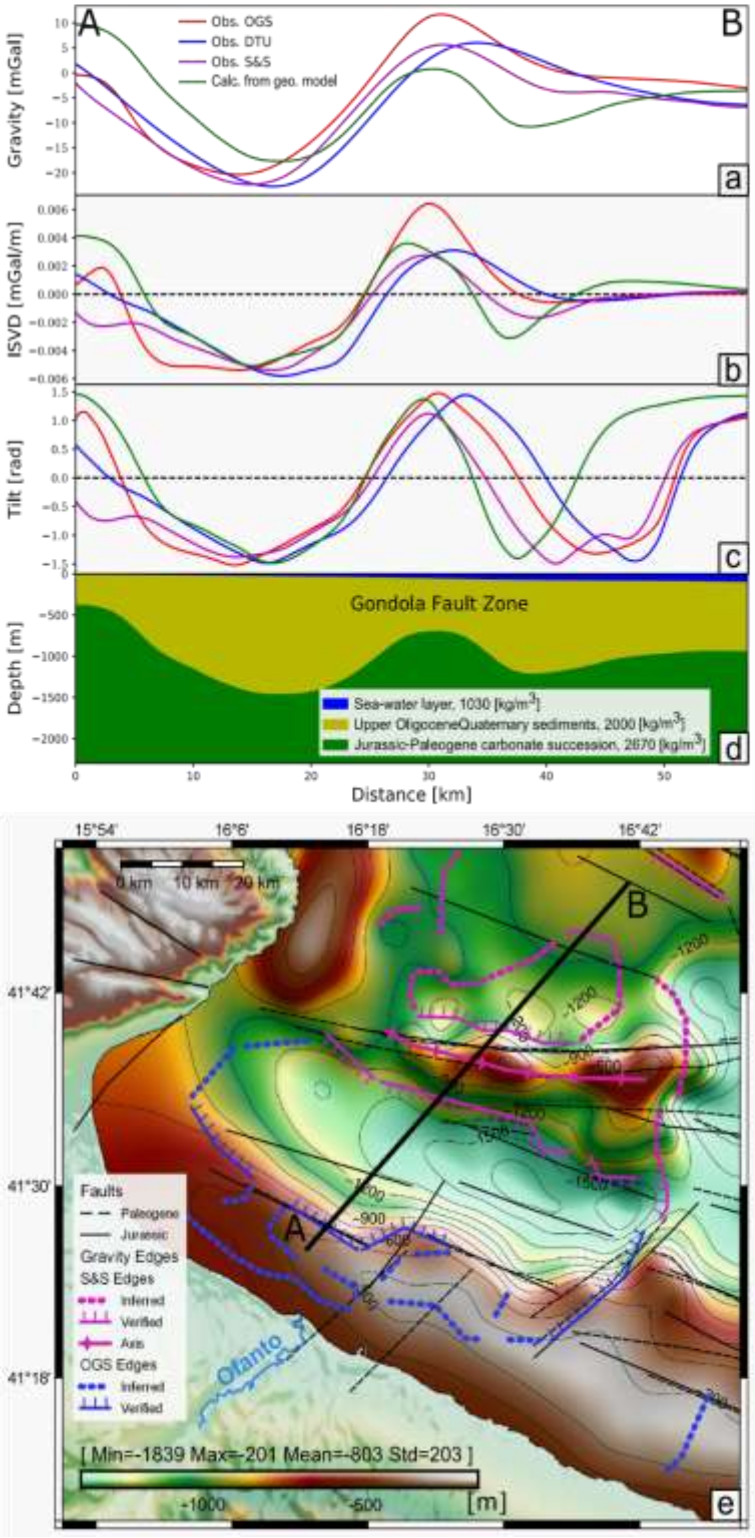

Figure 7. Representative depth profile of the geological model derived from seismic interpretation, crossing the Gondola Fault Zone (d). Upper panels (a, b, c) show the trend of the observed residual gravity, ISVD, and Tilt functions, calculated for each different dataset (OGS, DTU, and S&S) and for the geological model. The zero values of both ISDV and Tilt mark the approximate upper edges of the carbonate platforms. The bottom map (e) shows results from the edge-

detection analysis, which combines OGS data up to 17 km from the coast and S&S data in the remaining areas. The gravity edges have been divided into two sets: the first set contains lines correlating with the general trend of the faults (verified edges) and the second set contains lines only recorded by gravity (inferred edges). The ridge axis outline the approximate top center of the Gondola ridge. The rock/sediment interface is imaged and contoured onto the offshore areas (Volpi et al., 2015). Jurassic-Paleogene faults are both based on seismic interpretations taken from previous works (D. Morelli (2002), and references therein).

ANNEX 2

Technical Report (OGS) - Project Livenza Tagliamento Acque (LTA)

Detailed gravimetric survey in the Fontanafredda - Budoia (PN) area

F. Palmieri[1], **L. S. Zampa**[1]

[1]National Institute of Oceanography and Applied Geophysics - OGS - Italy

Data Acquisition

As part of the project “Geophysical analysis for the CAMI LIFE + and WARBO LIFE + protocols for the protection of the aquifers of aqueduct interest in the Upper and Lower Plain on the right Tagliamento in the area between the Livenza river and the Cellina torrent” (Busetti et al., 2021) supported by the Livenza Tagliamento Acque S.p.A, in the context of the Upper Friulian Plain, in the period 29.09 - 05.11 2020, a detailed gravimetric survey was carried out in the area of Fontanafredda - Budoia (PN). The main aim of this survey was deducing, from the Bouguer anomalies, the distribution of densities in the subsoil, i.e., the geometry, thickness, tectonic structure, etc., of the geological elements that characterize this sector of the Friulian Plain just at the foot of the Alpine chain. The gravimetric survey covered an area of about 90 km^2. Instrument used was a LaCoste & -Romberg gravimeter mod. D-018, equipped with feedback.

Since the gravimeters measure differences in gravity (Δg), a "First Order Network" was first established consisting of two points inside the surveyed area (church of Ranzano and church of San Giovanni) and one outside (cemetery of Tamai di Brugnera), which represented the definition of the "gravimetric datum" as it belongs to a gravimetric network, previously established, and connected with the absolute station of Basovizza (TS).

The three points of the “First Order Network" were connected by means of the so-called “Passo del Pellegrino" and back, which provides for the measurement of 4 Δg for each gravimetric section. The scheme of the “1st Order Network" is shown in Fig. 1.

Figure 1 - Sketch of the gravimetric “First Order Network".

The “1st Order Network" data were compensated with the least-squares method by solving a linear system consisting of the observation equations (indirect observations method). The gravity values and the relative standard deviation of the individual stations of the “1st Order Network" are shown in Tab. 1.

Standard deviation for unit weight 0.0023 mGal			
BSN	g	σ	Wt.
	mGal	mGal	
Tamai	980630.441	0.0000	8
Ranzano	980623.029	0.0008	8

San Giovanni	980624.966	0.0008	8

Table 1 - Gravity and standard deviation values of the "1st Order Network" stations.

Starting from these points of known gravity, closed circuits have been organized during data acquisition. In total, 29 gravimetric circuits have been set up for a total of 246 detailed gravimetric stations, as homogeneously distributed throughout the territory, with an average density of about 3 stations per km^2. In Fig. 2 is shown the areal distribution of the gravimetric points.

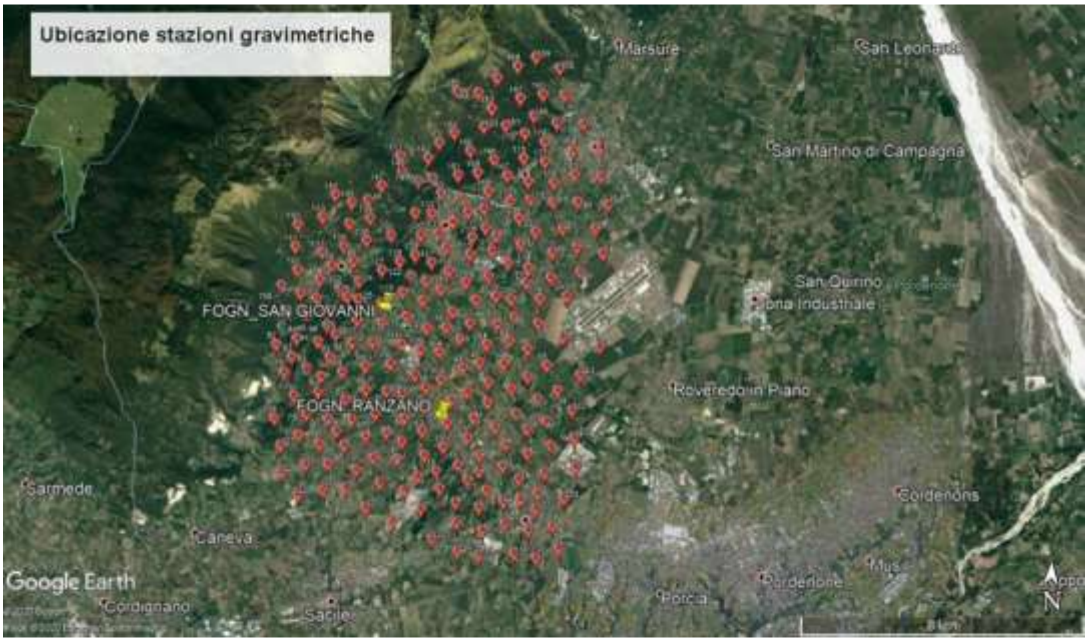

Figure 2 – Distribution of the gravimetric stations.

Data acquisition took place according to the following scheme: 1001-1-2-3-4-... -1002-1001, with stations 1001-1002 belonging to the "1st Order Network", the remaining 1-2-3 -4-... belonging to the detailed network. Closing in the same station 1001 (FOGN_Ranzano) allowed calculating the term of instrumental drift while closing in station 1002 (FOGN_San Giovanni) allowed calculating the closing error of the gravimetric circuit. In addition, a sample of 25 stations, equal to about 10%, was repeated for an estimate of the errors.

In Fig. 3, the instrumental drift term, expressed in mGal/h, the closure errors, expressed in mGal, of the gravimetric circuits, Δg, expressed in mGal, in the repeated stations, are represented.

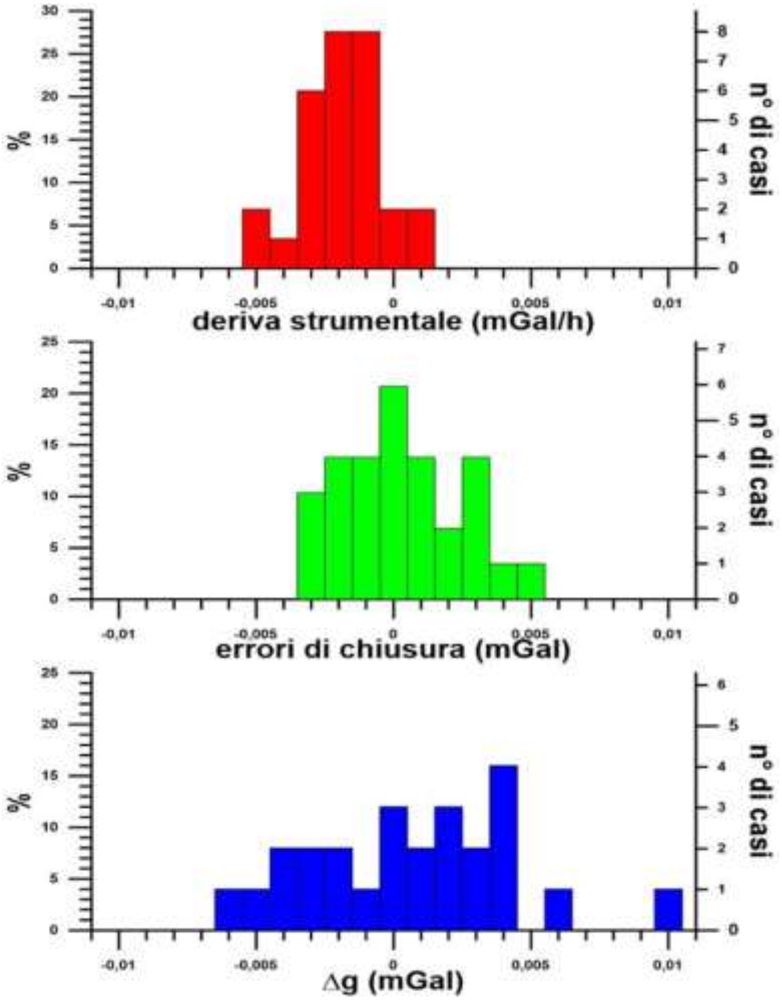

Figure 3 - Instrumental drift, closure errors and Δg in repeated stations.

For the calculation of the Bouguer anomalies, defined at the measuring point, the gravity values measured in the field were compared with the theoretical gravity values (calculated according to the formula that refers to the Geodetic Reference System 1980), appropriately corrected (CF, Faye Correction, CB, Bouguer Correction, CT, Topographic Correction).

The Faye Correction calculates the effect of the vertical distance (h) between the measurement station and the reference equipotential surface without taking into account the interposed masses, the Bouguer Correction calculates the effect of the interposed masses between the height of the reference surface and that of measurement, considering a hemispherical cap of constant density and thickness h, the Topographic Correction calculates the effect of topographic irregularities.

For the execution of the topographical correction, the calculation process was divided into two distinct phases, using for different intervals (RMIN and RMAX) of distances from the measurement point, different dimensions of the grid of the average altitudes. For this, two distinct DTMs have been created:

1) starting from the data of the digital terrain models (DTM) of the Veneto and Friuli-Venezia Giulia regions, a DTM with 10 x 10 meters cells was created: in total, the model consisted of 6,000,000 cells. This DTM was used to calculate the Topographic Correction in the range from 5 (RMIN) to 5,000 (RMAX) m away from the measurement point. So, it was possible to accurately describe the most significant topographical discontinuities located in the vicinity of the measurement points.
2) starting from the SRTM data, having an original spacing of 1"x 1" (for our latitudes/longitudes that is equal to about 30 x 22 m), a DTM with 20x20 meters cells was created: in total the model consisted of 16,250,000 cells. This DTM was used for the calculation of the Topographic Correction in the range from 5,000 (RMIN) to 30,000 (RMAX) m away from the measurement point.

For the calculation of the Bouguer and topographical corrections, a density of 2400 kg m^3 was used.

Therefore, the observed gravity values are compared with the theoretical ones (g_{teor}), calculated according to standardized formulas, appropriately corrected (CF, Faye correction; CB, Bouguer correction; CT, topographic correction):

$$g_{geol} = g_{oss} - (g_{teor} - CF + CB) + CT$$

Their difference (g_{geol}) is defined as a gravity or Bouguer anomaly at the measurement point. Therefore, it can be defined as the difference between the observed gravity and the theoretical gravity, appropriately corrected, of the measurement point calculated on a "theoretical" model of Earth. It is important to underline that, unlike what is sometimes written in various applied geophysics texts, the measured gravity (g_{oss}) is not "reduced", or moved, to a particular surface (geoid) to be compared with the other values, but is "reduced" the theoretical gravity value.

The Bouguer anomaly is determined by a lateral variation (contrast) of density ($\Delta\rho=\rho_1-\rho_2$) inside the Earth. Therefore, the sign of the anomaly is linked to the sign of the density contrast ($\Delta\rho$): with reference to Fig. 4, the Bouguer anomaly is negative for $\rho_1 < \rho_2$, Fig. 4 (a); zero for $\rho_1 = \rho_2$, Fig. 4 (b); positive for $\rho_1 > \rho_2$, Fig. 4 (c).

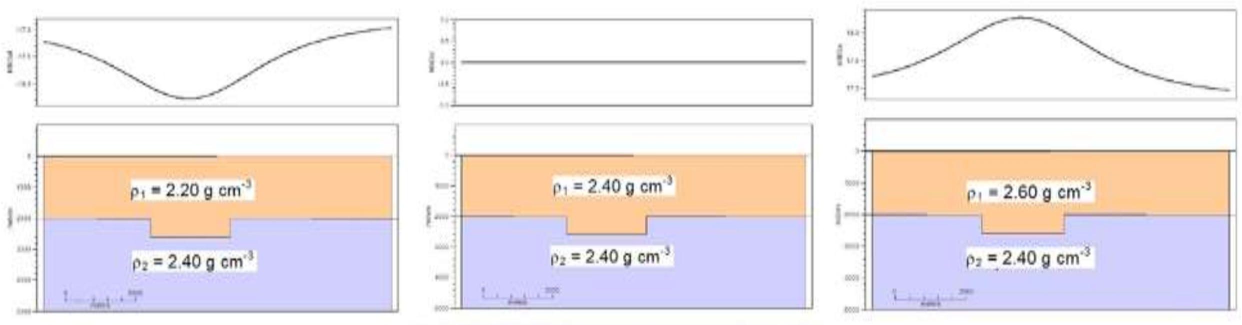

Figure 4 – Bouguer anomaly according to the density contrast.

The Bouguer anomaly map, which reflects the lateral variations in density within the Earth, is shown in Fig. 5. However, the gravimetric map obtained after making the corrections described above is the result of the superposition of anomalies of different origin and entities: any (potential) source will contribute to the potential field; therefore, complex distribution of sources to the Earth's interior, will give rise to a (potential) field which, for interpretative purposes, must be decomposed into its regional and local components. The regional field consists of isoanomalies with a slight curvature showing a regular trend and, therefore, a constant gradient in one direction over a vast area: this anomaly, at low spatial frequency or large wavelength, is caused by heterogeneity deep, in relation to the scale of the problem. Overlaid or masked by this field, there may be anomalies, at high frequency or small wavelength, comparable to distortions of the regional field, which are characterized by a spatial irregularity and a greater curvature of the isoanomaly: they are determined by "local" masses of interest for prospecting purposes: these anomalies define the local or residual field.

For the separation of the two components, a polynomial approximation (of the first and second-order) of the regional field was carried out in this first phase. The residual is the difference between the Bouguer anomaly and the calculated regional field. Fig. 6a shows the residual anomaly obtained using a polynomial of degree 1. Incidentally, it should be noted that, by increasing the order of the polynomial, the amplitude of the residual anomaly decreases; that is, increasingly external sources are highlighted, but the complexity of the residual trend is also accentuated because a gravimetric "noise" may be amplified.

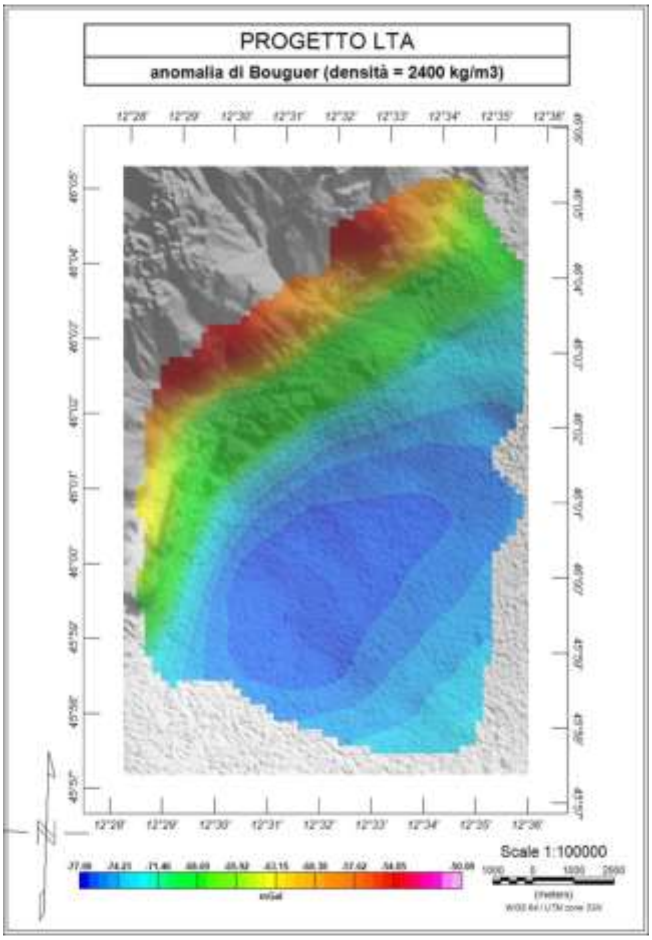

Figure 5 – Bouguer anomaly map.

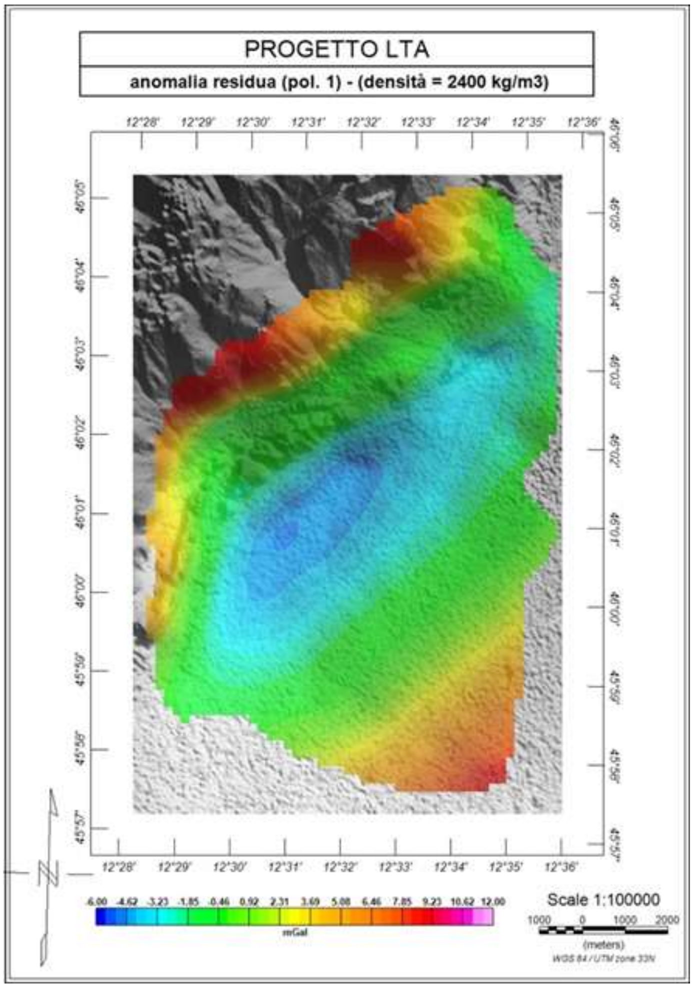

Figure 6 - Map of residual anomalies: with pol. 1

To visualize the longer-term component, i.e., low-frequency anomalies, the analytical extension technique was used upwards: with this technique, the field at higher altitudes than the measurement one is calculated, thus attenuating the signal in its higher frequency components (amplitude attenuation and noise reduction). For two altitudes: -1000 m and -4000 m, the results are shown in Fig. 7a and 7b, respectively.

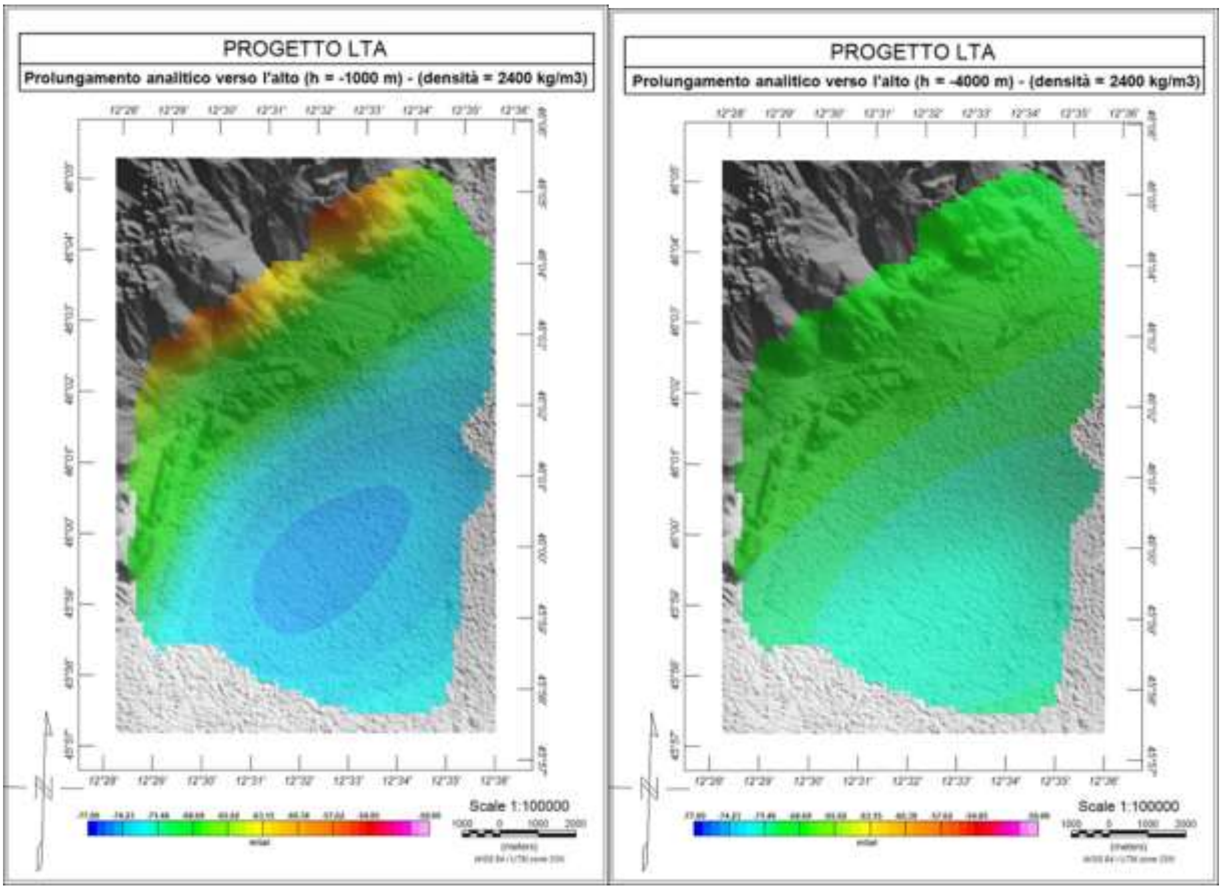

Figure 7 - Analytical extension upwards: (a) -1000 m – (b) -4000 m.

6.2 Modeling of gravimetric data

In general, the modeling of the gravimetric data has the objective of quantifying three parameters: (1) depth (2) geometry, and (3) relative density of the materials making up the subsoil. From the variations in density, it is then possible to estimate other correlated quantities, such as the speed of seismic waves or porosity of materials, known as lithologies. However, due to the intrinsic ambiguity of the method, it is theoretically impossible to obtain all this information simultaneously (Dentith & Mudge, 2014; Fairhead, 2016). Therefore, it is necessary to establish a priori to which of the three parameters is to be solved to solve the problem. Once chosen, it is possible to modify the two remaining parameters from the start through other geophysical and/or geological data. The ultimate goal is to obtain a density model consistent with the observed data and the geological-structural set-up of the area under study.

In the present work, multichannel seismic reflection profiles represented the main available data to be integrated with gravimetry. Previous works have used seismic to reconstruct the depths and geometries, (1) of the Quaternary base (Nicolich et al., 2004) and (2) of the carbonate surface (Barison, 2008). This information was used as the first starting constraint on the initial model.

The geological cartography (Carulli, 2006) and the data from the exploration wells have made it possible to group the lithologies present in the area into three main units, whose lateral contact can be identified starting from the gravimetric anomaly: (1) Jurassic-Cretaceous limestones, (2) Miocene molasses (marls and sandstones) and (3) Quaternary sediments (Fig. 8).

Furthermore, the geological section "D" of the Maniago sheet (Zanferrari et al., 2008), adjacent to the area of interest and perpendicular to the axis of the main tectonic structures, allowed us to hypothesize the geometry of the thrusts, which tend to verticalize near the topographical surface.

In addition to the geological data and the seismic data, some functions derived from the gravimetric data itself allow identifying contacts between different lithologies (i.e., only the lateral contacts, not the vertical ones). This information can be used as an additional constraint on the final model. In particular, the horizontal and vertical gradients, calculated starting from the Bouguer anomaly, are significant in the study area.

The horizontal gradient is given by the Cartesian sum of the derivatives of the anomaly along with the X and Y coordinates in the projected cartographic reference system UTM33 WGS84. In the study area, this function highlights some of the geological contacts between carbonates, molasses, and sediments, according to the spatial resolution limits of the data (Fig. 9a).
Maximum values of the horizontal gradient can be correlated with the tectonic features of Polcenigo-Maniago and Cansiglio. A summary of the information derived (1) from the geological survey and (2) from the gravimetry can therefore lead to a better definition of the trend of the faults on the map, especially in the sections where they do not emerge.

The vertical gradient, which can be calculated using the Fourier transform starting from the Laplace equation, tends to emphasize the components of the high-frequency signal generated by the most superficial density contrasts among those identifiable (Blakely, 1996).
Like for the gravity anomaly, the vertical gradient values are negative if the density of the source is less than that of the surrounding material, positive otherwise. This property allows circumscribing in greater detail the local anomalies generated by bodies with a relatively small horizontal extension (up to the maximum spatial resolution limit of the data). The zero value of the derivative is generally used to define the limits of high-density contrast structures (Fairhead, 2016).

From the comparison between the geological data and the vertical gradient map (Fig. 9b), maximum positive values are highlighted in correspondence of the molasses outcrops near Budoia and Polcenigo and of the carbonates on the northernmost alpine slopes (i.e., rock/sediment contrast). Instead, the minimum negative values of the vertical gradient saturate at the face of the Polcenigo - Maniago overthrow, distributed on a band parallel to the latter that widens in a S-W direction. This band constitutes a local minimum that could be partially explained as a numerical effect of the filter used for calculating the derivative: a noise that occurs at high horizontal gradients and is difficult to remove without making changes to the real signal (Gibbs effect). However, this minimum also coincides with a confluence area of the surface torrential waters coming from the mountain (Gorgazzo and Artugna streams), which join in the SW to form the Livenza river. This evidence may suggest the presence of relatively lower densities in the sediments that characterize the western sector compared to the SE sector of the alluvial plain (more significant clayey component and/or greater porosity). Furthermore, the polynomial residual of the second-order (Fig. 9d), close in terms of frequency to the vertical gradient and free from the mentioned disturbance, also shows a local minimum, similar to that of the gradient. This strengthens the interpretation of the minimum as a real signal rather than a simple filter effect.

The Cartesian sum of the horizontal and vertical derivatives of the gravity anomaly is defined as the "analytical signal" (Fig 9c). The latter summarizes the characteristics of both gradients described above, emphasizing (1) lateral contacts between bodies of different densities and (2) local minima.

The maximum spatial resolution limit of the gravimetric anomaly is linked to the distribution of the measurement points: an anomaly can be solved if it is sampled regularly from stations spaced at most half of its wavelength (Nyquist sampling theorem - Shannon). This means that local maxima or minima with a smaller extension than the distance between two measurements cannot be identified and/or considered reliable. In this case, the survey consists of homogeneously distributed stations with an average relative distance of ~ 700 m. Therefore, the minimum reliable wavelength in the observed anomalies is ~1400 m. This limit also implies that surface bodies with smaller dimensions cannot be interpreted and modeled correctly.

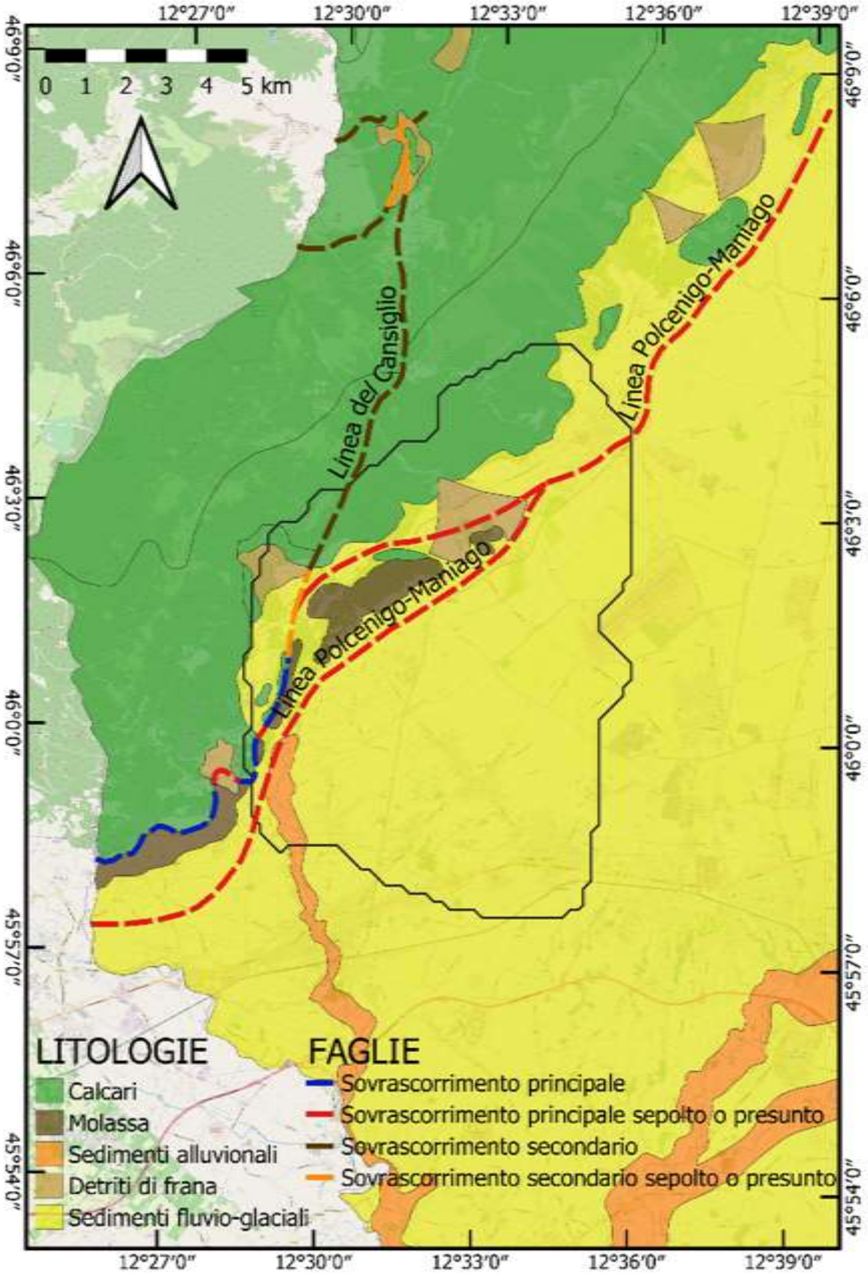

Figure 8 - Geological map of the study area, used to construct the initial density model (Carulli, 2006); the black polygon encloses the area covered by the gravimetric stations.

The depth of investigation also depends on the wavelength of the signal. Since the extension of the mapped area does not exceed 12 km, the effect of deep sources, such as the crystalline base and/or the Moho, will be approximable to a constant or at most to a linear trend (Rapolla 1986; Fedi and Rapolla 1983). The remaining non-linear variations of the signal are instead mainly attributable to (1) density variations in Quaternary sediments, (2) vertical variations of the rock/sediment interface, and (3) density variations within the bedrock up to maximum depths of 4 ÷ 6 km (Jung, 1961). The degree of uncertainty for the values of the Bouguer anomaly (observed data) was estimated to be around 0.1 mGal, a value obtained by considering the possible approximation errors in the heights of the digital terrain model in the calculation of the topographical effect. In addition, the interpolated anomaly on a regular grid is affected by possible edge effects, which could suggest "false" minimum/maximum, local or regional, for an extended area range ~0.7 km parallel to the internal perimeter of the mapped anomaly. The edge effects could be resolved by extending the relief area for a distance at least equal to the size of the local anomalies identified within the latter; this would also allow to resolve the ambiguity on the regional or local character of these effects.

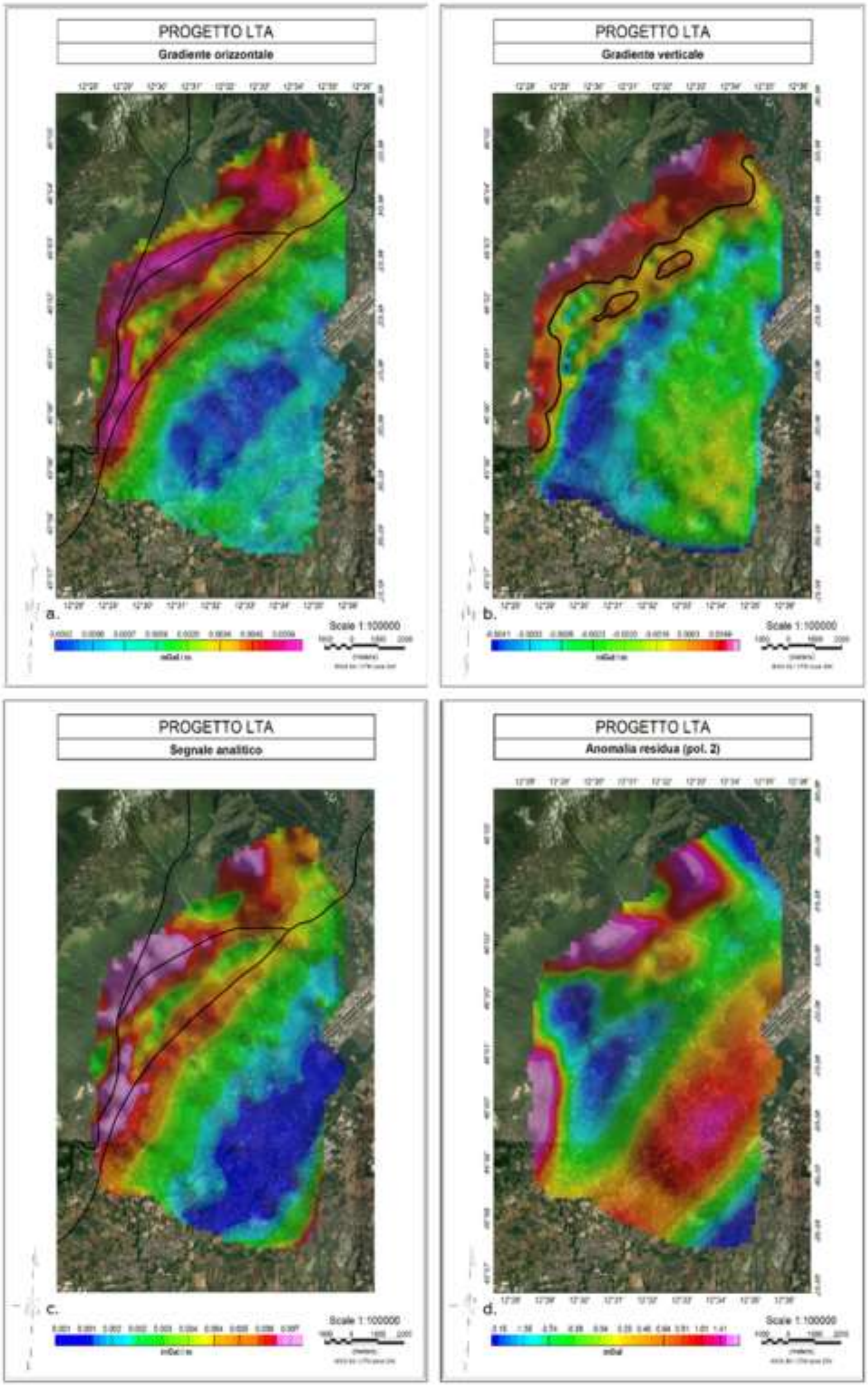

Figure 9 - Gravimetric maps. (a) Horizontal gradient with the interpretation of the corrected tectonic features taken from Carulli (2006); (b) vertical gradient with black contour line identifying the value 0, which approximates the areas of lateral contact between compact rock and loose sediment; (c) analytical signal superimposed on the interpretation of the tectonic features; (d) residual anomaly calculated by removing the second-order polynomial surface from the Bouguer anomaly.

Through the constraints provided by seismic and geology, an initial two-dimensional model was defined using the GM-SYS application of the Oasis Montaj (Seequent) software. The calculation of gravity, in this case, is limited by the assumption that in the dimension perpendicular to those represented, the model is repeated equally to itself for approximately infinite distances (Talwani et al., 1959). For this assumption to be a valid first approximation, the 2D profiles have been oriented perpendicularly to the main axes of the geological structures in the study area, which are the NE-SW oriented thrusts (Fig. 6.10).

The densities of the various modeled geological bodies have been chosen within reasonable intervals reported in the literature (Grant and West, 1965; P.V. Sharma, 1997):

- Jurassic-Cretaceous limestones 2.5 ÷ 2.75 g/cm^3
- Miocene molasses 2.4 ÷ 2.75 g/cm^3
- Quaternary sediments 1.6 ÷ 2.25 g/cm^3

The rocky substrate of the molasse raised by the overthrust of Polcenigo-Maniago and emerging upstream of the latter is made up of intensely fractured rock and displaced by tectonics; it has been hypothesized to have a slightly lower density than the rocky substrate belonging to the same formation and located below the Quaternary sediments south of the thrust. The densities of each body have been finally chosen within the ranges indicated through a least-squares solution in order to find the best agreement, geologically consistent, between the gravity calculated by the model and that measured in the field.

Finally, it is essential to specify that the gravimetric method is sensitive to variations in density in the subsoil, not to the absolute values of the parameter: by adding or subtracting a constant value to all the densities of the model, the calculated anomaly does not change but is at most translated of a negative or positive constant that does not change its trend.

The gravity calculated from the initial model results to approximate the observed data to less than an error of ± 0.738 mGal located in the south-eastern half of the study area, in correspondence with the alluvial plain (Fig. 9). In this area, the minimum relative to the thrust front (the same observed in the vertical gradient) corresponds to a mass deficit, which the initial model does not contemplate. In the SE sector of the profile, on the other hand, there is an excess of mass (negative error). Due to the already mentioned inherent ambiguity of the gravimetric method, the error can be solved by adopting several solutions: (1) by vertically varying the depth of the rock/sediment interface, (2) by laterally varying the density of Quaternary sediments, (3) by varying both vertically and laterally the density of the sediments, or (4) through a combination of the previous hypotheses (Fig. 10).

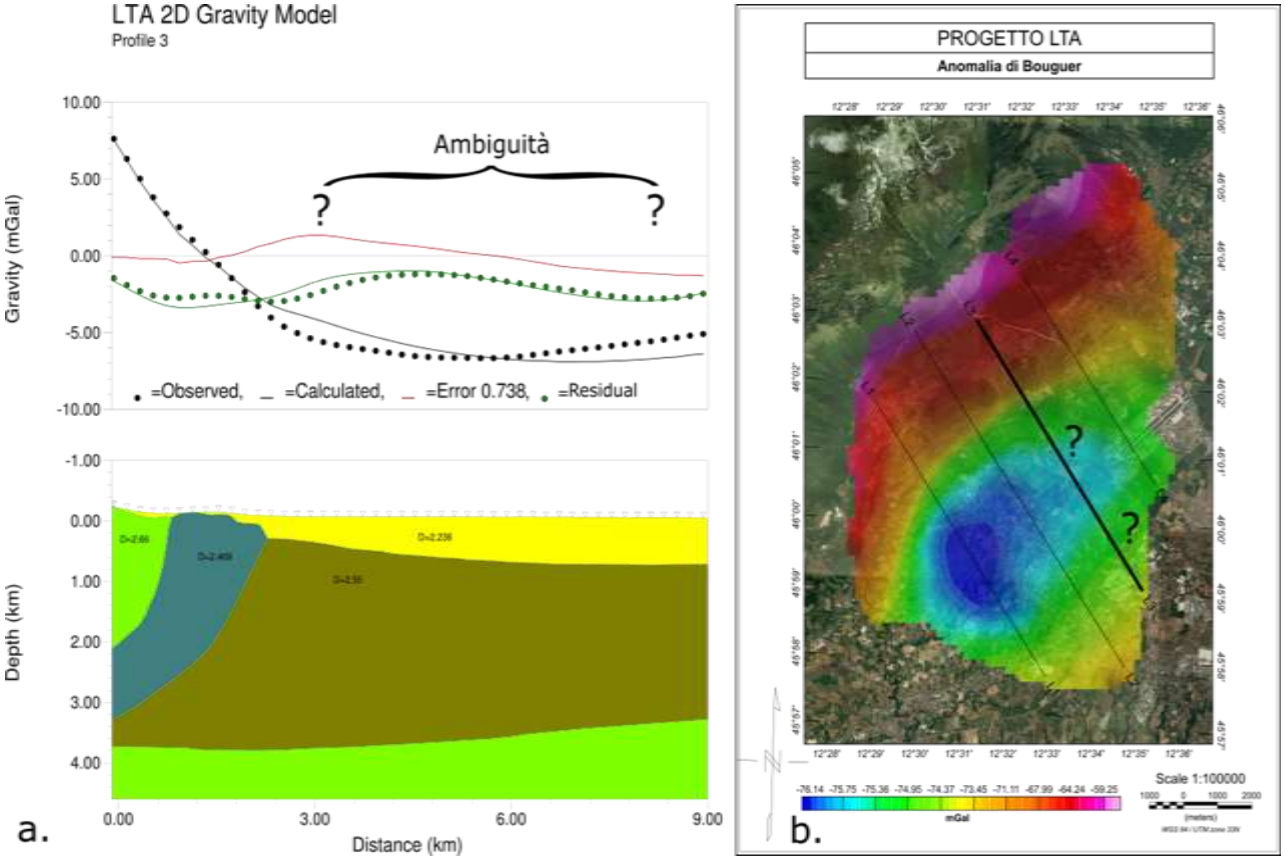

Figure 9 - (a) Gravimetric profile and relative initial density model (the densities are indicated above the corresponding bodies with the letter D. The areas in which the initial model has the greatest inconsistencies with the observed data are highlighted. (b) Map of gravimetric profiles superimposed on the Bouguer anomaly map (profile 3 is highlighted with greater thickness).

A partial solution to the problem of ambiguity can also be found in the geodynamic characterization of the area. In fact, although this is a relatively small area to record wavelengths due to deep structures, it must still be affected to a certain extent by the isostatic effect generated by the Alpine chain immediately in front, which reaches within a few kilometers from the stations' altitudes over a thousand meters. This massive lithostatic load folds the underlying crustal layer generating a variation in gravity that can be recorded on a regional scale (Simpson, 1986). Assuming that (1) the Earth's crust-mantle system is in a state of isostatic equilibrium and (2) that the elastic resistance of the crust is zero (Airy hypothesis), the gravimetric effect of crustal lowering has been calculated starting from a digital terrain model extended over a radius of ~40 km from the survey area (Fig. 11a). The regional isostatic effect locally takes the form of a weakly inclined plane and, once removed from the Bouguer anomaly, can partially justify the increase in gravity in the S-E direction (Fig. 11b, c).
However, even accepting this hypothesis, the local minimum problem at the thrust front remains, which cannot be solved by a simple first-order polynomial surface. To justify the latter, in addition to removing the isostatic effect, it was decided to "lower" the rock-sediment interface by ~200 m compared to the initial constraint posed by the seismic (Nicolich et al., 2004). This solution is plausible if we consider, with a good approximation, an average speed of ~2000 m/s of the sound waves in Quaternary sediments. Finally, the hypothesis was verified on four parallel gravimetric profiles covering the survey area (Fig. 12).

In conclusion, with this gravimetric survey, we can state that:

- The data allows to highlight the lateral density contrasts mainly attributable to the rock/sediment contact;
- the horizontal and vertical gradients of the gravimetric data allow to identify and map of the main tectonic features with a good approximation;
- The initial model built starting from seismic and geological constraints is able to justify the trend of the Bouguer anomaly in the NW sector, where the surface lithology is mainly made up of compact rock (limestone or molasses), but fails to adequately image density

contrasts in the SE sector, where the surface lithology is mainly made up of loose sediments;

The difference between the anomaly calculated and observed in the SE sector can be solved by:

1. a vertical variation of the rock/sediment interface, verifiable through targeted seismic investigation (by refraction or possibly by reflection);
2. a strong lateral variation in the density of sediments starting from the N-W towards the S-E (variation of the clay component or porosity), verifiable through a geo-electric survey capable of reaching depths greater than 200 m;
3. a combination of the first two hypotheses to which is added a possible deeper regional effect, verifiable only through an expansion of the survey area in the E, S, and W directions, for a radius of ~5 ÷ 10 km.

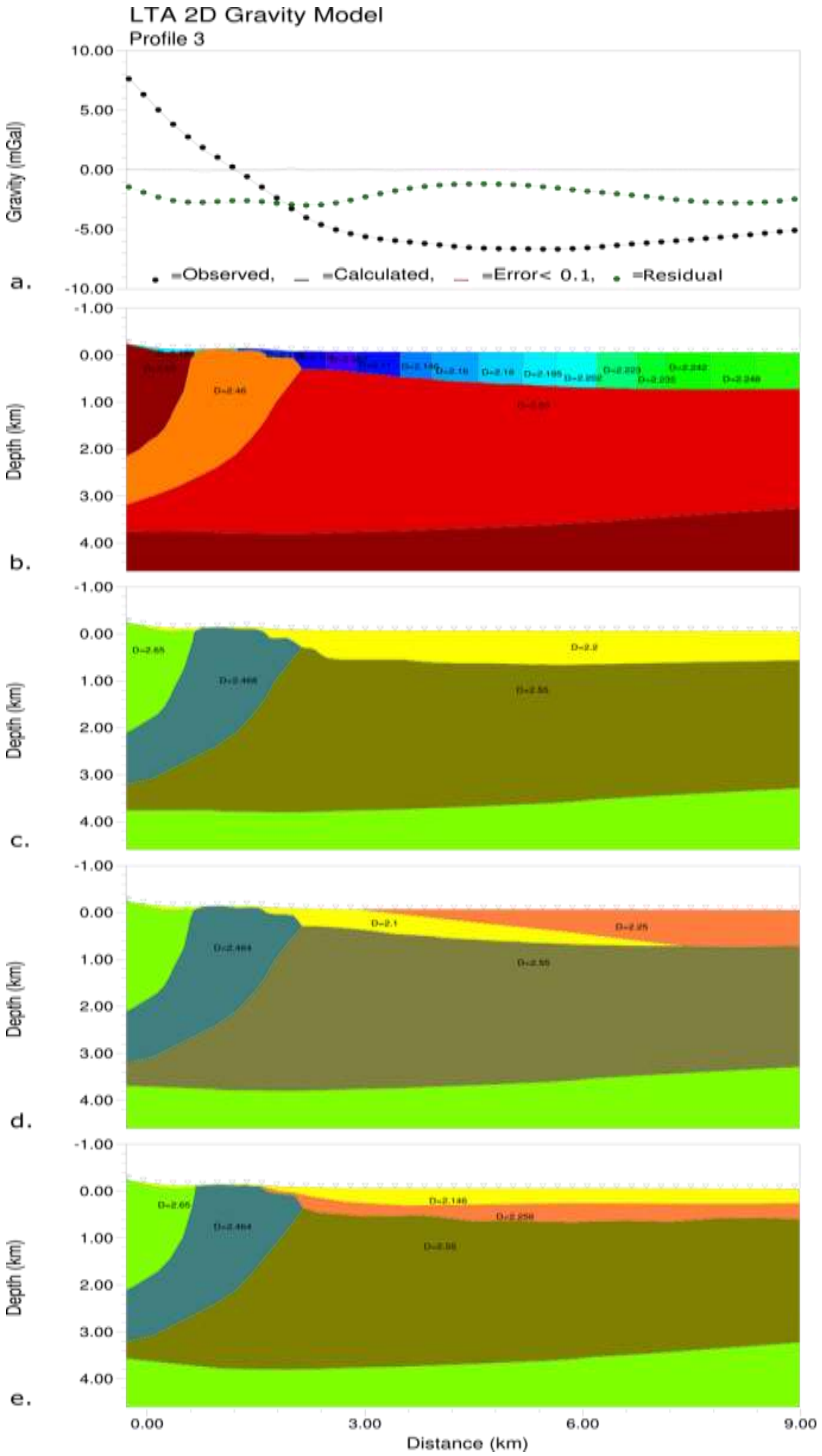

Figure 10 - Possible resolving sections of the initial model, which lead to a difference between the calculated and measured data of less than 0.1 mGal (a). Changes to the initial model consist of: (b) lateral variations in sediment density, (c) variations in bedrock depth (Molass, D = 2.55g/cm^3), (d) lateral and vertical variations in sediment densities, (e) vertical variations in sediment density and bedrock depth.

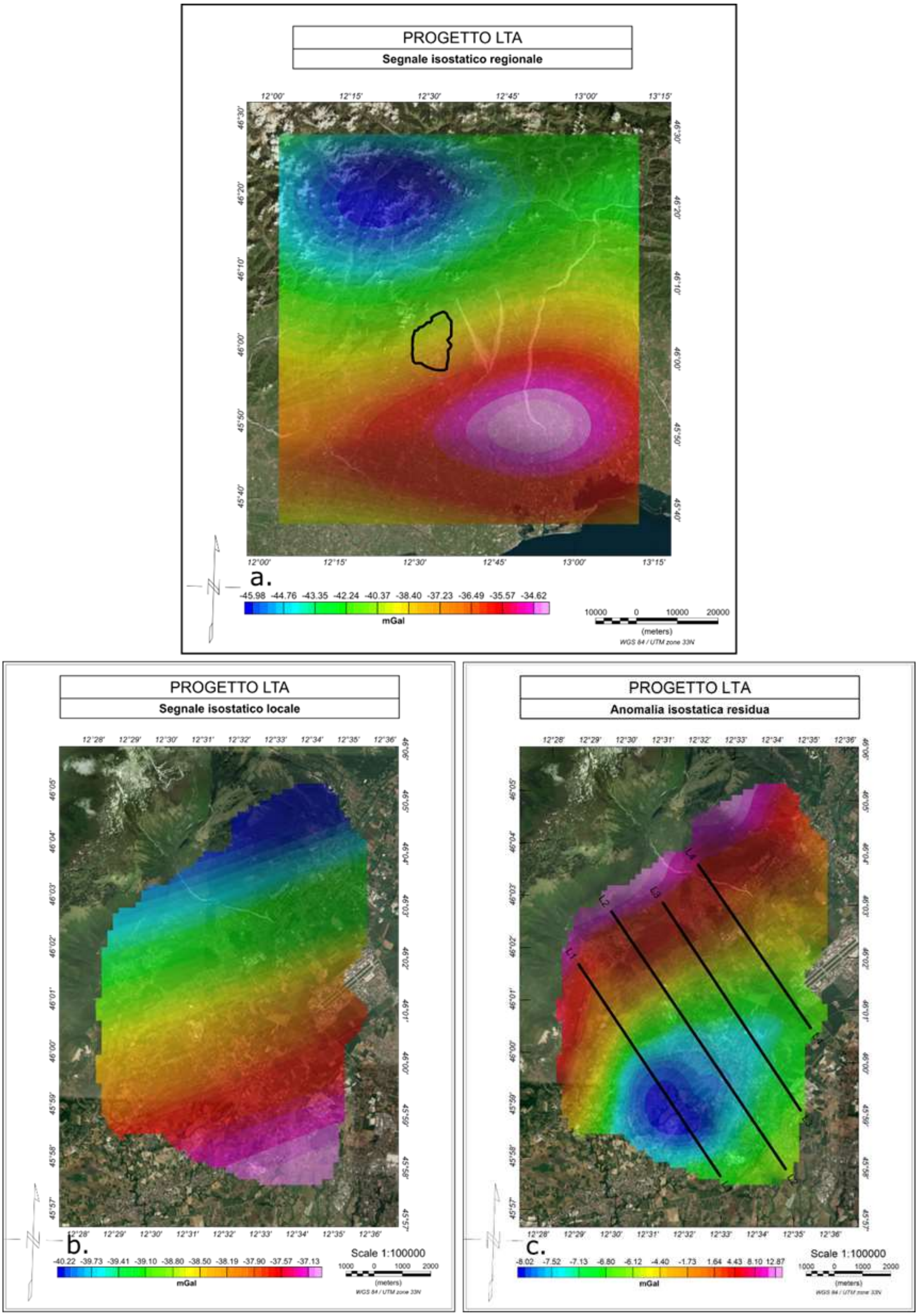

Figure 11 - (a) Regional isostatic effect calculated starting from the topography (black polygon represents the survey area, (b) local map of the regional effect and (c) Bouguer anomaly corrected for the isostatic effect, to which is superimposed the position of the modeled gravimetric profiles (Fig. 12).

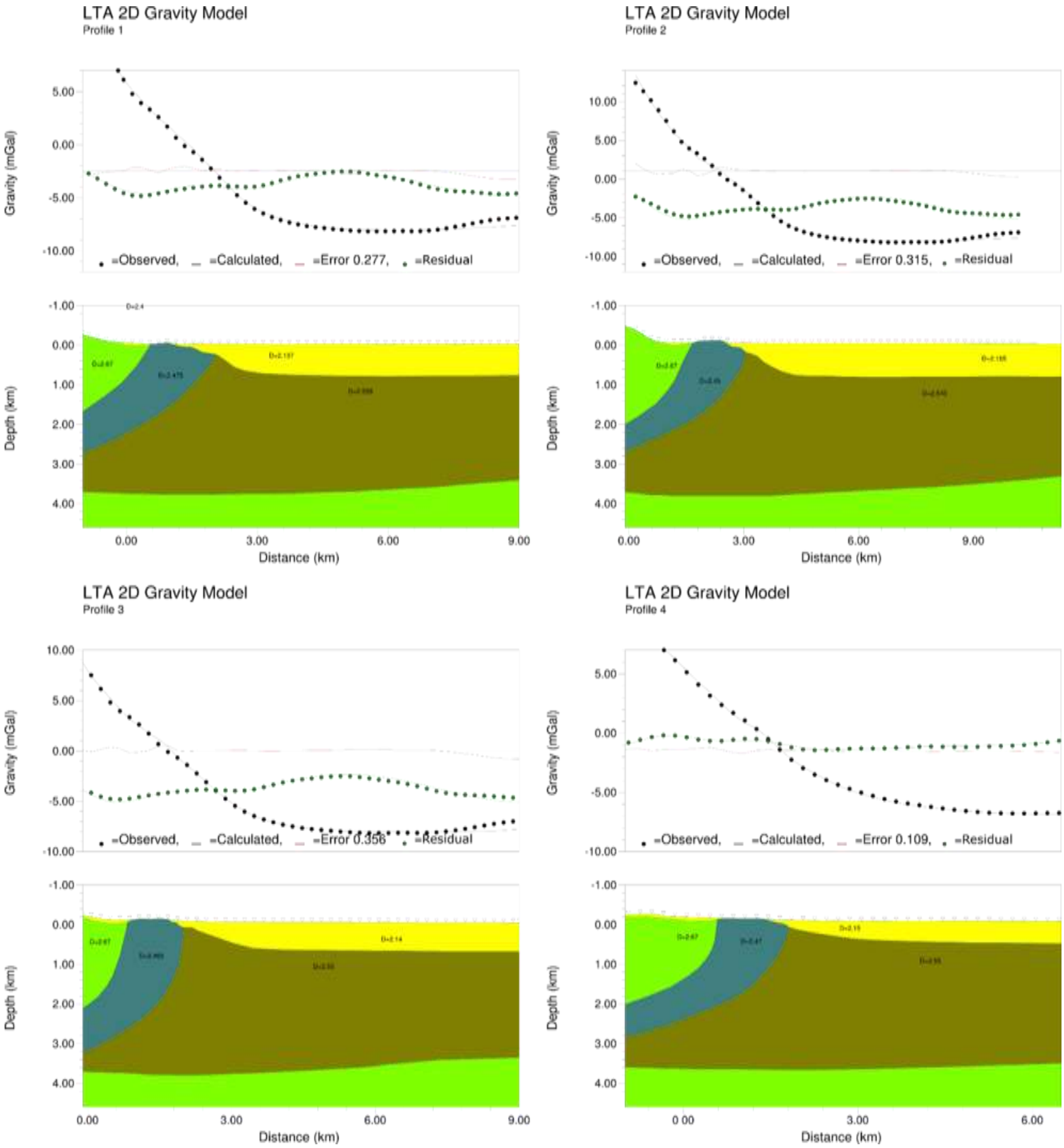

Figure 12 - Gravimetric profiles modeled starting from the Bouguer anomaly corrected for the regional isostatic effect and modified with respect to the initial model by lowering the depth of the bedrock by ~200 m compared to the initial hypothesis deriving from the maps of Nicolich et al. (2004).

References

Barison E., 2009 – Il contributo dei dati sismici per la valutazione delle risorse idriche e geotermiche nella Pianura friulana. PhD thesis, Università degli Studi di Trieste.

Blakely, R. J., 1996 – Potential theory in gravity and magnetic applications. Cambridge university press, pp. 323 - 327.

Busetti M., Palmieri F. Giorgi M., Dal Cin M., Giustiniani M., Nieto D., Zampa L. S., 2021. Analisi geofisiche in applicazione dei protocolli CAMI LIFE+ e WARBO LIFE+ per la salvaguardia degli acquiferi di interesse acquedottistico dell'Alta e Bassa Pianura in destra Tagliamento nell'area compresa tra il fiume Livenza ed il torrente Cellina. Relazione 2021/26 Sez. GEO 6 GEOS, 20 marzo 2021, 115 pp.

Dentith, M., & Mudge, S. T., 2014 – Geophysics for the mineral exploration geoscientist. Cambridge University Press, pp. 78-80.

Fairhead, J. D., 2016 – Advances in gravity and magnetic processing and interpretation. European Association of Geoscientists & Engineers Pubblication.

Fedi, M., & Rapolla, A., 1993 – I metodi gravimetrico e magnetico nella geofisica della Terra solida. Liguori, pag. 287.

Grant, F. S., & West, G., 1965 – Interpretation theory in applied geophysics. McGraw-Hill, New York, 583, 322-341.

Jung, K., 1961 – Schwerkraftverfahren in der angewandten Geophysik. Akademische Verlagsgesellschaft Geest and Portig, Leipzig.

Nicolich R., Della Vedova B., Giustiniani M., Fantoni R., 2004 – Carta del Sottosuolo della Pianura Friulana. Regione Autonoma Friuli Venezia Giulia, Direzione centrale Ambiente e Lavori Pubblici, Servizio Geologico Regionale, 4 Tav., Note Illustrative, 32 pp.

Rapolla, A. 1986 – Crustal structure of Central and sorthern Italy from gravity and magnetic data. Giornale di Geologia, 48(1-2), 129-143.

Sharma, P. V., 1997 – Environmental and engineering geophysics. Cambridge university press, pag. 17.

Simpson, Robert W., Jachens, Robert C., Blakely, Richard J., and Saltus, Richard W., 1986 – A new isostatic residual gravity map of the conterminous United States, with a discussion on the significance of isostatic residual anomalies, JGR, 91, p8348-8372.

Talwani, M., Worzel, J. L., and Landisman, M., 1959 – Rapid gravity computations for two-dimensional bodies with application to the Mendocino submarine fracture zone: J. Geophys. Res., 64, 49-59.

Zanferrari A., Avigliano R., Grandesso P., Monegato G., Paiero G., Poli M.E., Stefani C., 2008a – Note Illustrative della Carta geologica d'Italia alla scala 1:50.000 – Foglio 065 Maniago. APAT - Servizio Geologico d'Italia; Regione Friuli Venezia Giulia - Servizio Geologico 224 pp.